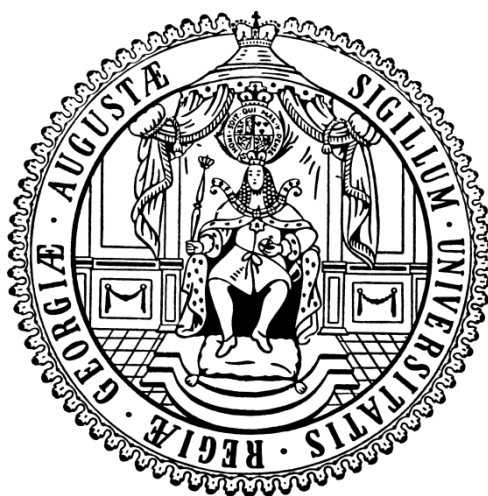


Exploring Metal-Ligand Interactions of Pyrrole Based Pincer Ligands



Dissertation

zur Erlangung des mathematisch-naturwissenschaftlichen Doktorgrades

„Doctor rerum naturalium“

der Georg-August-Universität Göttingen

im Promotionsprogramm CaSuS

der Georg-August University School of Science (GAUSS)

vorgelegt von

Christian Maaß

aus Rotenburg an der Fulda

Göttingen, 2013

Betreuungsausschuss

Prof. Dr. Dietmar Stalke, Institut für Anorganische Chemie

Prof. Dr. Lutz Ackermann, Institut für Organische und Biomolekulare Chemie

Prof. Dr. Oliver Wenger, Departement für Chemie, Universität Basel

Mitglieder der Prüfungskommission

Referent Prof. Dr. Dietmar Stalke, Institut für Anorganische Chemie

Korreferent Prof. Dr. Lutz Ackermann, Institut für Organische und Biomolekulare Chemie

Weitere Mitglieder

Prof. Dr. Franc Meyer, Institut für Anorganische Chemie

Dr. Inke Siewert, Institut für Anorganische Chemie

Jun.-Prof. Dr. Thomas Waitz, Institut für Anorganische Chemie

Prof. Dr. Konrad Koszinowski, Institut für Organische und Biomolekulare Chemie

Tag der mündlichen Prüfung: 16. Oktober 2013

“Der Zufall ist der einzig legitime Herrscher des Universums“

Napoleon I. Bonaparte

Abkürzungsverzeichnis

PMDETA	Pentamethyldiethylene-triamine	CSD	Cambridge Crystallographic Database
HSAB	Hard and soft acids and bases	hmds	Bis-trimethylsilylamide
dipp	Diisopropylphenyl	S _N	Nucleophilic substitution
pyrr	Pyrrole	Nu	Nucleophile
BOX	Bis-oxazoline	<i>t</i> Bu	<i>tert</i> -Butyl
Hal	Halide	Ph	Phenyl
PTE	Periodic Table of the Elements	HF	Hartree-Fock
HOMO	Highest occupied molecular orbital	DFT	Density Functional Theory
LUMO	Lowest unoccupied molecular orbital	LCAO	Linear combination of atomic orbitals
<i>n</i> -Buli	<i>n</i> -Butyllithium	Tol	Toluene
BOC	Butyloxycarbonyl	au	Atomic units
TMS	Trimethylsilyl	NBO	Natural Bond Orbital
NBS	<i>N</i> -bromosuccinimide	BO	Bond Order
NCS	<i>N</i> -chlorosuccinimide	LP	Lone pair
DMF	<i>N,N</i> -dimethylformamide	kcal	Kilocalorie
DIBAL-H	Diisobutylaluminiumhydride	MeLi	Methylolithium
Me	Methyl	BASF	Batch Scale Factor
Et	Ethyl	TMEDA	Tetramethylethylenediamine
Ar	Aryl	d	Distance / Doublet
NMR	Nuclear Magnetic Resonance	K	Kelvin
		NICS	Nucleus Independent Chemical Shift

ppm	Parts per million	h	Hour
eV	Electron volts	MHz	Megahertz
pm	Picometer	M	Molar
Å	Angström	mL	Milliliter
°C	Degree Centigrade	mmol	Millimol
T	Temperature	g	Gram
El	Electron Ionization	s	Singlet
MS	Mass spectrometry	THF	Tetrahydrofuran
m	Mass	mg	Milligram
z	Charge	mm	Millimeter

Table of Contents

1	Introduction	1
1.1	Pincer Ligands	1
1.2	Pyrrole	5
1.3	Chemistry of Low Valent Group 14 Elements	7
2	Scope	15
3	Results and Discussion	17
3.1	The pyrrole based pincer ligand	17
3.1.1	2,5-Bis((dimethylamino)methyl)pyrrole (1)	22
3.1.2	2,5-Bis((pyrrolidino)methyl)pyrrole (2)	24
3.1.3	2,5-bis((3,5-dimethylpiperidino)methyl)pyrrole (3)	25
3.1.4	Ligand derivatization	26
3.1.5	{SNS}-Pyrrole based pincer ligand	28
3.1.5.1	2,5-Bis((<i>tert</i> butyl-thiolato)methyl)pyrrole (5)	28
3.1.5.2	2,5-Bis((thiophenolato)methyl)pyrrole (6)	28
3.1.6	General remarks on the computational methods	32
3.2	Lithium pyrrolide complexes	34
3.3	Group 13 Metal Pincer Complexes	47
3.3.1	Aluminium-dichloro-{2,5-bis((3,5-dimethylpiperidino)methyl)-pyrrolide} (10)	47
3.3.2	2,5-Bis((pyrrolidino)methyl)pyrrole · 2 trimethylaluminium (11)	54
3.3.3	Indium-dibromo-{2,5-bis((pyrrolidino)methyl)pyrrolide} (12)	59
3.4	Group 14 Metal Pincer Complexes	61
3.4.1	Silicon-dichloro-hydrido-{2,5-bis((pyrrolidino)methyl)-pyrrolide} (13)	61
3.4.2	Germanium-chloro-{2,5-bis((pyrrolidino)methyl)-pyrrolide} (15)	69
3.4.2.1	Germanium-chloro-{2,5-bis((dimethylamino)methyl)-pyrrolide} (16)	77
3.4.2.2	Reactivity of the {NNN}germanium-chloride pincer complexes	79
3.4.2.2.1	Germanium-chloro-[2,5-bis(dimethylamino)methyl]pyrrolidido]-thione (17)	80
3.4.2.2.2	Oxidative addition of hydrogen	83
3.4.2.2.3	Ligand substitution reactions	84
3.4.3	Tin-chloro-{2,5-bis((pyrrolidino)methyl)-pyrrolide} (18)	86
3.4.4	Lead-chloro-{2,5-bis((pyrrolidino)methyl)-pyrrolide} (21)	90
3.4.5	Structural comparison of the prepared group 14 species	94
3.5	Group 15 Metal Pincer Complexes	99
3.5.1	Antimony-dichloro-{2,5-bis((pyrrolidino)methyl)-pyrrolide} (22)	99
3.5	Transition Metal Pincer Complexes	101
3.5.1	Nickel-chloro-{2,5-bis((<i>tert</i> butyl-thiolato)methyl)pyrrolide} (23)	101
3.5.2	Palladium-dimethylamino-chloro-{2,5-bis((dimethylamino)methyl)-pyrrolide} (26)	105
4	Synthesis and Structure	108

4.1	General.....	108
4.1.1	Spectroscopic and analytic methods	108
4.2	Synthesis	109
4.2.1	2,5-bis((dimethylamino)methyl)pyrrole (1)	109
4.2.2	2,5-bis((pyrrolidino)methyl)pyrrole (2)	109
4.2.3	2,5-bis((3,5-dimethylpiperidino)methyl)pyrrole (3)	110
4.2.4	2,5-bis((<i>tert</i> butyl-thiolato)methyl)pyrrole (5)	111
4.2.5	2,5-bis((thiophenolato)methyl)pyrrole (6)	112
4.2.6	Lithium[2,5-bis((dimethylamino)methyl)pyrrolide] (7)	113
4.2.7	Lithium[2,5-bis((pyrrolidino)methyl)pyrrolide] (8)	113
4.2.8	Lithium[2,5-bis((3,5-dimethylpiperidino)methyl)pyrrolide] (9)	114
4.2.9	Aluminium-dichloro-{2,5-bis((3,5-dimethylpiperidino)methyl)-pyrrolide} (10)	115
4.2.10	2,5-bis((pyrrolidino)methyl)-1H-pyrrole · 2 trimethylaluminium (11)	115
4.2.11	Indium-dibromo-{2,5-bis((pyrrolidino)methyl)-pyrrolide} (12)	116
4.2.12	Silicon-dichloro-hydrido-{2,5-bis((pyrrolidino)methyl)-pyrrolide} (13)	116
4.2.13	Germanium-chloro-{2,5-bis((pyrrolidino)methyl)-pyrrolide} (15)	117
4.2.14	Germanium-chloro-{2,5-bis((dimethylamino)methyl)-pyrrolide} (16)	118
4.2.15	Germanium-chloro-[2,5-bis(dimethylamino)methyl]pyrrolidido]-thione (17)	119
4.2.16	Tin-chloro-{2,5-bis((pyrrolidino)methyl)-pyrrolide} (18)	119
4.2.17	Lead-chloro-{2,5-bis((pyrrolidino)methyl)-pyrrolide} (21)	120
4.2.18	Antimony-dichloro-{2,5-bis((pyrrolidino)methyl)-pyrrolide} (22)	121
4.2.19	Nickel-chloro-{2,5-bis((<i>tert</i> butyl-thiolato)methyl)pyrrolide} (23)	121
4.2.20	Palladium-dimethylamino-chloro-{2,5-bis((dimethylamino)methyl)-pyrrolide} (26)	122
5	Crystallographic section	123
5.1	General	123
5.2	Determined Structures	124
5.2.1	2,5-Bis((pyrrolidine)methyl)pyrrole (2)	124
5.2.2	2,5-bis((thiophenolato)methyl)pyrrole (6)	126
5.2.3	Lithium-2,5-bis(dimethylamino)methyl pyrrolide (7)	128
5.2.4	Lithium[2,5-Bis((pyrrolidine)methyl)pyrrolide] (8)	131
5.2.5	Lithium-[2,5-bis((3,5-dimethylpiperidino)methyl)pyrrolide] (9)	134
5.2.6	Aluminium-dichloro-{2,5-bis((3,5-dimethylpiperidino)methyl)-pyrrolide} (10)	137
5.2.7	2,5-bis((pyrrolidino)methyl)-1H-pyrrole · 2 trimethylaluminium (11)	139
5.2.8	Indium-dibromo-{2,5-bis((pyrrolidino)methyl)-pyrrolide} (12)	141
5.2.9	Silicon-dichloro-hydrido-{2,5-bis((pyrrolidino)methyl)-pyrrolide} (13)	144
5.2.10	Silicon-dichloro-hydrido-2,5-bis((pyrrolidino)methyl)pyrrolide (13a)	146
5.2.11	Germanium-chloro-{2,5-bis((pyrrolidino)methyl)-pyrrolide} (15)	148
5.2.12	Germanium-chloro-{2,5-bis((dimethylamino)methyl)-pyrrolide} (16)	150
5.2.13	Germanium-chloro-[2,5-bis(dimethylamino)methyl]pyrrolidido]-thione (17)	152

5.2.14	Tin-chloro-{2,5-bis((pyrrolidino)methyl)-pyrrolide} (18).....	154
5.2.15	Lead-chloro-{2,5-bis((pyrrolidino)methyl)-pyrrolide} (21).....	156
5.2.16	Antimony-dichloro-{2,5-bis((pyrrolidino)methyl)-pyrrolide} (22).....	158
5.2.17	Nickel-chloro-{2,5-bis((tertbutyl-thiolato)methyl)pyrrolide} (23).....	160
5.2.18	Palladium-dimethylamino-chloro-{2,5-bis((dimethylamino)methyl)-pyrrolide} (26)	162
6	Conclusion and outlook	164
7	Crystal structure determination in collaborations	168
7.1	Structures determined for Dr. Tim Hungerland (Prof. Dr. Dr. h. c. L. F. Tietze)	168
7.2	Structures determined for Dr. Tobias Schneider (Prof. Dr. D. B. Werz)	173
7.3	Structures determined for Dr. Johannes Kaschel (Prof. Dr. D. B. Werz)	177
7.4	Structures determined for Matrin Pawliczek (Prof. Dr. D. B. Werz).....	178
7.5	Structures determined for Svenia C. Düfert (Prof. Dr. Dr. h. c. L. F. Tietze)	179
8	References	180

1 Introduction

1.1 Pincer Ligands

Pincer Ligands were synthesized first by *van Koten*¹ and *Moulton*² in the late 1970s. Their unexpected properties arouse great interest in the research area of coordination chemistry. With a rapidly increasing number of publications in the following years, they nowadays embody a well-known class of compounds, with application in catalysis³ as well as in inorganic coordination chemistry.⁴

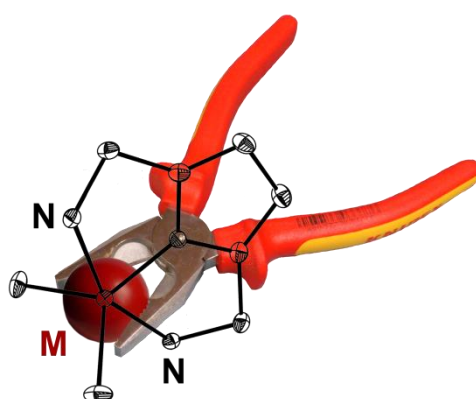
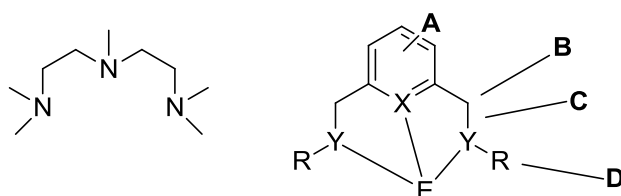


Figure 1. Simplified scheme of a pyrrole based pincer complex.

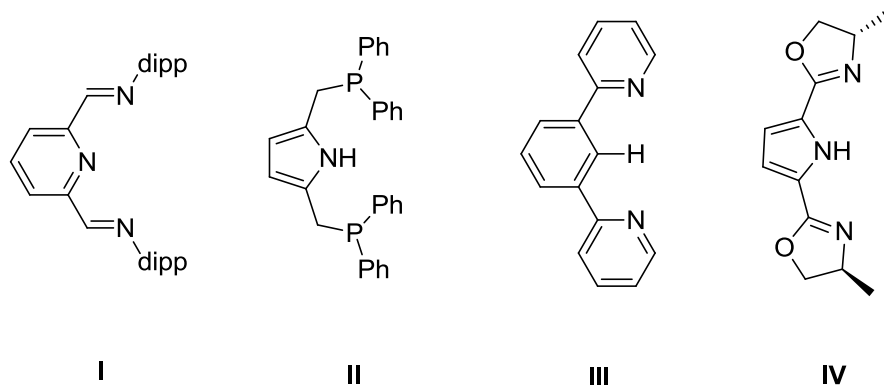
The name pincer ligand stems from their typical coordination motif, chelating the metal ion in a tridentate, meridonal fashion, like a pincer (Figure 1). The general abbreviation of a pincer ligand is {YXY} with *Y* as the donor functions located at the side arms and *X* as the central donor function (Scheme 1, right). These donor functions are connected by linker units, which are very often alkyl chains. The most facile pincer ligand one can think of is pentamethyldiethylenetriamine (PMDETA) (Scheme 1, left). With three nitrogen donor atoms connected by two ethylene moieties, it represents a neutral, tridentate pincer ligand.



Scheme 1. Exemplary non-aromatic (left) and aromatic (right) pincer ligands.

Through derivatization it is possible to adjust the ligand properties to the target metal moiety. Scheme 1 (right) shows the variable parameters of the pincer ligand (**A** –

D). Besides tuning the donor atoms according to the HSAB principle⁵ it is also possible to vary the backbone (**A**). It can be aliphatic or aromatic and within these species one can discriminate between electron rich or electron poor backbones. The linkers (**B**) can be aromatic providing a delocalized π -system between the donor centers or aliphatic and highly flexible alkylene groups. Moreover, the length of the linker determines the size of the coordination pocket. A linker consisting of two atoms will result in five-membered metallacycles, whereas a linker consisting of three atoms yields less strained six-membered metallacycles. In addition, it is possible to introduce electron deficient or electron donating substituents (**C**) to the linker system in order to fine-tune the ligand's electronic system. Besides the electronic properties, the steric demand can be varied. To protect reactive metal species, side arm donor functions with bulky groups can be introduced to the ligand (**D**) rising the kinetic stability of labile complexes.

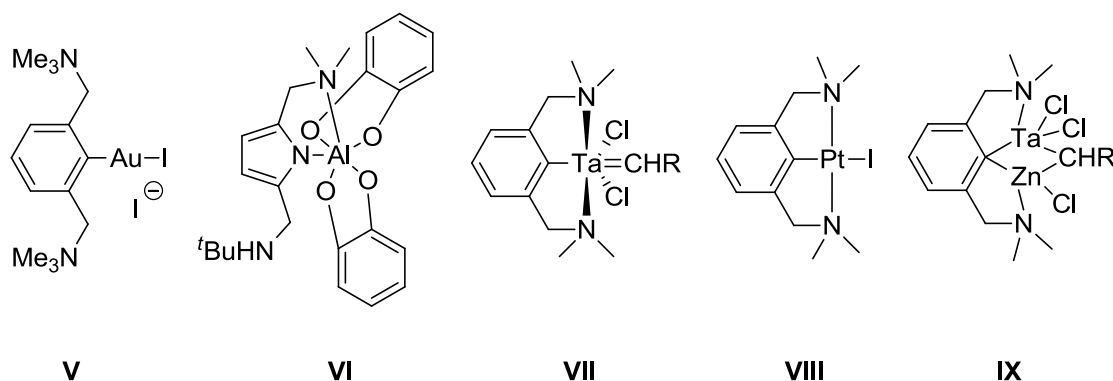


Scheme 2. Selected examples of pincer ligands.

Scheme 2 shows literature-known examples of pincer ligands. **I** is a neutral pincer ligand and characterized by a delocalized π -system between all donor atoms.⁶ A pyridine heterocycle serves as backbone and the side arm donors carry bulky 2,6-diisopropylphenyl (dipp) groups. It was used by *Roesky et al.* for coordination of reactive germanium species with the dipp moieties providing the required kinetic stability.⁷ Compound **II** is an anionic ligand with two phosphorus donor atoms in the side arm moieties.^{3d} A highly electron rich pyrrole heteroaromatic system serves as backbone and the linkers are flexible methylene groups. *Gade et al.* synthesized transition metal complexes based on **II**, with the purpose to use them as catalyst.^{3d} Ligand **III** is anionic with an aromatic system delocalized all over the ligand.⁸ It is used as building block for a metal coordination site in material science and in bioinorganic chemistry.⁸ The pyrrBOX ligand **IV** is anionic, containing a pyrrole heterocycle as backbone⁹ with the side arm

donor functions implemented in a chiral oxazoline moiety. The alkyl chains bonded to the oxazoline heterocycle induce asymmetry which makes the ligand feasible for asymmetric catalysis as it was demonstrated by *Gade et al.*⁹ These selected examples give an idea of the variety of properties in the class of pincer ligands.

A common feature of all ligands mentioned above is that kinetic stability gained through multiple coordination of the metal ion is combined with a high flexibility illustrated by the different metal coordination modes shown in Scheme 3. In compound **V**,¹⁰ the ligand acts a monodentate two electron donor. The ligand in **VI**¹¹ serves as a bidentate four electron donor whereas in **VII**¹² the typical tridentate coordination motif is present with the ligand acting as a six electron donor. Remarkable is the facial coordination of the pincer within an octahedral tantalum compound. In **VIII**¹³ the ligand functions as a six electron donor in a square planar platinum complex. **IX**¹⁴ is a rare example of a bridging (4+4) electron donating pincer ligand.



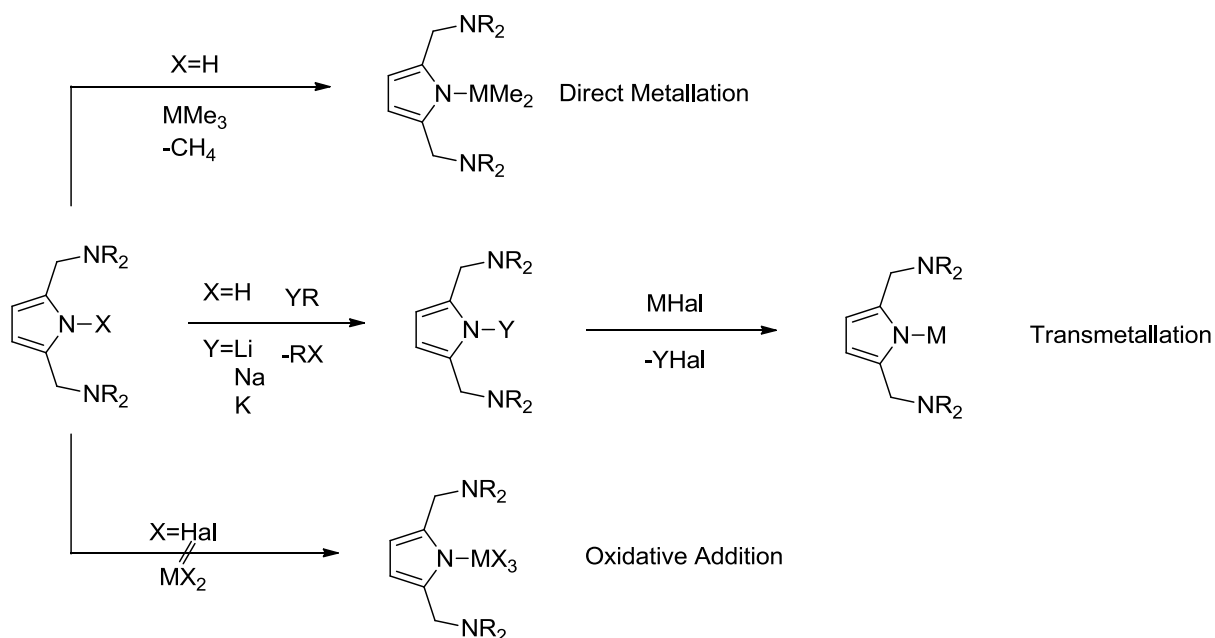
Scheme 3. Observed coordination modes within pincer complexes.

These selected examples mirror the coordination flexibility of the pincer ligands. In **VI** the rather bulky catechol can coordinate to the aluminium ion with one of the side arms bent aside, and in **IX** even two metals fit in the ligand's coordination pocket to form a heterobimetallic species. Within these five examples a variety of metal compounds is shown. By modifying the ligand properties it becomes feasible to coordinate the soft and rather big gold(I) ion as well as the hard and small aluminum(III) ion.

There are three procedures known to literature to obtain metal complexes based on pincer ligands. Most common is the transmetallation *via* salt elimination (Scheme 4).¹⁵ For this procedure, the ligand requires an acidic proton. Through deprotonation with a

basic alkaline metal compound, the group one metal-ligand complex is generated. It serves as precursor for the desired compounds which are obtained in a subsequent transmetallation reaction with a metal halide. The advantage of this reaction is that the equilibrium is shifted towards the product due to precipitation of the group one metal-halide compound.

Furthermore, it is possible to metallate the ligand directly¹⁶ using basic metal compounds like trimethylaluminum. This method offers two advantages. It skips one step compared to the transmetallation and the workup is simplified because of gaseous or at least volatile side products. The direct metallation is often preferred but the basic metal species can be highly reactive or unstable, therefore in some cases the transmetallation is the most promising method.



Scheme 4. Possible Synthetic routes to pyrrole based pincer complexes.


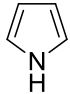
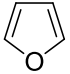
The third well established synthetic access to pincer complexes is the oxidative addition.¹⁷ The disadvantage herein is the need of a prefunctionalized ligand system. With pyrrole as backbone, there is no example of an oxidative addition yet. With halogenated benzene as backbone, however, this method works properly and offers the substantial advantage of no byproducts.

1.2 Pyrrole

Pyrrole was first isolated from coal tar by *Runge* in 1834.¹⁸ The name is derived from Runge's pyrrole detection test. A pine splint, wetted with hydrochloric acid, turns red if the pyrrole concentration (vapor) exceeds 3.3 ppm.¹⁹ He named the substance pyrrole, from *pyrros* (greek) meaning blazing red.

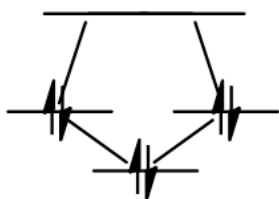
Pyrrole is a five membered heteroaromatic cycle with the lone pair of the nitrogen atom being involved in the π -system. The aromatic character is considerably higher than in related heterocycles containing oxygen, sulfur or phosphorous.²⁰ With six electrons dispersed on five atoms, the aromatic system is rather electron rich and activated for electrophilic substitution in the 2- and 5- position.²¹

Table 1. Comparison of cyclopentadienide and related heterocycles.

			
Av. Double bond [pm]	139.7 ^{22,23}	137 ²⁴	135 ²⁴
C-C Single bond [pm]	139.7 ^{22,23}	143 ²⁴	144 ²⁴

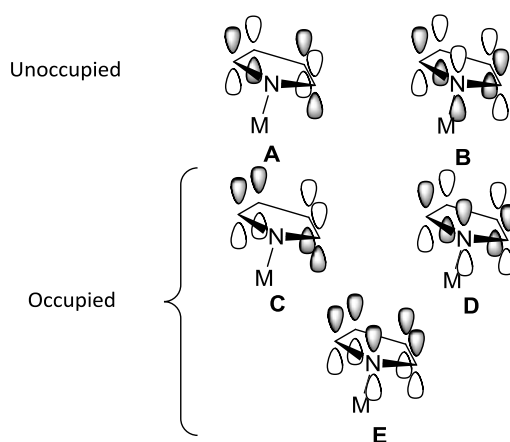
As shown in Table 1 the aromatic character decreases going from carbon to oxygen, although they all are perfectly planar and fulfill the *Hückel* rule.²⁵ Within the cyclopentadienide all bonds are equal in length, the six π -electrons are entirely delocalized on the five carbon atoms ending up in a benzene like bonding situation. When substituting one carbon for a nitrogen atom, the bond lengths diverge significantly but are still different from pure single or double C-C bond lengths (154 pm / 134 pm).²⁶ The nitrogen atom is sp^2 -hybridized having the p_z -orbital involved in the π -system. This loss of electron density decreases the pK_a value of the NH-proton to 17.8,²⁷ which is remarkable in comparison to the pK_a value of pyrrolidine (44),²⁸ the non-aromatic analogue of pyrrole. Furan, however, does not show the typical chemical behavior of aromatic cycles. Instead of reacting in an electrophilic aromatic substitution, it shows the reactivity of a diene, although the bond lengths still indicate a delocalization of the π -electrons.²¹

Investigation of the pyrrole π -system using a *Frost-Musulin* projection²⁹ afforded that it contains five π -orbitals, distributed over three certain levels of energy (Scheme 5).



Scheme 5. Frost-Musulin projection of pyrrole.

The different levels of energy arise from an increasing number of nodal planes with rising energy level. Taking this into account the molecular orbitals shown in Scheme 6 can be derived. This simplified model does not display the reality in detail but give an idea of how the π -system is organized. It is possible to draw inferences about the π -interaction of pyrrole with the *N*-bonded substituent from analyzing the C-C bond lengths.



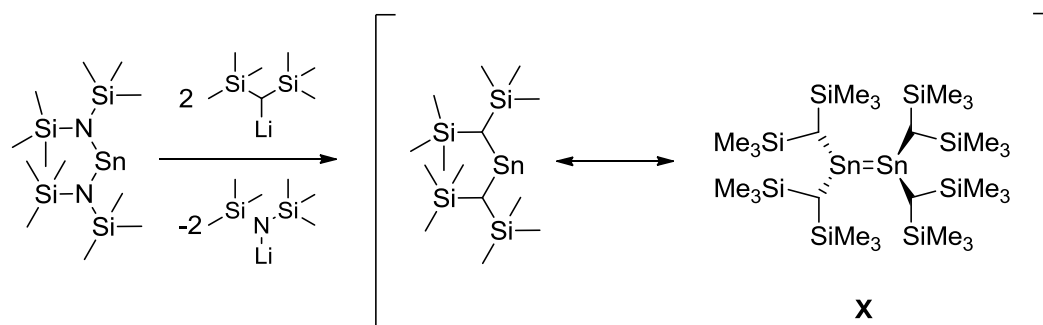
Scheme 6. Schematic depiction of the pyrrole molecular orbitals.

The molecular orbitals shown in Scheme 6 display the frontier orbitals of pyrrole. For investigation of the metal-pyrrole π -interaction, the left structures (A and C) can be neglected due to the lack of metal-nitrogen π -overlap. The orbital having the lowest energy (E) can be disregarded likewise because it affects all bonds in the same way. The orbitals shown on the right, however, are suitable for analyzing the character of the π -interaction. π -donation from the occupied molecular orbital D towards a *N*-bonded metal would shorten the formal double bonds (Scheme 6) and elongate the C-C single bond, whereas π -donation from the metal towards the unoccupied molecular orbital B causes the opposite effect.

By using this model, the changes of bond lengths within the pyrrole heterocycle in a hypothetical pyrrole-metal complex compared to free pyrrole can be traced back to the nature of the metal-ligand π -interaction.

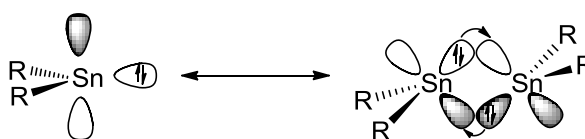
1.3 Chemistry of Low Valent Group 14 Elements

Since the middle 1970s a new class of compounds falsified fundamental rules in inorganic chemistry. The so-called “double bond rule”, stating that main group elements of the third period or heavier are unable to form homonuclear double bonds,³⁰ was shown to have limited validity. In 1976 *Lappert et al.* synthesized the first stable dimeric tin(II) alkyl compound (**X**),³¹ assuming a double bond in between the metal ions. The single crystal X-ray analysis of **X** revealed a local geometry at the tin ions, indicating sp^2 -hybridization. The Sn–Sn bond length of 277 pm fits nicely with the Sn–Sn distance in elemental tin (280 pm),³² and thus can be regarded to be of rather weak nature. This assumption is confirmed by the dissociation of **X** into the monomeric form in solution (Scheme 7).³¹



Scheme 7. Synthesis of the dimeric alkyl tin species and its equilibrium in solution.

Besides the Sn–Sn bond length, the sum of angles at the tin atoms as an indicator for local geometries can be used to draw inferences about the tin-tin interaction. The observed sum of angles of 342° at the tin atoms neither match the expected 360° found in ethylene nor the 327° for tetrahedral geometry. The explanation *Lappert* gave was that the bond is represented by a donor acceptor interaction of the empty p_z -orbital with the lone pair located in a sp^2 -orbital (Scheme 8).³³ This model was revised in the following years, however, the original version of *Lappert* is still used as edge case model for the heaviest main group elements like lead.^{31a,34,35,36}

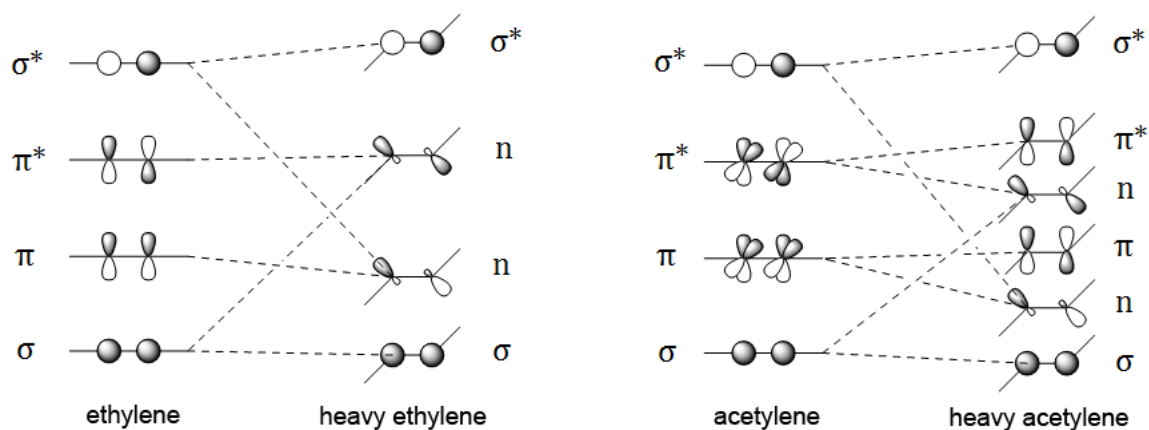


Scheme 8. Dimerization of dialkyltin(II) to a *trans* bent distannene.

The first R_2SiSiR_2 compound was published five years later by *West et al.*³⁷ resembling the ethylene structure much more precise compared to compound **X**. With a Si-Si bond length of 216.0 pm it is roughly 20 pm shorter than a Si-Si single bond (234 pm)²⁶ and the local geometry at the silicon atoms with a sum of angles of 355° deviates only by 5° from planarity.

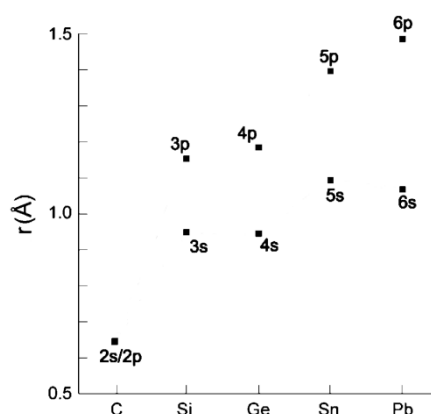
In 1984 *Lappert et al.* filled the gap between silicon and tin by successfully preparing R_2GeGeR_2 .³⁸ Investigating its geometry, the solid state structure shows that the dimeric germanium alkyl compound is within the expected range with less sp^2 character than silicon but more than tin. It is noteworthy that for the first time *Lappert et al.* described a high *Lewis*-basic reactivity of the monomer (R_2Ge) towards a wide range of *Lewis*-acids, which can be seen as the beginning of the modern main group chemistry in the area of (small) molecule activation.

Unexpectedly, it took until 1998 until the first solid state structure of a stable dimer of a dialkyl lead (II) compound was published.³⁹ This delayed publication of the diplumbene compared to the other group 14 dimetallenes is due to a high instability with a strong tendency to dissociate, forming R_2Pb . The selected examples for heavy ethylenes within this chapter show an increasing *trans*-bent character and a weaker metal-metal bond strength descending group 14. In the same way the bond strength weakens, the lone-pair character at each metal rises. This can be attributed to a second order *Jahn-Teller* effect⁴⁰ (Scheme 9), meaning a mixing of a bonding π -molecular orbital (MO) with an anti-bonding σ^* -MO of the dimetallene, yielding a more stabilized but nonbonding MO with sp -hybrid character.



Scheme 9. The second order Jahn-Teller effect in multiple bonded group 14 species.

In the same way, the bonding σ -MO mixes with the anti-bonding π^* -MO. This effect becomes more dominant the heavier the element gets, because the energy gap between σ - and π -orbital decreases as the main quantum number increases. The smaller this energy gap the more likely is a mixing between the σ - and π -orbitals.³⁶ A further weakening of the metal–metal bond results from the size separation of the s- and p-orbitals within one period of the *Periodic Table of the Elements* (PTE) (Scheme 10).⁴¹



Scheme 10. Radii of the valence s- and p-orbitals in group 14 elements.

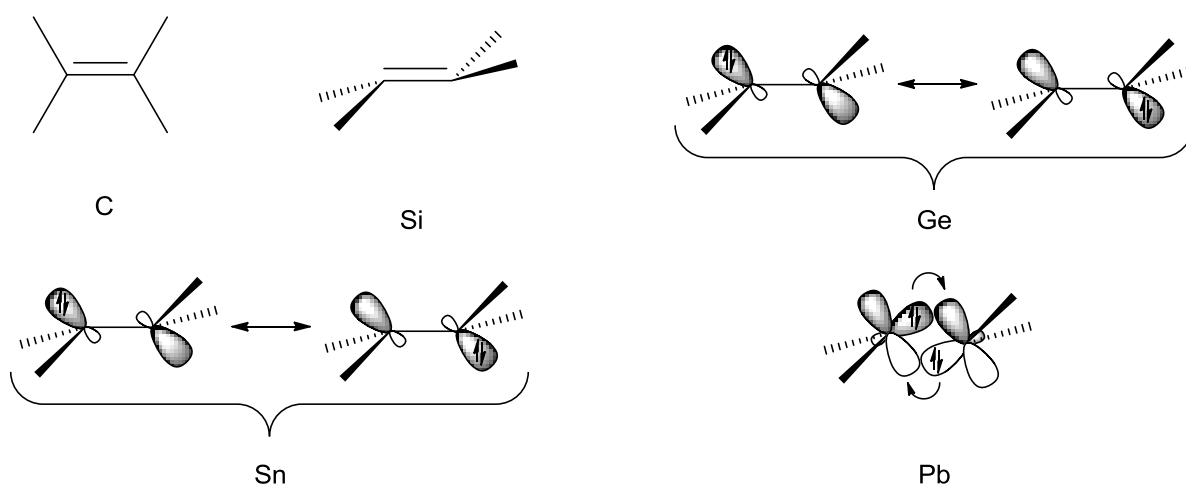
This makes sp hybridization less feasible and leaves the valence s-electrons as a non-reactive lone pair excluded from bonding.⁴¹ To illustrate the consequences of these effects on the structures, Table 2 shows selected properties of the heavy ethylene compounds. Descending group 14 the *trans*-bent character of the structures increases in accordance with a rising lone pair character at the metal atoms. Computations performed on the compounds listed in Table 2 confirm the experimentally observed tendencies. Going from carbon to lead, the increasing *trans*-bent character as well as the weakening of the metal-metal bond are supported by a decreasing σ - and π - interaction.

Table 2. Structural properties of the heavy ethylenes. The very right column contains computed metal-metal interaction energies.

Dimetallene	M–M [pm]	M–M–C bent angle [°]	σ/π Interaction
			energies ⁴² [kcal/mol]
C=C	134.0 ²⁶	0.0	81/62
Si=Si*	214.4 ⁴³	3.0	47/28
Ge=Ge*	234.7 ^{31b, 38}	32.0	39/26
Sn=Sn*	276.8 ^{31b}	41.0	35/11
Pb=Pb*	412.9 ^{39a}	34.2	23/--

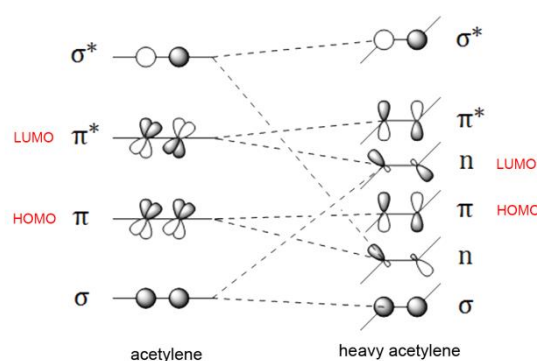
* The selected heavy group 14 metallenes with the exception of silicon consist of the same ligand, namely the CH(SiMe₃)₂ ligand. The disilene is stabilized by the 2,4,6-triisopropylphenyl (Trip) ligand.

The local geometry at the metal atoms can further be influenced by the bulkiness of the alkyl groups. With a bulky substituent, a slightly higher *trans*-bent character is observed as these substituents show an increased interference with increasing ligand bulkiness. Remarkably, the metal-metal bond lengths do not correlate with their bond strength.⁴⁴ The distannene with a tin-tin distance identical to a Sn-Sn single bond has a rather small bond enthalpy compared to reported single bond strengths.⁴⁵ Consequently, for tin and especially lead, the metal-metal bond is rather a donor-acceptor interaction than a covalent bond (Scheme 11).



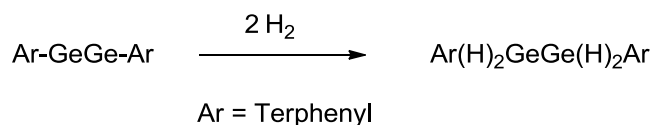
Scheme 11. Weakening of the double bond character in heavy ethylenes, descending group 14. The orbitals are taken from Scheme 9 (left) and visualize the increasing lone pair character descending group 14.

Soon after the preparation of the heavy ethylenes the analogous acetylenes were synthesized. The corresponding compounds were prepared in 2000 (Pb, *Power et al.*),⁴⁶ 2002 (Ge, *Power et al.*),⁴⁷ 2002 (Sn, *Power et al.*)⁴⁸ and 2004 (Si, *Sekiguchi et al.*)⁴⁹ and they resemble the geometry of the ethylenes. However, they contain a fundamental difference. As schematically depicted in Scheme 12, the HOMO-LUMO gap decreases in the heavy acetylenes as the σ - π^* mixing increases. The former π - π^* gap in acetylene is narrowed as the non-bonding orbital, resulting from the mixing of the σ - and π^* -orbitals, is lowered in energy compared to the π^* -orbital. Energetically close lying frontier orbitals were unknown for main group elements until the preparation of the first stable heavy acetylenes and founded a new field of research in inorganic chemistry. Further



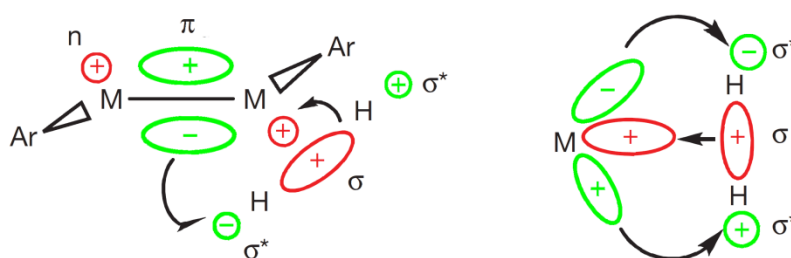
Scheme 12. Molecular orbital diagram of acetylene and its heavier analogues.

research based on the tin and especially the germanium acetylenes as well as intense studies on their molecular orbitals revealed a similar frontier orbital situation than observed for transition metal complexes. This feature provides reactivity of the main group compounds towards small molecules like hydrogen and ethylene which, until recently, was an exclusive property of transition metal complexes.⁵⁰



Scheme 13. Reaction of a digermine with two equivalents of hydrogen.

However, after the preparation of the digermine it took until 2005 when *Power et al.* described the stepwise oxidative addition of hydrogen to digermine (Scheme 13).⁵¹ *Schnöckel et al.* computed earlier that the hydrogenation reaction of HGeGeH to give H_2GeGeH_2 is highly exothermic ($\Delta H_R = -250 \text{ kJ/mol}$),⁵² and the publication of *Power et al.* gave the experimental evidence for the computational results which displayed a breakthrough in the activation of small molecules by main group compounds. For this kind of reaction, it is vital that the energy gap between the involved frontier orbitals (π and n) does not exceed 4 eV,³⁶ meaning a rather narrow energy separation of HOMO and LUMO. According to *Power et al.* this frontier orbital situation can be described as quasi-open shell.⁵³



Scheme 14. Orbital interaction of heavy acetylenes (left) and transition metal complexes (right) with hydrogen.³⁶

Scheme 14 depicts the corresponding orbital interaction of a heavy group 14 acetylene species with hydrogen. The π -orbital of the acetylene species (HOMO) attacks the σ^* -orbital of the hydrogen molecule, whereas the σ -orbital of hydrogen attacks the non-bonding orbital (LUMO) at the heavy acetylene, resulting in an oxidative addition of hydrogen.⁵⁴ For comparison, the transition metal interacts with hydrogen in a similar way, using the set of d-orbitals.

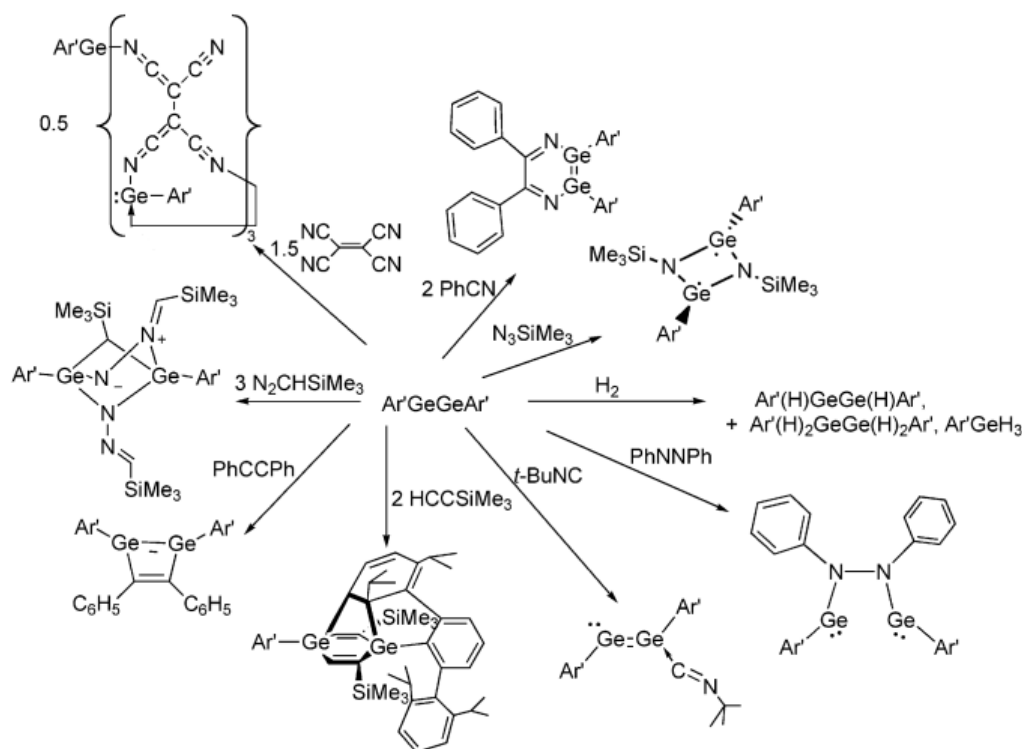
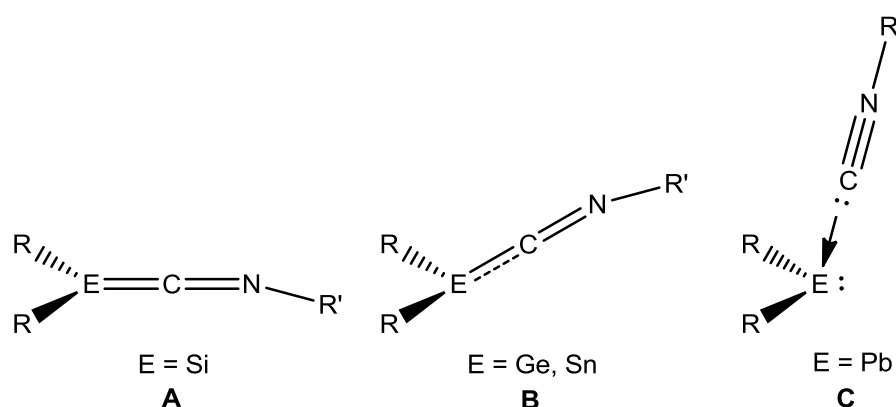


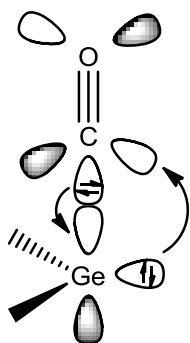
Figure 2. Reactivity of digermynes towards a range of small molecules.⁵¹

In the following years, research in the area of small molecule activation by main group compounds was ramped up⁵⁵ due to the discovery of *Power et al.* Another landmark in the area of small molecule activation was published in 2007 by *Bertrand et al.* They described the activation of hydrogen using carbenes,⁵⁶ resurrecting a species, first discovered in 1974,³¹ the metallocenes. Their name is derived from the carbene which describes a divalent carbon species, the methylene (CR_2). Most of the reported metallocenes carry two bulky substituents to prevent dimerization to the dimetallenes. The reactivity of the metallocenes was not realized by *Lappert* and co-workers in the 70s. They simply described a kind of *Lewis-acid/Lewis-base* interaction with solvents leading to dissociation of the desired dimetallenes as mentioned earlier in this chapter. However, they consist of high potential in the activation of small molecules as well as C–H and N–H bond activation. With an empty p-orbital and a sp^2 -type lone pair, they contain the properties of the *Frustrated Lewis Pairs*⁵⁷ at a single atom (Scheme 8). Their reactivity is best described by *Power et al.* within the related germylene-isocyanide complexes (Scheme 15).^{58,59}



Scheme 15. Different types of metalylene isocyanide interaction.

The E–C single bond (σ -bond) is formed by the interaction of the isocyanide lone pair with the empty p-orbital at the metalylene. The corresponding π -bond results from π -back donation from the metal centered sp^2 lone pair into the C–N π^* -orbital (Scheme 16).



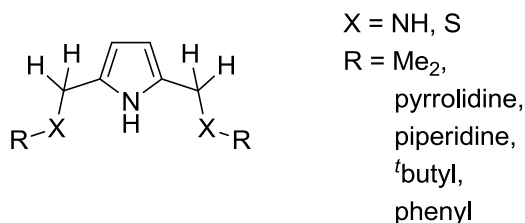
Scheme 16. Orbital interaction in a germylene-carbon monoxide complex.

Silicon is interacting strongly with the isocyanide, tending to form heterocumulenes (**A**).⁶⁰ The opposite is displayed by the plumbylenes. They weakly interact with a coordinated isocyanide, forming *Lewis-base* adducts (**C**).⁶¹ The germylenes^{58,59} and stannylenes^{59,61,62} are in-between, with germanium forming stronger E=C bonds than tin. Theoretical investigations conducted by *Power et al.* confirm these assumptions by determining the amount of π -interaction energy in a range of hypothetical metalylene-isocyanide model complexes (Si, Ge and Sn).⁵⁹ It turned out that the amount of π -

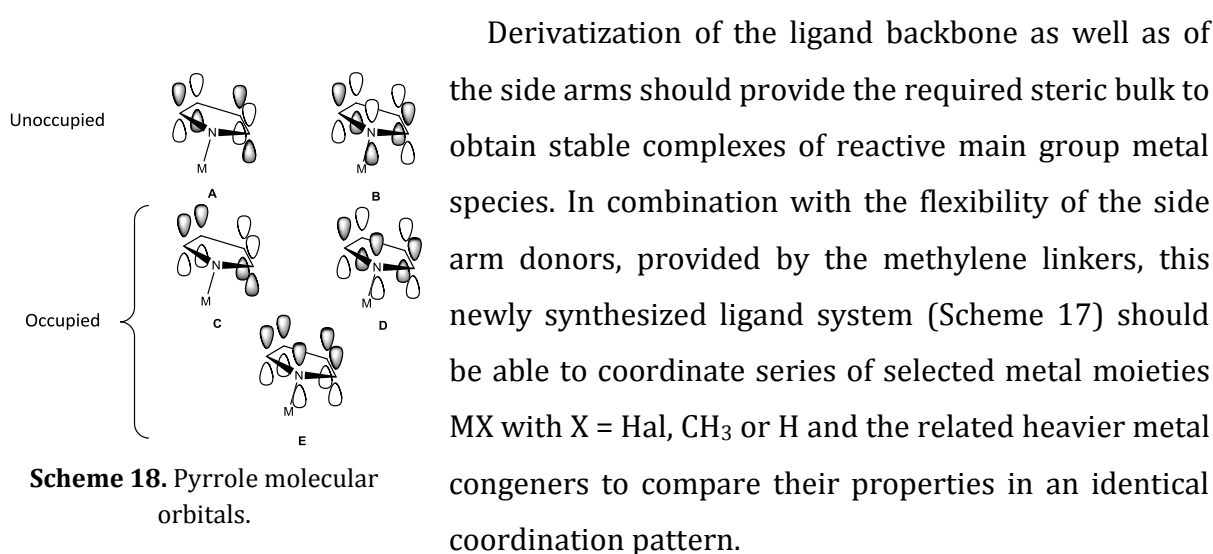
interaction decreases strongly going from silicon to germanium and further decays descending group 14. Besides the isocyanide model complexes, many other small molecules have been used for bond activation reactions (Scheme 16) such as carbon monoxide,⁶³ ammonia⁶⁴ and hydrazine⁶⁵ to name selected examples that emphasize the synthetic potential of the group 14 metalylenes.

2 Scope

This thesis is based on the work accomplished during my diploma thesis,⁶⁶ in which the pyrrole based pincer ligand was proven to be feasible for the coordination of main group metals.



Scheme 17. Variations of the pyrrole based ligand used within this thesis.



Scheme 18. Pyrrole molecular orbitals.

As the pyrrole backbone seems to be well suited to analyze the metal-ligand interactions inferences should be drawn from the observed bond length within the heterocycle about the nature of the metal ligand interaction (Scheme 18). To guarantee a high accuracy high quality single crystals are required and the resulting X-ray diffraction datasets should have a fairly high resolution of $2\theta \geq 60^\circ$ (Mo- $K\alpha$) (Figure 3).

To verify the assumptions made from the C-C bond lengths of the pyrrole heterocycle the molecular orbitals of the specific compound should be computed. For selected complexes, high level computations were conducted to gain a detailed insight into the ligand-metal interaction.

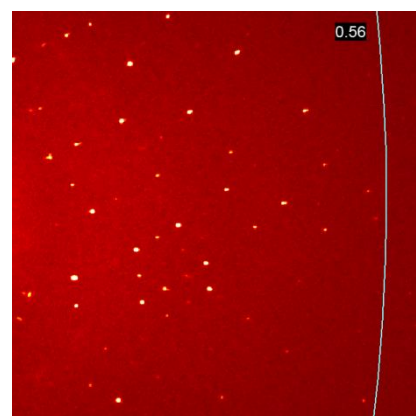


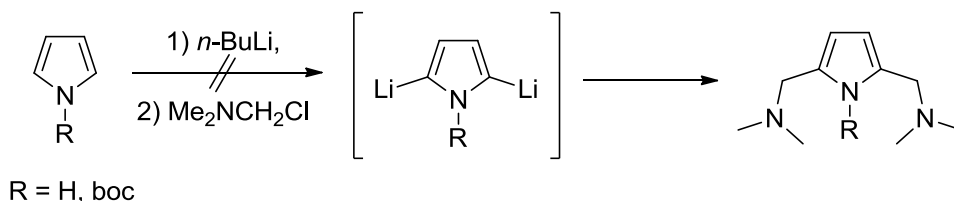
Figure 3. High resolution diffraction pattern up to $2\theta = 78.8^\circ$ recorded of a single crystal of compound **11**, *vide infra*.

3 Results and Discussion

3.1 The pyrrole based pincer ligand

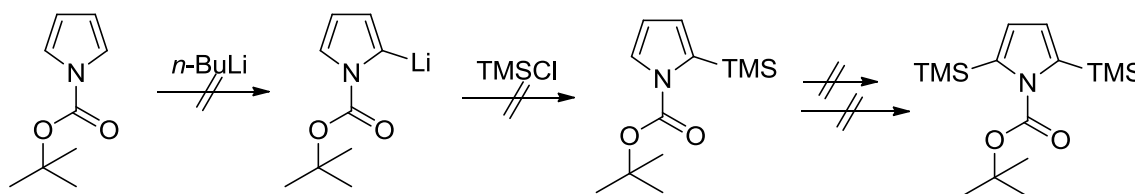
For the synthesis of the pyrrole based pincer ligand, there is a wide range of possible routes, yielding the desired product.

The most intuitive way is the direct lithiation of pyrrole in 2- and 5-position with *n*-butyllithium, followed by substitution with an electrophile (e.g. α -chloro-amine) (Scheme 19). This double lithiation is known for thiophene⁶⁷ but is not feasible for pyrrole due to the acidic NH proton (pK_a : 17.8)²⁷ which would be deprotonated at first. For that reason, *N*-boc protected pyrrole was used for the direct lithiation. Besides the protection of the amine functionality, it bears another useful effect. The carbonyl oxygen atom serves for precoordination of the lithium organic compound, ending up in the *ortho*-metallated species (directed *ortho* metallation).⁶⁸



Scheme 19. Double lithiation of pyrrole followed by electrophilic substitution.

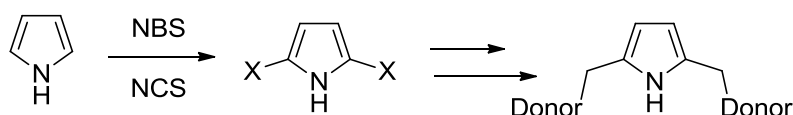
However, the double lithiation of an electron rich system like pyrrole is awkward, due to rapid decomposition into an insoluble brownish tar under any condition. The stepwise lithiation seems to be more promising. Chlorotrimethylsilane was used to protect the carbanion in the second lithiation step. The target compound was 2,5-bis(trimethylsilyl)-*N*-boc-pyrrole but the synthesis failed due to instability of the desired molecule (Scheme 20).



Scheme 20. Stepwise lithiation of *N*-boc-pyrrole

A possible reason for the decomposition is the labile pyrrole-TMS bond. On the one hand, it makes it easy to remove the protecting group on the other hand it enables the molecule for polymerization/decomposition as well.

Because of the difficulties occurring with the deprotonation in 2- and 5-position of pyrrole another pathway for further functionalization was developed. Radical halogenation, as it is known for the group 16 analogues of pyrrole,⁶⁹ using *N*-bromosuccinimide (NBS) or the corresponding chlorine derivative NCS should yield the 2,5-bis-halogenopyrrole (Scheme 21). These electron withdrawing substituents should reduce the electron density within the heterocycle and provide sufficient stability to purify the halogenated pyrrole.

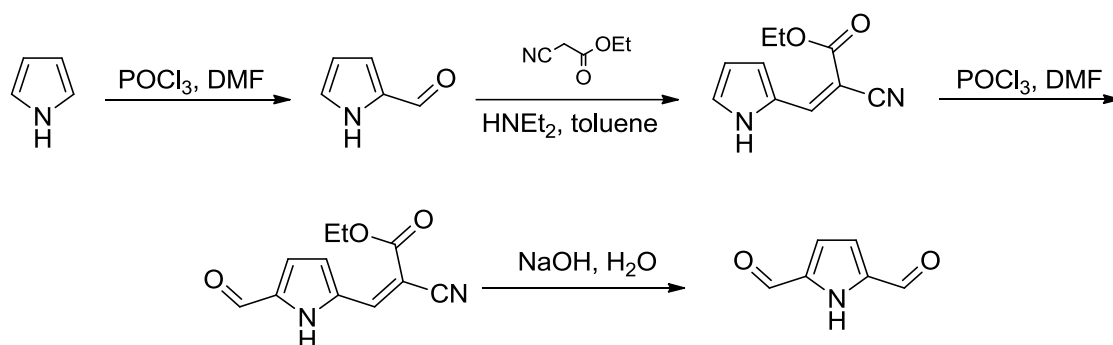


Scheme 21. Functionalization of pyrrole via radical reaction halogenation.

Various attempts were conducted to purify the halogenated compound but it decomposed readily upon warming it up to room temperature. Another approach published by *Gilow* describes the use of the crude 2,5-dibromopyrrole without any purification directly below $-30\text{ }^{\circ}\text{C}$.⁷⁰ However, none of the used *C*-nucleophiles yielded the desired 2,5-disubstituted pyrrole species. Instead, the blue solution of the 2,5-dibromopyrrole turned into a brownish black tar after addition of a nucleophile. The only species that could ever be verified to be in the solution by doing ^1H -NMR spectroscopy was the 2,5-dibromopyrrole.

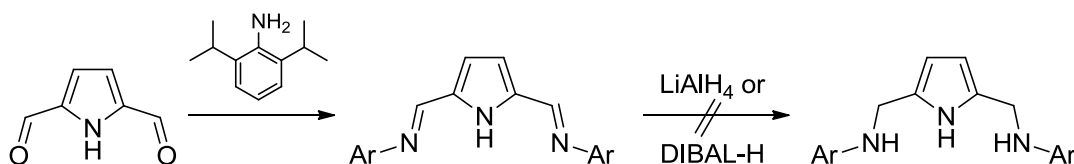
These examples display the lability of 2,5-hetero-substituted pyrroles and it was refrained from using them as intermediates on the way to synthesize the desired ligand.

A very promising synthetic pathway was reported by *Knizhnikov et al.*,⁷¹ describing a ligand synthesis with pyrrole-2,5-dicarbaldehyde as key intermediate (Scheme 22).



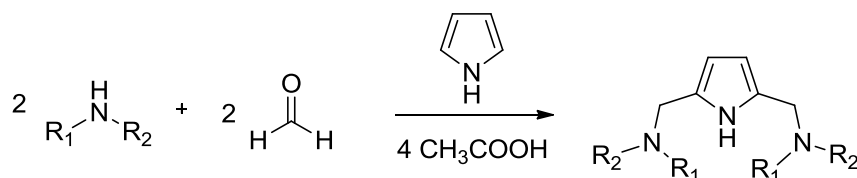
Scheme 22. Synthesis of pyrrole-2,5-dicarbaldehyde according to *Knizhnikov et al.*

The pyrrole-2,5-dicarbaldehyde could be prepared in really good yields and the preparation of the ligand precursor was already known and published by *Roesky et al.*⁷² However, in the last step, the attempted reduction of the C=N double bonds, to form flexible methylene linker moieties failed (Scheme 23). There could not even traces of the desired product be detected in the NMR-spectra.



Scheme 23. Reaction of pyrrole-2,5-dicarbaldehyde with a substituted aniline and the subsequently attempted reduction.

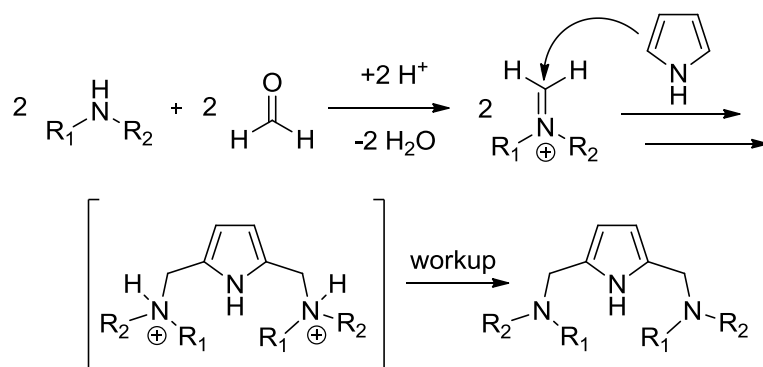
Finally, the most promising approach is to synthesize the ligand in a one-step synthesis making use of the *Mannich* reaction.⁷³ The procedure, reported earlier by *Elsenbaumer et al.*⁷⁴ was modified within this work to obtain highly pure product suitable for metallation reactions. However, this method is limited to primary or secondary amines that do not carry tertiary or quaternary carbon atoms in α -position due to their limited nucleophilicity (e.g. diisopropylamine) (Scheme 24).



Scheme 24. Synthesis of the pyrrole based pincer ligand via *Mannich* reaction.

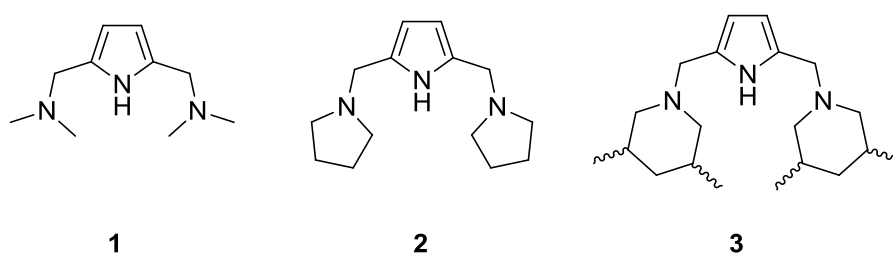
Under acidic conditions with a pH-value around four like in the *Mannich* reaction, the polymerization of pyrrole is faster than the reaction of pyrrole with a sterically hindered *Mannich* base. This polymerization can be controlled by temperature, but cooling is

limited to the melting point of the reaction mixture which is slightly below 0 °C, depending on the used amine. The bulkier the amine, the slower is the product formation and the more favored is the pyrrole-polymerization. Other reaction modifications like the use of a solvent or the use of less acid failed. It turned out that two equivalents of acid are essential for the reaction, otherwise the yield of the desired compound drops down and significant amounts of the mono-substituted pyrrole are detected. The need of two equivalents of acid can be explained by Scheme 25. Two protons are consumed by each product molecule which, under aqueous conditions, is present as a bis-ammonium ion in solution. Consequently, for the elimination of water in the first step, an external proton source like acetic acid is necessary.



Scheme 25. Consumption of protons in the *Mannich* reaction for the synthesis of pyrrole based {*NNN*}-pincer ligands.

Following this procedure, 2,5-bis((dimethylamino)methyl)pyrrole (**1**), 2,5-bis((pyrrolidino)methyl)pyrrole (**2**) and 2,5-bis((3,5-dimethylpiperidino)methyl)pyrrole (**3**) were successfully prepared.



Scheme 26. {*NNN*}-Pincer ligands prepared within this work.

Molecule **1** has been prepared earlier by *Elsenbaumer et al.* in 1998⁷⁴ but with the exception of a few metal complexes containing **1** the flexible type of the pyrrole based pincer ligand is not present in literature.^{11,75,76,77} The investigation of **1** was already object of my diploma thesis. It turned out that this type of ligand is perfectly suited for

metal complexation. The methylene moieties provide the flexibility needed for the coordination of different metal ions with large size distribution. Additionally, the electron rich pyrrole π -system strongly interacts with *Lewis*-acidic metal ions, yielding highly stable chelate complexes. Furthermore, the pyrrole heteroaromatic system appeared to be feasible for analyzing the pyrrole-metal interaction by investigating changes in bond lengths within the pyrrole ring (chapter 1.2).

The free ligands **1** and **2** show a solid state structure dominated by hydrogen bondings which is underlined by the absence of disorder within these molecules and the rapid formation of high quality single crystals. The following chapters will provide an insight into the properties of the free ligands and their intermolecular interactions, mainly derived from the obtained X-ray diffraction data.

3.1.1 2,5-Bis((dimethylamino)methyl)pyrrole (**1**)

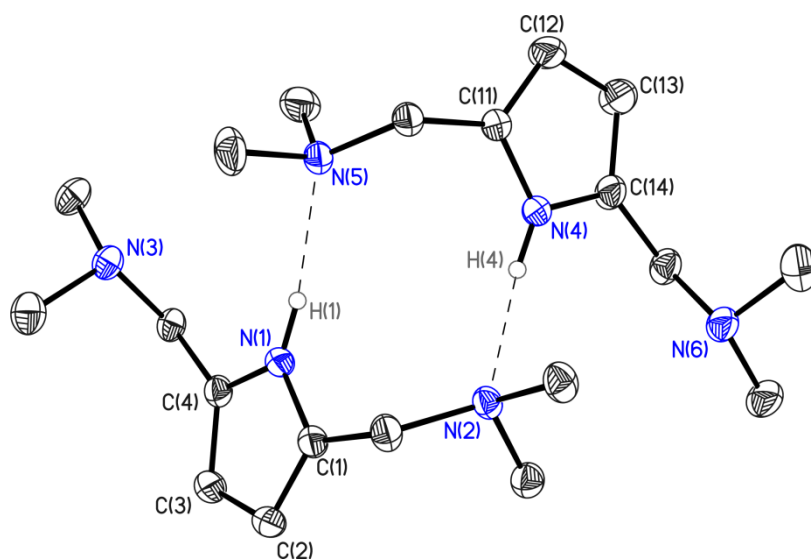


Figure 4. Crystal structure of 2,5-bis((dimethylamino)methyl)pyrrole (**1**). Thermal ellipsoids are depicted at the 50% probability level. Hydrogen atoms, besides H1 and H4, which have been freely refined, are omitted for clarity.

The crystal structure of **1**, obtained already in my diploma thesis, is shown for the sake of completeness within the series of the free ligands. It crystallizes in the monoclinic space group $P2_1/n$ enclosing two molecules in the asymmetric unit which

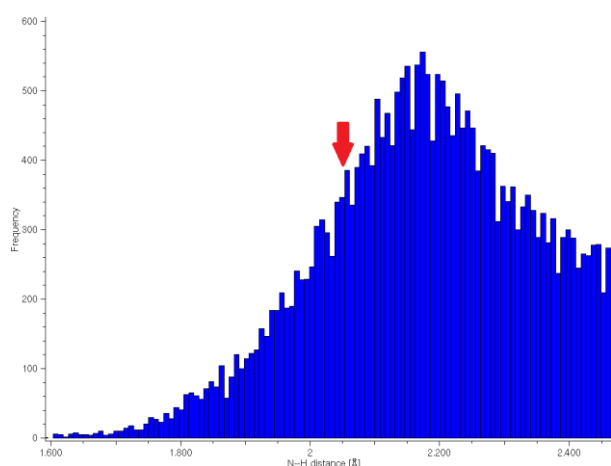


Figure 5. Bond distances of all intermolecular N...H...N interactions contained in the CSD.

are linked to dimers by hydrogen bondings. With lengths of 205.1 pm (H1–N5) and 210.2 pm (H4–N2) they are among the strongest hydrogen bondings found in the entire family of pyrrole based pincer ligands. Within the intermolecular N...H–N contacts contained in the Cambridge Structural Database (CSD),

they are considered to be rather short (Figure 5). Although the dimeric appearance seems to be quite rigid, it has to be monomeric in solution. Otherwise, the NH protons are encapsulated and do not take part in a deprotonation reaction, in particular not with a large base like lithium(bis-(trimethylsilyl)amide) (Li(hmds)). The room temperature ^1H -NMR spectrum of **1** shows a symmetric behavior of both side arms, hence indicating a monomer. Furthermore, it shows a doublet for the two pyrrole CH protons (Figure 6, left). This results from a 4J -coupling to the NH-proton of 2.6 Hz and can be used as an indicator for N-metallation. In the absence of the NH proton, the doublet is converted

into a singlet. This observation is unknown for unsubstituted pyrrole because of a superimposing 3J - and 4J -coupling (4.3 Hz and 2.2 Hz) between the protons in 3- and 4-position (former doublet) and the protons in 2- and 5-position (Figure 6, right).

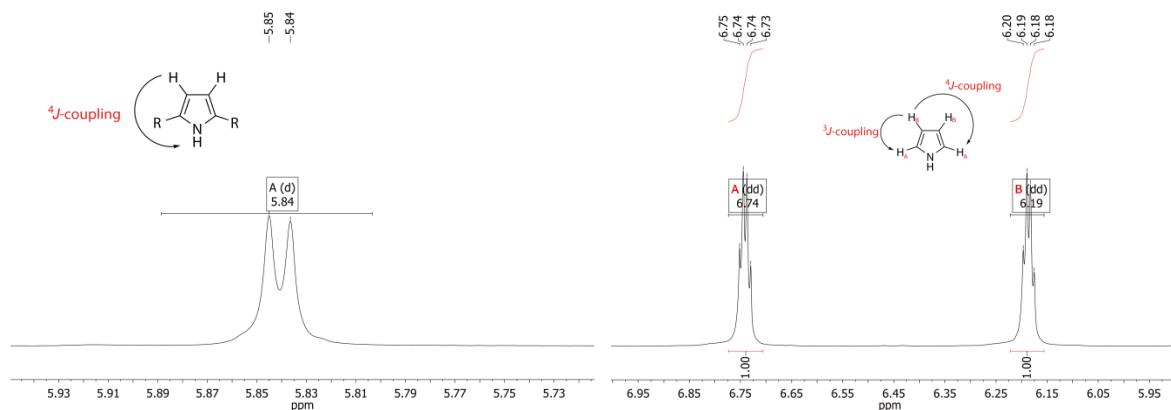


Figure 6. Left: Section out of the ^1H -NMR spectrum of **1**, showing the signal for the protons in 3- and 4-position of pyrrole. Right: ^1H -NMR signals of the protons in 3- and 4-position in free pyrrole.

The bond lengths within the pyrrole heterocycle (Table 3) indicate an intact aromatic system, the single bond length is 142.00(16) pm and the average double bond length is 137.20(15) pm. The resulting difference ($\Delta_{\text{SB-DB}}$) of 5.2 pm can be used as reference for investigating the metal–ligand bonding situation within metal complexes of **1** using the orbital scheme depicted in Scheme 6. However, this number can be misleading because the N–H bond has a dominant covalent character which addresses different molecular orbitals of the heterocyclic system compared to main-group metal complexes which form in principal less covalent bonds. Consequently, for comparability reasons, the lithium pyrrolide, which will be described in chapter 3.2, is used as reference compound.

3.1.2 2,5-Bis-((pyrrolidino)methyl)pyrrole (**2**)

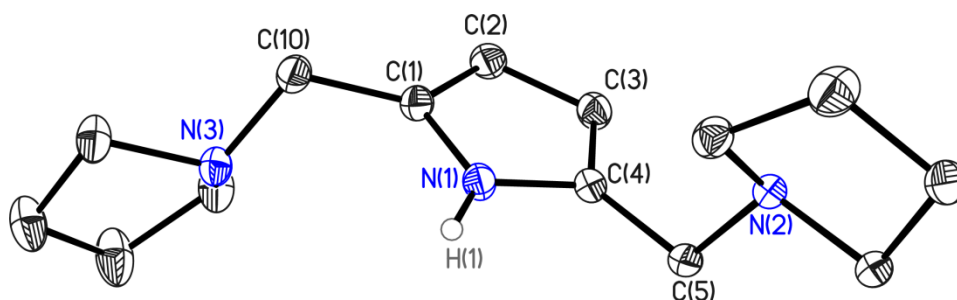


Figure 7. Crystal structure of 2,5-bis((pyrrolidino)methyl)pyrrole (**2**). Thermal ellipsoids are depicted at the 50% probability level. Hydrogen atoms, besides H1 which was freely refined, are omitted for clarity.

Although the crystal structure of **2** is already known and published in the Cambridge Structural Database (CSD),⁷⁸ it is included within this thesis, because the published structure does not fulfill our internal crystallography quality standards by far. When discussing bond lengths, it is fundamental to have minimized standard deviations

resulting from high quality data sets. This is why a new high quality data set of **2** was collected in order to establish reliable bond lengths as a benchmark.

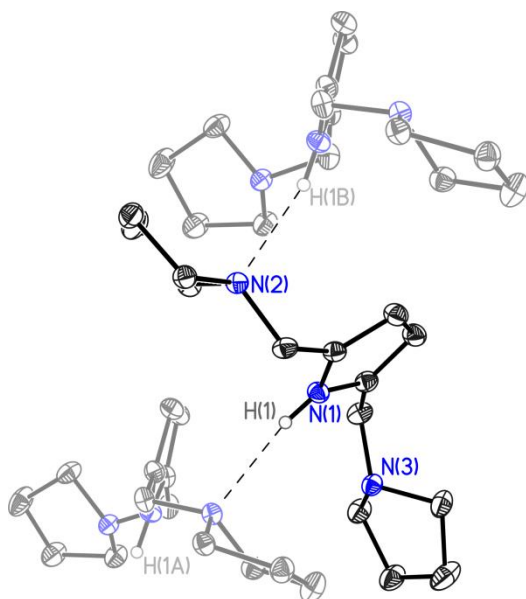


Figure 8. Oligomerization of **2** via hydrogen bonding.

Compound **2** crystallizes in the orthorhombic space group *Pbca*, including one molecule in the asymmetric unit. The asymmetric units are linked by hydrogen bondings between H1 and N2 of a neighboring molecule, forming linear oligomers. The hydrogen bonding is significantly longer than those in **1**, being 226.3 pm long. The larger pyrrolidine groups induce steric strain which leads to separation of both ligands with

respect to **1** and therewith elongation of the hydrogen bonding. Hence it is not surprising that the monomeric form of **2** is present in solution. The less rigid surrounding in solution allows a flipping of the envelope structure of the pyrrolidine moieties, displayed by broadened signals in the ¹H-NMR spectrum.

Table 3. Selected bond lengths of the free ligand structures **1** and **2**. Those marked with an asterisk are the average bond lengths of the equivalent bonds in the dimer depicted in Figure 4.

Bond lengths [pm]	1	2
C1–C2	137.07(14)*	137.69(15)
C2–C3	142.00(16)*	141.98(15)
C3–C4	137.33(15)*	137.46(15)
N1–H1	90.5(14)/89.2(14)	85.2(17)
N–H...N (1)	205.1	226.3
N–H...N (2)	210.2	---

Table 3 illustrates the electron withdrawing effect of the pyrrole bonded substituent perfectly. In **1** there are rather strong hydrogen bondings present and thus the corresponding pyrrole N–H bond is weaker than in **2**, where the hydrogen bond is considerably longer. The stronger pyrrole N–H bond in **2** withdraws more electron density from the heterocycle than that in **1**. Consequently, the C1–C2 and C3–C4 bonds are elongated going from **1** to **2**.

3.1.3 2,5-bis((3,5-dimethylpiperidino)methyl)pyrrole (**3**)

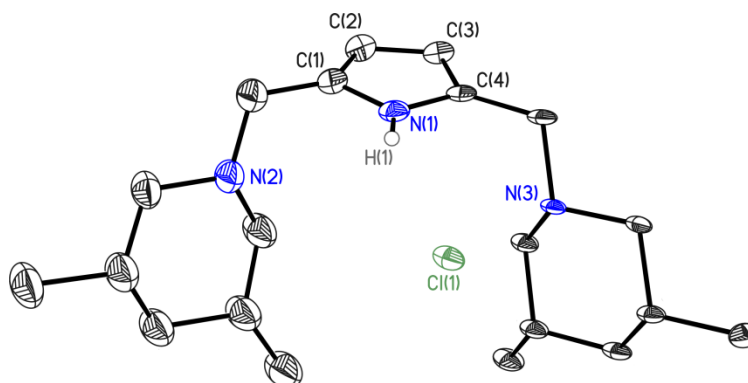
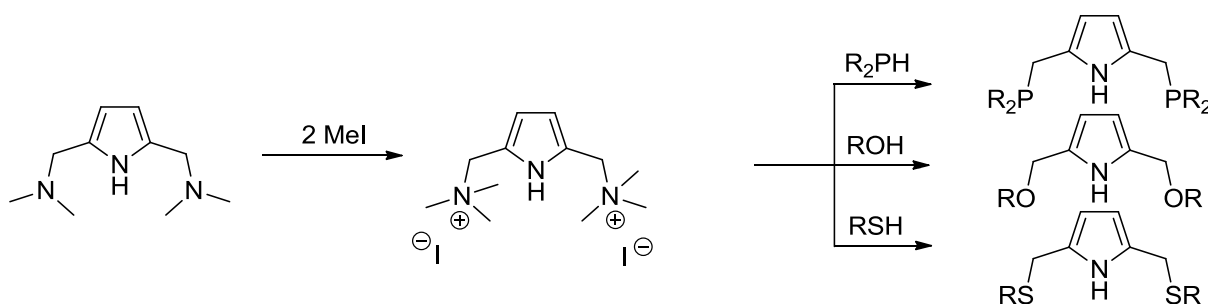


Figure 9. Crystal structure of 2,5-bis((3,5-dimethylpiperidino)methyl)pyrrole (**3**). Thermal ellipsoids are depicted at the 10% probability level. Hydrogen atoms, besides H1, are omitted for clarity.

Compound **3** does not crystallize in a similar arrangement like **1** and **2**. The piperidine moieties appear to be too bulky to generate a similar hydrogen bonding situation. Lacking this structure determining factor the piperidine fragments with its methyl groups in 3- and 5-position are too flexible to crystallize in a sufficiently short period of time. The addition of one equivalent of acid finally led to crystallization of the hydrochloride adduct of **3** after one year. It does not comprise any hydrogen bondings. The charge introduced by the acid apparently provides an ordering effect that slightly overcomes the flexibility and leads to crystallization. Nonetheless, the data quality is rather poor and consequently the bond lengths and angles of **3** are not discussed.

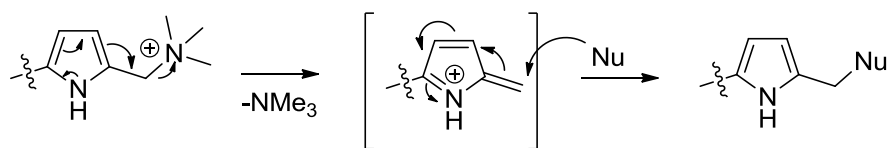
3.1.4 Ligand derivatization

Within the compounds **1**, **2** and **3**, **1** is superior, serving as key intermediate for the substitution of the nitrogen donor atoms. By addition of two equivalents of iodomethane the bis-ammoniumsalt is prepared which evolves trimethylamine when treated with a nucleophile. Using *P*-, *O*- and *S*-nucleophiles the {*NNN*} chelating ligand can be converted into a {*PNP*}, {*ONO*} or {*SNS*} pincer ligand system (Scheme 27). This variation of donor atoms increases the variety of possible target metals either to harder ({*ONO*}) or to softer metals ({*PNP*} and {*SNS*}). However, the method is limited to highly nucleophilic and non-basic substrates.



Scheme 27. Synthesis of {*PNP*}-, {*ONO*}- and {*SNS*}-pincer ligands.

With a rather weak base like a sodium thiolate, the reaction follows a S_N2 mechanism with participation of the neighboring aryl (pyrrolyl) group. It is known that substitution reactions at the benzylic position (phenyl) follow the S_N2 mechanism.⁷⁹ Similar assumptions can be made for pyrrole as aryl group. Furthermore it should be even more activated due to the stabilization of the intermediate (Scheme 28).



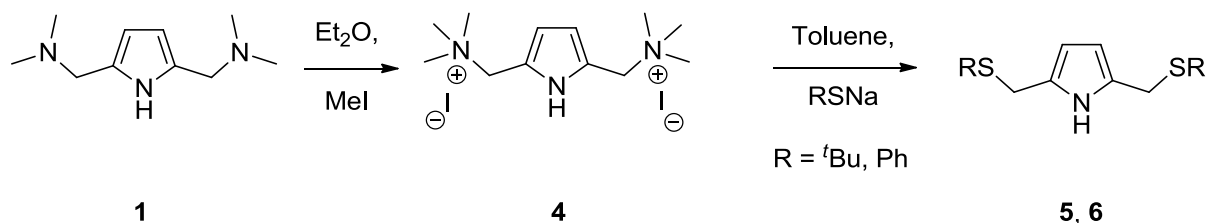
Scheme 28. Mechanism of the S_N2 reaction with the neighboring group effect of pyrrole.

If the nucleophile is basic enough to deprotonate the pyrrole amine, the heterocycle becomes highly electron rich causing a very dominant neighboring group effect. The addition of the former pyrrole N–H proton to the nucleophile weakens its nucleophilicity and the intermediate decomposes to unidentifiable products. The use of four equivalents of nucleophile, two as base for the deprotonation and the remaining two equivalents for

the nucleophilic attack does not show any improvement of the reaction. The intermediate then decomposes in an unknown pathway to an unidentifiable black tar.

3.1.5 {SNS}-Pyrrole based pincer ligand

The {SNS}-pyrrole based pincer ligands were prepared following the procedure explained in chapter 3.1.4 and summarized in Scheme 29.



Scheme 29. Synthesis of the {SNS}-pyrrole based pincer ligands.

3.1.5.1 2,5-Bis((*tert*butyl-thiolato)methyl)pyrrole (5)

5 has been prepared following Scheme 29 and was obtained as a yellow oil. Unfortunately it was impossible to obtain single crystals of **5**, thus its presence was proven by NMR-spectroscopy. The ^1H -NMR spectrum is very much alike the related free ligand species. **5** was used within this thesis for the synthesis of complexes with rather soft late transition metals.

3.1.5.2 2,5-Bis((thiophenolato)methyl)pyrrole (6)

6 has been prepared along a protocol similar to **5**. After recrystallization, single crystals suitable for X-ray diffraction experiments were obtained.

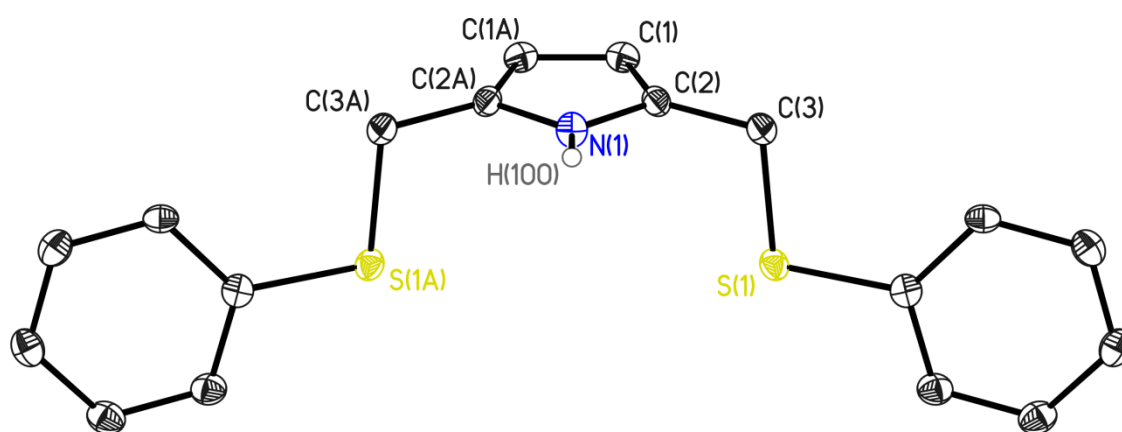


Figure 10. Crystal structure of 2,5-bis((thiophenolato)methyl)pyrrole (**6**). Thermal ellipsoids are depicted at the 50% probability level. Hydrogen atoms, besides H100, which was freely refined, are omitted for clarity.

6 crystallizes in the orthorhombic space group *Pnma* with half a molecule in the asymmetric unit. The molecule is completed by a mirror plane going through N1 and H100, being perpendicular to the heterocyclic plane. **6** seems to be perfectly suited as a

reference for the protonated pyrrole based pincer ligand system, as there are no hydrogen bondings present, which could vitiate the resulting C–C bond length of the pyrrole heterocycle.

A very useful tool to detect these weak interactions is the *CrystalExplorer*⁸⁰ program. Starting from a cif file, it calculates the promolecule density of the selected compound. The resulting output is a surface which includes the space that is dominated (>0.5) by the electron density of the selected molecule. The intermolecular close contacts can be mapped onto this surface by taking the distance of the enclosed atoms to the surface (d_i), the distance of the external atoms to the surface (d_e) and the van der Waals radii of the involved atoms into account (Equation 1). The resulting value is the normalized distance d_{norm} describing the distance of an atom inside the surface from an atom outside the surface normalized to their van der Waals radii.⁸¹

$$d_{\text{norm}} = \frac{d_i - r_i^{\text{vdW}}}{r_i^{\text{vdW}}} + \frac{d_e - r_e^{\text{vdW}}}{r_e^{\text{vdW}}}$$

Equation 1. The normalized contact distance.

The d_{norm} value is calculated for each pixel of the surface, negative values are labeled in red (indicating a possible close contact), positive values are labeled in blue. The resulting colored surface is named the *Hirshfeld* surface⁸² and is a powerful tool to detect intermolecular interactions within a crystal structure.

A closer investigation of the crystal structure of compound **6** using the *Hirshfeld* surface tool within the *Crystal Explorer*⁸⁰ program revealed a η^5 -N–H– π interaction that can be considered rather strong (Figure 11). The bond lengths and angles at H100 hint to the strength of this interaction. A CSD search for hydrogen–centroid distances to pyrrole and cyclopentadienide between 100 pm and 400 pm yielded a mean value of 353 pm, with the shortest distance being 240 pm⁸³ long. With a hydrogen– π -system distance of only 244(4) pm, a H–centroid distance of 248 pm and an N–H–centroid angle of 173.3° the N–H– π interaction in **6** is among the strongest reported in the CSD until today.

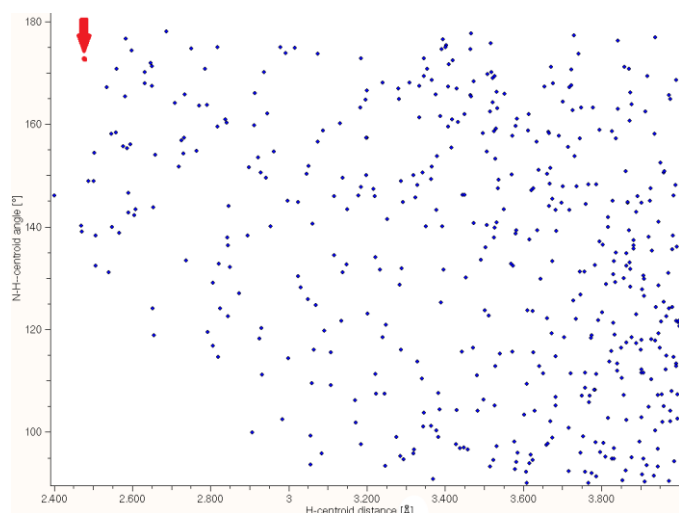


Figure 12. Results of a CSD search for N-H... π interactions. X-axis: H-centroid distance [pm]; Y-axis: N-H...centroid angle [°].

Theoretical calculations rank N-H- π interactions as being between 0.7 kcal/mol and 17.3 kcal/mol (hypothetical alanine-benzene interaction).⁸⁴ However, *Mohan et al.* recognized a strong dependency on the N-H polarization. The values for protonated alanine vary between 10.7 kcal/mol and 17.3 kcal/mol, whereas the range for neutral alanine is given by 0.7 kcal/mol and 4.7 kcal/mol. Similar observations

were made by *Tsuzuki et al.*, showing that substituted methyl moieties have higher C-H- π interaction energies than methane.⁸⁵ Furthermore, he stated that the interaction energy is orientation dependent, with the maximum interaction energy at a donor-H-acceptor angle of 180°. ⁸⁶ With an angle close to the ideal 180°, and the short hydrogen- π -plane distance in combination with the rather acidic pyrrole N-H proton, the N-H- π interaction found in **6** is considered to be among the strongest present in literature until today (Figure 12). According to *Mohan et al.* the interaction is worth between 5 kcal/mol and 10 kcal/mol, which is a wide range, however, these values strongly depend on the

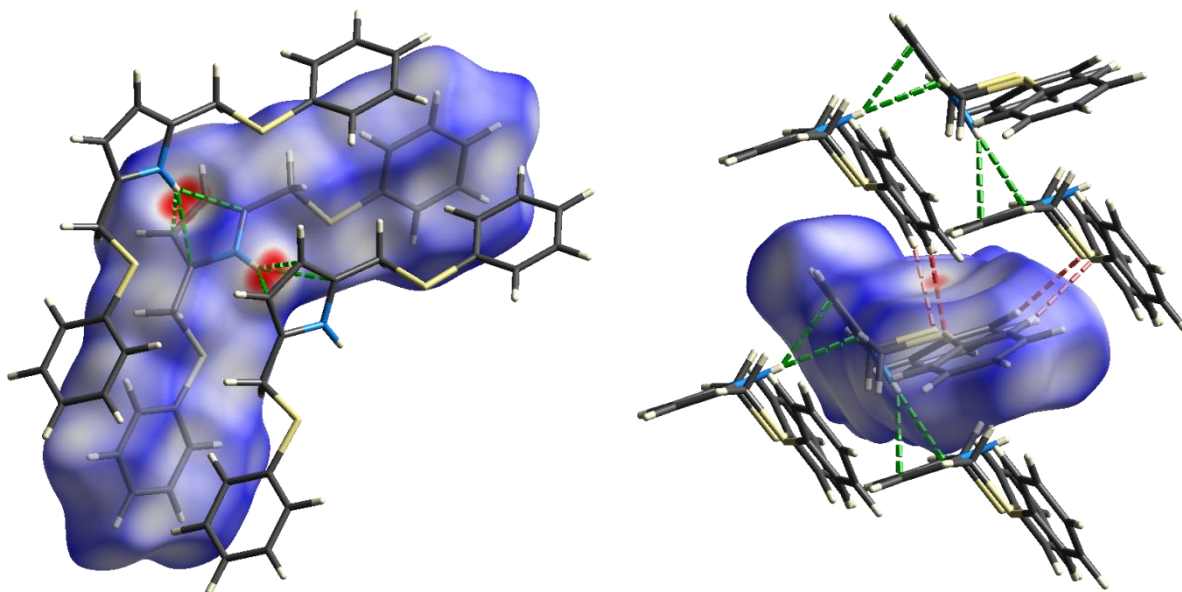


Figure 11. Hirshfeld surfaces for compound **6**. Left: N-H- π interaction forming a chain like arrangement (green dashed lines). Right: Interconnection of these chains (red dashed lines) via Ph-H-S interaction.

used computational method and rather precise determinations of non-covalent interactions are associated with an enormous computational effort.⁸⁴

This interaction can be regarded as structure determining effect as selected molecules arrange themselves to chains via this N-H- π interaction. The planes of the respective pyrrole heterocycles are tilted within a chain by 66.6(3)°. These chains are further connected by phenyl-H-S interactions forming a two-dimensional network in the crystal. The hydrogen-sulfur distance is 288.0 pm long and the C-H...S angle measures 165.9°.

3.1.6 General remarks on the computational methods

There are in principle two different approaches used in this thesis to compute the desired parameters like the molecular orbitals of a selected compound. A very convenient tool to access the electronic structure of a molecule is to make use of the *Hartree-Fock* (HF) approximation.⁸⁷ It is based on the quantum mechanics and computes the energy for every single electron (i) of a given system. Equation 2 summarizes the single contributions to the energy expectation value (E_{HF}) of a given system. The HF method is non-expensive in computation time and reveals highly accurate results as long as the interactions are of covalent nature. It becomes imprecise when the structure includes non-covalent interactions, as those cannot be taken into account by the used formalism.

The diagram illustrates the decomposition of the Hartree-Fock energy equation into its constituent integrals. At the top, the equation for the expectation value of the Hartree-Fock Hamiltonian is shown:

$$E_{HF} = \langle \Psi^{SD} | \hat{H} | \Psi^{SD} \rangle = V_{NN} + \sum_i^N \langle i | \hat{h} | i \rangle + \frac{1}{2} \sum_i^N \sum_j^N [\langle ii | jj \rangle - \langle ij | ji \rangle]$$

Arrows point from the terms in this equation to boxes below:

- One-electron integrals** points to the term $\sum_i^N \langle i | \hat{h} | i \rangle$.
- Two-electron integrals** points to the term $\frac{1}{2} \sum_i^N \sum_j^N [\langle ii | jj \rangle - \langle ij | ji \rangle]$.

The **One-electron integrals** box is further decomposed into:

- Kinetic energy** points to the $-\frac{1}{2} \nabla^2$ term in the integral $\langle i | \hat{h} | i \rangle = \int \chi_i(x_1) \left[-\frac{1}{2} \nabla^2 - \sum_{A=1}^M \frac{Z_A}{r_{1A}} \right] \chi_i(x_1) dx_1$.
- Electron-nucleus attraction** points to the $-\sum_{A=1}^M \frac{Z_A}{r_{1A}}$ term in the same integral.

The **Two-electron integrals** box is further decomposed into:

- Coulomb-integrals** points to the $\langle ii | jj \rangle = \iint \chi_i(x_1) \chi_i(x_1) \frac{1}{r_{12}} \chi_j(x_2) \chi_j(x_2) dx_1 dx_2$ term.
- Exchange-integrals** points to the $\langle ij | ji \rangle = \iint \chi_i(x_1) \chi_j(x_1) \frac{1}{r_{12}} \chi_j(x_2) \chi_i(x_2) dx_1 dx_2$ term.

Equation 2. Expectation value of the *Hartree-Fock* Hamiltonian and the individual contributions.⁸⁷

Roothaan modified this formalism, to obtain orbital energies instead of electron energies.⁸⁸ His procedure is named the Linear Combination of Atomic Orbitals (LCAO)⁸⁹ and obtains the energy values for the molecular orbitals of the investigated molecule. The accuracy depends on the basis set applied to the HF calculation. A basis set contains the mathematical description of the orbitals for each element. They vary in accuracy and complexity and determine the expense as well as the accuracy of a calculation.

The more accurate, but also more expensive method concerning computation time is the Density Functional Theory (DFT).⁹⁰ It computes the electron density of the investigated molecule which already contains the information about all observable parameters. There are various functionals available to compute the electron density, however, they extremely vary in accuracy. The most frequently used is the B3LYP functional.⁹¹ It produces rather accurate results but is not too expensive in computation time which is, similar to the HF method, depending on the basis set chosen for the computation.

The computational methods used within this thesis are abbreviated as follows: “HF/*basis set*” for a quantum mechanical computation and “*functional/basis set*” for a computation based on the DFT. Quantum mechanical computations were run using the *Crystal Explorer* program⁸⁰ and the DFT calculations were conducted by *D. M. Andrada* and *R. A. Mata*. The software they used will be named when discussing the results of their computations.

3.2 Lithium pyrrolide complexes

For the synthesis of metal complexes it is vital to deprotonate the free ligand. The most feasible pathway would be to use basic metal compounds that deprotonate and metallate in one step such as trimethylaluminium. However, these compounds are available only for selected metals and an application can be problematic due to solubility problems. Thus, *n*-butyllithium or lithium(hmds) were used as deprotonation reagents, yielding the lithium pyrrolides as intermediate compounds for transmetallation reactions.

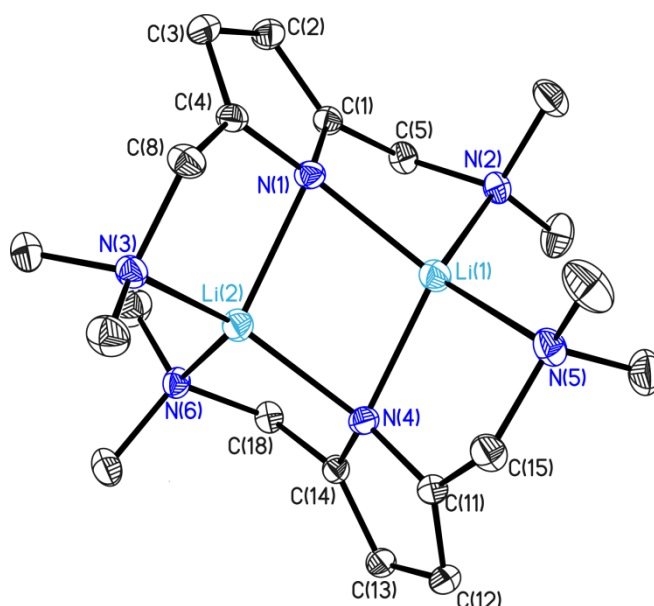


Figure 13. Crystal structure of lithium-2,5-bis(dimethylamino)methyl pyrrolide (**7**). Thermal ellipsoids are depicted at the 50% probability level, hydrogen atoms are omitted for clarity. Selected bond lengths and angles are shown in Table 4.

Compound **7** crystallizes in the monoclinic space group $P2_1/c$ containing a dimer in the asymmetric unit. The structure of **7** has already been published by *Kuo et al.* as a room temperature dataset.⁷⁵ It is included within this thesis because of its brilliant quality crystals, superior to those of compounds **8** and **9**. Furthermore, the obtained 100 K data set is of excellent quality, and thus feasible to analyze the structure in a very detailed manner. The pyrrole heterocyclic planes are twisted by $59.6(4)^\circ$ with respect to each other. Both lithium ions are coordinated in a tetrahedral distorted fashion with an angular range of $87.14(3)^\circ$ to $139.54(4)^\circ$ at Li1 and $89.80(3)^\circ$ to $137.14(4)^\circ$ at Li2. This asymmetry is induced by a stronger lithium coordination of the pyrrole nitrogen atoms (N1 and N4) relative to the side arm donors (N2, N3, N5 and N6). As a consequence, the lithium atoms are shifted further towards the center of the coordination pocket

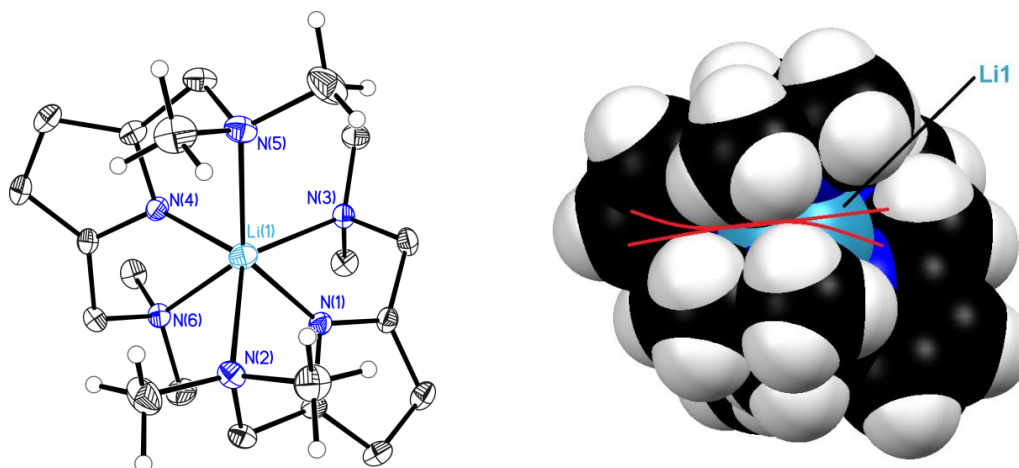
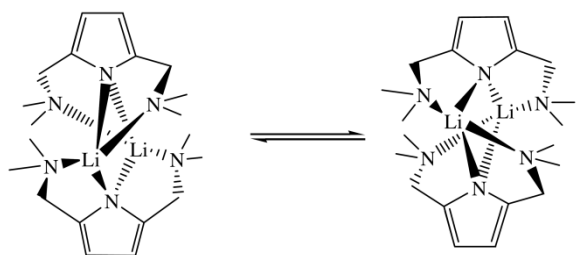


Figure 14. Crystal structure of **7**, view along the Li1...Li2 axis. Left: Thermal ellipsoid depiction; right: Space filling model.

provided by the ligands but steric repulsion prevents the side arms from following the lithium ions. They bent aside, maintaining the coordination to lithium, on the other hand distorting the tetrahedral geometry. Figure 14 clarifies that the methyl groups attached to N2 and N5 are almost touching, they cannot move further to Li1 and have to bent away to avoid each other. The data contained in Table 4 displays that the appearance of both ligands is symmetric concerning bond lengths and angles. Interestingly, the orientation of the lithium ions differs with respect to pyrrole although the Li1–N1–Li2 and Li1–N4–Li2 angles are similar. By looking at the lithium positions along the pyrrole plane it turned out that the Li1–N4–Li2 angle is approximately halved by the pyrrole plane, whereas, the pyrrole plane forms a narrow angle to the N1–Li1 bond and thus the N1–Li2 bond ascends steeply from the pyrrole plane regarding the Li1–N1–Li2 angle (Table 4). Nonetheless, the complex is quite symmetric and the crystal structure does not contain any disorder.

Table 4. Selected bond lengths [pm] and angles [°] of **7**.

Bond	Bond length [pm]	Atoms	Angle [°]
C1–C2	138.75(5)	Li1–N1–Li2	76.49(3)
C2–C3	142.22(5)	Li1–N4–Li2	77.81(3)
C3–C4	138.83(5)	N1–Li1–N2	87.14(3)
N1–Li1	204.47(8)	N2–Li1–N5	116.38(4)
N1–Li2	212.05(10)	N5–Li1–N4	88.58(3)
N2–Li1	211.46(8)	N4–Li1–N1	102.66(3)
N3–Li2	211.47(8)	N4–Li2–N1	101.25(3)
N4–Li1	207.09(10)	N1–Li1–N5	139.54(4)
N4–Li2	203.56(8)	N2–Li1–N4	127.88(4)



Scheme 30. Fluctuating coordination behavior of the side arms in **7**.⁷⁵

For that reason, the ^1H -NMR spectrum was expected to show sharp singlet signals. In contrast, the spectrum shows broad signals for the methylene protons. For this flexible type of pincer ligand bearing methylene linker moieties this behavior was already observed by *Kuo et al.*⁷⁵

They describe a fluctuating behavior for the methylene linker protons and explain it with a flipping of the side arms donors from Li1 to Li2 (Scheme 30). These different bonding situations seem to be chemically unequal, although the atomic environment is identical. This statement was confirmed using low temperature ^1H -NMR experiments (Figure 15).⁷⁵ It turned out that at room temperature, the unidentifiable broad singlet signal of the methylene linkers splits into two doublets upon cooling to less than 285 K. According to *Kuo et al.*, the estimated activation energy for flipping of the ligand side arms is 13.8 kcal/mol. There were no low-temperature ^1H -NMR experiments run for compound **7**, as the room temperature spectrum is equivalent to that of *Kuo et al.* However, compound **8** shows a different behavior and will be investigated in the next section.

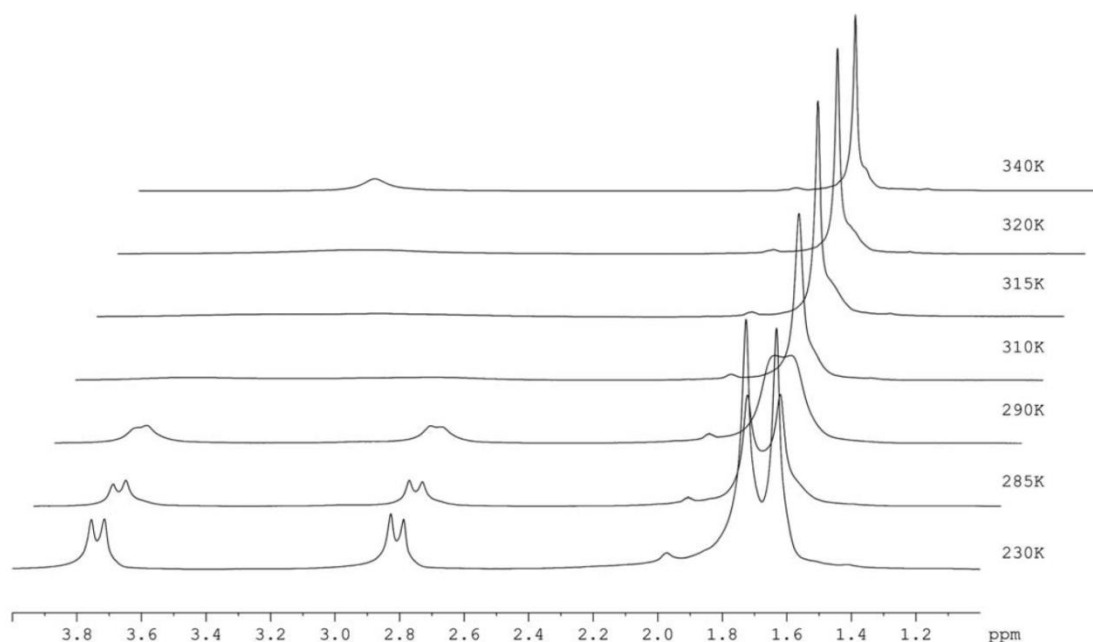


Figure 15. ^1H -NMR experiments conducted at variable temperatures, showing the methylene and methyl protons of **7**.⁷⁵

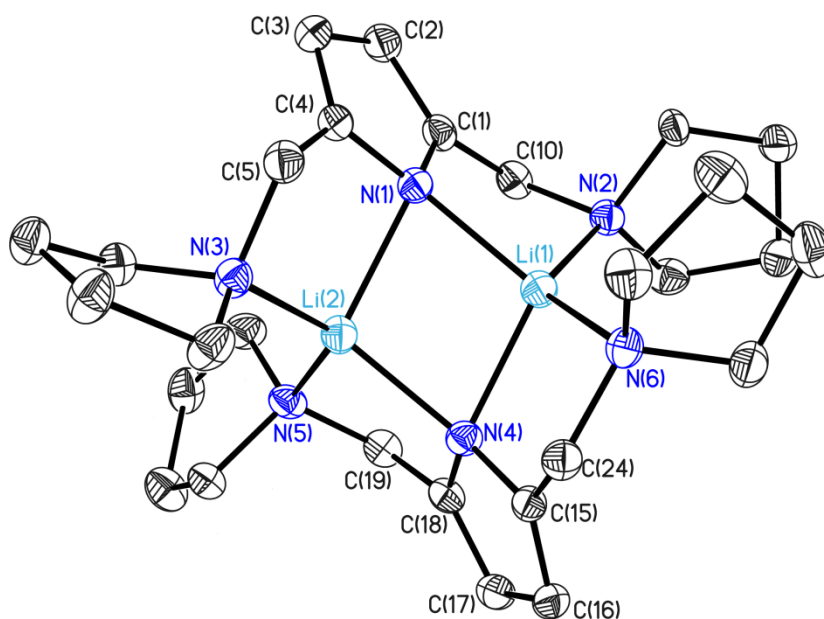


Figure 16. Crystal structure of lithium-2,5-bis(pyrrolidino)methyl pyrrolide (**8**). Thermal ellipsoids are depicted at the 50% probability level, hydrogen atoms are omitted for clarity. Selected bond lengths and angles are shown in Table 5.

Compound **8** crystallizes in the monoclinic space group $P2_1/n$ containing a dimer in the asymmetric unit and is almost isosterical to **7**. The tetrahedral geometry at the lithium ions is significantly distorted and bond lengths and angles at Li1 are similar to those at Li2 resembling the coordination motif of **7**. The marginal differences between **7** and **8** can be displayed by superposition plots. When increasing the bulkiness of the side arms (dimethylamino- to pyrrolidino-) bonded to the linker, the effect on the

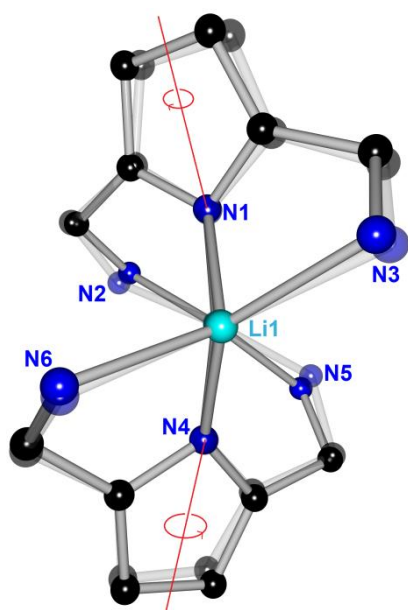


Figure 17. Superposition plot of compounds **7** (light) and **8** (dark) along the Li1–Li2 axis. The structures are fixed at N1, Li1 and N4.

coordination geometry is not drastic, although it becomes apparent as can be seen in Figure 17. The coordination motif itself is not affected but the nitrogen atoms of the side arms are even more bent aside than in **7**. This structural change is attenuated by the whole ligand system. By rotation, the pyrrole follows the movement of its side arms reducing the strain caused by coordination of the lithium atoms. As a consequence the tilting angle of the heterocyclic planes is slightly reduced from $59.63(4)^\circ$ in compound **7** to $56.73(9)^\circ$ in **8**, similar to all the other structural parameters that only changed marginally (Table 5). With one exception, the lithium atoms are located closer to the pyrrole nitrogen atoms. With bond

lengths of 201.9(2) pm (Li1) and 208.3(2) pm (Li2) both lithium atoms in **8** significantly form shorter bonds to N1 (and to N4) than those in **7**. A consequence of this lithium reorientation is a weakening of the side arm lithium interaction displayed by longer Li–N_{pyrrolidine} bonds.

Table 5. Selected bond lengths [pm] and angles [°] of **8**.

Bond	Bond length [pm]	Atoms	Angle [°]
C1–C2	138.03(19)	Li1–N1–Li2	76.32(9)
C2–C3	141.0(2)	N1–Li1–N2	87.21(9)
C3–C4	138.21(19)	N2–Li1–N6	127.77(11)
N1–Li1	201.9(2)	N6–Li1–N4	89.08(9)
N1–Li2	208.3(2)	N4–Li1–N1	102.88(10)
N2–Li1	213.3(2)	N1–Li1–N6	129.25(12)
N3–Li2	208.0(2)	N2–Li1–N4	121.50(11)

Figure 18 includes the room temperature ¹H-NMR spectrum of compound **8**. The methylene protons show a broad singlet signal at $\delta = 3.69$ ppm. A similar broadening was observed in compound **7** but at the elevated temperature of 340 K. By conducting low temperature ¹H-NMR experiments (243 K – 293 K) it could be shown that the activation energy of the side arm flipping in compound **8** is considerably less than in **7** as the distinct doublet signals for the methylene protons already appear at 285 K for compound **7**, whereas the sample of compound **8** needs to be cooled to 243 K to show a similar set of doublets.

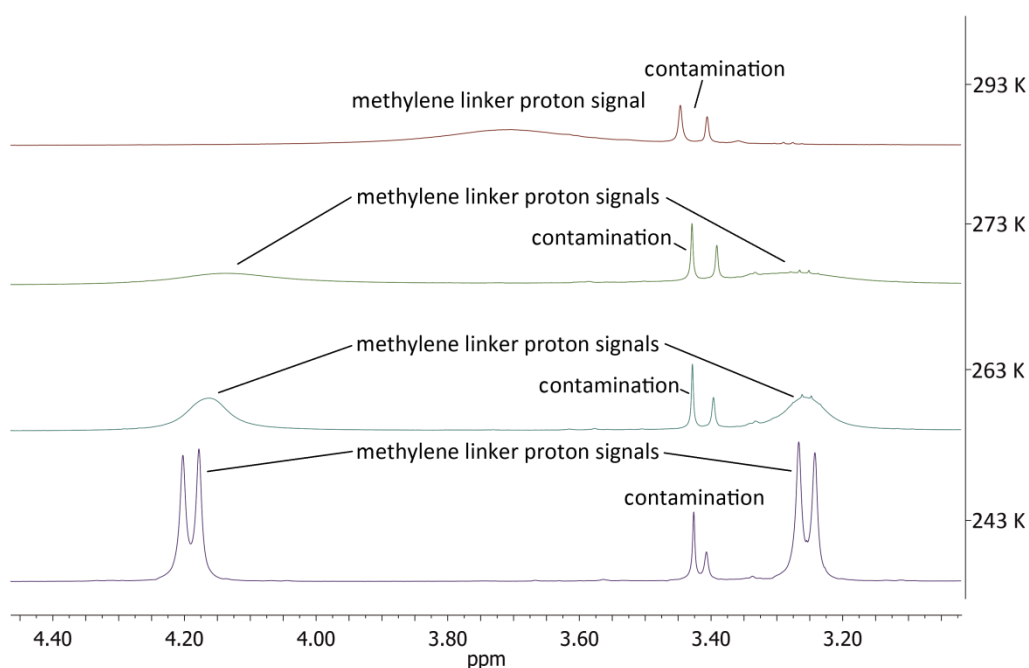


Figure 18. Variable temperature ¹H-NMR spectra of compound **8**. They were recorded from crystalline material of **8**, dissolved in Tol-d₈

Apart from shifting towards the pyrrole nitrogen atoms when going from **7** to **8**, the lithium ions adopt a different orientation relative to the pyrrole planes for both ligand molecules in **7** (Figure 19, left). Li1 is closer to the heterocyclic plane coordinated by the N1 sp^2 orbital than Li2 which is located way off the pyrrole plane, being closer to the heterocyclic π -electron density. At N4 this difference is less pronounced (Figure 19, right).

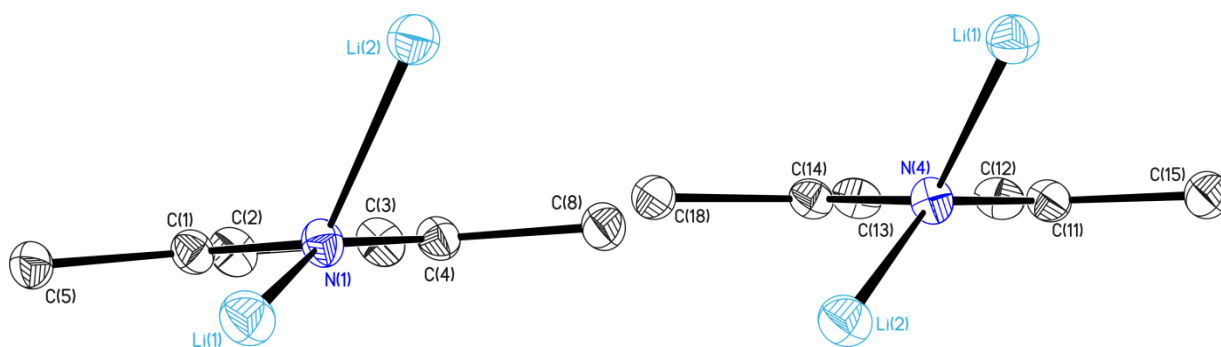


Figure 19. Section of compound **7**. Different orientation of the lithium atoms at N1 (left) and at N4 (right).

This bonding situation is known for a few more compounds of this type and *Stalke et al.*⁹² focused on the amido–lithium interaction within lithium anilide in detail. They found two different nitrogen–lithium bonds (198.9(3) pm and 208.7(3) pm, Li–N–Li 76.8(1)°) and stated that the geometry within the N_2Li_2 four-membered ring suggests sp^2 character at the nitrogen atom and thus an interaction of the nitrogen based p-orbital with the lithium ion (Figure 20). Figure 19 displays the nitrogen–lithium bonding situation in **7**. With a Li1–N1–pyrrole plane angle of 17.4° Li1 is interacting primarily with the N1 sp^2 lone pair, whereas Li2 forms a Li2–N1–pyrrole plane angle of 46.5° being almost exactly in between the outermost values for pure sp^2 - or p-interaction. Hence, Li2 can be assumed to interact with the pyrrole π -system via the N1 p-orbital as well.

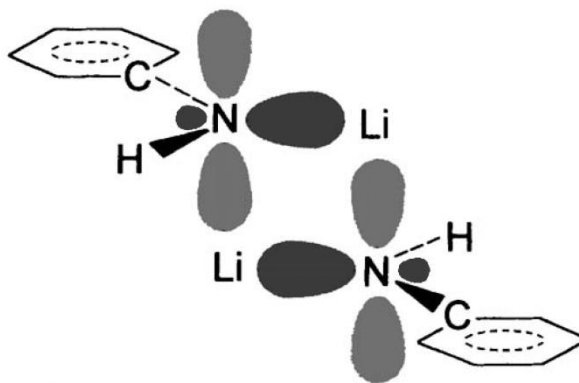


Figure 20. Nitrogen–lithium interaction within the structure of lithium anilide as suggested by *Stalke et al.*

To prove this unusual type of bonding, calculations were performed on compounds **7** and **8** by *D. M. Andrada*. All the geometry optimizations were performed by using the *ORCA* 2.9 program package.⁹³ Both, geometry optimizations and frequency calculations of the complexes were carried out at DFT level, using the B3LYP functional.⁹¹ The def2-

SVP and def2-TZVP basis set was used on all atoms.⁹⁴ The density differences were carried out with *Molpro*2012.1 program package.⁹⁵ The densities were calculated with the density fitted local MP2 method.⁹⁶ In these calculations the cc-pVTZ basis set⁹⁷ was used for carbon, nitrogen and the hydrogen atoms and the cc-pCVTZ basis set⁹⁸ was used for the lithium atoms. Wiberg Bond Order, Natural Population Analysis and donor-acceptor interactions have been computed using the natural bond order (NBO) method⁹⁹ with the with *GAUSSIAN* 09 suite of programs.¹⁰⁰

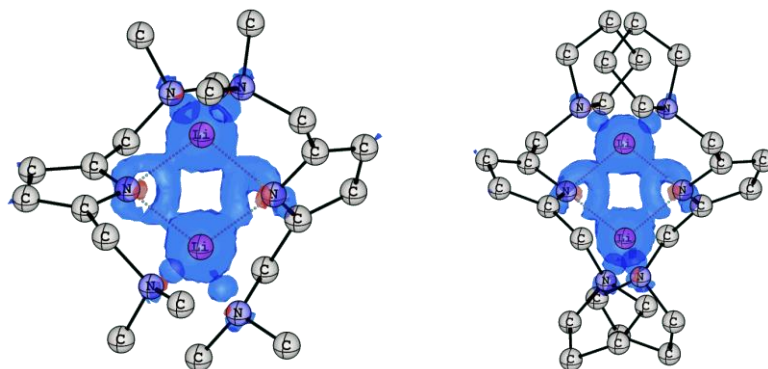


Figure 21. Density difference map of compounds **7** and **8** computed on the geometry-optimized structures. Hydrogen atoms are omitted for clarity. Isosurface: 0.01 au.

A density difference map was computed to visualize the effect of lithium coordination on the electronic structure. Figure 21 displays the difference of electron density computed for the geometry-optimized structures of **7** and **8** with and without the lithium ions ($\rho[\{NNN\}Li] - \rho[\{NNN\}^-]$). Positive values, meaning a concentration of electron density in the lithium compound compared to the anionic species, are displayed by the blue areas. Negative values, indicating a depletion of electron density in the lithium species compared to the hypothetical metal free compound are displayed in red. It becomes apparent that the lithium ions withdraw electron density from the ligand, mainly from the pyrrole nitrogen atoms but admittedly in lower amounts from the side arm nitrogen donor atoms as well (blue areas). Both lithium ions are enclosed in a sphere of withdrawn electron density whereas the pyrrole nitrogen atom shows a red bulb, hinting to a depletion of electron density at the position at the sp^2 lone pair in the lithium species. The red spots at the side arm donor atoms are rather small and in good agreement with the weaker side arm donor strength. However, the density difference map cannot shed further light on the nature of the lithium–pyrrole interaction. It can only hint to where the electron density is shifted through metal coordination and thus where the main interactions are.

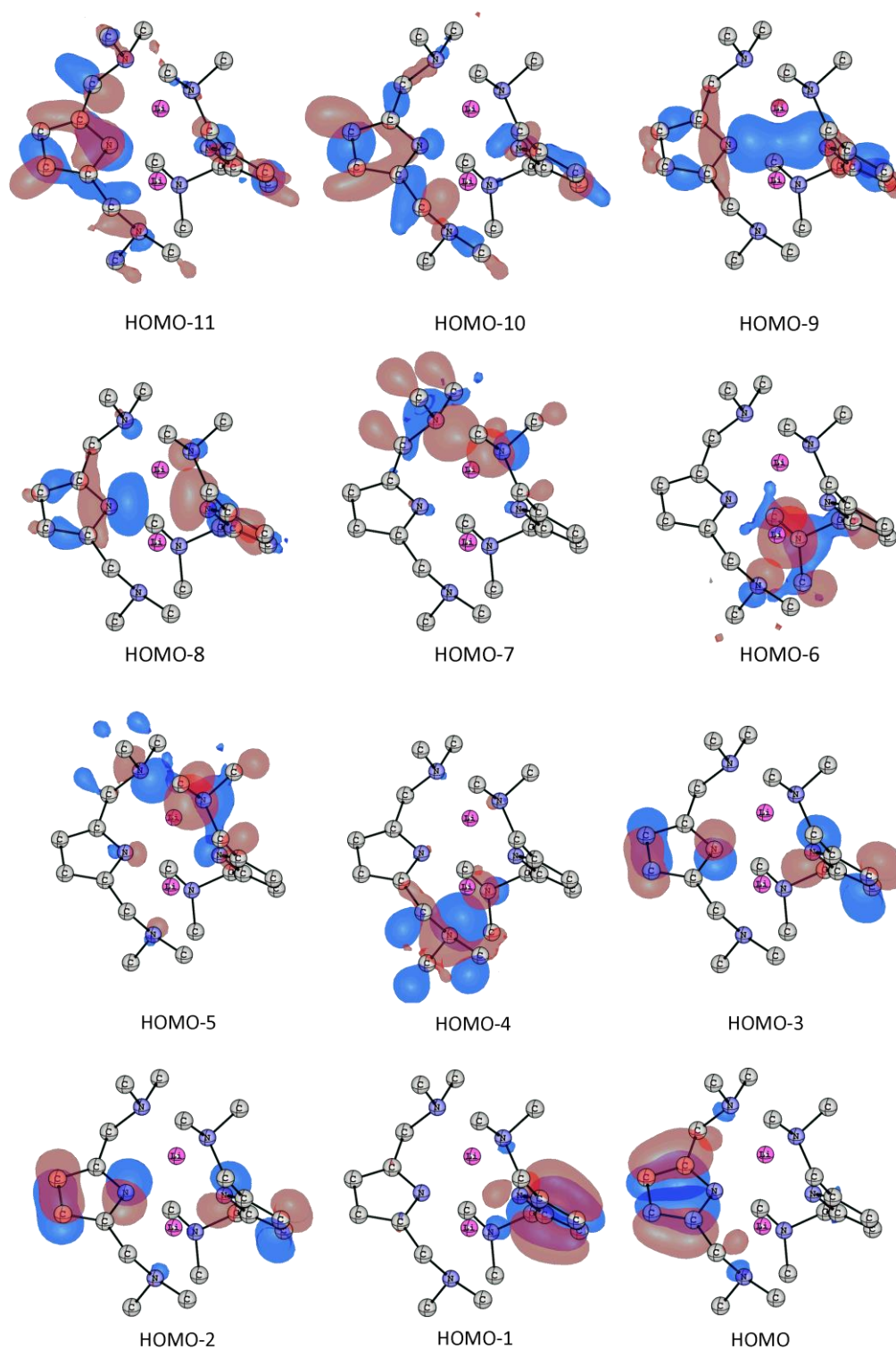
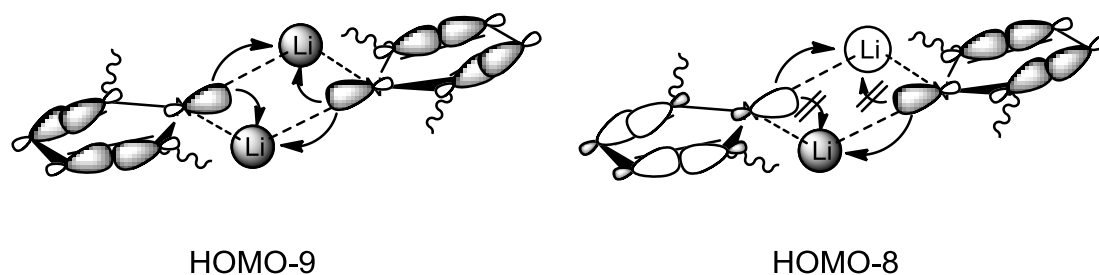


Figure 22. Shape of the twelve energetically highest occupied molecular orbitals of **7**.

To gain further insight, the molecular orbitals of **7** were investigated. The orbital interactions therein assist to analyze the metal ligand interaction in a more detailed way than it is possible using the density difference map. Molecular orbitals down to HOMO-11 were computed (Figure 22) but no covalent lithium nitrogen interaction was found at

The energetically lower lying molecular orbitals HOMO-4 to HOMO-7 exclusively contain the side arm donor–lithium interaction. Energetically lower lying orbitals than HOMO-7 start having σ -character. HOMO-8 and HOMO-9 enclose the pyrrole nitrogen sp^2 orbital as well as sp^2 σ -bonds from within the heterocycle. They are the bonding and anti-bonding combination of the interaction of both pyrrole nitrogen sp^2 -orbitals, but due to the fact that both are fully occupied, there is no covalent interaction in between the pyrrole moieties. However, the very distinct lone pairs at the pyrrole nitrogen atoms in HOMO-8, generated by the negative overlap of both sp^2 orbitals provide electron density in close proximity to the *Lewis* acidic lithium ions (Scheme 32). HOMO-9 as the positive overlap of the sp^2 orbitals exhibits the same effect. The anti-bonding molecular orbitals depicted in Scheme 31 and Scheme 32 (HOMO-8 and HOMO-2) have a nodal plane between the pyrrole units that does not permit a positive orbital overlap with both lithium ions. Instead, only one of the lithium ions is coordinated by pyrrole. Hence, each of the lithium atoms has a preferred coordination towards one of the pyrrole units, and a weaker interaction with the other pyrrole. This imbalanced interaction can be regarded as the origin for the asymmetric lithium coordination.



Scheme 32. Pyrrole – lithium interaction within the HOMO-8 and HOMO-9 molecular orbitals of compound 7.

To quantify the interaction, a Natural Bond Orbital (NBO)⁹⁹ analysis was conducted (Table 6). It confirms the inferences drawn from the density difference map (Figure 21). The lithium ions contain a considerable amount of electron density, resulting in a charge ($Q(\text{Li})$) of +0.581 and +0.609, respectively. As expected, the charges of the nitrogen donor atoms ($Q(\text{N}_{\text{arm}})$) are slightly negative. The meager charge concentration (-0.631/-0.635) at the pyrrole nitrogen atoms ($Q(\text{N}_{\text{py}})$), the expected value was -1, can be explained by delocalization of the N1 p_z -orbital into the heteroaromatic system and the electron withdrawing effect of the lithium ions. This is confirmed by the value for the occupation of the N1 p_z -orbital which is app. 1.45 for both pyrrole nitrogen atoms.

Table 6. NBO Charges for the lithium ($Q(\text{Li})$) and nitrogen atoms ($Q(\text{N}_{\text{py}})$ and $Q(\text{N}_{\text{arm}})$) in [au], Wiberg bond order (BO) in [au], occupancy of the lone pair ($\text{LP}(\text{N}_{\text{py}})$ p_z and $\text{LP}^*(\text{Li})$) in [au] and second order perturbation energy in [kcal/mol] involving the lithium atoms of compound 7.

Properties		Properties	
$Q(\text{Li})$	+0.581/+0.609	$\text{LP}(\text{N}_{\text{py}})$ p_z	1.45787/1.45337
$Q(\text{N}_{\text{py}})$	-0.631/-0.635	$\text{LP}^*(\text{Li})$ sp	0.139/0.106
$Q(\text{N}_{\text{arm}})$	-0.451/-0.445	$\Delta E^{(2)} \text{LP}(\text{N}_{\text{py}}) \text{ sp}^2 \rightarrow \text{LP}^*(\text{Li})$	22.76/21.42
	-0.449/-0.441	$(\text{N}_{\text{py}} \rightarrow \text{Li } \sigma\text{-donation})$	23.39/20.60
$\text{BO}(\text{Li}-\text{N}_{\text{py}})$	0.1272/0.1413	$\Delta E^{(2)} \text{LP}(\text{N}_{\text{py}}) p_z \rightarrow \text{LP}^*(\text{Li})$	2.11/2.07
	0.1429/0.1327	$(\text{N}_{\text{py}} \rightarrow \text{Li } \pi\text{-donation})$	1.30/2.80
$\text{BO}(\text{Li}-\text{N}_{\text{arm}})$	0.0808/0.0828	$\Delta E^{(2)} \text{LP}(\text{N}_{\text{arm}}) \text{ sp}^3 \rightarrow \text{LP}^*(\text{Li})$	21.43/18.29
	0.0722/0.0775	$(\text{Side arm} \rightarrow \text{Li donation})$	22.45/18.51

The perturbation energy listed in Table 6 is the yield in energy gained by electron donation as specified. For N1, the interaction energy with Li1 via the sp^2 lone pair is 23.39 kcal/mol. Due to the spatial distance of Li2 to the N1 sp^2 lone pair, the interaction energy is reduced to 20.60 kcal/mol. In contrast, the interaction energies of N4 with the lithium ions are much more akin. Li2 which is much closer to the pyrrole plane than Li1 has a interaction energy with N4 of 22.76 kcal/mol. The corresponding value of the N4–Li1 interaction is 21.42 kcal/mol.

Remarkably, the energy values correlate with the spatial approximation of the lithium ions to the pyrrole plane, obtained by measuring the pyrrole plane–N1–Li angle (Table 7), whereas the distance of the lithium ion from the pyrrole nitrogen atom seems to be less important. At N4 the lithium ions have similar distances to the pyrrole plane and show intermediate interaction energy values. At N1 one of the lithium ions is located close to the pyrrole plane and the other one way off. Consequently, the obtained interaction energies are the maximum and minimum values for compound **7**.

The opposite effect is present investigating the lithium– π interaction. With increasing distance of the lithium ion from the pyrrole plane and thus a spatial approximation to the pyrrole π electron density, the lithium– π interaction energy rises. A correlation between the degree of π -overlap (distance centroid–lithium) and strength of the π -interaction is reasonable and was published earlier.¹⁰¹ Therefore it is not surprising that the maximum cation π -interaction energy value is obtained for the N1_{pZ}→Li2 π -interaction (2.80 kcal/mol) and the corresponding minimum value for the N1_{pZ}→Li1 π -interaction (1.30 kcal/mol) (Table 7).

Table 7. Comparison of the structural properties of **7** with the computed lithium–pyrrole interaction energies.

Bond	N-Li-pyrrole plane angle [°]	N-Li distance [pm]	N _{py} →Li σ -donation [kcal/mol]	N _{py} →Li π -donation [kcal/mol]
N1–Li1	15.72	204.5	23.39	1.30
N1–Li2	46.81	212.2	20.60	2.80
N4–Li1	38.87	207.1	21.42	2.11
N4–Li2	27.16	203.6	22.76	2.07

Gas phase calculations performed on lithium interacting with benzene resulted in a π -interaction energy value for the η^6 -interaction of 43.8 kcal/mol and 39.5 kcal/mol, respectively, depending on the used basis sets.¹⁰² However, these calculations neglect the remaining substituents at the lithium ion which would weaken the lithium benzene interaction. *Yuan et al.* focused on the cation π -interaction of lithium amide with benzene among others. They obtained lithium–benzene η^6 -interaction energy values of 8.56 kcal/mol and 7.17 kcal/mol, respectively, for the different basis sets used in their computation.¹⁰³ Taking these results into account, the 2.8 kcal/mol, resulting exclusively from the N1_{pZ}→Li2 π -interaction, sound reasonable. The orientation of the lithium ion in **7** is far off the ideal η^5 -orientation which should significantly reduce the interaction

energy values compared to those reported by *Yuan et al.*¹⁰³ Hence, the computations performed on compound **7** support the theory of the sp^2 amide nitrogen atom, donating electron density towards the lithium ion involving both lone pairs.

Table 8. NBO Charges for the lithium ($Q(\text{Li})$) and nitrogen atoms ($Q(\text{N}_{\text{py}})$ and $Q(\text{N}_{\text{arm}})$) in [au], Wiberg bond order (BO) in [au], occupancy of the lone pair ($\text{LP}(\text{N}_{\text{py}})$ p_z and $\text{LP}^*(\text{Li})$) in [au] and second order perturbation energy in [kcal/mol] involving the lithium atoms of compound **8**.

Properties		Properties	
$Q(\text{Li})$	+0.567/+0.613	$\text{LP}(\text{N}_{\text{py}}) p_z$	1.45350/1.45037
$Q(\text{N}_{\text{py}})$	-0.638/-0.634	$\text{LP}^*(\text{Li}) sp$	0.136/0.132
$Q(\text{N}_{\text{arm}})$	-0.450/-0.454	$\Delta E^{(2)} \text{LP}(\text{N}_{\text{py}}) sp^2 \rightarrow \text{LP}^*(\text{Li})$	23.74/26.58
	-0.452/-0.448	$(\text{N}_{\text{py}} \rightarrow \text{Li } \sigma\text{-donation})$	24.04/26.20
$\text{BO}(\text{Li}-\text{N}_{\text{py}})$	0.1214/0.1198	$\Delta E^{(2)} \text{LP}(\text{N}_{\text{py}}) p_z \rightarrow \text{LP}^*(\text{Li})$	1.00/2.32
	0.1383/0.1391	$(\text{N}_{\text{py}} \rightarrow \text{Li } \pi\text{-donation})$	0.95/2.48
$\text{BO}(\text{Li}-\text{N}_{\text{arm}})$	0.0780/0.0780	$\Delta E^{(2)} \text{LP}(\text{N}_{\text{arm}}) sp^3 \rightarrow \text{LP}^*(\text{Li})$	17.26/19.81
	0.0679/0.0691	$(\text{Side arm} \rightarrow \text{Li donation})$	19.17/18.75

To investigate the structural differences of **7** and **8**, the computations were performed on **8** as well. The fact that the lithium ions are located closer to the pyrrole nitrogen atom in **8** is reflected by a greater value for the $\text{N}_{\text{py}}(sp^2) \rightarrow \text{Li } \sigma$ -interaction energy (Table 8). The analogous interaction energy of the side arms with the lithium ions is consequently decreased. Other values like the atom charges or lone pair occupation as well as the bond order show ambiguous tendencies. The increased pyrrole–lithium interaction energy is not reflected by the lithium–pyrrole bond order, which surprisingly decreased slightly. However, the values for the $\text{BO}(\text{Li}-\text{N}_{\text{arm}})$ are lower in **8** compared to **7**, matching the expectations from the crystal structure comparison.

Table 9. Comparison of the structural properties of **8** with the computed lithium–pyrrole interaction energies.

Bond	N-Li-pyrrole plane angle [°]	N-Li distance [pm]	$\text{N}_{\text{py}} \rightarrow \text{Li } \sigma\text{-donation}$ [kcal/mol]	$\text{N}_{\text{py}} \rightarrow \text{Li } \pi\text{-donation}$ [kcal/mol]
N1–Li1	17.42	201.9	26.58	0.95
N1–Li2	46.48	208.3	23.74	2.48
N4–Li1	41.07	207.3	24.04	2.32
N4–Li2	24.05	201.3	26.20	1.00

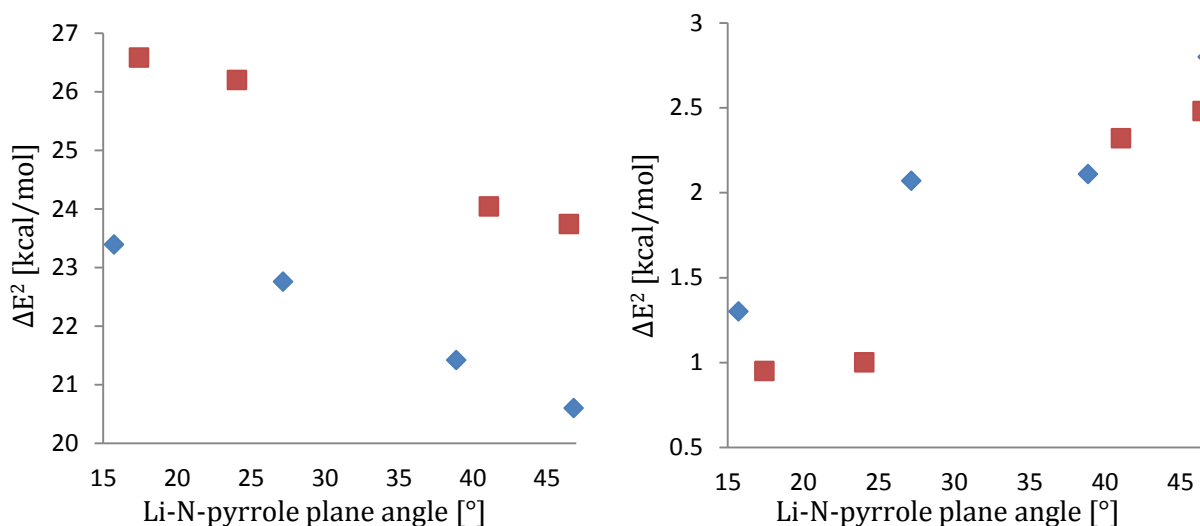


Figure 23. Lithium–pyrrole interaction energy [kcal/mol] in dependence of the Li-N-pyrrole plane angle [°]. Pyrrole–lithium σ -interaction (left) and pyrrole–lithium π -interaction (right) for **7** (blue) and **8** (red).

The computational results show in general that both lithium ions are much more alike in **8** than in **7**. Both lithium atoms in **8** form unequal bonds to the pyrrole moieties, with a considerable stronger bond to one of the pyrrole moieties than to the remaining pyrrole unit. This is underlined by the values for the lithium–pyrrole interaction energies and the bond order values that are similar for equivalent interactions of the respective lithium atoms.

Table 9 contains the orientation of the lithium ions relative to the pyrrole nitrogen atoms in **8**. The same tendencies as in compound **7** could be observed. The lithium–pyrrole interaction energies are correlated with the pyrrole plane–N1/N4–Li angle, as already observed for **7**. The dependence of the N–Li interaction energy from the N–Li distance becomes obvious when comparing the energy values at a given N–Li–pyrrole plane angle of two different structures (**7** and **8**) (Figure 23). At a fixed N–Li–pyrrole plane angle, the sp^2 -lithium interaction energy in **8** is about 3 kcal/mol higher than in **7**. This effect is less pronounced for the π -interaction energies, however, the values for **7** at a given pyrrole plane–N1/N4–Li angle are higher than those in **8** by in average 0.5 kcal/mol.

3.3 Group 13 Metal Pincer Complexes

3.3.1 Aluminium-dichloro-{2,5-bis((3,5-dimethylpiperidino)methyl)-pyrrolide} (10)

The lithium pyrrolide complex discussed in the previous chapter plays a key role for the synthesis of other metal complexes. Via the salt elimination process, mentioned in chapter 1.1, a wide range of metal complexes is accessible. By the addition of aluminiumchloride to a stirred solution of the corresponding lithium pyrrolide (9) in toluene, the dichloroaluminium-pincer complex could be obtained.

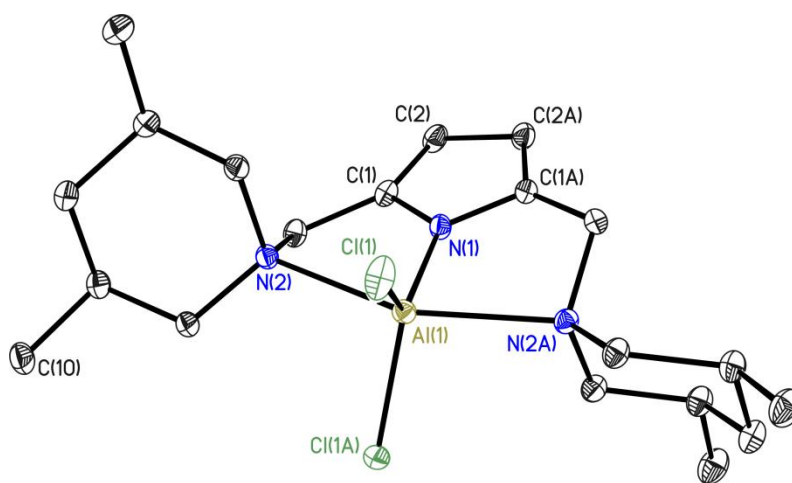


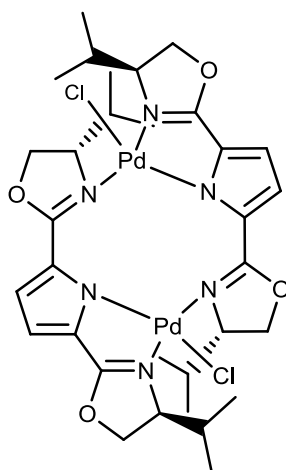
Figure 24. Crystal structure of aluminium-dichloro-{2,5-bis((3,5-dimethylpiperidino)methyl)-pyrrolide} (10) ($\{NNN\}AlCl_2$). Thermal ellipsoids are depicted at the 50% probability level, hydrogen atoms are omitted for clarity. Selected bond lengths and angles are shown in Table 10.

10 crystallizes in the monoclinic space group $C2/c$ enclosing half a formula unit and a toluene solvent molecule in the asymmetric unit.

Table 10. Selected bond lengths and angles of $\{NNN\}AlCl_2$ (10).

Bond	Bond length [pm]	Atoms	Angle [°]
C1–C2	137.82(18)	N1–Al1–Cl1	123.872(18)
C2–C2A	143.8(3)	Cl1–Al1–Cl1A	112.26(3)
N1–Al1	181.72(16)	N2–Al1–N2A	155.26(6)
N2–Al1	225.22(11)	N1–Al1–N2	77.63(3)
Al1–Cl1	214.30(5)	C1–C3–N2	107.15(10)
N2–N2A	440.0(3)	Σ (Al1–N1–Cl1–Cl1A) plane	360.00

Surprisingly, the aluminium(III) ion is coordinated in the {NNN} fashion although the ion radius of aluminium(III) with a value of 48 pm¹⁰⁴ is smaller than the radius for lithium(I) (59 pm)¹⁰⁴ and the lithium pyrrolide complexes are known to form highly stable dimeric compounds (chapter 3.2).



Scheme 33.
Palladium complex
reported by *Gade et al.*⁹

Besides these dimeric compounds (7-9) with the rather small lithium(I)-ion, an example of a dimeric palladium(II) pincer complex has been reported in literature by *Gade et al.* using the BOX-ligand with a pyrrole backbone (pyrrBOX).⁹ With an ion radius of 64 pm¹⁰⁴ the larger palladium(II) seems to fit perfectly into the coordination pocket provided by the dimeric ligand species as bond lengths and angles do not reflect a very tensed structure. Hence, the aluminium(III) ion having $\frac{3}{4}$ of the palladium(II) ion size should induce a dimeric motive to reduce tension caused by the hypothetical coordination of both ligand side arms to one metal ion.

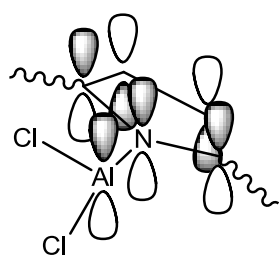
Unexpectedly, as can be seen in Figure 24, the structure is monomeric with both side arms having the identical distance to the aluminium(III) ion which is due to a two-fold axis going through the molecule. As it is quite unexpected for this compound showing monomeric appearance, it is consequently strained visualized by the selected bond angles shown in Table 10 (C1-C3-N2) which represents a rather narrow angle at the methylene linker. The coordination geometry at the aluminium ion is distorted trigonal-bipyramidal. Although the triangular plane is perfectly planar with a sum of angles of 360.00°, the axial positions are bent towards the pyrrole heterocycle (N2-Al1-N2A 155.26(6)°). The linear arrangement of the two side arm donors and the metal ion is not feasible for the ligand, because of the ligand geometry which exclusively permits a convex shape. The methylene linkers are simply not long enough to coordinate a metal ion in a linear or concave shape. Within the triangular plane, the chlorine atoms claim less space than the pyrrole unit displayed by comparison of the Cl1-Al1-Cl1A angle (112.26(3)°) with the Cl1-Al1-N1 angle (123.872(18)°). Each chlorine atom occupies 118.1° whereas the pyrrole moiety occupies the residual 123.9° of the triangular plane. The N1-Al1 bond with a length of 181.72(16) pm is one of the shortest nitrogen-(dichloro)aluminium distances found in the CSD. The N-donor side-arms however, show longer N-metal distances with 214.30(5) pm for each bond. An explanation can be the

negative charge of the pyrrole unit, interacting stronger with the highly *Lewis*-acidic aluminium(III) ion than the neutral piperidyl nitrogen atoms. Additionally, the pyrrole π -system can interact with the aluminium ion, whereas the side arm donor atoms are cut off from the π -system and can simply donate with their lone-pair. The sum of these differences makes the N1–Al1 43.50 pm shorter than the N2–Al1 bond.

Table 11. Comparison of bond length within the pyrrole moiety in **9** and **10**.

	[NNN]Li (9)	{NNN}AlCl ₂ (10)
Single bond [pm]	141.2(4)	143.8(3)
Avg. double bond [pm]	137.7(5)	137.82(18)
$\Delta_{\text{SB-DB}}$ [pm]	3.5	6.0

To gain insight into the metal ligand bonding, the bond lengths within the pyrrole heterocycle were investigated and the loss of electron density within the pyrrole moiety becomes obvious. The difference in-between single and double bonds is increased by 2.5 pm compared to the lithium pyrrolide (**9**) (Table 11). By using the simple orbital model explained in chapter 1.2, the occupied π -orbital of pyrrole obviously donates electron density towards the aluminium ion. According to Scheme 34 this interaction results in a shortening of the formal C=C double bonds and an elongation of the formal single bond thus increasing the difference between single- and double-bonds. But exclusively taking the bond lengths into account is misleading when evaluating the nature of the N1–Al1 bond. It turned out that the use of the simple orbital model is problematic as well. The orbitals shown in Scheme 6 are plausible, but the position of the nodal plane can be different for heterocycles like pyrrole as they are adopted from



Scheme 34.
Pyrrole→aluminium
 π -donation.

the cyclopentadienide molecule and not derived from pyrrole itself. Therefore, quantum mechanical calculations using the *TONTO*¹⁰⁵ program within the *CrystalExplorer*⁸⁰ program package were run with the HF/cc-pVDZ⁹⁷ level of theory. The computational results show that the occupied pyrrole π -orbitals are located in the HOMO and the HOMO-1 and do not overlap with aluminium centered p-orbitals at an isolevel of 0.04 au (Figure 25). The aluminium- p_z -orbital is lower in energy, overlapping with the lone-pairs of the piperidine nitrogen atoms in the HOMO-3 without interfering with pyrrole centered orbitals. Taking the energetically low lying molecular orbitals down to HOMO-10 into account, it turned out that there is only HOMO-3 showing p-orbital character at the

aluminium atom (Figure 25, right). The different algebraic signs of the orbitals displaying the side arm–aluminium interaction are only in agreement with a p-orbital at the aluminium atom. Thus, sp^2 -type hybridization is assumed for the frontier orbitals of aluminium, explaining the textbook planarity in the Cl–Al–Cl plane and the coordination geometry in general. However, the investigation of the energetically low lying molecular orbitals can be misleading as these orbitals are very close in energy and an orbital mixing of different orbitals becomes likely.

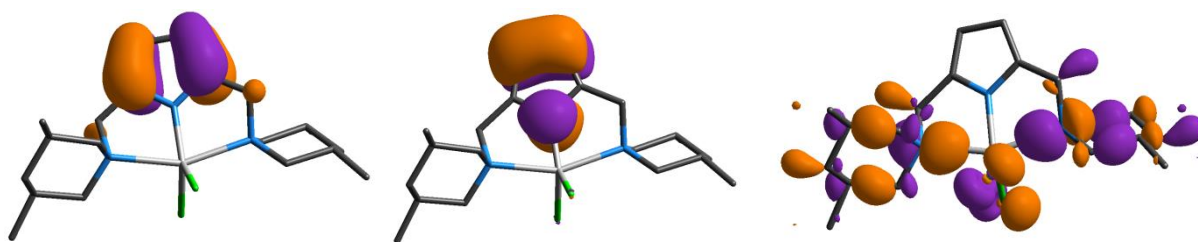


Figure 25. Molecular orbitals of **10**, depicted at an isolevel of 0.04 au, were obtained by quantum mechanical calculations based on the crystal structure using the HF/cc-pVDZ⁹⁷ level of theory. HOMO (left), HOMO-1 (middle) and HOMO-3 (right).

Nonetheless, the molecular orbitals obtained within this calculation contradict a ligand-metal π -interaction. Thus, the $N1_{sp^2} \rightarrow Al1$ donation must be responsible for the short N–Al bond observed in **10**, but it does not explain the observed bond lengths. A strong *Lewis* acid like aluminium(III) may influence the formal double bonds, however, the withdrawal of electron density from N1 towards Al1 could hardly elongate the C2–C3 bond by 2 pm. The only valuable explanation must be a π -donation from the $N1_{p_z}$ orbital into the Al–Cl σ^* -orbitals, although the computed molecular orbitals do not confirm the presence of a π -overlap between N1 and Al1. This π -donation would perfectly explain the elongated C2–C3 bond. The almost unchanged C1–C2 and C3–C4 bonds, with respect to **9**, can be explained by a compensation of the shortening caused by a withdrawal of electron density via the $N1_{sp^2} \rightarrow Al1$ donation.

An effect that cannot be quantitatively traced back to bond elongation or shortening within the pyrrole heterocycle is the intermolecular interaction in the solid state. Most of the intermolecular interactions are not realized by simply refining the crystal structure. Additionally, if the interaction is rather weak, it can hardly be displayed by any structure refinement software. It can only be found by carefully checking all close contacts but an oversight cannot be excluded, in particular if it is a weak interaction.

The structure of **10** does not show any close contacts to other molecule parts. The molecules are clearly separated from each other and the co-crystallized solvent is just occupying voids within the unit cell. However, the *Hirshfeld* surface⁸² revealed some red areas hinting to an intermolecular interaction (Figure 26). After a careful investigation of the *Hirshfeld* surface,⁸² it turned out that the red areas, marked with red arrows, are caused by a close contact of the pyrrole π -system with a hydrogen atom belonging to a piperidine methyl moiety (Figure 27). The green arrow marks a red area which is not caused by an intermolecular interaction. The C–H– π interaction moves other molecule parts in close approximation, which do not show any kind of interaction.

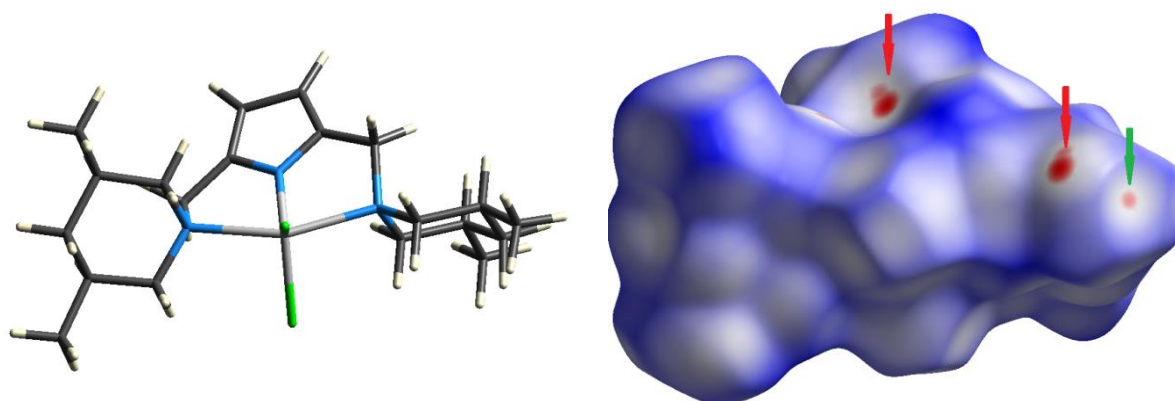


Figure 26. Crystal Structure (left) and *Hirshfeld* surface of **10** (right), computed with a molecule orientation as seen on the left.

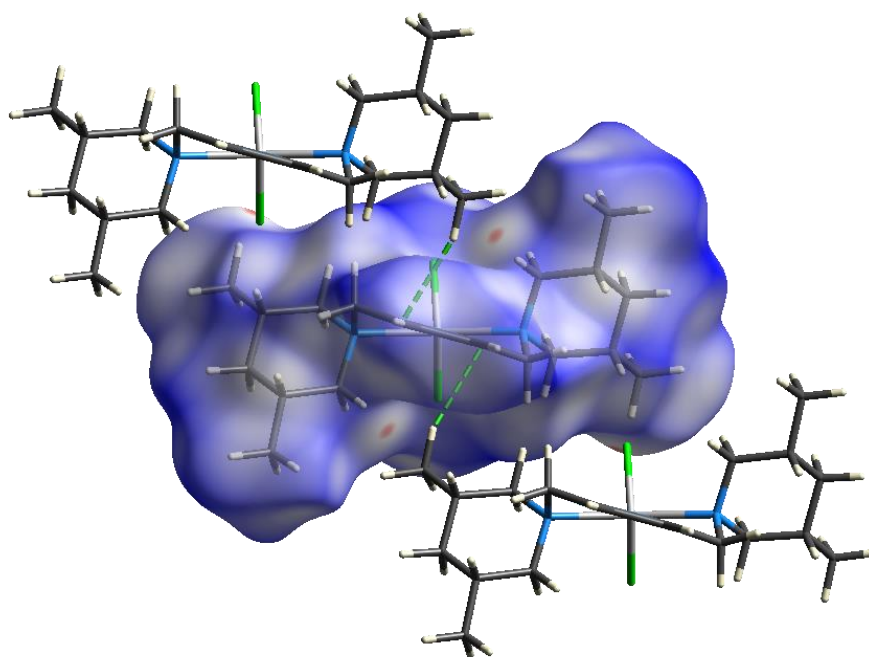


Figure 27. Hirshfeld surface of **10**, including the corresponding close contact molecules.

In Figure 27, the molecules within close contact were added to the *Hirshfeld* surface⁸² plot, clarifying that the C–H– π interaction is present on both sides of the pyrrole π -system (green dashed lines). Both C–H– π interactions are identical concerning bond lengths and angles and coordinate to the pyrrole heterocycle in the η^5 -mode. The shortest distance of the hydrogen atom (H10B) to the aromatic plane is 259.8(2) pm, the H-centroid distance is 262.8 pm with a C–H-centroid angle of 173.48°. An analysis of the crystal structures contained in the CSD for C–H– π interactions towards five membered aromatic cycles revealed that compound **10** contains a rare example of a considerable short C–H– π interaction with an almost linear C–H– π arrangement. Theoretical calculations rank methyl– π interactions in the class of the weakest C–H– π interactions with approximately 2 kcal/mol.¹⁰⁶ However, the results of *Tsuzuki et al.* demonstrate that substituted methyl moieties have higher interaction energies than methane,⁸⁵ and described an angular dependence of the C–H– π

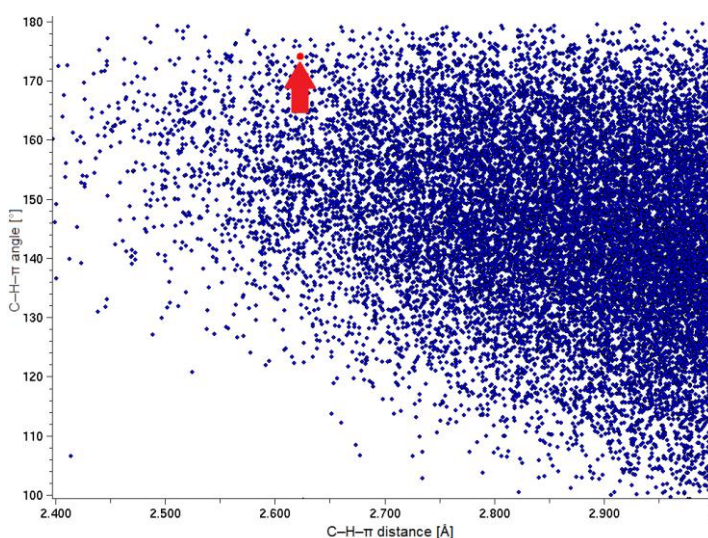
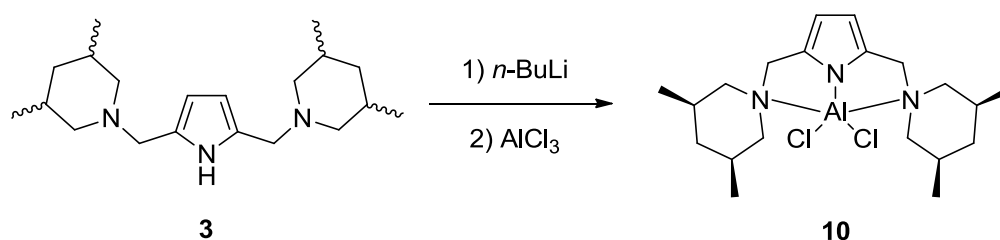


Figure 28. Scatterplot of all entries within the CSD containing C–H– π interactions to cyclopentadienide or pyrrole. The red dot marks the C–H– π interaction within **10**.

interaction energy. The wider the C–H– π angle becomes, the higher the interaction energy, reaching the maximum at an angle of 180°. ⁸⁶ With an angle close to the ideal 180°, and the short hydrogen– π -plane distance the C–H– π interactions found in **10** are considered to be of a rather strong nature with respect to the other reported C–H– π interactions (Figure 28).

In the field of computational chemistry there is an ongoing debate on whether these interactions are important intermolecular forces like hydrogen bondings or if they are kind of *London*-dispersion forces, having only weak influence on structures in the presence of other forces like hydrogen bondings. ^{106,107} However, it cannot be denied that C–H– π interactions are an important structure determining effect in crystal packing. In compound **10** the structure is determined by the C–H– π interactions.

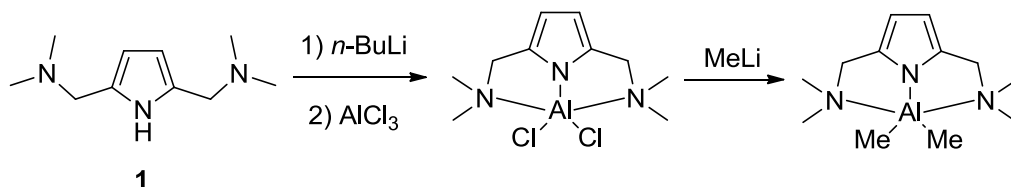


Scheme 35. Synthesis of compound **10** starting from the free ligand **3** via a salt elimination reaction.

As the reaction was performed using a racemic mixture of *cis/trans*-3,5-dimethylpiperidine the crystal structure was expected to contain both isomers, but it exclusively shows the *cis*-isomer (Scheme 35). The *trans*-isomer is obviously not able to crystallize in a similar orientation. It is most likely that the steric repulsion, caused by an axial methyl group of the *trans*-isomer, overcomes the energy gained from the C–H– π interaction. Finally, the complex containing the *trans*-isomer does not crystallize at all lacking intermolecular interactions, whereas the complex, containing the *cis*-isomer creates a C–H– π interaction network which leads to formation of single crystals suitable for X-ray diffraction experiments.

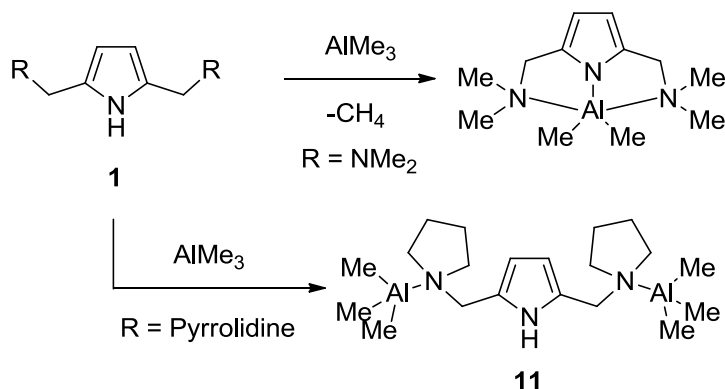
3.3.2 2,5-Bis((pyrrolidino)methyl)pyrrole · 2 trimethylaluminium (11)

In 2001 *Huang et al.* reported the synthesis of an aluminium pincer compound whose synthesis was quite inconvenient (Scheme 36).⁷⁶ Using methyllithium they converted the $\{NNN\}AlCl_2$ species into the dimethyl species with app. 80% yield.



Scheme 36. Synthesis of a $\{NNN\}AlMe_2$ species as described by *Huang et al.*

This $\{NNN\}AlMe_2$ species is of interest in the context of this thesis because of the evaluation of the consequences on the ligands π -system when changing the metal-substituents from chlorine to methyl. However, it should be possible to synthesize this $\{NNN\}AlMe_2$ species in a one-step synthesis, making benefit of the high basicity of trimethylaluminium.



Scheme 37. Different reactivity of the free ligands **1** and **2** towards trimethylaluminium.

Therefore the ligand 2,5-bis((dimethylamino)methyl)pyrrole was treated with an equimolar amount of trimethylaluminium and the resultant colorless solution was stored at $-28\text{ }^{\circ}\text{C}$ (Scheme 37). After three days, crystals, suitable for single crystal X-ray diffraction experiments, were obtained. The resulting structure is almost matching to that of *Huang et al.* However, the crystal system differs. *Huang et al.* reported an orthorhombic crystal system (space group *Pbca*) whereas the compound prepared within this thesis crystallizes as a twin (BASF 0.41) in the monoclinic space group *C2/c*. After having explored a new reaction pathway to organoaluminium pincer compounds, the free ligand 2,5-bis((pyrrolidino)methyl)pyrrole (**2**) was reacted with

trimethylaluminium. Crystals, suitable for single crystal X-ray diffraction experiments, were obtained after two days.

11 crystallizes in the monoclinic space group $P2_1/c$ with a whole molecule enclosed in the asymmetric unit (Figure 29). The geometry at the aluminium ions is slightly distorted from tetrahedral geometry, with the methyl ligands occupying marginally more space than the pyrrolidine nitrogen atoms (N2 and N3). The N–Al–C angles are in a range of 102.9° to 105.6° , whereas the C–Al–C angles are considerably larger with a range of 112.0° to 116.7° . The Al–N bond lengths (N2–Al1 204.48(4) pm; N3–Al2 203.76(5) pm) fit perfectly into the range of reported N–Al bond lengths of $N\cdots AlMe_3$ adducts.¹⁰⁸

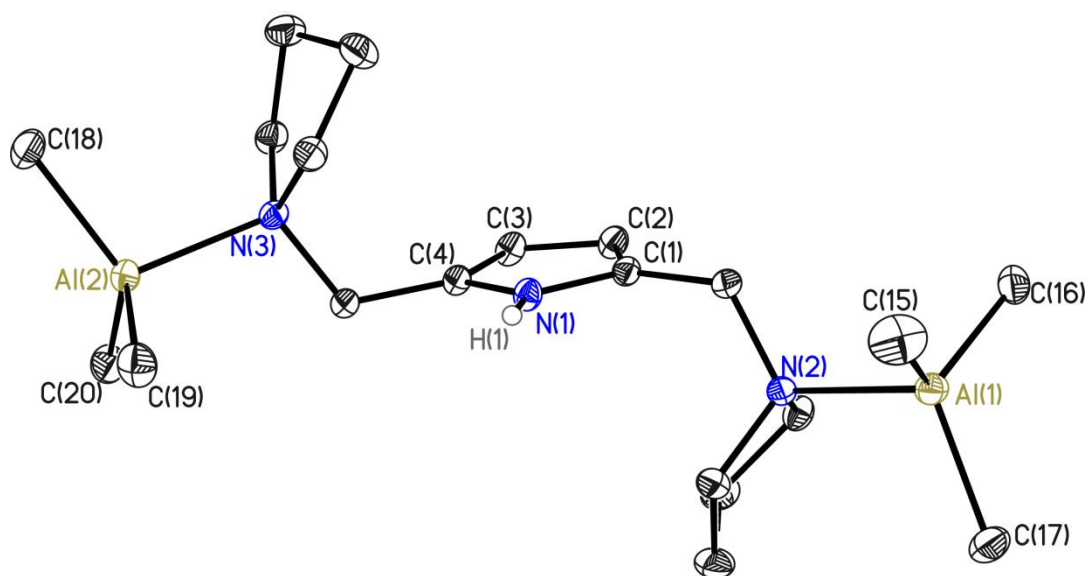


Figure 29. Crystal structure of 2,5-bis((pyrrolidino)methyl)pyrrole · 2 trimethylaluminium (**11**). Thermal ellipsoids are depicted at the 50% probability level, hydrogen atoms, besides H1 which was freely refined, are omitted for clarity.

It is somehow surprising that treatment of the free ligand with trimethylaluminium did not lead to a deprotonation of the pyrrole nitrogen atom as it occurred using the slightly smaller ligand 2,5-bis((dimethylamino)methyl)pyrrole. Comparing the pK_a values of the corresponding species it becomes even more curious. With a pK_a of 17.8,²⁷ pyrrole is comparable to ethanol (15.5)²⁷ concerning acidity and in sharp contrast to main group organometallic species who are among to the most basic compounds with pK_a values of about 50.¹⁰⁹ Thus there must be some kinetic effect present that prevents the compound from reacting to the thermodynamically most stable product, the dimethylaluminium-pyrrolide. Regarding bond lengths and angles of **11**, it becomes

apparent that C19 is slightly different from the other methyl groups. It forms the longest Al–C bond of all aluminium bonded methyl groups and the smallest N–Al–C angle in **11** (Table 12). Investigation of the crystal structure with regard on C19 afforded that compound **11** dimerizes through interaction of C19 with H1 of a neighboring molecule.

Table 12. Bond lengths and angles at the aluminium atoms in **11**.

Bond length [pm]		Bond Angle [°]	
Al1–C15	197.59(7)	N2–Al1–C15	103.69(3)
Al1–C16	198.59(6)	N2–Al1–C16	103.30(2)
Al1–C17	198.68(7)	N2–Al1–C17	105.59(2)
Al2–C18	198.38(7)	N3–Al2–C18	104.59(2)
Al2–C19	199.04(6)	N3–Al2–C19	102.90(2)
Al2–C20	197.52(6)	N3–Al2–C20	104.59(2)

This assumption is confirmed by the *Hirshfeld* surface⁸² analysis, indicating intermolecular H–H and C–H interactions (Figure 30). C19 is highly negative polarized as it is bonded to an electropositive aluminium(III) ion. It interacts with the positive polarized hydrogen atom bonded to the pyrrole nitrogen atom of a neighboring molecule. But instead of the expected methane evolution leading to the

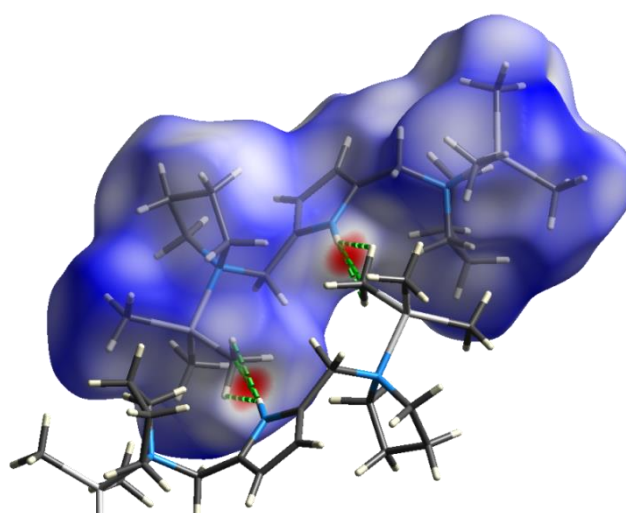
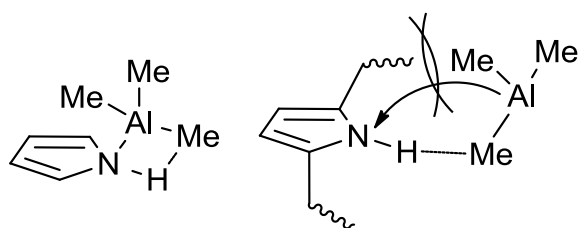


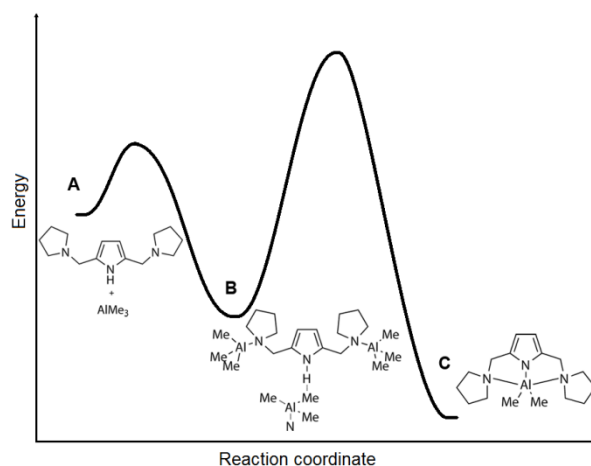
Figure 30. *Hirshfeld* surface of compound **11**, including the interactions with a neighboring molecule.

{*NNN*}AlMe₂ compound a stable dimeric compound is formed. The bulkier pyrrolidine groups (with respect to dimethylamine) prohibit the formation of a four-membered ring as is necessary for a cyclometallation¹¹⁰ reaction (Scheme 38). In Scheme 40 the energy



Scheme 38. Left: Transition state of a cyclometallation reaction. Right: The bulky side arms do not permit the essential arrangement for the cyclometallation reaction.

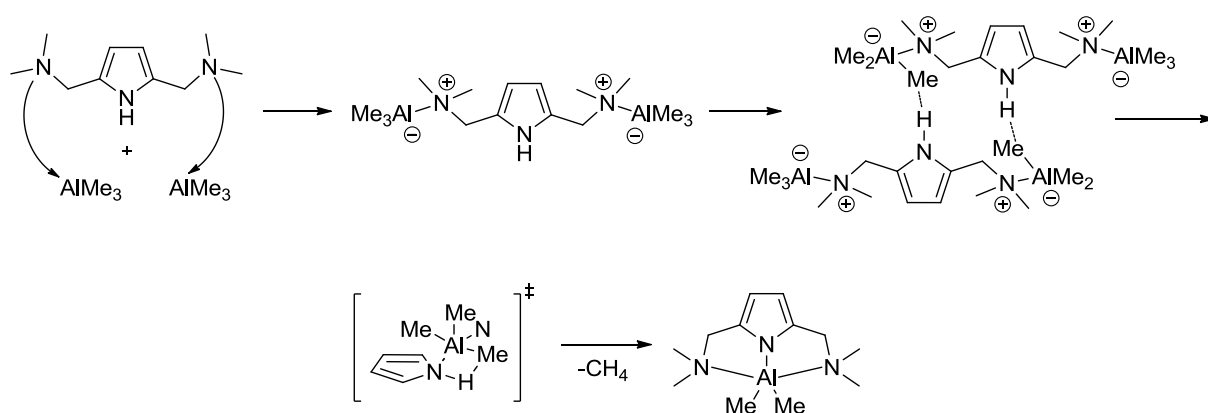
profile of such a cyclometallation reaction is shown schematically. The transition state on the way to the thermodynamic product (**C**) could not be passed and consequently the intermediate product (**B**) was crystallized. As almost the complete amount of trimethylaluminium



Scheme 40. Schematic depiction of the energy profile of the unsuccessful cyclometallation of **2** using trimethylaluminum.

was consumed by the formation of **11** the energy value of the intermediate compound must be lower than the corresponding value of the starting materials. The observed N-H \cdots CH₃ interaction could be the reason for the stabilization of **11**. With the C19-H1 distance being 251.2(9) pm long and the N1-H1-C19 angle of 172.7°, it is among the shortest intermolecular CH₃ \cdots H distances reported in the CSD until today.

Remarkably, there are exclusively C-H \cdots N interactions present in literature where nitrogen acts as the acceptor and not even one report of a R-H₃C \cdots H-N interaction with carbon as the base. Thus this interaction cannot be compared to related structures and theoretical calculations have to be done in the future to evaluate this interaction in detail.



Scheme 39. Proposed mechanism for the cyclometallation of **1** using trimethylaluminum.

The discovery of the intermediate compound facilitates the formulation of a reaction mechanism for the cyclometallation of the pyrrole based pincer ligand using trimethylaluminum. In combination with the known cyclometallation transition state, the following mechanism is proposed (Scheme 39). In a first step, trimethylaluminum precoordinates at the side arm nitrogen donor atom. One of the methyl moieties then orientates towards the pyrrole NH proton of a neighboring molecule which results in a dimerization. Finally, with side arms as small as dimethylamino groups the side arm can rotate and place the aluminium atom in close approximation to the pyrrole nitrogen

atom of the neighboring molecule to form a four membered ring. Methane is cleaved off from the four membered ring and the dimethylaluminium moiety coordinates to the deprotonated ligand to form the desired $\{NNN\}AlMe_2$ compound.

3.3.3 Indium-dibromo-{2,5-bis((pyrrolidino)methyl)pyrrolide} (12)

After having successfully prepared the lighter group 13 pincer complexes a heavy group 13 metal should be coordinated by 2,5-bis((pyrrolidino)methyl)-pyrrole (**2**) to investigate the interactions of the pyrrole based pincer ligand with a fifth row group 13 element. However, the reaction afforded non identifiable set of signals in the ^1H -NMR spectra. A tiny crystal could be taken from the precipitated solid obtained after storage of the filtrate for four weeks at -28°C which was suitable for single crystal X-ray diffraction experiments. Compound **12** crystallizes in the monoclinic space group $P2_1/c$, containing a whole molecule in the asymmetric unit.

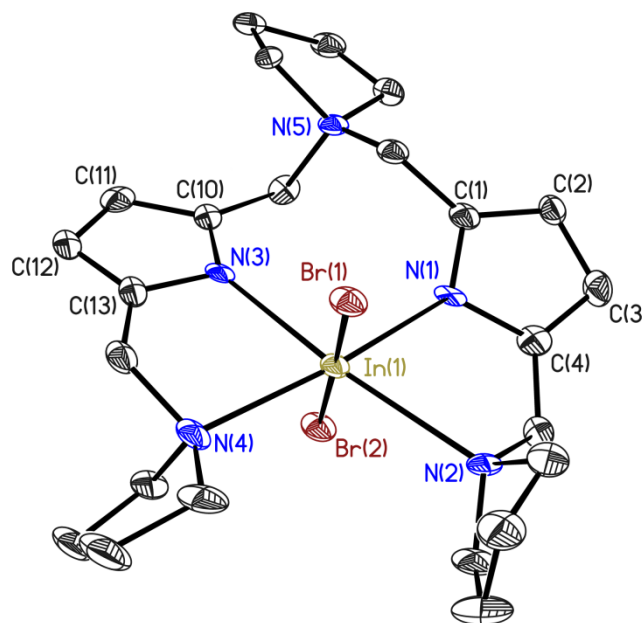
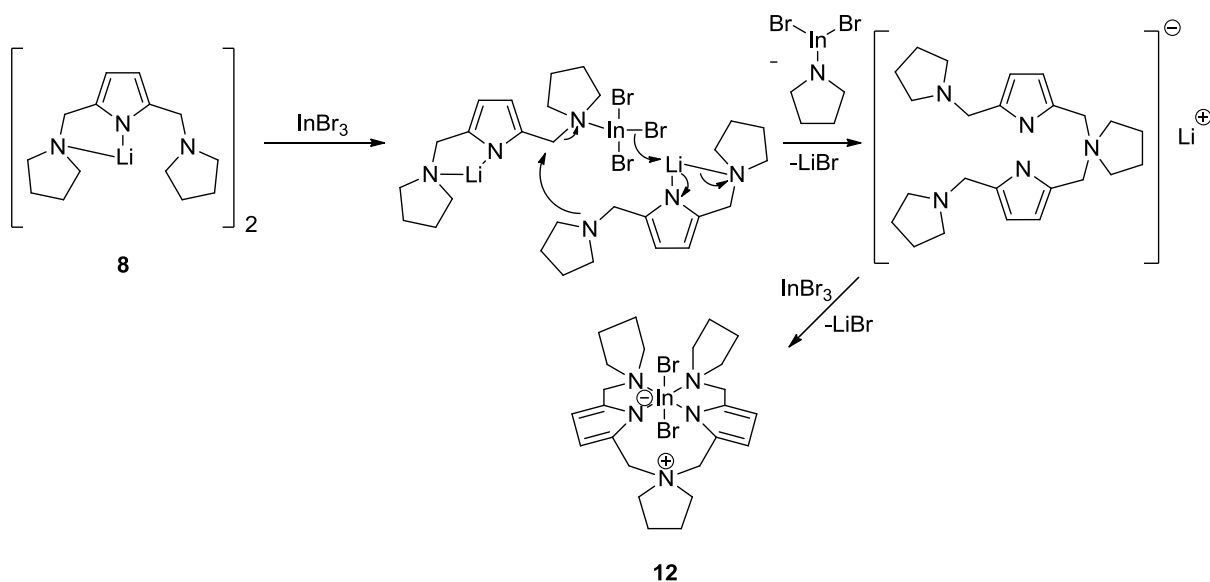


Figure 31. Crystal structure of compound **12**. Thermal ellipsoids are depicted at the 50% probability level, hydrogen atoms are omitted for clarity.

The data quality is rather poor and does not allow a discussion of bond lengths in detail. The coordination geometry at the indium ion is slightly octahedral distorted. The bromide ions are arranged in an almost linear fashion ($\text{Br-In-Br } 176.91(3)^\circ$) and the four nitrogen atoms chelate the indium ion in a nearly planar geometry (sum of angles 360.2°). Nonetheless the nitrogen atoms of the ligand coordinate to the indium atom in an asymmetrical manner thus distorting the octahedron. N1 and N2 form bonds of different lengths to the indium ion whereas the bond lengths of N3 and N4 to In1 are quite similar which causes the distortion.

However **12** turned out not to be the desired product.. It must have been formed in a decomposition mechanism (Scheme 41) starting from the indium(III)bromide adduct to one of the ligands side arms, as it was observed for **11**.



Scheme 41. Possible decomposition mechanism leading to **12**.

The coordination of indium seems to withdraw considerable amounts of electron density polarizing the neighboring methylene carbon atom to be rather positive. Thus, a nucleophilic attack of another ligand molecule via the pyrrolidine side arm moiety could occur, resulting in the mono-lithium salt. This compound undergoes a salt elimination reaction with another indium(III)bromide molecule, yielding **12**.

3.4 Group 14 Metal Pincer Complexes

Group 14 metal complexes have particularly attracted interest of many research groups worldwide because of their unusual frontier orbital situation with respect to other main group compounds (Chapter 1.3). Several group 14 species have been prepared within this thesis to further investigate their reactivity.

3.4.1 Silicon-dichloro-hydrido-{2,5-bis((pyrrolidino)methyl)-pyrrolide} (**13**)

By adding trichlorosilane to a solution of the lithium pyrrolide, the desired silicon(IV)-pincer complex could be prepared. Single crystals suitable for X-ray diffraction experiments could be obtained, after storing a toluene solution of **13** for a month at $-40\text{ }^{\circ}\text{C}$.

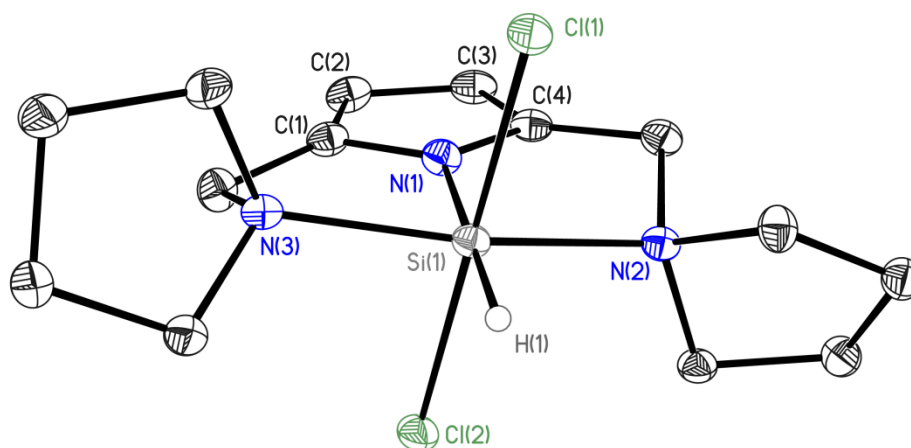


Figure 32. Crystal structure of silicon-dichloro-hydrido-2,5-bis((pyrrolidino)methyl) pyrrolide (**13**). Thermal ellipsoids are depicted at the 50% probability level, hydrogen atoms, with exception of the silicon bonded H1, which was freely refined, are omitted for clarity.

13 crystallizes in the monoclinic space group $P2_1/c$ with one molecule enclosed in the asymmetric unit. The coordination geometry at the silicon atom is a distorted octahedron. The linkers connecting pyrrole and pyrrolidine are too short to allow a linear arrangement of N3–Si1–N2 ($164.61(5)^{\circ}$), which consequently distorts the octahedron. The Cl1–Si1–Cl2 angle ($178.11(2)^{\circ}$) as well as the N1–Si1–H1 angle ($178.9(9)^{\circ}$) are almost linear and the sum of angles at Si1 (360.03°) indicates a perfectly planar arrangement of the ligand and the hydrogen atom. The ligand coordination is highly symmetric with similar pyrrolidine-silicon bonds ($206.88(14)\text{ pm}$ and $207.23(14)\text{ pm}$). With a N1–Si1 bond length of $174.72(14)\text{ pm}$ this bond is an average nitrogen–silicon bond when compared to related structures within the CSD. Among the compounds containing six-fold coordinated silicon atoms the N1–Si1 bond in **13** is fairly short which is further illustrated in Figure 33.

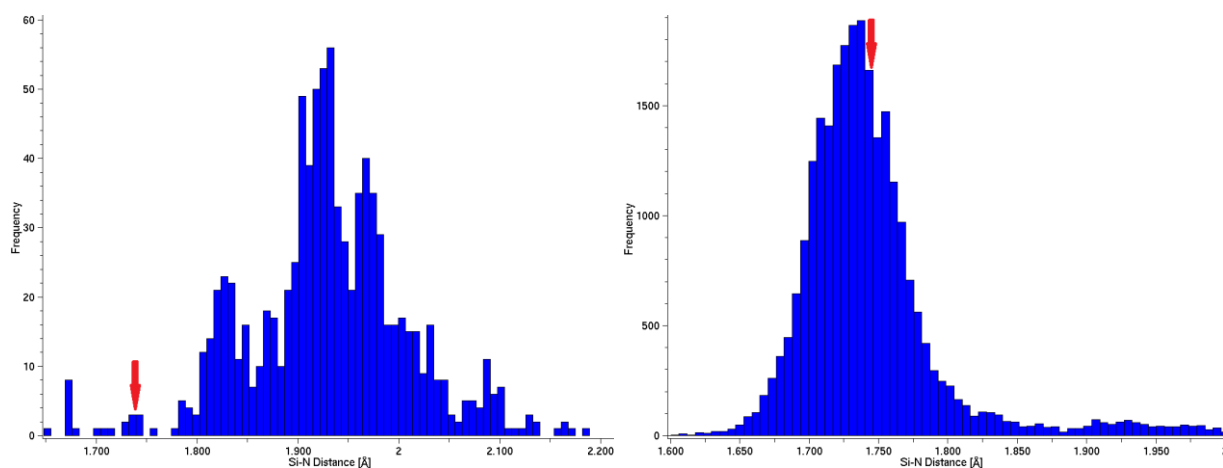
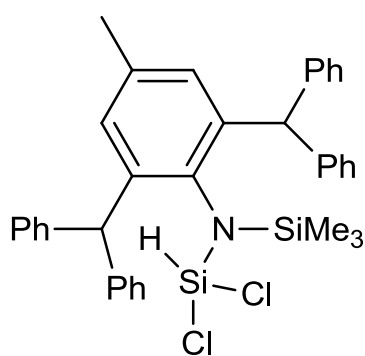


Figure 33. Silicon–nitrogen bond lengths reported in the CSD for six-fold coordinated silicon (left) and for all coordination numbers (right).

There is only one compound similar to **13** published in literature, however, the data quality of the corresponding crystal structure does not permit a detailed structure comparison.¹¹¹ Another related compound containing the neutral HSiCl_3 moiety coordinated by a TMEDA solvent molecule¹¹² can hardly serve for structural comparison due to substantial structural and electronic differences. *Jones et al.* published a compound containing a HSiCl_2 moiety coordinated by a nitrogen atom that belongs to an amidic ligand (**14**). However, the coordination number at silicon is different to that in **13** (Scheme 42),¹¹³ and the bond lengths in **14** are also different to those in **13** (Table 13). The $\text{Si-N}_{\text{amide}}$ distance in **13** is about 1.4 pm shorter than the related bond in **14**. Remarkably the Si-Cl bond lengths differ by almost 25 pm. This surprising elongation of the Si-Cl bonds in **13** cannot be explained by a higher coordination number or crystal packing effects.



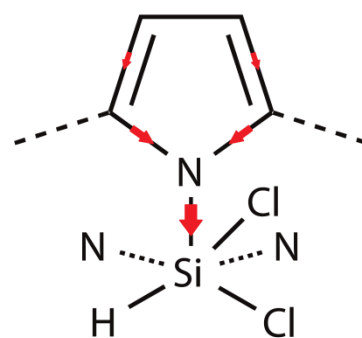
Scheme 42. Crystal structure of the silicon compound prepared by *Jones et al.* (**14**).

A close investigation of the ligand-metal orbital interaction should shed further light on the Si-Cl interaction as well as on the rather short N1-Si1 bond. Therefore the molecular orbitals of **13** were computed based on the crystal structure using the HF/6-31g* level of theory.¹¹⁴ The obtained occupied molecular orbitals do not explain the unusually long silicon–chlorine bond, as there are no hints towards an orbital interaction of the pyrrole π -system with the σ^* -orbital of the Si-Cl bonds. Nonetheless,

the changes in bond lengths within the pyrrole moiety can partially be explained by the withdrawal of electron density towards the highly *Lewis*-acidic silicon(IV) species via

the $N1_{sp^2} \rightarrow Si$ donation, leading to an elongation of the corresponding σ -bonds (Scheme 43).

This also provides an explanation for the short $N1-Si1$ bond in **13**. As the pyrrole heterocyclic system is supposed to be very electron rich high amounts of electron density can be withdrawn by the silicon atom which results in a short $Si1-N1$ bond. This phenomenon was already



Scheme 43. Schematic depiction of the electron withdrawal effect caused by the silicon atom in **13**.

observed for the aluminium compound and is present within all pincer complexes of the groups 13, 14 and 15 of the Periodic Table of the Elements (PTE), which have been prepared with this thesis. The concentration of electron density at the silicon ion compared to related silicon(IV) species is further confirmed by the ^{29}Si -NMR chemical shift, which is -90.3 ppm for compound **13** and rather shifted to high field with respect to the related compound **14** (-21.2 ppm).

Table 13. Comparison of selected bond lengths [pm] at the silicon atoms in compounds **13** and **14**.

Bond length [pm]	$\{NNN\}HSiCl_2$ (13)	$[(Ar)(TMS)N]HSiCl_2$ (14)
Si-N1 / Si-N2	174.72(14)	176.1
Si-Cl1	228.42(7)	205.5
Si-Cl2	229.47(7)	203.1
Si-H1 / Si-H37	139(2)	140.8

This withdrawal of electron density, as mentioned in chapter 3.1.1 could slightly elongate the formal double bonds of pyrrole but it cannot affect the C2-C3 bond in a significant manner. The C2-C3 bond length can, similar to that of compound **10**, only be explained by a π -donation from an occupied pyrrole π -orbital into σ^* -orbitals of the corresponding Si-Cl bonds. In combination with the withdrawal of electron density, the observed pyrrole C-C bond lengths mirror the result of both effects (Table 14).

Table 14. C-C bond lengths within the pyrrole heterocycle in **13** and **8**.

Bond length [pm]	$\{NNN\}HSiCl_2$ (13)	$\{NNN\}Li$ (8)
C1-C2	138.2(2)	138.03(19)
C2-C3	143.5(3)	141.0(2)
C3-C4	138.1(2)	138.21(19)

Nevertheless, the effects discussed above still do not explain the extraordinarily long silicon-chlorine bonds (avg. Si-Cl distance in the CSD: 209.0 pm) as there are no orbital

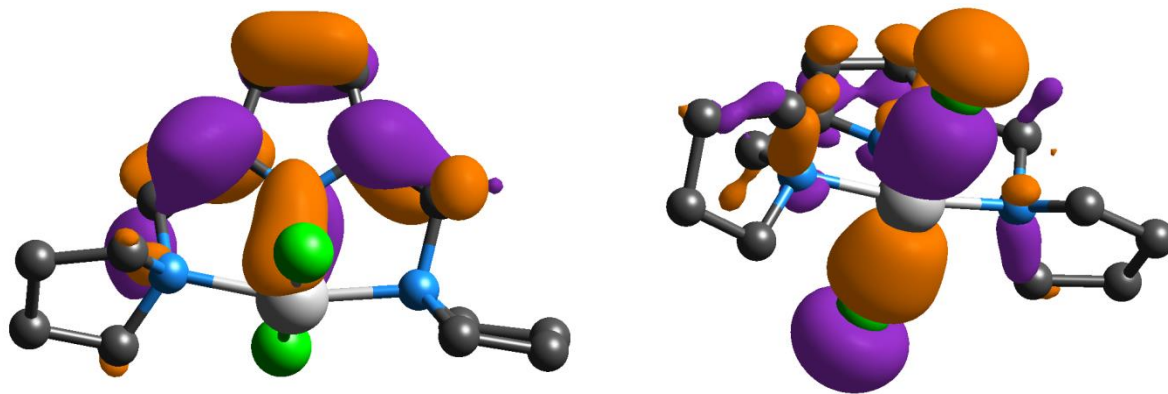


Figure 34. Left: LUMO of compound **13**. Right: HOMO-8 of compound **13**, both are depicted at the 0.04 au isovalue and computed using the HF/6-31g* level of theory.¹¹⁴

interactions causing a depletion of electron density of the Si-Cl σ -orbital. However, they give a hint to what may be the reason for this unusual bond length. In Figure 34 (right) HOMO-8 unambiguously shows that the chlorine atoms are interacting with the same silicon p-orbital. This phenomenon is called the *trans-effect*¹¹⁵ and weakens the bonds of the opposing chlorine atoms to the silicon ion. In a tetrahedral environment like in **14**, this *trans-effect* is absent and the related Si-Cl bonds are considerably shorter than in **13**. Another, assumingly weaker, impact on the Si-Cl bond has the LUMO of **13** (Figure 34, left). The antibonding pyrrole π -orbital overlaps with the p-orbital at silicon which is involved in the Si-Cl σ^* -orbital. When using a lower isovalue the orbital coefficients of the Si-Cl σ^* -orbital appear at the chlorine atoms but for clarity reasons an isovalue of 0.04 was chosen in Figure 34. According to the shape of the LUMO a population would strengthen the N1-Si1 bond and simultaneously weaken the Si-Cl bonds. However, as the occupation of the LUMO would shorten the formal single bond in the pyrrole heterocycle the π -back donation cannot be significant. The only effect that would be in good agreement with the experimentally observed pyrrole bond lengths is, as mentioned before, a π -donation via the N1_{pZ} orbital.

Investigation of the intermolecular interactions to detect long distance interactions of chlorine, similar to those of the lead structure (chapter 3.4.4), could be another source for the Si-Cl bond elongation. Using the *Hirshfeld* surface⁸² revealed that there are no intermolecular interactions present for both chlorine atoms. Furthermore, the whole molecule does only show weak intermolecular dispersion forces being responsible for the molecule packing in the crystal. Thus, it should be possible to alter the crystal structure by varying the crystallization conditions (temperature, solvent etc.). By removing the solvent from a toluene solution of **13** and subsequently storing the oily

residue at room temperature for three days, single crystals different from those gained at $-40\text{ }^{\circ}\text{C}$ could be obtained.

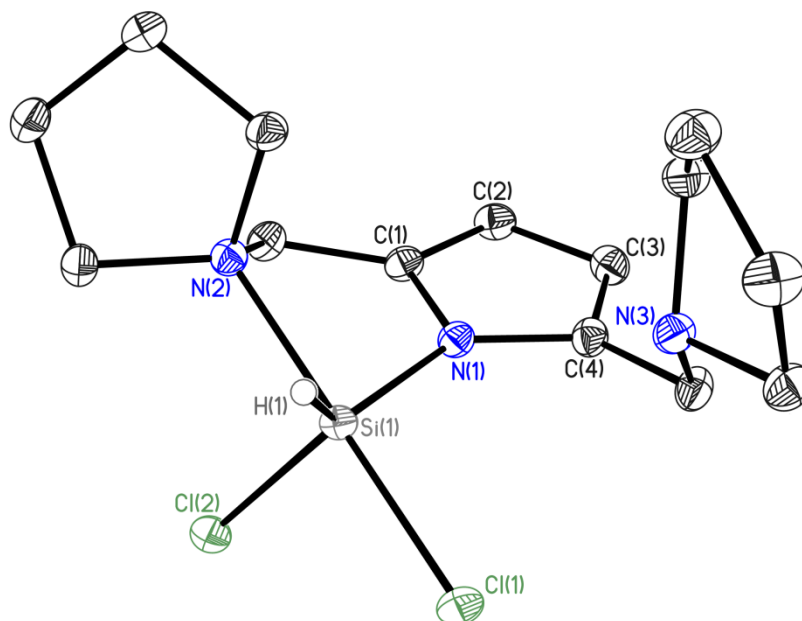


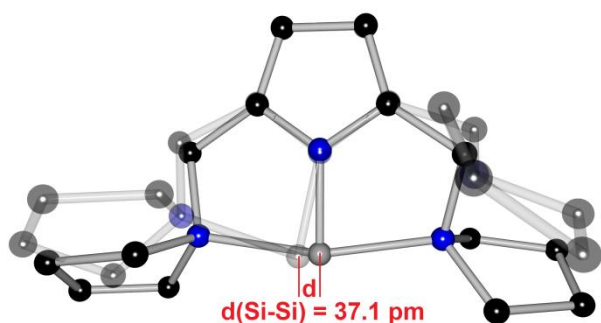
Figure 35. Crystal structure of silicon-dichloro-hydrido-2,5-bis(pyrrolidino)methylpyrrolide (**13a**). Thermal ellipsoids are depicted at the 50% probability level, hydrogen atoms, with exception of the silicon bonded H1 which was freely refined, are omitted for clarity.

13a crystallizes in the monoclinic space group $P2_1/n$ having one molecule in the asymmetric unit. It is astonishing that **13a** shows a different solid state structure than **13** as they contain identical molecule fragments, namely the pyrrolide ligand and the HSiCl_2 moiety. One of the pyrrolidine side arms does not take part in silicon coordination in **13a** reducing the Si-coordination number from six to five. Consequently, the coordination geometry changes from octahedral to trigonal bipyramidal. The triangular plane is formed by N1, H1 and Cl1 (sum of angles at Si1: 357.85°) and N2 and Cl2 form the tips of the bipyramid with a Cl2–Si1–N2 angle of 178.82° . Although the composition of the compounds **13** and **13a** is identical, the bond lengths of the corresponding structures differ significantly (Table 15).

Table 15. Selected structural parameters of **13** and **13a** in comparison with **14**.

Bond length [pm]	{NNN}HSiCl ₂ (13)	{NN}HSiCl ₂ (13a)	14
C1–C2	138.2(2)	136.78(11)	---
C2–C3	143.5(3)	142.66(12)	---
C3–C4	138.1(2)	137.10(11)	---
N1–Si1	174.72(14)	177.23(7)	176.1
Si1–Cl1	228.42(7)	210.34(4)	205.5
Si1–Cl2	229.47(7)	217.28(12)	203.1
Si1–H1	139(2)	136.3(14)	140.8
N2–Si1	Avg. 207.06	204.46(7)	---

The shorter and asymmetric Si–Cl bonds in **13a** (210.2 pm and 217.6 pm, respectively) represent the most apparent difference between **13** and **13a**. Additionally, the Si1–N1 bond is slightly elongated and all C–C bonds within the pyrrole heterocycle are shortened by app. 1 pm. This can be explained by slightly less N1_{pZ}→σ*(Si–Cl) π -

**Figure 36.** Overlay graphic of **13** (dark) and **13a** (light), showing the shift of the silicon atom.

donation, causing the slight shortening of the C2–C3 bond and by a more distinct weakening of the N1_{sp2}→Si donation which diminishes the electron withdrawal and thus causes a shortening of the formal double bonds. A structural feature in **13a** that can serve to explain the changes within the pyrrole unit as well as the elongation of the N1–Si1 bond is the in-plane shift of the silicon atom towards one of the side arms (Figure 36). This would reduce the overlap of the N1 sp²-orbital with the Si1 sp²-orbital resulting in an elongation of the N1–Si1 bond. Consequently, the electron withdrawal from the pyrrole σ -orbitals towards Si1 is reduced. The loss of electron density at the silicon atom is compensated by a stronger donation of the coordinated pyrrolidine. The N2–Si1 bond is 204.46(7) pm long which is an avg. shortening of 2.4 pm compared to the pyrrolidine–silicon bonds in **13**.

The shortening of the chlorine–silicon bonds in **13a** is primarily caused by the coordination geometry. In the octahedral environment in **13** both chlorine atoms are located on opposing sites of the silicon atom with the *trans-effect* elongating the corresponding Si–Cl bonds. In **13a** however, only one of the chlorine atoms (Cl2) is

subjected to the *trans*-effect being located opposite to a pyrrolidine nitrogen atom (N2) with respect to the silicon atom. N2 seems to have a weaker *trans*-effect on Cl2 than Cl1 has on Cl2 in the octahedral compound **13**. This assumption is supported by a shorter Cl2–Si1 bond in **13a** compared to **13**. Cl1 is located in the triangular plane and consequently cannot be affected by the *trans*-effect. The same can be postulated for H1. Hence the Si1–H1 bond as well as the Si1–Cl1 bond are shorter in **13a** than the corresponding bonds in **13**.

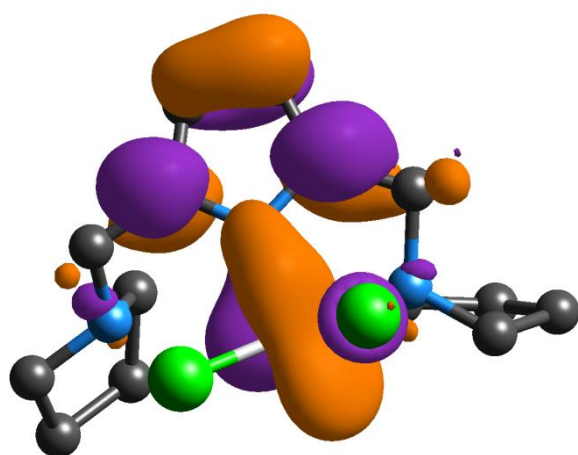


Figure 38. LUMO of compound **13a**, depicted at the 0.04 au isolevel. Computed using the HF/6-31g* level of theory.¹¹⁴

However, the Si1–Cl1 bond is still longer by app. 5 pm than the Si–Cl bonds at the tetrahedral coordinated silicon atom in compound **14**. The Si1–Cl1 bond is arranged almost coplanar to the N1_{p_z} orbital and quantum mechanical calculations using the HF/6-31g* level of theory¹¹⁴ confirmed that the antibonding pyrrole π -orbital overlaps with the σ^* -orbital of the Si1–Cl1 bond (Figure 38).

This effect cannot be quantified however, it should have only a minor effect on the Si1–Cl1 bond. It is usual that in a compound containing five-fold coordinated silicon, the avg. Si–Cl bonds are longer than in those compounds containing silicon atom which has only four coordination sites, which is a trend throughout all structures of the CSD. Taking this into account a significant elongation by an occupation of the LUMO of **13a** becomes doubtful.

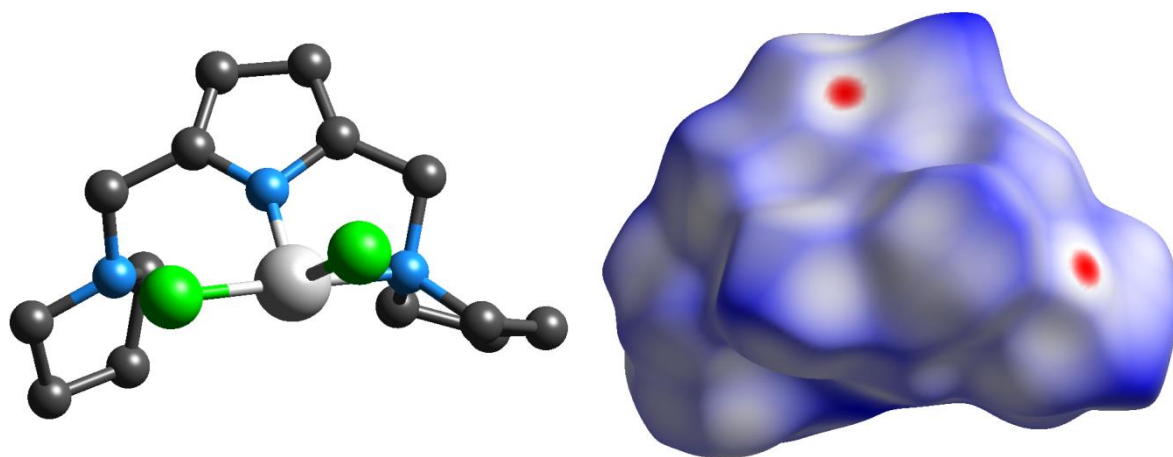


Figure 37. Molecule orientation of **13a** (left) within the *Hirshfeld* surface (right).

Careful investigation of the molecular structure and the computed molecular orbitals does not give a hint why this crystal structure is favored over the coordination mode in **13** at the described crystallization conditions. However, the *Hirshfeld* surface⁸² analysis using the *Crystal Explorer*⁸⁰ program revealed an intermolecular $\eta^1\text{-C-H}\cdots\pi$ interaction. A side arm of a neighboring molecule is arranged on top of the pyrrole π -system, with one of the CH-bonds pointing towards a carbon atom of pyrrole (Figure 37, Figure 39). The $\text{C-H}\cdots\text{C}$ angle with 164.92° indicates a rather linear arrangement. Combined with the $\text{C}\cdots\text{H}$ bond length of 270.2 pm this interaction can be considered structure determining.

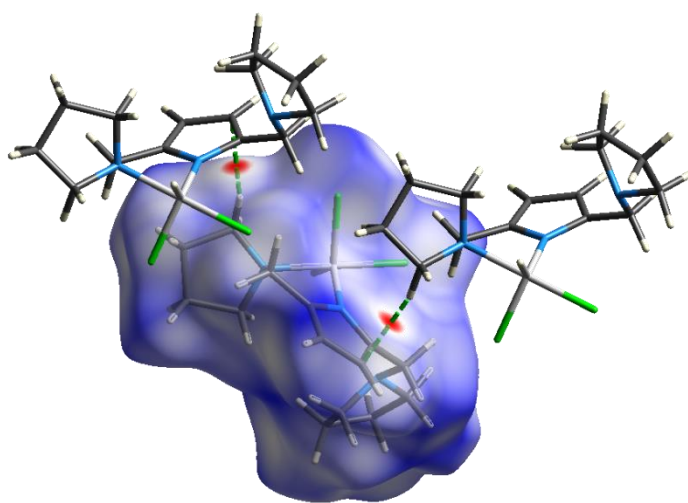


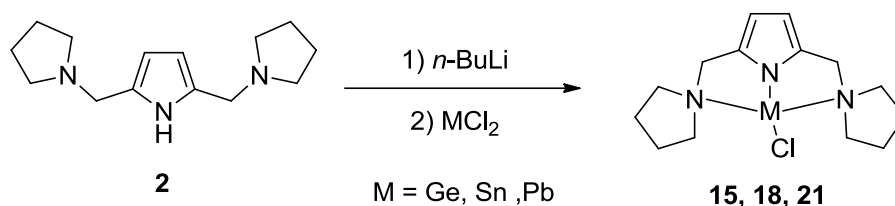
Figure 39. *Hirshfeld* surface of compound **13a**, including short contacts to neighboring molecules.

As already discussed investigating the $\text{C-H}\cdots\pi$ bonding within the aluminium structure these interactions are worth 2-6 kcal/mol depending on the carbon bonded substituents. Therefore, the octahedral coordination in **13** must overcompensate this stabilization energy, otherwise **13** would not be a stable coordination motif for

$\{\text{NNN}\}\text{HSiCl}_2$. Due to the different crystallization conditions, a diluted toluene solution causing a very slow crystallization was used to yield **13** whereas **13a** was obtained after solvent removal in a very rapid crystallization process. **13a** is considered to be the kinetic crystallization product and **13** the thermodynamic one. This phenomenon is unknown in literature and is reported for the first time within this thesis. To confirm this assumption, high level theoretical computations were conducted by *R. A. Mata*.

In order to compare the stability of the five- and six-fold coordinated isomers, the Gibbs free energy at 298.15 K was calculated, based on the B3LYP-D3¹¹⁶/def2-TZVP¹¹⁷ geometry optimized structures, computing the electronic energy at the MP2¹¹⁸/CBS[3:4] level of theory using the *Orca* program package⁹³ and the *Molpro2012.1* program package.⁹⁵ The energy difference between the two isomers is relatively small. Including the thermodynamic and electronic corrections a ΔG value of 7.8 kJ/mol (gas phase) is obtained, with the six-fold coordinated isomer being more stable approving the six-fold coordinated isomer to be the thermodynamic crystallization product.

3.4.2 Germanium-chloro-{2,5-bis((pyrrolidino)methyl)-pyrrolide} (15)



Scheme 44. Synthesis of low valent group 14 pincer complexes.

In chapter 3 of the introduction the importance of energetically close lying frontier orbitals was already pointed out, however, those species have been prepared in a rather complicated synthesis. In contrast, the pyrrole based pincer ligand provides a simplification of the synthetic access to the low valent group 14 species (Scheme 44) but should generate a similar frontier orbital situation by a pyrrole-metal π -interaction. In the following chapters, these group 14 complexes will be investigated with a focus on the metal-ligand π -interaction.

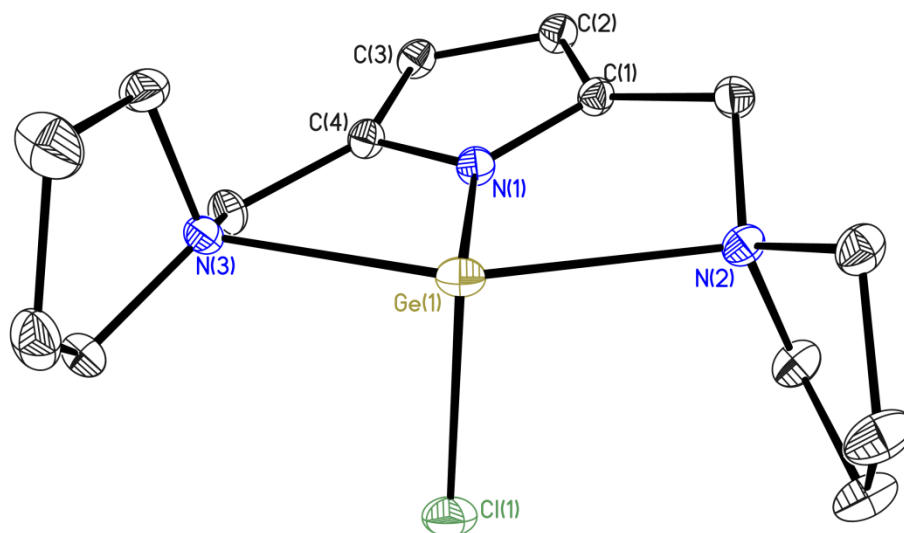


Figure 40. Crystal structure of germanium-chloro-[2,5-bis(pyrrolidino)methyl]pyrrolide (15). Thermal ellipsoids are depicted at the 50% probability level, hydrogen atoms are omitted for clarity.

15 crystallizes as a racemic twin in the tetragonal space group $I\bar{4}$ with a whole molecule in the asymmetric unit. The geometry at the germanium atom is distorted trigonal bipyramidal with a stereochemically active lone pair in the triangular plane, proving germanium to be in the oxidation state +2. The N2–Ge1–N3 angle with $147.59(3)^\circ$ describes the typical convex shaped {NNN} metal coordination of the pyrrole based pincer ligand. With an N1–Ge1–Cl1 angle of $98.49(3)^\circ$ the lone pair occupies approximately 163.02° within the N1–Ge1–Cl1 plane. The germanium ion is coordinated

in an asymmetrical fashion by the pyrrolidine side arms and seems to be wrong in size, as the smaller silicon(IV)-ion and the bigger tin(II)-ion clearly fit better into the coordination pocket of the pincer ligand. With bond lengths of 249.78(9) pm for Ge1–N2 and 238.01(10) pm for Ge1–N3 they differ by more than 10 pm which is remarkable as they are chemically equivalent in the crystal structure.

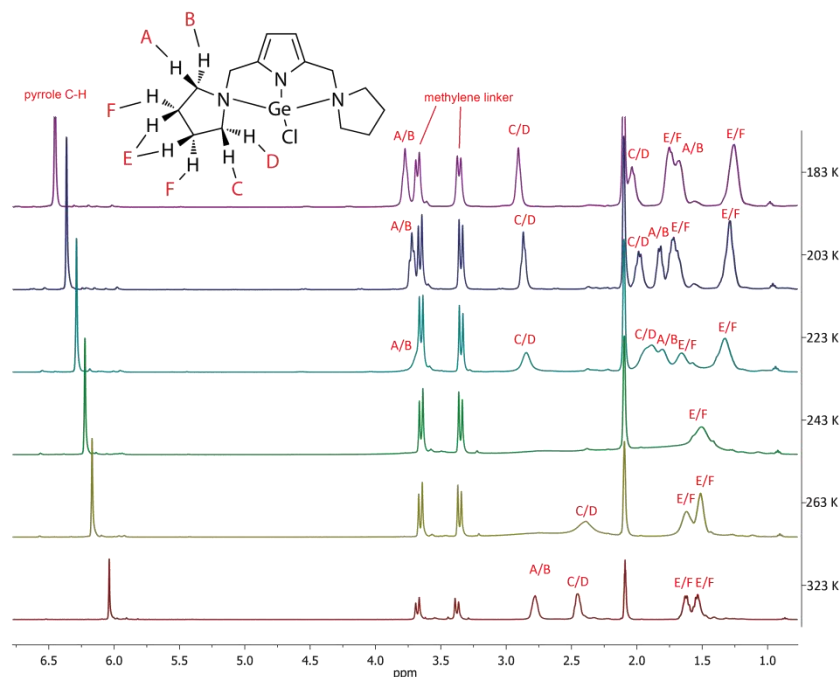


Figure 41. Variable temperature ^1H -NMR spectra of compound **15**, recorded from dissolved crystals of **15** in Tol- d_8 .

Figure 41 shows non fluctuating behavior for the methylene protons of compound **15**. They are forming two stable doublets at chemical shifts between 3.0 ppm and 4.0 ppm. In contrast, the methylene protons of the lithium compound (**8**) show a broad singlet at room temperature explained by a flipping of the linker. The coordination in **15** seems to be quite rigid. Even at the elevated temperature of 323 K the methylene protons still show two sharp signals. Instead, the pyrrolidine moieties show a fluctuating behavior of the envelope conformation. At 323 K the pyrrolidine moieties show four signals. Each CH_2 group can be assigned to an individual chemical shift. Upon cooling, the appearance of the spectra considerably changes. At approximately 243 K the coalescence temperature is reached. The former four signals split into six signals at 183 K. Each CH_2 group is now split into one signal for the equatorial and one for the axial position, however, the chemical shift of the equatorial (E) and the axial (F) protons at the 3- and 4- position is equivalent.

Finally, these ^1H -NMR spectra confirms the solid state structure to be present in solution as well, which is also valid for the prepared tin and lead compounds. Consequently, inferences could be drawn about the reactivity in solution by investigation of the crystal structure.

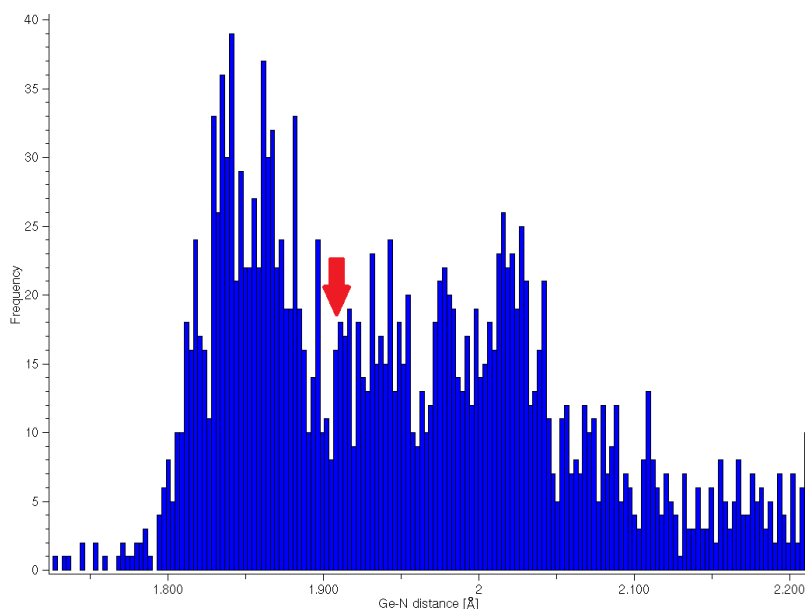
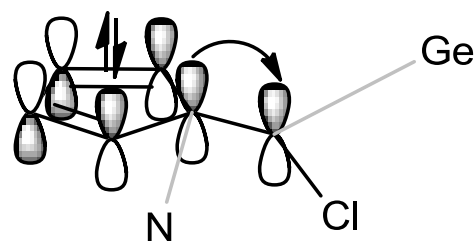


Figure 42. Germanium–nitrogen distances of all germanium containing structures reported in the CSD.

germanium(IV) species or extraordinary low coordination numbers at the germanium ion (Figure 42), which comprise shorter metal-nitrogen bonds than a four-coordinated germanium(II) species. In low valent group 14 pincer complexes another effect increases the pyrrole metal interaction: Orientation of the metal lone pair coplanar to the $\text{N}1_{\text{pz}}$ orbital and therewith the pyrrole π -system will cause an overlap of the metal lone pair with the pyrrole π -system if the corresponding orbitals are of similar energy (Scheme 45). A resulting ligand-metal π donation as well as a metal-ligand π -back donation would further shorten the $\text{N}1\text{--Ge}1$ bond.



Scheme 45. Ligand-metal π -donation in **15**.

In most of the pyrrole based pincer complexes the pyrrole–M bond is quite short compared to compounds containing similar bonds. The $\text{Ge}1\text{--N}1$ bond with a length of $190.95(9)$ pm is considered to agree to this observation. Most of the compounds listed in the CSD, containing a shorter Ge–N bond than compound **15** consist of a

Table 16. Selected parameters of the high resolution dataset of **15**.

Max. resolution	0.44 Å
$R1 (I > 2\sigma(I))$	1.76%
wR2 (all data)	4.22%
Data/ $R(\text{int})$	9581/3.74%
Parameter	173

It is described in chapter 1.2 how a ligand-metal π -interaction would affect the bond lengths within the pyrrole heterocycle. To experimentally quantify these interactions a high resolution X-ray diffraction dataset of **15** was collected (Table 16). From this dataset it was possible to obtain a standard deviation for the C–C bonds in pyrrole as low as 0.14 pm, which is an essential requirement for discussing changes in bond length of a few picometers. The C–C bond lengths within the pyrrole heterocycle in compound **15** show values of 137.74(13) pm and 137.91(13) pm for the formal C=C double bonds and a value of 143.48(14) pm for the corresponding C–C single bond. According to the frontier orbital scheme of pyrrole (Scheme 6) π -donation from the ligand towards the metal should have caused an elongation of the single bond and a shortening of the double bonds within the pyrrole heterocycle. However, the double bonds remain almost unchanged compared to the lithiated ligand whereas the single bond length is in agreement with a ligand→metal π -donation (Table 17). With the withdrawal of electron density towards the germanium ion, the shortening of the formal C=C double bonds of pyrrole caused by the mentioned π -donation is counterbalanced. A metal→ligand π -back donation can be excluded as well. This kind of π -interaction would shorten the C–C single bond in pyrrole which in contrast is shown to be significantly elongated.

Table 17. Comparison of C–C bond length within the pyrrole moiety in compounds **15** and **8**.

Bond length [pm]	{NNN}GeCl (15)	{NNN}Li (8)
C1-C2	137.74(13)	138.03(19)
C2-C3	143.48(14)	141.0(2)
C3-C4	137.91(13)	138.21(19)
$\Delta_{\text{SB-DB}}$	5.7	2.9

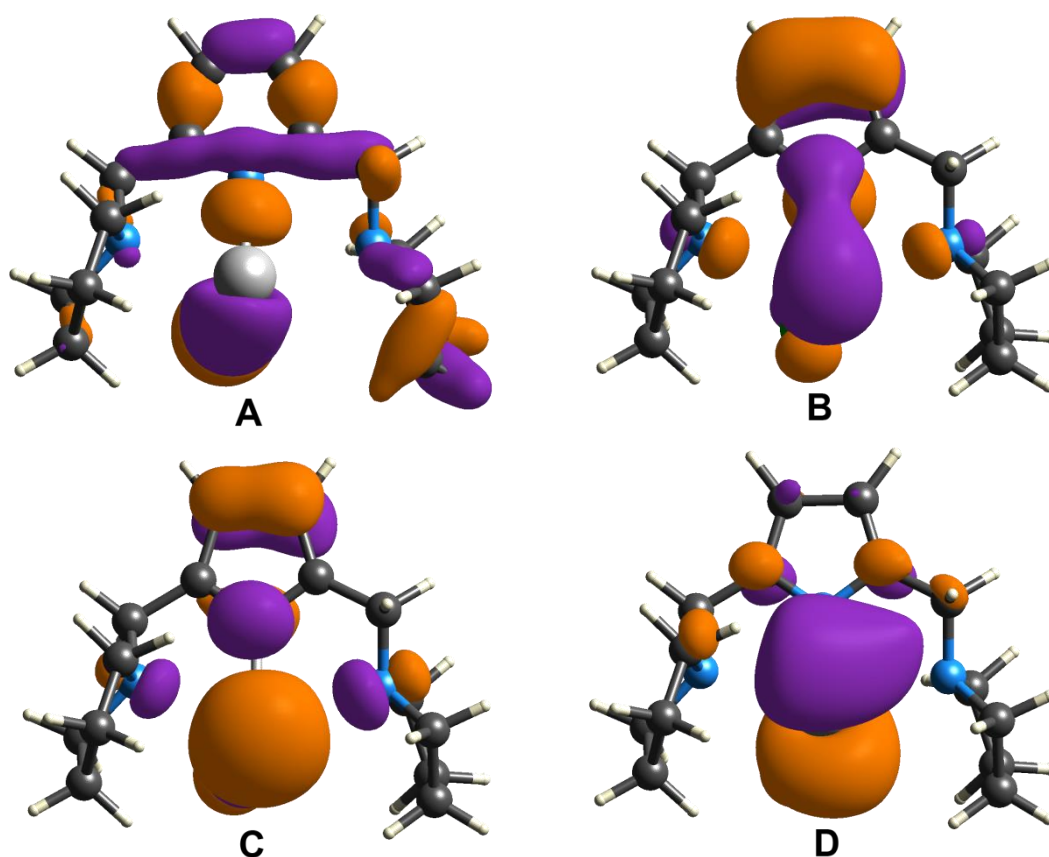


Figure 43. Selected molecular orbitals of **15**, computed using quantum mechanical methods on the HF/cc-pVDZ⁹⁷ level of theory. A: HOMO-8; B: HOMO-2; C: HOMO-1; D: LUMO.

To prove this assumption the molecular orbitals of **15** were computed using quantum mechanical calculations based on the HF/cc-pVDZ⁹⁷ level of theory (*Crystal Explorer*⁸⁰ program). The energetically low lying σ -orbitals of the pyrrole backbone confirm the thesis of a withdrawal of electron density from the pyrrole σ -bonds towards the germanium ion (Figure 43, **A**). HOMO-8 unambiguously shows the participation of the σ -orbitals of the pyrrole C–C bonds in the $N1_{sp^2} \rightarrow M$ donation. A quantification of this effect is rather difficult as not only the degree of overlap determines the strength of the withdrawal, but also the *Lewis*-acidity of the metal species has a significant influence.

Investigation of the ligand-metal π -interaction revealed that HOMO-2 and HOMO-1 contain the bonding/antibonding combination of the overlap of the $N1_{p_z}$ -orbital with the lone pair at Ge1 (Figure 43, **B** and **C**). Thus these effects cancel out. Furthermore the LUMO shows a weak interaction of the Ge1–Cl1 σ^* -orbital with an unoccupied π -orbital of pyrrole (Figure 43, **D**). This would cause a shortening of the C–C single bond of pyrrole and an elongation of the corresponding C=C double bonds and is in contradiction to the observed changes in bond lengths.

For a more detailed investigation of the ligand-metal π -interaction high level computations were performed by *D. M. Andrada*.¹¹⁹ A ligand \rightarrow metal π -donation would lead to depletion of electron density in the pyrrole π -system. As a consequence, the aromaticity of the heterocycle should be less developed, experimentally monitored by the divergent C–C bond lengths of the pyrrole heterocycle. A computational value to investigate the aromaticity of a compound or a fragment within a compound is the NICS(0) (Nucleus Independent Chemical Shift) value.¹²⁰ It describes the absolute magnetic shielding at the center of the investigated ring structure and corresponds to the NMR chemical shift convention. A shielding effect at the ring center like in benzene is indicated by a high-field shifted value for the NICS(0) (NICS(0) for benzene: -9.7 ppm¹²⁰ (6-31+G* basis set)¹²¹). Anti-aromatic systems will yield a positive (down-field sifted) NICS(0) value. This magnetic shielding value is contaminated by the contribution of the σ -orbitals of C–C and C–H bonds of the cyclic system.¹²² This contribution can be minimized by computing the NICS(1) value which is based on the magnetic shielding 1 Å above the ring center. Furthermore the NICS_{zz} was developed which exclusively uses contributions to the magnetic field in Z-direction (out-of-plane component).¹²³ Further improvements on the NICS were made, but they drastically increase the computation time, while the use of the NICS(1)_{zz} already reveals highly precise results.^{120c}

Table 18. NICS(1)_{zz} values [ppm] for the anionic ligand and the germanium compound (**15**).

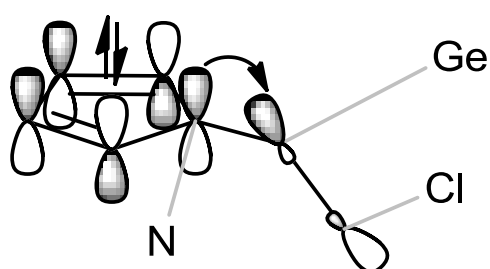
Compound	NICS(1) _{zz} [ppm]
{NNN} ⁻	$-30.2 / -29.8$
{NNN}GeCl	$-25.0 / -24.9$
Pyrrole	-31.8
Benzene	-28.7^{124}

The computed NICS(1)_{zz} values (Table 18) indicate a decrease in aromaticity through metal coordination. It drops from app. -30 ppm for the anionic ligand to about -25.0 ppm for the germanium compound (**15**). However, this significant change cannot be assigned to a specified orbital interaction within the molecule. It describes a less distinct π -system at pyrrole in **15** than in the anionic ligand which can be caused by π -donation effects or a loss of electron density through σ -interactions that affect the pyrrole π -orbitals.

Table 19. NBO results for compound **15**. Partial charges (Q) (in au) and occupation numbers (LP) (in au), Wiberg bond order (BO) and second-order acceptor-donor interaction energies ($\Delta E^{(2)}$) (in kcal/mol) are given.

Q(M)	LP(M)	LP(N1)	BO(N1-M)	$\Delta E^{(2)}$	
				LP(N1 _{pZ}) → LP*(M)	LP(N1 _{pZ}) → $\sigma^*(\text{M-Cl})$
1.042	1.978	1.544	0.456	1.08	6.0

To get an idea which effect exactly causes the change in the NICS(1)_{zz} value a Natural Bond Orbital (NBO) analysis⁹⁹ was conducted. Obtained values are listed in Table 19. It turned out that the metal charge is reduced by almost 1 au via ligand to metal electron donation. Almost half of this amount is contributed by the N1_{sp2} lone pair, the remaining electron density is donated by the pyrrolidine moieties and *via* π -donor-acceptor interaction of the pyrrole heterocycle and the germanium atom. A significant donation from the metal lone pair towards the antibonding pyrrole π -orbital can be excluded as this lone pair is almost fully occupied with 1.978 au. Shifting the focus to the N1-germanium π -interaction, namely the HOMO-2 and the LUMO, indicating a ligand-metal π -interaction via the N1_{pZ} orbital. The LP(N1_{pZ})→LP*(M) donation is equivalent to the interaction depicted in the HOMO-2 with the N1_{pZ} orbital donating electron density into



Scheme 46. Schematic drawing of the N1_{pZ}→ $\sigma^*(\text{M-Cl})$ donation in **15**.

an unoccupied orbital located at the germanium ion. However, with an energy benefit of app. 1 kcal/mol it can be considered rather weak. In contrast, the N1_{pZ}→ $\sigma^*(\text{M-Cl})$ donation, corresponding to the LUMO, is worth 6 kcal/mol (Scheme 46). This significant energy value should have consequences on the resulting structure. As

the germanium-chlorine σ^* -orbital is occupied, the corresponding Ge-Cl bond should be elongated. Related structures exclusively containing negatively charged ligands with nitrogen donor atoms show similar Ge-Cl bond lengths.¹²⁵ Thus the Ge-Cl bond in **15** does not seem to be unusually elongated.

The consequences of a N1_{pZ}→ $\sigma^*(\text{M-Cl})$ donation on the π -system are barely detectable, if at all. The orbital coefficients of the pyrrole π -system in the LUMO are tiny and in combination with the effect of the electron depletion via the N1_{sp2} lone pair that additionally affects the electron density of the heterocycle, it is impossible to quantify the consequences of the N1_{pZ}→ $\sigma^*(\text{M-Cl})$ donation on the pyrrole C-C bond lengths. The

fundamental requirement for this kind of interaction is an occupation of the LUMO. It is located energetically in the bonding area with an orbital energy of -0.23 eV (Table 20). This makes an occupation of the LUMO likely, however, the HOMO-LUMO gap of approximately 5 eV unambiguously contradicts a possible LUMO occupation. It is still most probable that the π -donation of an occupied pyrrole π -orbital towards the $\sigma^*(\text{Ge-Cl})$ orbital causes the experimentally observed bond lengths.

Table 20. Frontier orbital energies of compound **15**, computed using DFT calculations on the B3LYP⁹¹/cc-pVTZ⁹⁷ level of theory.

Orbital	HOMO-2	HOMO-1	HOMO	LUMO
Energy [eV]	-6.429	-5.915	-5.300	-0.230

The crystal structure of compound **15** contains two intermolecular interactions that have been identified using the *Hirshfeld* surface⁸² analysis of the *Crystal Explorer*⁸⁰ program (Figure 44). These contacts are $\eta^1\text{-C-H-}\pi$ interactions. The first interaction is formed by a CH moiety of a pyrrolidine side arm. The CH moiety is located below the heterocyclic plane of a neighboring molecule and points directly towards C4, displaying a H6B-C4 distance of 276.3 pm and a C6B-H6B...C4 angle of 157.1° . The second interaction is formed by a pyrrole CH moiety being located on top of a neighboring molecule, with the C3A-H3A bond pointing directly towards C4. Independent from the H3A-C4 bond length of 283.1 pm and a C3A-H3A...C4 angle of 171.5° , the second interaction can be considered to be stronger than the first one as the C-H bond of pyrrole is by far more polarized than the C-H bond of a CH_2 fragment from pyrrolidine.

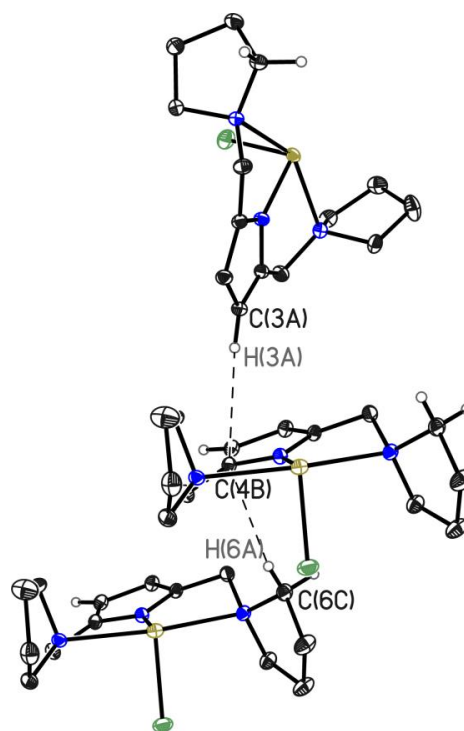


Figure 44. C-H- π interactions in the crystal structure of **15**.

To investigate this interaction in a more detailed way the ligand was modified. The pyrrolidine side arms were replaced by dimethylamine moieties. This should give a deeper insight into the influence of the side arm bulkiness on the electronic situation of the π -system, as the intermolecular interactions like the C-H- π interaction should change with varying bulkiness of the side arms.

3.4.2.1 Germanium-chloro-[2,5-bis((dimethylamino)methyl)-pyrrolide] (**16**)

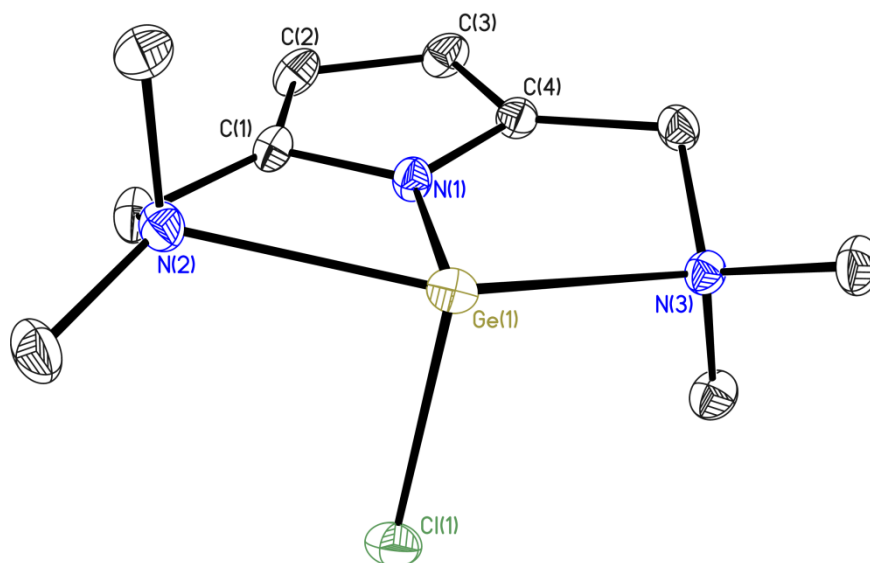


Figure 45. Crystal structure of germanium-chloro-[2,5-bis(dimethylamino)methyl]pyrrolide] (**16**). Thermal ellipsoids are depicted at the 50% probability level, hydrogen atoms are omitted for clarity.

16 crystallizes in the monoclinic space group $P2_1/c$ enclosing a whole molecule in the asymmetric unit. The local geometry at the germanium atom as well as adjacent bond lengths do not differ considerable from those in **15** as it is shown in Table 21.

Table 21. Comparison of selected bond lengths and angles of compounds **15** and **16**.

Bond length [pm] or angle [°]	{NNN}GeCl (15)	{NNN}GeCl (16)
N1–Ge1	190.95(9)	191.56(8)
Ge1–Cl1	230.69(5)	231.14(5)
N2–Ge1	249.78(9)	236.24(9)
N3–Ge1	238.01(10)	250.22(11)
C2–C3	143.48(14)	143.22(14)
N1–Ge1–Cl1	98.49(3)	97.52(3)

The same is observed for the computed molecular orbitals of **16** (HF/cc-pVDZ).⁹⁷ The orbital shape as well as the orbital coefficients at specific atoms are almost identical. However, an investigation of the intermolecular interactions reveals that the crystal structure of compound **16** (Figure 45) does not show a similar motif like compound **15**.

As expected the intermolecular C–H– π interactions differ considerably. In contrast to **15**, there is only one intermolecular C–H– π interaction present in **16**. A methyl group of a side arm is located below the heterocyclic plane and an attached C–H moiety interacts with the pyrrole π -system in a distorted η^3 -fashion (Figure 46). The H10A– π distance is 273.6 pm long, which is about 3 pm less than the shortest C–H– π interaction in **15**. However, this methyl– π interaction can be considered weaker than those C–H– π

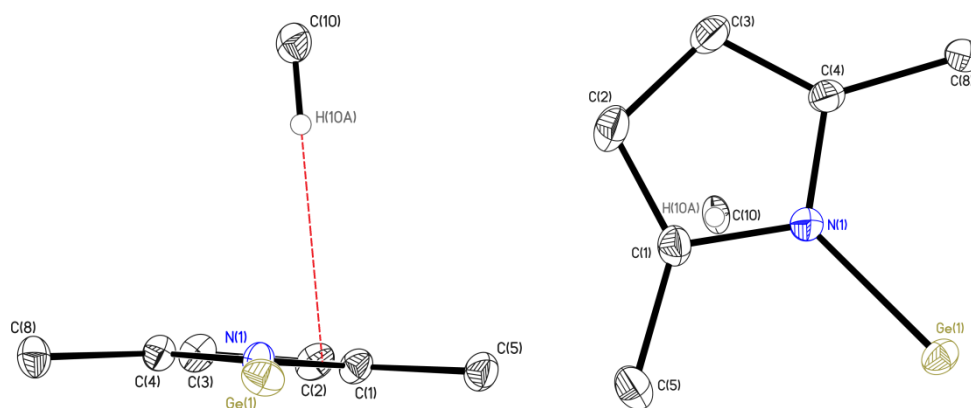
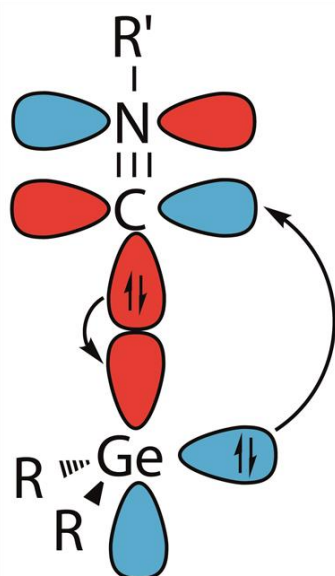


Figure 46. C–H– π interaction in **16**. Left: View from the side; right: View from top.

interactions of a CH₂-group or an aromatic CH moiety as observed in **15**.⁸⁵ Besides this C–H– π interaction, the *Hirshfeld* surface⁸² of **16** showed numerous dispersive intermolecular H–H interactions. There is an ongoing discussion in literature whether these H–H interactions are structure determining in sum, or if they are a kind of weak *London* dispersion forces. Due to these uncertain opinions it is not reliable to estimate the energy benefit of those interactions.^{106,107}

The investigation of the intermolecular interactions of **15** and **16** revealed that only marginal differences have been induced by changing the bulkiness of the ligands side arm. These changes neither affected the structure of the compounds nor the electronic situation of their corresponding π -system. They remain almost untouched and only slight changes in the bond lengths were observed (Table 21). By the comparison of **15** and **16** it was shown that the C–H– π does not influence the pyrrole π -system at all. The observed C–C bond lengths within the pyrrole heterocycle result from the interplay of the withdrawal of electron density by the germanium ion and the ligand→metal π -donation.

3.4.2.2 Reactivity of the {NNN}germanium-chloride pincer complexes



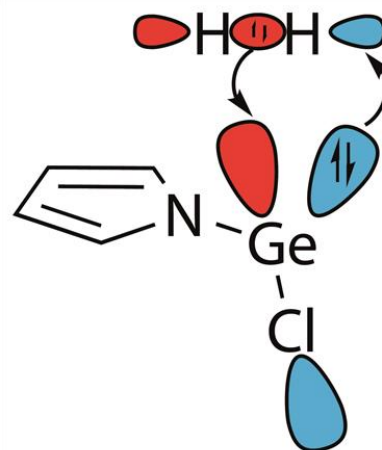
Scheme 47. Germylene-isocyanide orbital interaction.

R = Ar*, R' = ^tBu.⁵⁸

The frontier orbital situation at the germanium ion with an energetically low lying LUMO and a lone pair located in the HOMO-1 gives rise to the idea of a frustrated Lewis-pair sited at a single atom. This orbital situation would be similar to that of a germylene (Scheme 47). However, the frontier orbitals in **15** are molecular orbitals resulting from the metal ligand interaction similar to the frontier orbitals of the digermynes and in contrast to the atomic orbitals (p and sp²) of the germylene (chapter 1.3). When comparing the synthesis and handling of those known open shell main group compounds like digermynes with **15** the synthesis and handling of **15** is rather convenient. The metal does not need to be reduced and the yield is excellent as there are

only two reaction steps starting from pyrrole. Furthermore it is stable for years under an inert gas atmosphere.

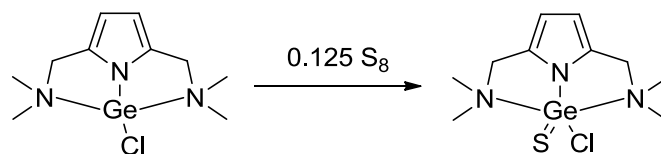
Scheme 48 describes the hypothetical interaction of the frontier orbitals of **15** with the σ -orbitals of hydrogen. The HOMO-1 of **15** containing the germanium lone pair, interacts with the σ^* -orbital of hydrogen. Simultaneously, the σ -orbital of hydrogen interacts with the LUMO (M-Cl σ^* -orbital) of **15**. The described process is similar to an oxidative addition of hydrogen to a transition metal species and yields a germanium(IV) species. The questionable parameter in this proposed mechanism is the energy gap between the HOMO-1 and the LUMO. It is computed to be 5.69 eV (Table 20), which is slightly more than the ideal HOMO-LUMO gap estimated by Power.³⁶



Scheme 48. Hypothetical interaction of germanium centered frontier orbitals with the molecular orbitals of hydrogen.

To explore the frontier orbital situation at the germanium atom in pyrrole based pincer complexes in a more detailed approach, several reactions were run which are described in the following.

3.4.2.2.1 Germanium-chloro-[2,5-bis(dimethylamino)methyl]pyrrolidido]-thione (17)



Scheme 49. Oxidation of compound **16** using elemental sulfur.

First of all, it was studied whether the germanium centered lone pair is chemically active or not. As mentioned in chapter 1.3 descending group 14 the lone pair is of rising s-character and is excluded from bonding. Analogously to the oxidation of phosphines, compound **15** was treated with an equimolar amount of sulfur (Scheme 49). Storage of a solution of the oxidation product at -28°C yielded crystals suitable for single crystal X-ray diffraction analysis after five days.

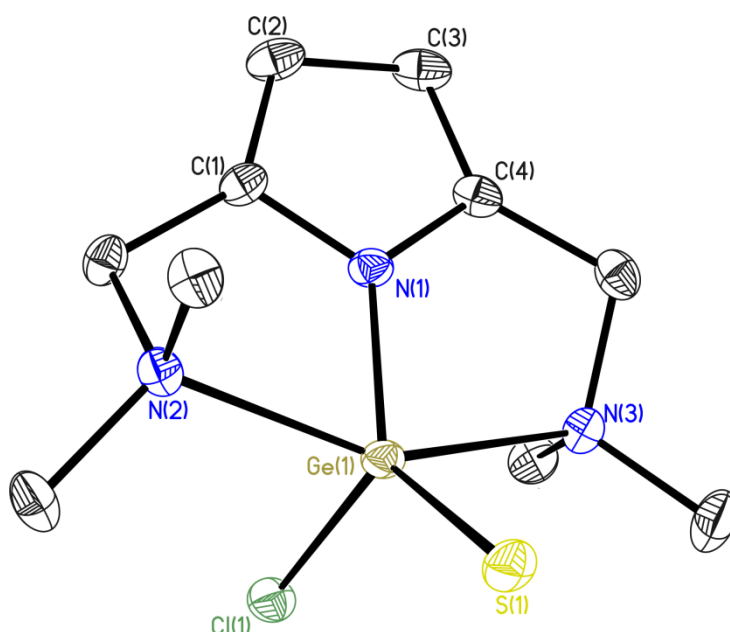


Figure 47. Crystal structure of germanium-chloro-[2,5-bis(dimethylamino)methyl]pyrrolidido]-thione (**17**). Thermal ellipsoids are depicted at the 50% probability level, hydrogen atoms are omitted for clarity.

17 crystallizes in the monoclinic space group $P2_1/c$ enclosing one molecule of **17** and a toluene solvent molecule in the asymmetric unit. The geometry at the germanium atom is slightly distorted trigonal bipyramidal with N1, S1 and Cl1 forming the triangular plane (sum of angles 359.71°). The N2–Ge1–N3 axis is slightly bent towards the heterocycle forming an angle of $151.71(4)^\circ$. The absence of a sulfur bonded

hydrogen atom and the Ge-S bond length, which is in perfect agreement with related germanium-sulfur double bond lengths¹²⁶ (208.07(6) pm), prove the obtained species **17** to contain germanium in the oxidation state +IV. The consequences of the metal oxidation yielding a germanium(IV) species become apparent when comparing **17** with the non-oxidized germanium(II) species (**15**). The higher Lewis acidity accompanied by a larger electron withdrawing effect shortens the N1-Ge1 bond by about 5 pm and the Ge1-Cl1 bond by about 13 pm. Another parameter that was changed by oxidizing the germanium ion is the ion size. The smaller size of germanium(IV) (39 pm)²⁷ compared to germanium(II) (73 pm)²⁷ is displayed best by the pyrrolidine-germanium bonds. As mentioned earlier in this chapter they are asymmetric with a difference in bond length of about 11 pm in **15**. In contrast, they differ by almost 24 pm in **17** (Table 22).

Table 22. Comparison of selected structural parameters of the germanium(II) species (**15**) and the germanium(IV) species (**17**).

Bond length [pm] / bond angle [°]	{NNN}GeCl (15)	Bond length [pm] / bond angle [°]	{NNN}Ge(S)Cl (17)
Ge1-N1	190.95(9)	Ge1-N1	185.03(11)
Ge1-Cl1	230.69(5)	Ge1-Cl1	217.12(5)
Ge1-N3	238.01(10)	Ge1-N2	219.48(12)
Ge1-N2	249.78(9)	Ge1-N3	243.21(13)
N2-N3	468.4	N2-N3	448.7
N1-Ge1-Cl1	98.49(3)	N1-Ge1-Cl1	107.12(4)
N1-Ge1-N3	74.44(3)	N1-Ge1-N2	78.30(5)
N1-Ge1-N2	73.22(3)	N1-Ge1-N3	73.56(5)

However, the {NNN} tridentate coordination is still kept upright as it is shown by the coordination geometry of **17**. The more likely a bidentate coordination becomes, the

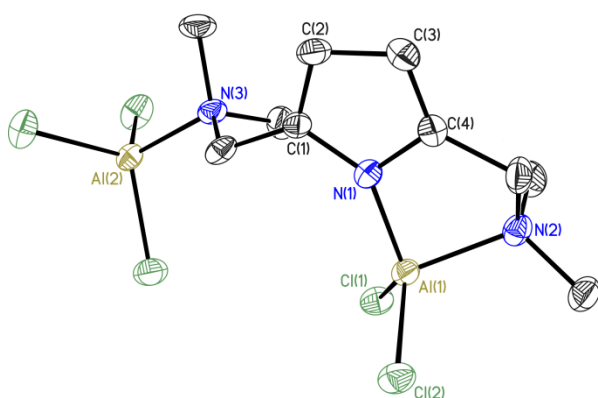


Figure 48. Crystal structure of {NN}AlCl₂ · AlCl₃. This compound has already been prepared within my diploma thesis.⁶⁶

larger becomes the corresponding N_{arm}-Ge-N_{py} angle. In typical bidentate coordination motifs like in the {NN}AlCl₂ · AlCl₃ compound (Figure 48), the N_{arm}-Al-N_{py} angle with 88.63(19)° is considerably larger than the reported 78.30(5)° for the N_{arm}-Ge-N_{py} angle in **17**. Furthermore, the adjacent N1-Ge1-N3 angle of the pending side arm would have

been increased in a bidentate dominated coordination motif. However, this angle changes only marginally from 73.22° to 73.56°. Thus the smaller germanium(IV) ion increases the asymmetry of the {NNN} coordination concerning bond lengths but the corresponding bond angles verify an almost ideal tridentate meridional coordination motif (Figure 49).

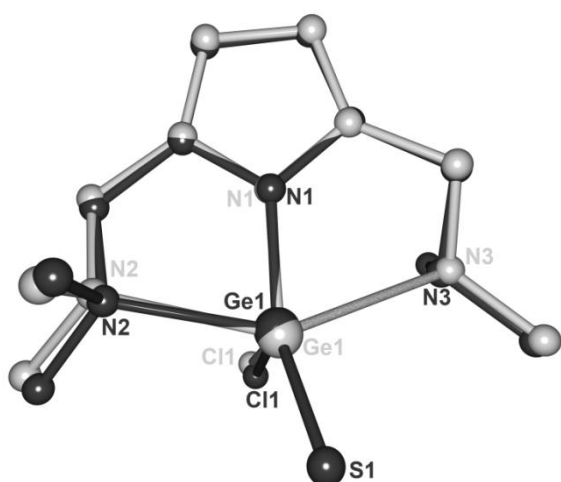


Figure 49. Superposition plot of **15** (light gray) and **17** (dark gray).

The bond lengths of the heterocyclic system are almost not affected by the oxidation of the coordinated germanium atom. With the formal C=C double bonds being 137.68(19) pm and 137.39(19) pm long and a C-C single bond length of 143.2(2) pm the $\Delta_{\text{SB-DB}}$ parameter is, analogous to that in compound **15**, 5.7 pm (Table 23). The stronger electron withdrawing effect induced by the germanium(IV) ion seems to be

compensated by π -interaction. Nonetheless, it is impossible to quantify the contribution of π -donation as the observed changes are marginal and do not indicate a significant increase of the named effects. Another dissimilarity in **17** compared to the germanium(II) species is the lack of the interaction of the pyrrole π -system with the germanium centered lone pair. It was computed to be worth only about 1 kcal/mol in **15** by *D. M. Andrada*¹¹⁹ but it should be carefully taken into account when discussing very small differences.

Table 23. Comparison of the bond lengths within the pyrrole moiety of compounds **15** and **17**.

Bond length [pm]	{NNN}GeCl (15)	{NNN}Ge(S)Cl (17)
C1-C2	137.74(13)	137.68(19)
C2-C3	143.48(14)	143.2(2)
C3-C4	137.91(13)	137.39(19)
$\Delta_{\text{SB-DB}}$	5.7	5.7

Like most of the pyrrole based pincer complexes the crystal structure of **17** contains an intermolecular C-H- π interaction. A proton of the methylene linkers is located on top of the pyrrole heterocycle of a neighboring molecule forming a dimer. The C-H- π

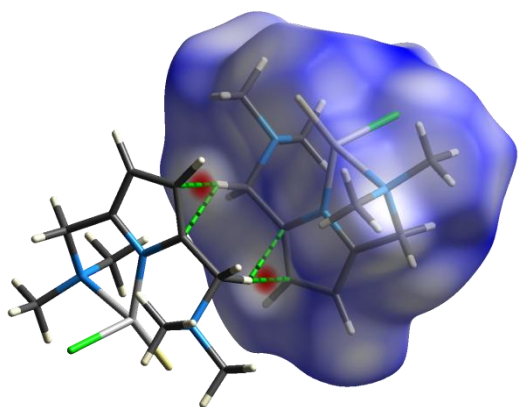


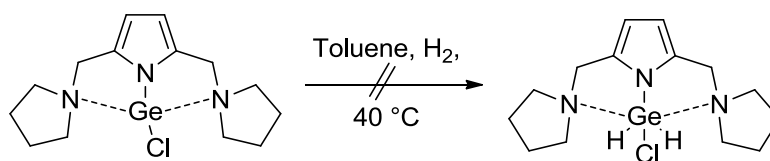
Figure 50. Hirshfeld surface of **17** including the short contacts to a neighboring molecule.

distance is 266.6(3) pm, the C–H–centroid distance is 273(2) pm and the C–H–centroid angle is 159.7°. This interaction can be regarded as an η^5 -C–H– π interaction with the hydrogen atom slightly shifted towards one of the formal C–C double bonds of the pyrrole moiety as it is indicated by the short contacts in Figure 50.

The successful oxidation of compound **15** using sulfur confirmed the chemical activity of the germanium lone pair. However, effects of the oxidation on the electronic structure of the pyrrole heterocycle are marginal. The effects of a higher *Lewis*-acidity and the missing lone pair seem to be counterbalanced by the ligand→metal π -donation.

3.4.2.2 Oxidative addition of hydrogen

With the successful preparation of the sulfur oxidized germanium species it could be proven that the lone pair is chemically active. The next challenge was to confirm the quasi open shell orbital configuration of the $\{NNN\}\text{GeCl}$ compound as it was described within this chapter. To prove this point, hydrogen was bubbled through a toluene solution of **15** at the elevated temperatures (40 °C) (Scheme 50). After 15 Minutes the hydrogen inlet was removed and the solvent was evaporated under reduced pressure. NMR spectroscopic analysis of the obtained solid did not confirm the formation of the desired species.

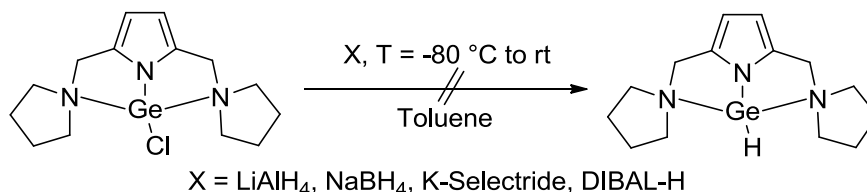


Scheme 50. Oxidative addition of hydrogen to germanium-chloro-{2,5-bis((pyrrolidino)methyl)-pyrrolide}

Instead, a mixture of the starting material and an unidentifiable decomposition product was detected. The most probable explanation for this observation is a too large HOMO-1/LUMO energy gap which does not fulfill the requirements for a quasi-open shell orbital configuration.

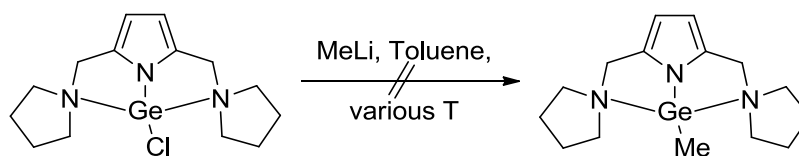
3.4.2.2.3 Ligand substitution reactions

The most promising way to modify this HOMO-1/LUMO gap is a variation of the substituents bonded to the germanium atom. Preparation of the $\{NNN\}\text{GeH}$ species would provide a different reactivity as already shown by *Roesky et al.*, who reported the first stable germanium(II) monohydride species in 2001.¹²⁷ In 2009, the activation of carbon dioxide by using the germanium(II) monohydride species was reported¹²⁸ and subsequently, the activation of carbonyl groups and many related species was discovered.¹²⁹ Mechanistical studies revealed a nucleophilic attack of the germanium hydride as the key step. As the reactivity of the hydride differs considerably from that of the chloride, the molecular orbitals may be affected as well by the change from chlorine to hydrogen. Unfortunately, there was not even one computational study containing a proper investigation of the corresponding molecular orbitals. Thus, various attempts to synthesize the $\{NNN\}\text{GeH}$ compound were conducted (Scheme 51) with the aim of comparing the molecular orbitals of the hydride species with those of the already known chloride compound. Unfortunately, every single approach failed.

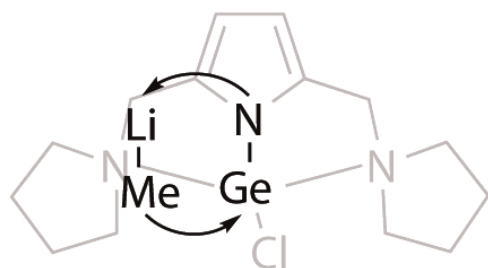


Scheme 51. Synthesis of the $\{NNN\}\text{GeH}$ compound.

Another substituent that will have an impact on the electronic situation at the germanium species is the methanide anion. *Roesky et al.* reported the first synthesis of such a compound in 2002 and described the oxidative addition of methyl iodide to germanium initiated by an increased nucleophilicity of the germanium lone pair.¹³⁰ This reactivity was absolutely unknown for the halide species and prompted *Barrau et al.* to do a computational investigation of the germanium methanide species.¹³¹ It turned out that the energy values for the occupied frontier orbitals of the germanium methanide compound are raised by almost 1 eV with respect to the chloride species.



Scheme 52. Synthesis of the $\{NNN\}\text{GeMe}$ compound.



Scheme 53. Probable explanation for the formation of the lithium pyrrolide **8** instead of the desired $\{NNN\}\text{GeMe}$ species.

Awkwardly, reacting the $\{NNN\}\text{GeCl}$ compound (**15**) with methyllithium exclusively yielded the lithium pyrrolide species (**8**) under any condition applied to the reaction (Scheme 52). An explanation can be found in the proposed reaction mechanism of Scheme 53. The pyrrolidine side arms are not bulky enough to prevent the methyllithium molecule from initiating a kind of cyclometallation that yields compound **8** and MeGeCl . However, the aluminium compound **11** encourages to use bulkier alkyl lithium species like trimethylsilylmethyllithium (TMSMeLi) comprising a similar bulkiness than AlMe_3 . The increased bulkiness should prevent the alkyl lithium compound from approaching the amidic pyrrole nitrogen atom and therewith the formation of a lithium pyrrolide compound.

3.4.3 Tin-chloro-{2,5-bis((pyrrolidino)methyl)-pyrrolide} (**18**)

As it was already mentioned in the introduction, the chemical behavior of tin is different from that of germanium. A more dominant s-orbital character at the lone pair makes sp^3 hybridization less feasible. To evaluate these differences in a metal ligand interaction a tin compound analogous to **15** was prepared.

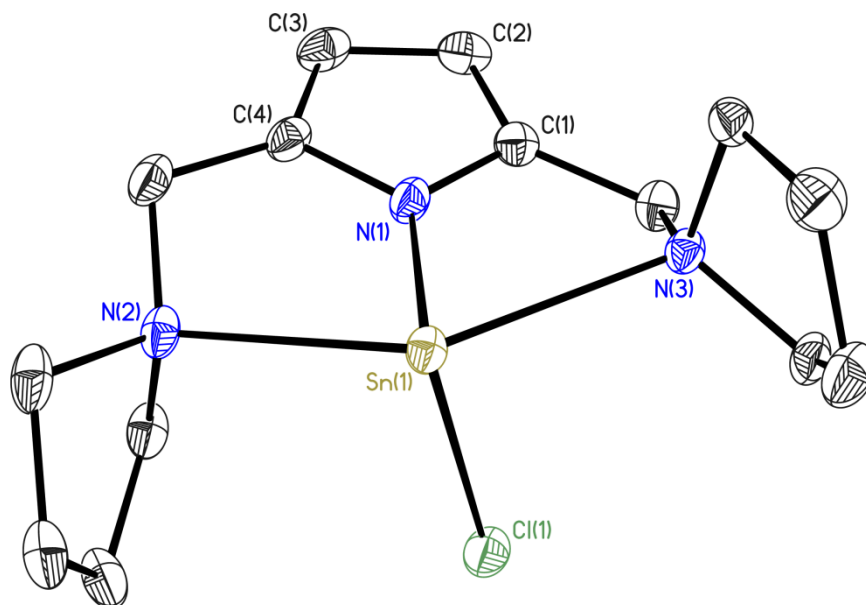
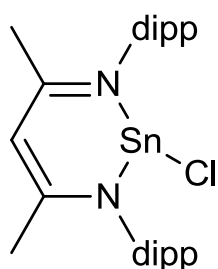


Figure 51. Crystal structure of tin-chloro-[2,5-bis(pyrrolidino)methyl]pyrrolide] (**18**). Thermal ellipsoids are depicted at the 50% probability level, hydrogen atoms are omitted for clarity.

18 crystallizes in the monoclinic space group $P2_1/c$ with a whole molecule in the asymmetric unit. The geometry at the tin ion is distorted trigonal bipyramidal with a stereochemically active lone pair in the triangular plane. The distortion is caused on the one hand by the lone pair which occupies more space ($\sim 169.98^\circ$) than the chlorine or the N1 nitrogen atom (N1–Sn1–Cl1: $95.01(4)^\circ$) and on the other hand by the inability of the linkers to provide a linear N3–Sn1–N2 (observed angle: $138.39(4)^\circ$) arrangement. Apart from this distortion the size of the tin(II) ion seems to be well suited for the coordination pocket of the used ligand system underlined by similar N–Sn side arm



Scheme 54. Tin compound prepared by Roesky *et al.*

donor bond lengths (N2–Sn1: 257.68(12) pm; N3–Sn1: 258.56(12) pm). The N1–Sn1 bond (211.83(12) pm) is one of the shortest N–Sn bonds among related species¹³² containing an amidic ligand which coordinates a Sn–Cl moiety. A selected example is the complex of Roesky *et al.* (Scheme 54).^{125w} It contains two similar amidic N–Sn bonds with bond lengths of 217.9 pm and 218.6 pm, respectively. Unexpectedly, they are longer by more than 6 pm

compared to the N1–Sn1 bond in **18**. An explanation can be that in **18**, the tin ion is perfectly positioned for N1–Sn1 orbital overlap. The tridentate ligand with symmetrical side arms usually coordinates in a meridional fashion with the metal ion in the heterocyclic plane directly in front of the pyrrole nitrogen atom. The weakening of the pyrrole metal interaction in a hypothetical bidentate coordination motif becomes obvious when comparing the $\{NNN\}AlCl_2$ compound (**10**) with the four-fold coordinated $\{NN\}AlCl_2 \cdot AlCl_3$ compound (**19**) and a literature known pincer compound⁷⁶ coordinating an $AlCl_2$ fragment in the $\{NNN\}$ fashion (**20**) (Table 24). The N1–Al1 bond length in the bidentate coordination motif is longer by 1.88 pm and 0.80 pm, respectively (Table 24), which is caused by a poorer orbital overlap. At a given *Lewis*-acidity of the metal ion, the ligand-metal bonds behave proportional to the coordination number. This is because the *Lewis*-acidity has to be equalized by fewer donor atoms, which then have to donate more electron density towards the metal ion. Consequently, the ligand-metal bonds in low coordinate metal species should be shorter than those in their high coordinate congeners.

Table 24. Selected bond lengths of compounds **10**, **19** and **20**, showing the differences in bond lengths between a four-fold and a five-fold coordination motif.

Bond length [pm]	$\{NNN\}AlCl_2$ (10)	$\{NN\}AlCl_2 \cdot AlCl_3$ (19)	$\{NNN\}AlCl_2$ (20)
N1–Al1	181.72(16)	183.6(4)	182.8
Al1–N2	225.21(11)	195.8(5)	221.1
Al1–N3	225.22(11)	---	225.6
Al1–Cl1	214.30(5)	210.3(2)	213.4
Al1–Cl2	214.31(5)	211.9(2)	214.6

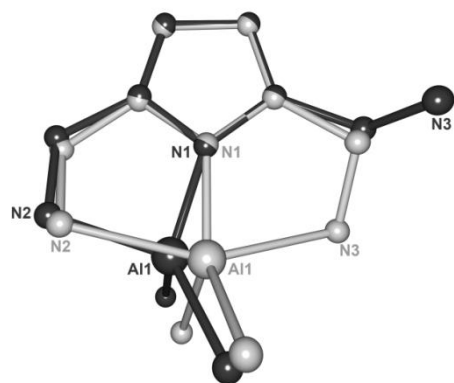


Figure 52. Superposition plot of compounds **10** (light gray) and **19** (dark gray).

Bond lengths contained in Table 24 confirm the assumptions made above. In **19**, all bonds to the aluminium ion are significantly shortened compared to **10** and **20**. Most apparent, the N2–Al1 bond is shortened by almost 30 pm indicating a strong increase of N→Al donation. The aluminium-chlorine bonds are slightly shortened by approximately 3 pm. Only the N1–Al1 bond is slightly elongated although it should be shortened

like the other bonds. This can be explained only by a poorer orbital overlap between N1 and Al1 caused by the shift of the aluminium ion (Figure 52).

Besides the assumed perfect overlap between the N1-sp² lone pair and tin there is another effect further fortifying the N1–Sn1 interaction the ligand-metal π -interaction. To gain insight into this π -interaction a high level computational investigation was conducted by *D. M. Andrada*.¹¹⁹

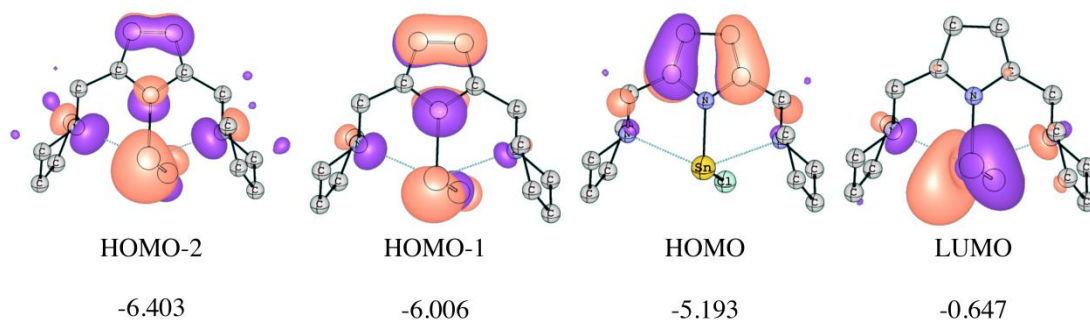


Figure 53. Molecular orbitals of **18** at the 0.045 au isolevel and their corresponding orbital energy in eV, computed using DFT calculations based on the M06¹³³/cc-pVTZ⁹⁷ level of theory.

DFT calculations based on the M06¹³³/cc-pVTZ⁹⁷ level of theory afforded the molecular orbitals depicted in Figure 53. It turns out that the orbital overlap between the pyrrole π -orbitals and the tin centered orbitals is barely visible at the given isolevel. The NBO analysis⁹⁹ (Table 25) revealed that the π -interaction, which is exclusively π -donation from pyrrole to the tin atom, is worth 4.33 kcal/mol. This value divides into 0.63 kcal/mol for the LP(N1_{pZ})→LP*(M) donation and 3.7 kcal/mol for the LP(N1_{pZ})→ σ^* (M–Cl) donation which is just half of the value obtained for the corresponding germanium compound (**15**).

Table 25. NBO results for compound **18**. Partial charges (Q) (in au) and occupation numbers (LP) (in au), Wiberg bond order (BO) and second-order acceptor-donor interaction energies ($\Delta E^{(2)}$) (in kcal/mol) are given.

Q(M)	LP(M)	LP(N1)	BO(N1-M)	$\Delta E^{(2)}$ LP(N1 _{pZ}) →LP*(M)	$\Delta E^{(2)}$ LP(N1 _{pZ}) → σ^* (M–Cl)
1.190	1.986	1.525	0.390	0.63	3.7

The effects of a tin coordination on the bond lengths of the pyrrole heterocycle are slightly less pronounced than in related metal complexes. The interplay of σ - and π -interaction afforded bond lengths of 137.8(2) pm and 138.1(2) pm, respectively, for the formal double bonds of pyrrole and 143.0(2) pm for the corresponding C–C single bond.

Table 26. Comparison of selected bond lengths of compounds **18** and **8**.

Bond length [pm]	{ <i>NNN</i> }SnCl (18)	Lithium pyrrolide (8)
C1–C2	137.8(2)	138.03(19)
C2–C3	143.0(2)	141.0(2)
C3–C4	138.1(2)	138.21(19)
$\Delta_{\text{SB-DB}}$	5.1	2.9

The bond lengths depicted in Table 26 indicate a considerable amount of ligand-metal π -donation as this would elongate the C2–C3 bond (Scheme 6). Simultaneously, the C1–C2 and C3–C4 bonds are shortened. However, the bond lengths for the C1–C2 and the C3–C4 bonds do not reflect this shortening compared to the lithium pyrrolide benchmark system. This is due to a compensation by the withdrawal of electron density from the heterocyclic system towards the tin ion *via* N1–Sn1 σ -interaction, which causes an elongation of the corresponding bonds. Thus, only the C2–C3 bond is elongated, the others remain almost untouched. The resulting $\Delta_{\text{SB-DB}}$ of 5.1 pm clearly indicates a different electronic situation in the heteroaromatic system in **18** with respect to **8**.

3.4.4 Lead-chloro-{2,5-bis((pyrrolidino)methyl)-pyrrolide} (**21**)

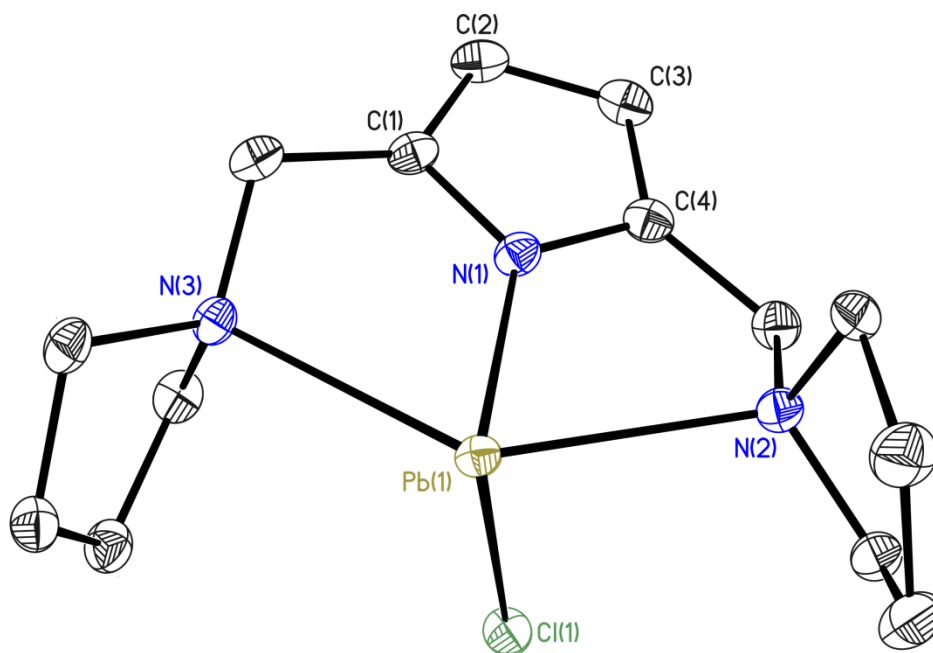


Figure 54. Crystal structure of lead-chloro-[2,5-bis((pyrrolidino)methyl)pyrrolide] (**21**). Thermal ellipsoids are depicted at the 50% probability level, hydrogen atoms are omitted for clarity.

21 crystallizes in the monoclinic space group $P21/c$ containing a whole molecule in the asymmetric unit. The geometry at the lead ion is somewhere halfway between distorted trigonal bipyramidal and distorted pyramidal. The N1–Pb1–Cl1 angle with $90.02(5)^\circ$ substantially deviates from the ideal 120° of a trigonal bipyramid. Simultaneously, the N2–Pb1–N3 angle with $136.05(6)^\circ$ is drastically narrowed compared to the 180° of an ideal trigonal bipyramid. The free space provided by this coordination motif is occupied by a bulky lone pair, which consumes about 179.96° of space in the former triangular plane (Sn: 169.98° ; Ge: 163.02°).

The lead ion is coordinated in a slightly asymmetrical fashion by the side arms. With bond lengths of $261.62(18)$ pm and $268.05(19)$ pm for the N2–Pb1 and the N3–Pb1 bond the bond lengths differ roughly by 7 pm. An explanation can be the size of the lead(II) ion. With 119 pm^{104} it seems to reach the upper limit of the ion size scale of those who are still suited for a {NNN} coordination by this ligand.

As the lead ion was shown not to participate in π -bonds⁴² the same was assumed for compound **21**. High level computations performed by *D. M. Andrada* were expected to confirm this assumption.¹¹⁹

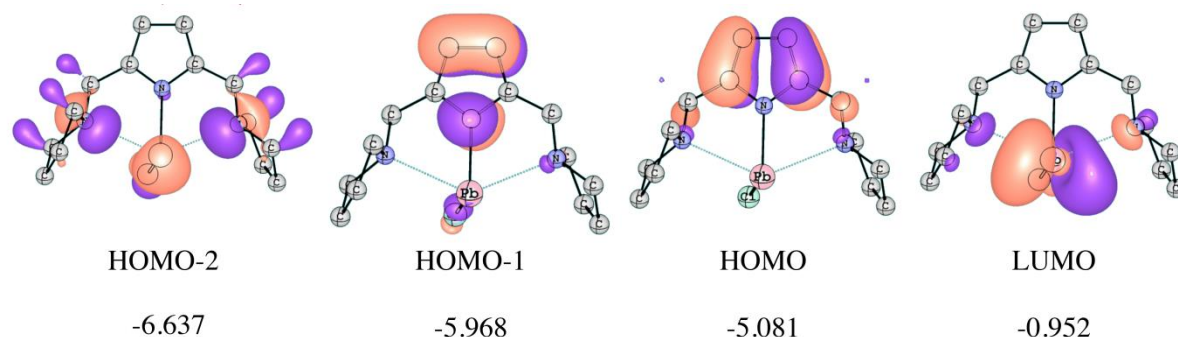


Figure 55. Molecular orbitals of **21** at the 0.045 au isolevel and their corresponding orbital energy in eV, computed using DFT calculations based on the M06¹³³/cc-pVTZ⁹⁷ level of theory.

The molecular orbitals perfectly reflect the reluctance of lead to undergo a π -interaction with the heteroaromatic system of pyrrole (Figure 55). The frontier orbitals, which contain the pyrrole π -system, do not even show a slight orbital overlap between the N1_{p_z} orbital and the lead centered orbitals. An additional NBO analysis⁹⁹ then challenged the inferences drawn from the molecular orbitals (Table 27). The stabilization energy of a hypothetical π -overlap between N1 and Pb1 is worth 4.11 kcal/mol, which is similar to the value of the tin compound, but should be close to zero according to previously performed computations investigating the nature of formal multiple bonded lead–lead species.⁴²

Table 27. NBO results for compound **21**. Partial charges (Q) (in au) and occupation numbers (LP) (in au), Wiberg bond order (BO) and second-order acceptor-donor interaction energies ($\Delta E^{(2)}$) (in kcal/mol) are given.

Q(M)	LP(M)	LP(N1)	BO(N1-M)	$\Delta E^{(2)}LP(N1_{pz})$ $\rightarrow LP^*(M)$	$\Delta E^{(2)}LP(N1_{pz})$ $\rightarrow \sigma^*(M-Cl)$
1.190	1.987	1.516	0.390	0.51	3.6

To find a solution for this mismatch within the computational results the experimental bond lengths in the pyrrole heterocycle were examined. They confirm the molecular orbitals which do not show any kind of π -interaction reflected by the relevant bond lengths in **21**. The C–C bond lengths in pyrrole do not differ significantly from those of the lithium pyrrolide compound (**8**) (Table 28). The C1–C2 and C3–C4 bond lengths are identical in both compounds merely the C2–C3 bond is elongated by 1 pm. This could be due to a weak N1_{p_z}→Pb π -donation. This would shorten the C1–C2 bond

and the C3–C4 bond and elongate the C2–C3 bond. The shortening could have been compensated by the effect of electron withdrawal by the lead atom and the combination of those effects yields the obtained bond lengths. As already mentioned for the tin compound it is not possible to quantify the change in bond length caused by each specific effect. However, it is possible to state that the influence of the π -interaction is rather weak if present at all. Otherwise, the difference between the C2–C3 bonds would have been more distinct (Table 28).

Table 28. Comparison of selected bond lengths of compounds **21** and **8**.

Bond length [pm]	{NNN}SnCl (21)	Lithium pyrrolide (8)
C1–C2	138.2(3)	138.03(19)
C2–C3	142.0(3)	141.0(2)
C3–C4	138.1(3)	138.21(19)
$\Delta_{\text{SB-DB}}$	3.9	2.9

As lead chloride complexes are known to form μ -Cl bridged compounds, the crystal structure was investigated with a focus on long distance lead–chlorine interactions. The *Hirshfeld* surface⁸² analysis revealed a rather short Pb–Cl interaction in addition to the Pb1–Cl1 bond (Figure 56). A chlorine atom of a neighboring molecule is located on top of Pb1 forming a dimer which further polymerizes by μ -Cl bridging ending up with long coordination polymer chains. The Pb1–Cl1' interaction is 300.56(7) pm long and the Cl1'–Pb1–Cl1 angle is 173.99(2)° wide. With approximately 300 pm the Pb–Cl1' interaction is located well within regular Pb–Cl bond lengths as a CSD search for Pb–Cl bond lengths revealed.

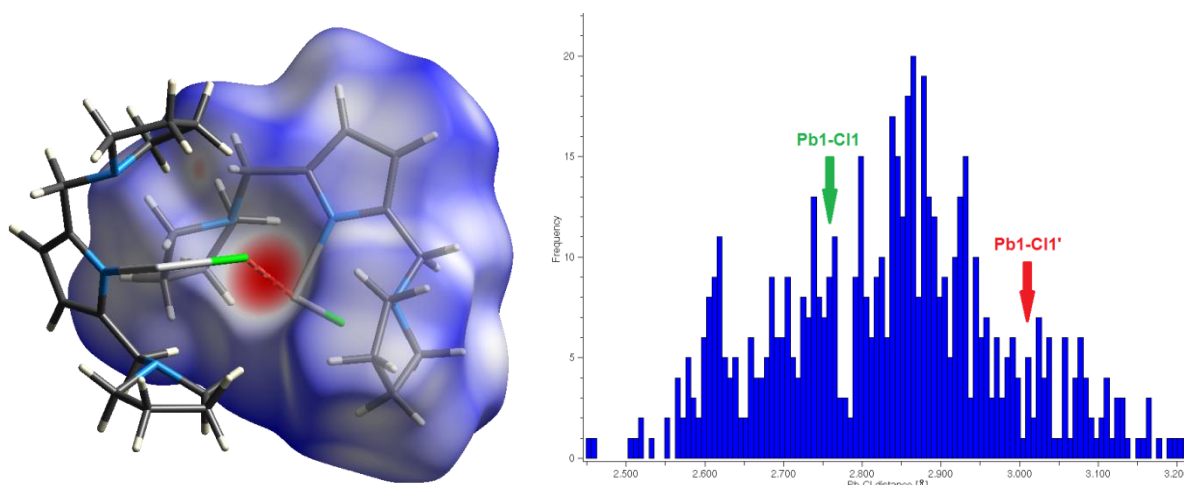
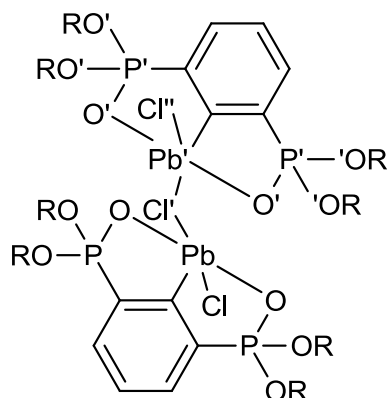


Figure 56. Left: *Hirshfeld* surface of compound **21** showing the Pb–Cl close contact to a neighboring molecule. Right: Result of a CSD search for Pb–Cl bond lengths. The Pb1–Cl1 and the Pb1–Cl1' bond lengths are labeled within the diagram.



Scheme 55. Crystal structure of the lead compound (**22**) reported by Jurkschat *et al.*

In 2003 *Jurkschat et al.* reported a similar compound (**22**) that comprises an almost identical structural feature at the lead atom (Scheme 55).¹³⁴ The Cl–Pb–Cl1' angle is 169.59° wide and therewith slightly narrower than in **21**. Due to the less bulky side arms in **22**, the single molecules can approach further than in **21** which comprise the pyrrolidine side arms proven to be stereochemically active. Thus, both Pb–Cl bonds are more alike with bond lengths of 279.5 pm and 290.1 pm, respectively. This Cl1–Pb1–Cl1' interaction *via* the lead

lone pair would drastically weaken a possible pyrrole–lead π -interaction and exclude the lone pair from other interactions or at least significantly weaken other lead π -interactions.

3.4.5 Structural comparison of the prepared group 14 species

In the first decade of the 21st century many discoveries were made in the area of low valent heavy group 14 compounds and their specific dissimilarities were investigated in a very detailed process, as described in the introduction. However, besides the reactivity towards small molecule substrates or intermetallic orbital interactions, the interaction with the ligand carrying such a metal species was neglected although it could provide useful information about the nature of these metal species in general and not merely towards selected molecules. Having a well-studied π -system like pyrrole embedded in the ligand makes a study of the π -interactions feasible.

Table 29. Comparison of selected structural properties of the prepared group 14 halide species and the lithium pyrrolide **8**.

Bond length [pm]	{NNN}Ge (15)	{NNN}Sn (18)	{NNN}Pb (21)	Lithium pyrrolide (8)
N1–M	190.95(9)	211.83(12)	220.00(18)	---
C1–C2	137.74(13)	137.8(2)	138.2(3)	138.03(19)
C2–C3	143.48(14)	143.0(2)	142.0(3)	141.0(2)
C3–C4	137.91(13)	138.1(2)	138.1(3)	138.21(19)
$\Delta_{\text{SB-DB}}$	5.7	5.1	3.9	2.9
N–M	187.2/	208.7/	222.2/	---
in M[hmds] ₂	187.8 ¹³⁵	209.5 ¹³⁶	226.0 ¹³⁶	

Table 29 summarizes selected structural properties of the prepared group 14 metal(II) species. Most eye-catching is the decrease in the $\Delta_{\text{SB-DB}}$ value the heavier the element gets. This effect is the result of an elongation of the C1–C2 and C3–C4 bonds along with a shortening of the C2–C3 bonds when descending group 14. The Lewis-acidity among these metal(II) species should be in a similar scale and thus should not be primarily responsible for the different $\Delta_{\text{SB-DB}}$ values observed. A π -donation from the N1_{pZ} orbital towards metal centered orbitals would elongate the C2–C3 bond and shorten the formal double bonds. Thus, this π -donation seems to be an explanation for the observed differences in bond lengths. Assumption of an increasing degree of this π -donation ascending group 14 would be in good agreement with the obtained bond lengths. Bond lengths observed in compound **8**, which does not show significant amounts of π -interaction, further confirms the theory of an increasing π -donation going from lead to germanium. Without this assumed loss of electron density via the N1_{pZ}→M donation the C2–C3 bond in **8** is quite short and the C1–C2 and C3–C4 bonds are in a similar range like in the group 14 complexes. The electron withdrawal effect which

should be considerably weaker for lithium than for the group 14 metals seems to be decreased in the same magnitude as the lacking π -donation. Thus the C1-C2 and C3-C4 bonds have approximately the same length in all the species described in Table 29.

The $N1_{pz} \rightarrow M$ donation would further shorten the N1-M bond as bonding orbitals between N1 and M are populated (HOMO-2 of compound **15**). Comparison with the $M(hmds)_2$ species, which form rather short N-M bonds with a coordination number as low as two, confirms group 14 pincer complexes to form short bonds between pyrrole and the metal ion.

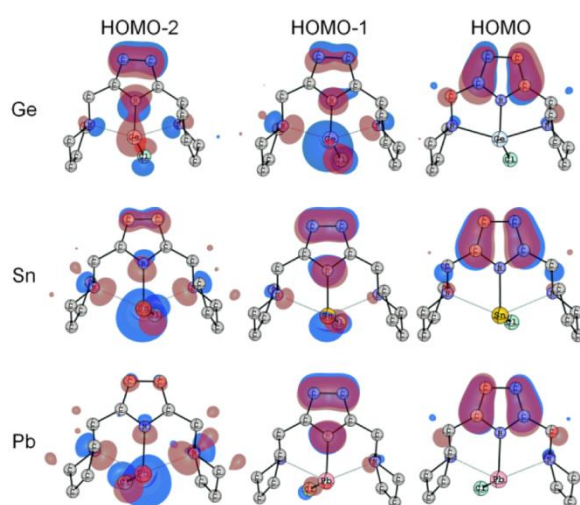


Figure 57. Frontier molecular orbitals of the prepared group 14 species, computed at the M06¹³³/cc-pVTZ⁹⁷ level of theory.¹¹⁹

As can be seen in Figure 57 the molecular orbitals suggest a stronger interaction between germanium and pyrrole than for its heavier homologues. In the germanium species, the orbital overlap is clearly visible at an isolevel of 0.045 au. In contrast, there is hardly any overlap detectable for the tin species, however, the orbitals at N1 and Sn1

have the same algebraic sign and would overlap at a lower isolevel. Within the lead compound, there is no π -overlap

detectable, even at a very low isolevel. Remarkably, the ordering of the molecular orbitals is changed. This is due to a decrease in energy of the lone pair going from germanium to lead. For germanium it is mainly located in the HOMO-1 (-5.915 eV). In the tin and lead species, it is located in the HOMO-2, with energy values of -6.403 eV and -6.637 eV, respectively. This observation is not surprising as the ability of the heavier elements to undergo sp hybridization decreases with increasing atomic number of the tetravalent element ending up at lead with an energetically low lying lone pair with mainly s-character. This has already been observed by *Lappert et al.* in 2007 when comparing a three coordinate lead species with its lighter congeners.¹³⁷ They computed the orbital character of the metal centered lone pair in a LPbCl ($s^{0.918}$, $p^{0.082}$), LSnCl ($s^{0.861}$, $p^{0.139}$) and LGeCl ($s^{0.816}$, $p^{0.184}$) species.

With the increasing divergence of the C-C bond lengths within the pyrrole heterocycle when ascending the group of the tetrel elements, the aromaticity should be reduced. To quantify the differences in aromaticity the NICS(1)_{zz} values, computed by *D. M. Andrada*, have been taken into account.¹¹⁹ They confirm the hypothesis that an increased divergence of bond length ($\Delta_{\text{SB-DB}}$) decreases the aromaticity of pyrrole, however, the differences are marginal (Table 30) and can hardly be used as an evidence.

Table 30. Computed NICS(1)_{zz} values for the prepared group 14 species.

Compound	NICS(1) _{zz} [ppm]
{NNN}Ge (15)	-25.0 / -24.9
{NNN}Sn (18)	-25.2 / -25.1
{NNN}Pb (21)	-25.6 / -25.5

The NBO analysis⁹⁹ in contrast creates a picture with more distinct differences between each element. Most noticeable are the obtained values for the acceptor-donor interaction energy $\Delta E^{(2)}$ (Table 31). For the metal→ligand π -back donation the obtained energy values are not significant and are neglected in the investigation. The donation from the N1_{pz} orbital towards the metal centered orbitals, however, clearly display the expected differences of the investigated species. The π -interaction within the lead compound is worth 4.11 kcal/mol. Going to tin the ligand→metal π -interaction is increased by 5.36% and further increased by 72.27% going from lead to germanium. Surprisingly, the values for the tin and lead compounds are almost identical. That is in sharp contrast to the experimentally observed results as well as to the computed molecular orbitals. This may be due to the intermolecular Pb–Cl interaction in **21** which was not taken into account for the computational investigations and could have had an influence on the experimentally observed bond lengths in **21**.

Table 31. NBO results for compounds **15**, **18** and **21**. Partial charges (Q) (in au) and occupation numbers (LP) (in au), Wiberg bond order (BO) and second-order acceptor-donor interaction energies ($\Delta E^{(2)}$) (in kcal/mol) are given.

Compound	Q(M)	LP(M)	LP(N1)	BO(N1-M)	$\Delta E^{(2)}$ LP(N1 _{pz}) →LP*(M)	$\Delta E^{(2)}$ LP(N1 _{pz}) → σ^* (M–Cl)
{NNN}Ge (15)	1.042	1.978	1.544	0.456	1.08	6.0
{NNN}Sn (18)	1.190	1.986	1.525	0.390	0.63	3.7
{NNN}Pb (21)	1.190	1.987	1.516	0.390	0.51	3.6

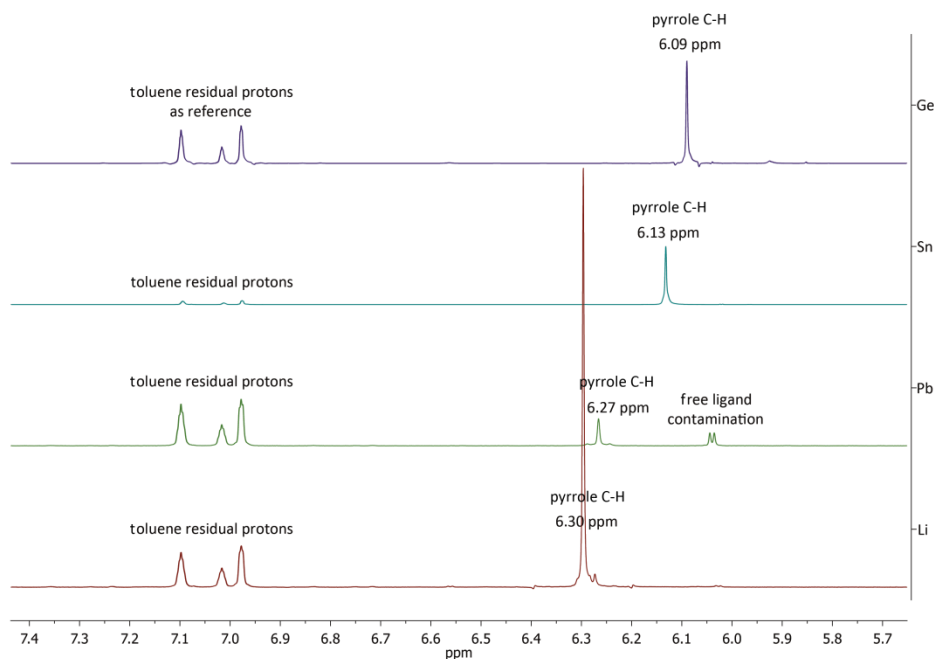


Figure 58. Extract from the ^1H -NMR spectra of the prepared group 14 compounds in the oxidation state +2 and the lithium pyrrolide compound (**8**), focusing on the signal of the pyrrole C-H protons.

Among the methods used above for explaining the ligand-metal interactions there is another very useful experimental tool to prove the capability for metal ligand π -interaction of each single group 14 metal. The chemical shift of the protons at the 3- and 4- position of the pyrrole moiety directly depends on the π -electron density of the heterocycle. The ring current effect is deshielding the protons, however, loss of electron density in the pyrrole π -orbitals weakens this effect and the corresponding protons are high-field shifted. Figure 58 shows extracts from the ^1H -NMR spectra of the prepared compounds $\{\text{NNN}\}\text{Ge}$ (**15**), $\{\text{NNN}\}\text{Sn}$ (**18**), $\{\text{NNN}\}\text{Pb}$ (**21**) and the lithium pyrrolide (**8**). The spectra have been recorded using crystalline material of the corresponding compounds, dissolved in toluene- d_8 . The chemical shift of the protons in 3- and 4-position of pyrrole is in perfect agreement with the inferences drawn from the experimentally observed bond lengths in the heteroaromatic cycle. Most remarkable, displaying a chemical shift of 6.13 ppm the signal for the tin compound is much closer to the chemical shift of the germanium compound (6.09 ppm) than to the lead species (6.27 ppm). The chemical shift of the lead compound on the other hand is similar to that of the lithium pyrrolide species (6.30 ppm). The same trend but much less pronounced is witnessed for the ^{13}C -NMR spectra. Although the concentrations of the samples vary (Sn vs Li) which could affect the resulting chemical shifts, the observed differences between the single compounds are too distinct to be caused by a different sample

concentrations. The computational results concerning the tin and lead species are somehow in contradiction to the experimental results, which have been proven by the high resolution X-ray data and by NMR spectroscopy. With some limitation the NICS(1)_{zz} values confirm the experimental results as well. However, the NBO analysis⁹⁹ does not fully support these results which may be due to some problems with the model in particular as the intermolecular interactions have not been taken into account, which may affect the final result.²³

Finally, it can be stated that the pyrrole-metal π -interaction decreases descending group 14. However, the change is not proportional to the atomic number of the corresponding elements. According to the discussed experiments it decreases in the following order Ge > Sn >> Pb (\geq Li).

3.5 Group 15 Metal Pincer Complexes

3.5.1 Antimony-dichloro-{2,5-bis((pyrrolidino)methyl)-pyrrolide} (22)

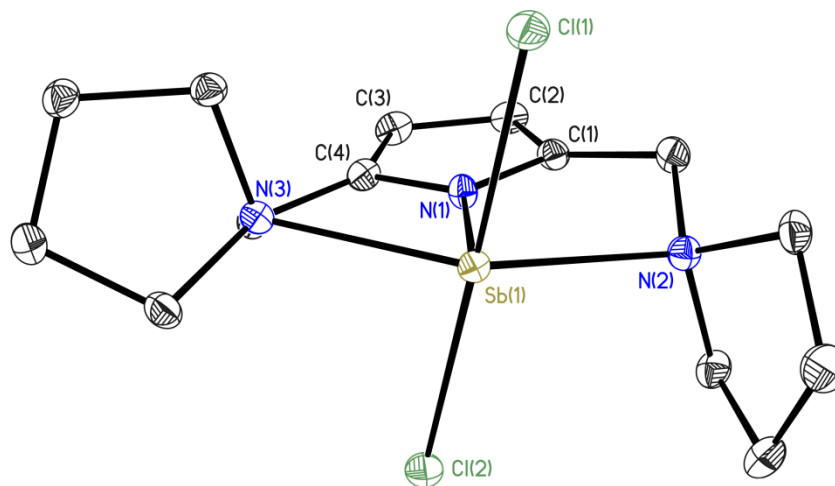


Figure 59. Crystal structure of lead-chloro-[2,5-bis(pyrrolidino)methyl]pyrrolide] (**22**). Thermal ellipsoids are depicted at the 50% probability level, hydrogen atoms are omitted for clarity.

After the observation of the dominant donation of electron density from the pyrrole heterocycle into the antibonding metal-chlorine bond, a species containing two metal chlorine bonds, orientated coplanar to the pyrrole π -orbitals should be prepared. The element of choice is antimony as the lightest metal in group 15. The resulting compound (**22**) crystallizes in the monoclinic space group $P2_1/n$ with a whole molecule in the asymmetric unit. The geometry at the antimony ion is distorted octahedral and the stereochemically active lone pair is located in the $\{NNN\}$ plane. The distortion is caused by the ligand creating convex shaped N2–M–N3 geometries (N2–Sb1–N3: $144.59(6)^\circ$) being unable to provide perfectly octahedral coordination pocket. Furthermore, the lone pair forces the chlorine atoms to bent slightly towards the pyrrole heterocycle (Cl1–Sb1–Cl2: $173.997(19)^\circ$). The antimony(III) ion seems to be slightly too small to fit perfectly into the coordination pocket provided by the ligand which is indicated by a slightly asymmetric coordination pattern of both side arms. However, this could be expected as the ion radius of antimony(III) is only 3 pm bigger than that of germanium(II).²⁷

In 2001, *Anderson et al.*^{115b} reported about the *trans*-effect¹¹⁵ in metal compounds and gave the example of an antimony(IV)chloride compound including an additional solvent molecule. The Sb–Cl bond lengths vary between 227.1 pm and 243.7 pm which confirms

the validity of the *trans*-effect for main group metals as well. In **22** both Sb–Cl bonds are unusually long accompanied by a rather short N1–Sb1 bond. This phenomenon was found for many related amidic ligand species coordinating a Sb–Cl₂ fragment.¹³⁸ The Sb–Cl bonds are always orientated perpendicular to the ligand's π -system if the ligand consists of an aromatic system. Unfortunately, the antimony atom is too heavy to compute the molecular orbitals for compound **22** in accurate manner using the *Crystal Explorer*⁸⁰ program. Thus, merely the experimental bond lengths are available for an analysis of the ligand metal interaction.

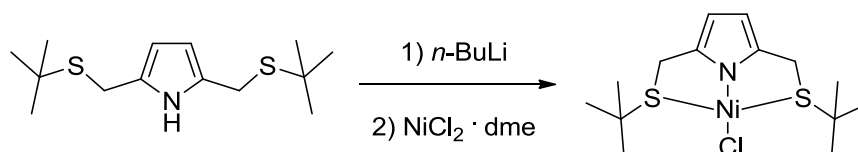
Table 32. Selected bond lengths of compound **22**.

Bond lengths [pm]	{NNN}SbCl ₂
C1–C2	137.2(3)
C2–C3	142.5(3)
C3–C4	137.5(3)
N1–Sb1	202.87(17)
Sb1–Cl1	258.05(7)
Sb1–Cl2	259.35(7)

Besides the *trans*-effect a ligand-metal π -donation could be the reason for the observed bond lengths. It would shorten the N1–Sb1 bond and elongate the Sb–Cl bonds. With 142.5 pm the C2–C3 bond is not unusually elongated (Table 32) which hints to a ligand→metal π -donation ($N1_{pz} \rightarrow \sigma^*(Sb-Cl)$) similar to the other main group complexes reported within this thesis and is too weak to explain the long Sb–Cl bonds. The π -donation must be ranked in between tin and germanium, probably superior to tin as the Sb1–Cl1 bonds are arranged perfectly coplanar to the $N1_{pz}$ -orbital. Finally, the *trans*-effect is responsible for the major part of the Sb–Cl bond elongation and the ligand metal π -donation seems to have only minor contributions to the Sb–Cl bond elongation.

3.5 Transition Metal Pincer Complexes

3.5.1 Nickel-chloro-{2,5-bis((tertbutyl-thiolato)methyl)pyrrolide} (23)



Scheme 56. Synthesis of compound **23** making use of the transmetallation reaction.

After the successful preparation and analysis of the main group compounds, proving them to participate in π -donor acceptor interactions with the heteroaromatic ligand, a related transition metal compound was prepared. It should display the landmark for strong metal–ligand π -interaction. Therefore a transition metal with d^8 -configuration was chosen with empty d -orbitals as π -acceptor and occupied ones, suitable for π -back donation. As the nickel(II) ion is regarded to be a rather soft *Lewis*-acid, the pincer ligand comprising the soft *Lewis*-bases as side arm donor atoms namely sulfur were used in the synthesis.

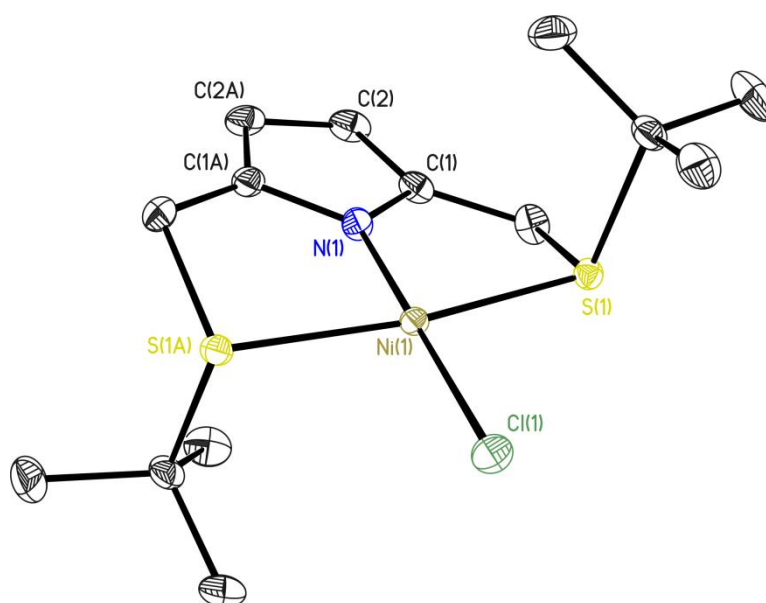


Figure 60. Crystal structure of nickel-chloro-{2,5-bis((tertbutyl-thiolato)methyl)pyrrolide} (**23**). Thermal ellipsoids are depicted at the 50% probability level, hydrogen atoms are omitted for clarity.

23 crystallizes in the orthorhombic space group *Pbcn* with half a molecule in the asymmetric unit. It is completed by a C_2 -axis located in the N1–Cl1 axis. Due to the considerable longer methylene–sulfur bonds (183.09(12) pm) in comparison to the previously described methylene–nitrogen bonds (147.62(12) pm/147.60(14) pm) in **15**

the donor–metal–donor arrangement becomes more linearly shaped. Thus, the geometry at the nickel(II) ion is almost perfectly squared planar with N1–Ni1–Cl1 and S1–Ni1–S1A angles of 180.0° and 170.375(17)°, respectively.

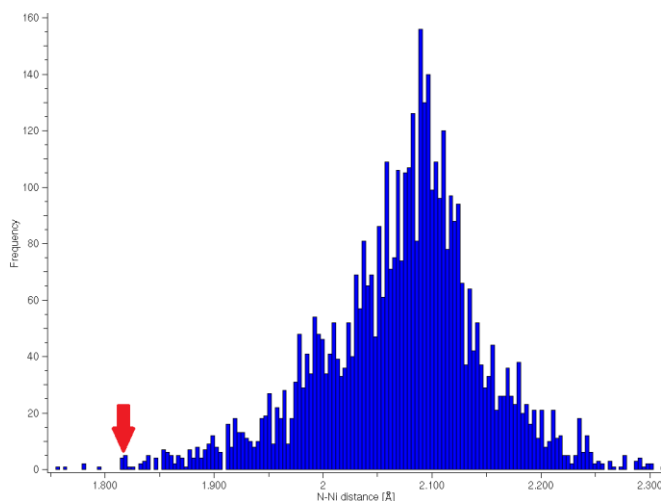
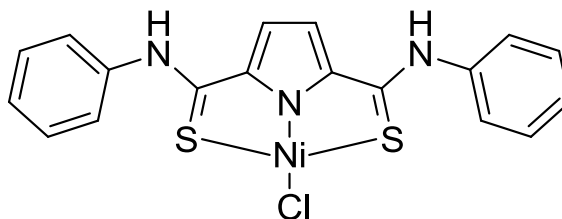


Figure 61. Result of a CSD search for N-coordinated Ni–Cl fragments.

Investigating the crystal structure of **23** it becomes apparent that the N1–Ni1 bond is significantly shortened compared to other nitrogen coordinated Ni–Cl fragments (Figure 61). With a bond length of 182.20(13) pm the Ni–Cl bond is almost as short as the N–Al bond in **10**, although the aluminium(III) ion has a drastically smaller ion radius. Thus, additional interactions with respect to

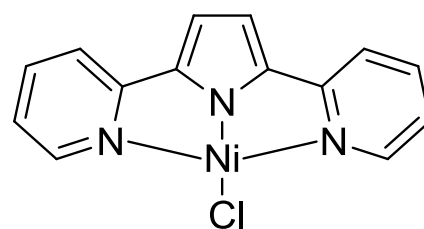
the N–Al interaction must be present in **23**. As the nickel(II) ion contains filled and an empty d-orbital, a N–Ni π -donor-acceptor interaction becomes likely. Structures comprising a similar N–Ni bond length than **23** all consist of a π -system, involving a nitrogen atom.¹³⁹ Within those, the compound reported by *Yamamoto et al.* stands out (Scheme 57).^{139e} The crystal structure includes a pincer compound (**24**), very similar to that in **23** but with a fully delocalized π -system between the {SNS} donor atoms. Bond lengths within the pyrrole heterocycle of **24** clearly indicate a π -back donation from the nickel atom into the unoccupied pyrrole π -orbital. With C1–C2 and C3–C4 bond lengths of 140.6 pm and 141.3 pm, respectively, and 138.9 pm for the C2–C3



Scheme 57. Crystal structure of the {SNS}NiCl pincer complex (**24**) prepared by *Yamamoto et al.*

bond, the bonding situation in the pyrrole moiety has been inverted. This is in sharp contrast to the situation in **23**. The heterocyclic C–C bonds resemble the motif already observed in the main group complexes reported earlier in this thesis. The C1–C2 bond is 138.23(16) pm, and the C2–C2A bond 142.4(3) pm long. Hence, **23** does not comprise a considerable amount of π -back donation. Another approach was conducted by *Wayland et al.* They studied the impact of a coordinated transition metal species (palladium and platinum) on the pyrrole π -system of the 2,5-bis(α -pyridyl)-pyrrolate (PDP) ligand

(Scheme 58).^{3c} PDP displays quite a rigid type of pincer with a delocalized π -system including the entire backbone and all donor atoms. Compound (**25**) displays a medium π -back donation in comparison with **23** and **24**. The C–C bond lengths of the pyrrole moiety in **25** are 140.2(8) pm and 140.0(13) pm for C6–C7 and C7–C7A.



Scheme 58. Crystal structure of the [PDP]PdCl complex (**25**) prepared by Wayland *et al.*

Table 33. C–C Bond length in the pyrrole moieties in **23** and related compounds from literature (**24** and **25**).

Bond length [pm]	{SNS}NiCl (23)	{SNS}NiCl (24)	[PDP]PdCl (25)
C1–C2	138.23(16)	140.6	140.2(8)
C2–C3	142.4(3)	138.9	140.0(13)
C3–C4	---	141.3	---
N1–C1	136.88(13)	135.8	134.1(6)
$\Delta_{\text{SB-DB}}$	4.2	–2.05	–0.2

Table 33 summarizes the C–C bond lengths of the compounds discussed above. It is apparent that there is almost no metal→ligand π -back donation from the nickel(II) ion present in **23** as the C2–C3 bond is elongated and not shortened compared to the lithium pyrrolide species (**8**). Nonetheless, all N_{Pyrrole}–metal bonds have similar lengths. This must be to a counterbalancing effect. A stronger σ - or π -donation from the ligand towards the nickel atom could be the reason for the N–Ni bond shortening. This additional interaction, with respect to **24** and **25**, is possible as the negative charge is concentrated in the pyrrole moiety in **23** and cannot be delocalized towards the side arms. The C2–C3 bond in **23** is slightly elongated compared to the lithiated compound (**8**) hinting to a weak ligand→metal π -donation. A quantification of the σ -donation is considerably more challenging than for the π -donation. Basically, the N1–C1 bond length can give a hint as it is directly bonded to the σ -donating pyrrole nitrogen atom and in fact the N1–C1 bond is longer in **23** than in the related compounds (Table 33). Thus, the withdrawal of σ -electron density caused by N1_{sp2}→Ni1 donation affects the N1–C1 bond in a more severe way than in **24** and **25**. In combination, the rather weak π -donation together with the stronger σ -donation compensates the π -back donation present in **24** and **25** and equalizes the pyrrole–metal bond length. Taking the N–C bond length in pyrrole into account can be misleading. It seems to work fine for compounds **23**, **24** and

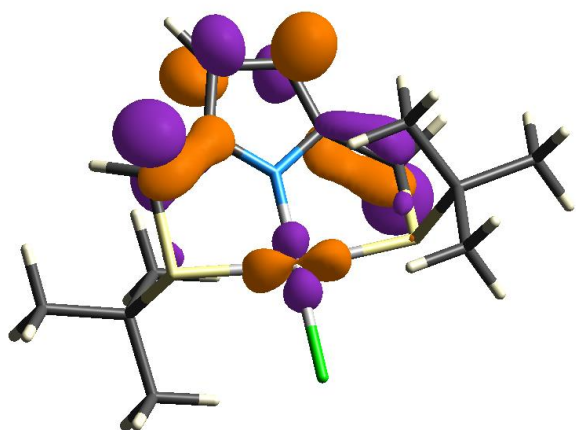


Figure 62. LUMO+8 of compound **23**, computed using the HF/6-31g* level of theory.¹¹⁴

25, however, the aluminium compound (**10**) comprises a shorter N1-C1 bond length although it is much more Lewis-acidic than nickel(II) or palladium(II).

The reason for the absence of the π -back donation in **23** can be found in the molecular orbitals computed on the HF/6-31g* level of theory¹¹⁴ (*Crystal Explorer*)⁸⁰. The unoccupied π -orbital can

be found in the rather diffuse LUMO+8. It is too high in energy to have any kind of interaction with the metal centered d-orbitals. The related compounds **24** and **25** show that a derivatization of the ligand backbone or the side arm residues can affect the orbital energies and therewith provide the requirements for a π -back donation.

The variation of the donor atoms seems to have no effect on the π -system. Going from nitrogen donor atoms to sulfur atoms does neither increase the energy of an occupied pyrrole π -orbital nor does it lower the energy of the LUMO of the pyrrole π -system. Furthermore, its effect on the energy level of the metal centered d-orbitals is marginal as well. As could be shown by compound **24** an enlargement of the heterocyclic π -system or a substitution of the metal bonded chlorine atom are the methods of choice to control the HOMO-LUMO gap.

3.5.2 Palladium-dimethylamino-chloro-{2,5-bis((dimethylamino)methyl)-pyrrolide} (26)

Unfortunately, the synthesis of a palladium analogue of compound **23** for a direct comparison of the nickel and palladium interactions with the pincer ligand bearing the sulfur donor atoms failed. Therefore the lithium pyrrolide {NNN}Li **7** was reacted with palladium(II)chloride.

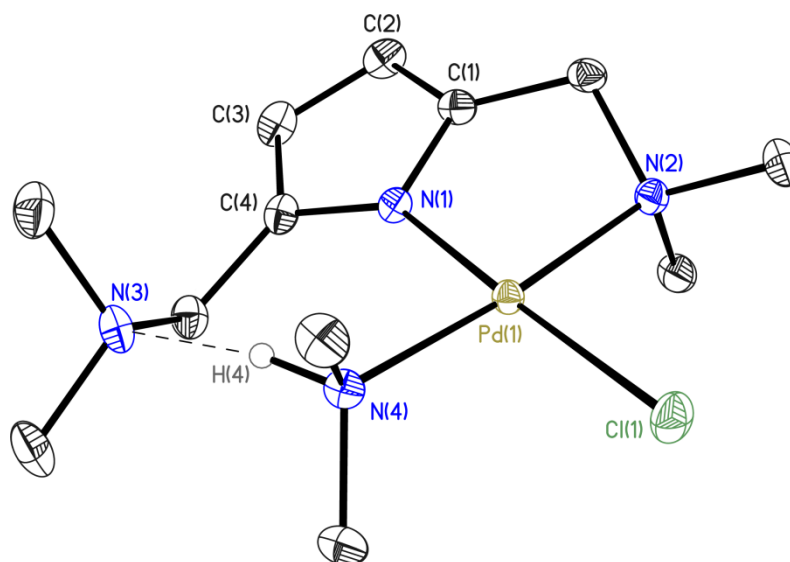


Figure 63. Crystal structure of Palladium-dimethylamino-chloro-{2,5-bis((dimethylamino)-methyl)pyrrolide} (**26**). Thermal ellipsoids are depicted at the 50% probability level, hydrogen atoms are omitted for clarity.

Surprisingly, the obtained compound was not the expected {NNN}PdCl species. Instead, a dimethylamine molecule replaces one of side arms ending up in a {NN}Pd(HNMe₂)Cl type structure. However, the source of the dimethylamine molecule is questionable. The free ligand was distilled in the purification process (5×10^{-2} mbar, $\sim 100^\circ\text{C}$), thus possible dimethylamine contaminations should have been removed. Nonetheless, a cleavage of one of the side arms from the pyrrole moiety is possible and would explain the presence of dimethylamine in the reaction solution and therewith in the crystal structure. **26** crystallizes in the monoclinic space group $P2_1/c$ with the whole molecule enclosed in the asymmetric unit. The coordination geometry at the palladium(II) ion is slightly distorted squared planar (N2–Pd1–N4: $175.11(5)^\circ$, N1–Pd1–Cl1: $175.25(4)^\circ$). The palladium bonded dimethylamine moiety is connected with the pending side arm *via* a N–H \cdots N hydrogen bond (N \cdots H distance: 189.7 pm, N–H \cdots N angle: 170.24°), which is the shortest non-covalent interaction of this whole thesis and can considered to be quite short in comparison to other N–H \cdots N hydrogen bondings reported in the CSD so far (chapter 3.1.1).

This structural feature is an evidence for the flexibility of the pyrrole based pincer ligand. Besides the coordination of metal ions with a wide ion size distribution (39 pm (Ge(IV)) to 119 pm (Pb(II))), the ligand can act as a hemi-labile species¹⁴⁰ in the presence of suitable substrates like dimethylamine.

Table 34. C-C Bond length in the pyrrole moieties in **26**, **23** and **8**.

Bond length [pm]	{NN}Pd(HNMe ₂)Cl (26)	{SNS}NiCl (23)	Lithium pyrrolide (8)
C1-C2	138.2(2)	138.23(16)	138.03(19)
C2-C3	141.5(2)	142.4(3)	141.0(2)
C3-C4	139.0(2)	---	138.21(19)
$\Delta_{\text{SB-DB}}$	2.9	4.2	2.9

The N1-Pd1 distance is, different from the N1-Ni1 bond in **23**, not unusually short. The bidentate {NN} coordination mode decreases the σ -overlap between N1 and Pd1. The effect of a decreased pyrrole-metal σ -interaction upon a shift of the metal ion towards one of the side arms has been discussed investigating the tin compound in chapter 3.4.3. The C-C bond lengths in the pyrrole heterocycle indicate a weak π -back donation (Table 34). The average bond lengths of the formal double bonds of pyrrole are the longest of all species investigated within this thesis and the C2-C3 bond is, besides the lithium pyrrolide (**8**), the shortest observed in this thesis. With a $\Delta_{\text{SB-DB}}$ value of 2.9 it cannot be compared to the nickel and palladium species discussed in the previous chapter as they show $\Delta_{\text{SB-DB}}$ values of -2.05 (**24**) and -0.2 (**25**), respectively. Thus the π -back donation must be rather weak. Additionally, the ligand→metal π -donation cannot be strong as the C2-C3 bond is not elongated compared to compound **8**. Together with the weakened σ -interaction, the resulting N1-Pd1 bond is, uncharacteristic for metal-pyrrole bonds in pyrrole based pincer complexes, of average length compared to other N-PdCl bonds reported in the CSD.

An interesting structural property of **26** was revealed after a closer investigation of the intermolecular interactions. **26** contains exactly the same intermolecular C-H- π interactions as the germanium(IV) species (**17**). It dimerizes due to the orientation of a methylene proton (H5B) on top of the pyrrole π -system of a neighboring molecule and *vice versa* (Figure 64). No structural feature could be detected for these two compounds that is absent in all the others and therewith probably responsible for this similarity.

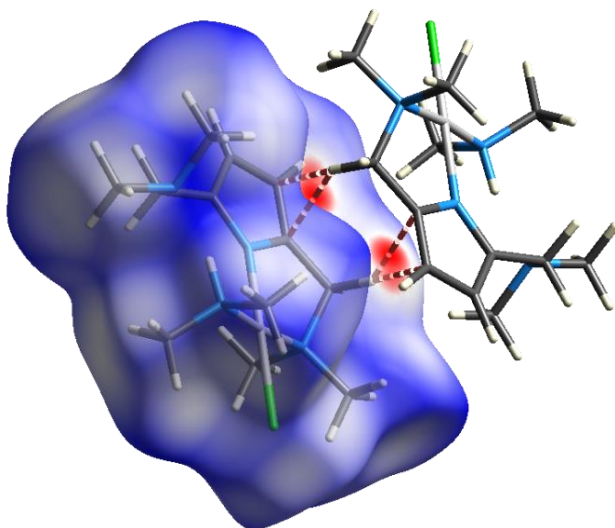


Figure 64. *Hirshfeld* surface of compound **26**, including the short contacts to a neighboring molecule.

The H- π distance is 246.7(2) pm (H-centroid: 249.7 pm) long and the C-H-centroid angle is 169.1° wide. These values reflect the probable strength of this interaction, when compared to compound **17** but also regarding the structures reported in the CSD, containing C-H- π interactions (Figure 28). Furthermore, this C-H- π interaction may be the reason for the short C2-C3 bond and the slight elongation C1-C2 and C3-C4. A loss of

electron density in the HOMO caused by a C-H- π interaction would cause exactly these changes. On the other hand, the free ligand **6** contains a N-H- π interaction which is considered to be much stronger than the C-H- π interaction in **26** and the C-C bond lengths in the pyrrole moiety of **6** do not even indicate a marginal loss of electron density in the HOMO. Unfortunately, the molecular orbitals could not be calculated due to the computational expense. Thus, it cannot be stated whether the π -back donation or if the C-H- π interaction is responsible for the bonding situation in the pyrrole heterocycle. However, a weak π -back donation is most probably the reason for the unfamiliar bonding situation in the pyrrole moiety.

4 Synthesis and Structure

4.1 General

All reactions were carried out with strict exclusion of air and moisture under nitrogen or argon atmosphere using modified *Schlenk*-techniques or in an argon dry box.¹⁴¹ All solvents were dried using standard laboratory procedures and were freshly distilled from sodium/potassium alloy prior to use. Solvents used for the synthesis or further reactions of the germanium and silicon compounds were degassed according to standard laboratory procedures. All employed reactants were commercially available or reproduced according to the given literature procedure.

4.1.1 Spectroscopic and analytic methods

Nuclear Magnetic Resonance

All samples were prepared and filled into *Schlenk*-NMR-tubes inside an argon dry box. The NMR-tube was sealed-off to exclude any impurities. Solvents were dried with potassium. Spectra were recorded at variable temperatures at a *Bruker Avance 300*, *Bruker Avance 400*, or a *Bruker Avance 500* NMR spectrometer. All chemical shifts δ are given in ppm, relative to the residual proton signal of the deuterated solvent. Assignments of the shifts were checked by two-dimensional correlation spectra.

Mass spectrometry

EI-spectra were recorded with a *MAT 95* device (EI-MS: 70 eV). Peaks are given as a mass to charge ratio (m/z) of the fragment ions, based on the molecular mass of the isotopes with the highest natural abundance.

Elemental analysis

Elemental analysis was performed as a combustion analysis by the *Analytischen Labor des Institutes für Anorganische Chemie* at the Georg-August Universität Göttingen with an *elementar vario EL III* device.

4.2 Synthesis

4.2.1 2,5-bis((dimethylamino)methyl)pyrrole (1)

1 was prepared along a modified protocol of *Elsenbaumer et al.*⁷⁴ At 0 °C, dimethylamine-hydrochloride (50.0 g, 613 mmol) was added to a solution of formaldehyde (36% in H₂O, 46.0 mL, 613 mmol) and stirred at that temperature for 15 minutes. Subsequently, pyrrole (21.4 mL, 306 mmol) was added drop wise. After completed addition, the cooling bath was removed and the solution stirred for 12 h at room temperature. Afterwards, the solution was treated with aqueous NaOH-solution (2 M), until the pH reached a value of 10. The layers were separated and the organic layer was washed with water (2 x 50 mL). The organic layer was then treated with aqueous HCl-solution (2 M) until the pH value was below 4. The layers were separated and the organic layer was extracted with water (2 x 50 mL). The combined aqueous layers were again treated with aqueous NaOH solution (2 M) until the pH value was approximately 10. Diethylether (100 mL) was added and the layers were separated. The aqueous layer was extracted with diethylether (2 x 50 mL) and the combined organic layers were dried using anhydrous Na₂SO₄. The solvent was removed under reduced pressure and the residue was distilled (0.05 mbar, 100 °C) yielding a colorless oil (43.8 g, 242 mmol, 79%), tending to crystallization after one day.

¹H-NMR (300 MHz, THF-d₈): δ (ppm) 9.87 (s_{br}, 1 H, pyrrole-NH), 5.74 (d, *J* = 2.6 Hz, 2 H, pyrrole-CH), 3.28 (s, 4 H, linker-CH₂), 2.12 (s, 12 H, NMe₂).

¹³C-NMR (75 MHz, THF-d₈): δ (ppm) 127.0 (pyrrole N-C), 104.7 (pyrrole CH), 55.73 (linker CH₂), 42.36 (NMe₂).

MS (EI, 70 eV): *m/z* (%) 181 (24), 137 (97), 93 (100), 58 (99).

4.2.2 2,5-bis((pyrrolidino)methyl)pyrrole (2)

Compound **2** was prepared along a modified protocol published by *Elsenbaumer et al.*⁷⁴ Pyrrolidine (14.2 g, 200 mmol) was added to glacial acetic acid (12 mL) and cooled to 0 °C. Formaldehyde (37% in MeOH, 15 mL, 200 mmol) was added followed by 10 mL of water. Stirring was continued for 1 h at 0 °C. Then pyrrole (7.2 mL, 100 mmol) was

added slowly and the mixture was allowed to warm up to room temperature. The mixture was then stirred for 18 h at room temperature. Chloroform was added (100 mL) and the pH was adjusted to approx. 10 using aq. NaOH (2 M). The organic layer was separated and the solvent removed under reduced pressure. The residue was dissolved in hexane and the desired compound (15.4 g, 65.9 mmol, 66%) was obtained as colorless crystals after storage for three days at -80°C .

$^1\text{H-NMR}$ (300 MHz, Tol-d_8): δ (ppm) 9.42 (s_{br} , 1 H, pyrrole-NH), 6.02 (d, $J = 2.6$ Hz, 2 H, pyrrole-CH), 3.41 (s, 4 H, 2 linker- CH_2), 2.37 (m, 8 H, N- CH_2 (pyrrolidine)), 1.58 (m, 8 H, N- $\text{CH}_2\text{-CH}_2$ (pyrrolidine)).

$^{13}\text{C-NMR}$ (75 MHz, Tol-d_8): δ (ppm) 129.7 (2 C, pyrrole N-C), 106.7 (2 C, pyrrole CH), 54.17 (2 C, linker CH_2), 53.44 (4 C, N- CH_2 (pyrrolidine)), 23.89 (4 C, N- $\text{CH}_2\text{-CH}_2$ (pyrrolidine)).

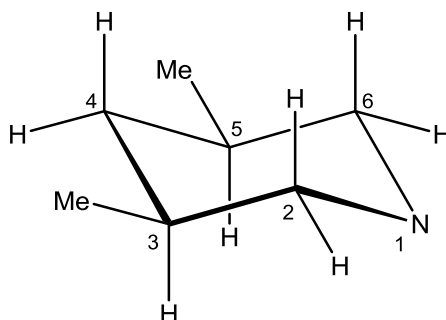
MS (EI, 70 eV): m/z (%) 233 (16), 163 (62), 93 (100), 70 (20).

Elemental Analysis Anal. Calcd for $\text{C}_{14}\text{H}_{23}\text{N}_3$: C, 72.06; H, 9.93; N, 18.01. Found: C, 71.93; H, 10.12; N, 18.03.

4.2.3 2,5-bis((3,5-dimethylpiperidino)methyl)pyrrole (3)

3 was prepared along a modified protocol of *Elsenbaumer et al.*⁷⁴ 3,5-Dimethylpiperidine (rac., 10.0 mL, 75 mmol) was added to glacial acetic acid (10 mL). The resulting mixture was stirred for 30 minutes and after cooling to room temperature, formaldehyde (37% in MeOH, 5.6 mL, 75 mmol) was added. The resulting mixture was stirred for 2 h. Then the solution was treated with aqueous NaOH-solution (2 M) until the pH reached a value of 10. The layers were separated and the organic layer was washed with water (2 x 50 mL). The organic layer was then treated with aqueous HCl-solution (2 M) until the pH value was below 4. The layers were separated and the organic layer was extracted with water (2 x 50 mL). The combined aqueous layers were again treated with aqueous NaOH solution (2 M) until the pH value was approximately 10. Diethylether (100 mL) was added and the layers were separated. The aqueous layer was extracted with diethylether (2 x 50 mL) and the combined organic layers were dried

using anhydrous Na_2SO_4 . After removal of the solvent, a highly viscous yellow oil was obtained (8.83 g, 27.8 mmol, 73%).



$^1\text{H-NMR}$ (300 MHz, CDCl_3): δ (ppm) 8.54 (s_{br} , 1 H, pyrrole N-H), 5.91 (s, 2 H, pyrrole C-H), 3.46 (s, 4 H, linker CH_2), 2.79 (m, 2 H, H-2_e + H-6_e (*cis*)), 2.36 (m, 2 H, H-2_e + H-6_a (*trans*)), 2.03 (m, 2 H, H-2_a + H-6_e (*trans*)), 1.90 (m, 2 H, H-3 + H-5 (*trans*)), 1.75 – 1.60 (m, 3 H, H-4_e + H-3 + H-5 (*cis*)), 1.43 (m, 2 H, H-2_a + H-6_a (*cis*)), 1.29 (m, 2 H, H-4 (*trans*)), 0.95 (d, 6 H, CH_3 (*trans*)), 0.84 (d, 6 H, CH_3 (*cis*)), 0.53 (q, 1 H, 4-H_a (*cis*)).

$^{13}\text{C-NMR}$ (75 MHz, CDCl_3): δ (ppm) 128.5 (2 C, pyrrole N-C), 106.9 (2 C, pyrrole C-H), 61.34 (2 C, C-2 + C-6 (*cis*)), 61.22 (2 C, C-2 + C-6 (*trans*)), 55.73 (2 C, linker CH_2), 42.26 (1 C, C-4 (*cis*)), 39.14 (1 C, C-4 (*trans*)), 31.24 (2 C, C-3 + C-5 (*cis*)), 27.46 (2 C, C-3 + C-5 (*trans*)), 19.63 (2 C, CH_3 (*cis*)), 19.13 (2 C, CH_3 (*trans*)).

MS (EI, 70 eV): m/z (%) 317 (8), 205 (50), 112 (100), 93 (27).

4.2.4 2,5-bis((*tert*butyl-thiolato)methyl)pyrrole (5)

*t*Butyl-mercaptan (2.0 mL, 17.8 mmol) was dissolved in THF (15 mL). Subsequently, sodium hydride (0.43 g, 17.8 mmol) was carefully added and the resulting mixture stirred for 30 minutes. The resulting mixture was added to a suspension of **4** (4.14 g, 8.9 mmol) in THF (20 mL), according to a literature known procedure.⁷⁴ The combined mixtures were stirred at 66 °C for one hour. After cooling to room temperature, the solvent was removed and the residue was dissolved in diethylether (50 mL). The

resulting suspension was filtered and the filtrate was dried over anhydrous Na₂SO₄. After removal of the solvent, the product was obtained as yellow oil (1.94 g, 7.2 mmol, 81%).

¹H-NMR (300 MHz, CDCl₃): δ (ppm) 10.58 (s_{br}, 1 H, pyrrole-NH), 5.74 (d, 2 H, pyrrole-CH), 3.67 (s, 4 H, 2 linker-CH₂), 1.27 (s, 18 H, S^tbu).

¹³C-NMR (75 MHz, CD₃CN): δ (ppm) 129.4 (2 C, pyrrole N-C), 108.2 (2 C, pyrrole C-H), 57.32 (2 C, CCH₃), 45.62 (2 C, linker CH₂), 31.44 (6 C, CH₃).

MS (EI, 70 eV): m/z (%) 271 (16), 182 (98), 126 (100), 93 (20).

4.2.5 2,5-bis((thiophenolato)methyl)pyrrole (6)

Thiophenol (1.82 mL, 17.8 mmol) was dissolved in THF (15 mL). Subsequently, sodium hydride (0.43 g, 17.8 mmol) was carefully added and the resulting mixture stirred for 30 minutes. The resulting mixture was added to a suspension of **4** (4.14 g, 8.9 mmol) in THF (20 mL), according to a literature known procedure.⁷⁴ The combined mixtures were stirred at 66 °C for one hour. After cooling to room temperature, the solvent was removed and the residue was dissolved in diethylether (50 mL). The resulting suspension was filtered and the filtrate was dried over anhydrous Na₂SO₄. After removal of the solvent, the crude product was obtained which was then recrystallized from hexane (20 mL) yielding compound **6** as colorless crystalline solid (2.12 g, 6.8 mmol, 76%).

¹H-NMR (300 MHz, Tol-d₈): δ (ppm) 8.22 (s_{br}, 1 H, pyrrole-NH), 7.30 – 7.18 (m, 10 H, 2 x Ph), 5.87 (d, *J* = 2.6 Hz, 2 H, pyrrole-CH), 4.09 (s, 4 H, 2 x linker-CH₂).

¹³C-NMR (75 MHz, Tol-d₈): δ (ppm) 135.7 (2 C, C_{ipso}-Ph), 130.2 (2 C, pyrrole N-C), 128.8 – 126.6 (10 C, (*o*, *m*, *p*)-Ph), 107.9 (2 C, pyrrole CH), 32.10 (2 C, linker CH₂).

MS (EI, 70 eV): m/z (%) 311 (4), 202 (100), 93 (55).

4.2.6 Lithium[2,5-bis((dimethylamino)methyl)pyrrolide] (7)

2,5-Bis{[(dimethylamino)methyl]}pyrrole (1.00 g, 5.52 mmol) was dissolved in *n*-hexane (20 mL) and cooled to 0 °C. A solution of *n*-butyllithium (*n*-hexane, 6.0 M, 0.92 mL, 5.52 mmol) was added drop wise and the solution was stirred for 1 h at 0 °C. Subsequently, the ice bath was removed and the solution stirred for 15 h at room temperature. The precipitated white solid was filtered off, washed with cold *n*-hexane (10 mL) and dried *in vacuo*. Recrystallization from diethylether (10 mL) at –28 °C yielded single crystals (0.89 g, 4.75 mmol, 86%) suitable for X-ray diffraction experiments.

¹H-NMR (400 MHz, THF-*d*₈): δ (ppm) 5.73 (s, 2 H, pyrrole CH), 3.95 – 2.75 (s_{br}, 4 H, linker CH₂), 2.11 (s, 12 H, NMe₂).

4.2.7 Lithium[2,5-bis((pyrrolidino)methyl)pyrrolide] (8)

2,5-Bis{[(pyrrolidino)methyl]}pyrrole (1.00 g, 4.29 mmol) was dissolved in toluene (20 mL) and cooled to 0 °C. A solution of *n*-butyllithium (*n*-hexane, 6.0 M, 0.71 mL, 4.29 mmol) was added drop wise and the solution was stirred for 1 h at 0 °C. Subsequently, the ice bath was removed and the solution stirred for 15 h at room temperature. Evaporation of all volatile materials afforded **8** as a white powder (0.92 g, 3.86 mmol, 90%). After recrystallization from diethylether, single crystals suitable for X-ray diffraction experiments were obtained.

¹H-NMR (300 MHz, Tol-*d*₈): δ (ppm) 6.33 (s, 2 H, pyrrole CH), 3.72 (s_{br}, 4 H, linker CH₂), 2.47 (s_{br}, 8 H, N-CH₂ (pyrrolidine)), 1.40 (m, 8 H, N-CH₂-CH₂ (pyrrolidine)).

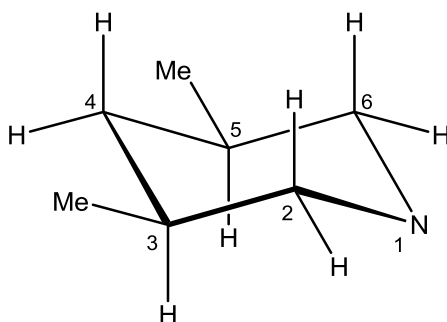
¹³C-NMR (75 MHz, Tol-*d*₈): δ (ppm) 138.7 (2 C, pyrrole N-C), 105.7 (2 C, pyrrole CH), 59.55 (2 C, linker CH₂), 54.14 (4 C, N-CH₂ (pyrrolidine)), 23.79 (4 C, N-CH₂-CH₂ (pyrrolidine)).

⁷Li-NMR (117 MHz, Tol-*d*₈): δ (ppm) 2.01 (s).

MS (EI, 70 eV): *m/z* (%) 239 (14), 169 (66), 99 (100), 70 (18).

4.2.8 Lithium[2,5-bis((3,5-dimethylpiperidino)methyl)pyrrolide] (**9**)

2,5-bis((3,5-dimethylpiperidino)methyl)pyrrole (1.00 g, 3.15 mmol) was dissolved in toluene (20 mL) and cooled to 0 °C. A solution of *n*-butyllithium (*n*-hexane, 6.0 M, 0.52 mL, 4.29 mmol) was added drop wise and the solution was stirred for 1 h at 0 °C. Subsequently, the ice bath was removed and the solution stirred for 15 h at room temperature. Evaporation of all volatile materials afforded **9** as a white powder (0.88 g, 2.71 mmol, 86%). After recrystallization from diethylether single crystals suitable for X-ray diffraction experiments were obtained.



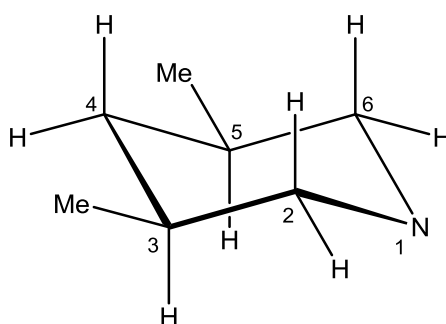
$^1\text{H-NMR}$ (300 MHz, CD_3CN): δ (ppm) 5.76 (2 H, pyrrole C-H), 3.36 (s_{br}, 4 H, linker CH_2), 2.73 (m, 2 H, H-2_e + H-6_e (*cis*)), 2.33 (m, 2 H, H-2_e + H-6_a (*trans*)), 1.98 (m, 2 H, H-2_a + H-6_e (*trans*)), 1.84 (m, 2 H, H-3 + H-5 (*trans*)), 1.73 – 1.52 (m, 3 H, H-4_e + H-3 + H-5 (*cis*)), 1.38 (m, 2 H, H-2_a + H-6_a (*cis*)), 1.27 (m, 2 H, H-4 (*trans*)), 0.92 (d, 6 H, CH_3 (*trans*)), 0.81 (d, 6 H, CH_3 (*cis*)), 0.48 (q, 1 H, 4-H_a (*cis*)).

$^{13}\text{C-NMR}$ (75 MHz, CD_3CN): δ (ppm) 126.5 (2 C, pyrrole N-C), 107.8 (2 C, pyrrole C-H), 62.51 (2 C, C-2 + C-6 (*cis*)), 61.85 (2 C, C-2 + C-6 (*trans*)), 56.77 (2 C, linker CH_2), 43.46 (1 C, C-4 (*cis*)), 40.36 (1 C, C-4 (*trans*)), 32.47 (2 C, C-3 + C-5 (*cis*)), 28.76 (2 C, C-3 + C-5 (*trans*)), 20.33 (2 C, CH_3 (*cis*)), 19.90 (2 C, CH_3 (*trans*)).

MS (EI, 70 eV): m/z (%) 323 (8), 211 (46), 112 (100), 99 (21).

4.2.9 Aluminium-dichloro-{2,5-bis((3,5-dimethylpiperidino)methyl)-pyrrolide} (10)

Lithium[2,5-bis((3,5-dimethylpiperidino)methyl)pyrrolide] (0.50 g, 1.54 mmol) was dissolved in toluene (25 mL) and subsequently aluminiumtrichloride (0.21 g 1.54 mmol) was added. The resulting mixture was stirred for 24 h at room temperature and was then filtered through Celite. The residue was washed with cooled toluene (2 x 5 mL) and the volume of the combined filtrates was reduced under reduced pressure to approximately 10 mL. Cooling of this solution to -28°C yielded colorless crystals of **10** (0.12 g, 0.29 mmol, 19%).



$^1\text{H-NMR}$ (300 MHz, Tol- d_8): δ (ppm) 6.04 (2 H, pyrrole C-H), 3.62 (s, 4 H, linker CH_2), 2.86 (m, 2 H, H-2_e + H-6_e (*cis*)), 1.85 – 1.62 (m, 3 H, H-4_e + H-3 + H-5 (*cis*)), 1.45 (m, 2 H, H-2_a + H-6_a (*cis*)), 0.84 (d, 6 H, CH_3 (*cis*)), 0.56 (q, 1 H, 4-H_a (*cis*)).

$^{13}\text{C-NMR}$ (75 MHz, Tol- d_8): δ (ppm) 128.6 (2 C, pyrrole N-C), 108.9 (2 C, pyrrole C-H), 65.74 (2 C, C-2 + C-6 (*cis*)), 59.38 (2 C, linker CH_2), 45.43 (1 C, C-4 (*cis*)), 35.87 (2 C, C-3 + C-5 (*cis*)), 21.98 (2 C, CH_3 (*cis*)).

MS (EI, 70 eV): m/z (%) 413 (9), 378 (16), 301 (48), 266 (64), 154 (18), 112 (100).

4.2.10 2,5-bis((pyrrolidino)methyl)-1H-pyrrole · 2 trimethylaluminium (11)

2,5-bis((pyrrolidino)methyl)pyrrole (**2**) (0.50 g, 2.14 mmol) was dissolved in toluene and cooled to 0°C . Afterwards, a trimethylaluminium solution (hexane, 1.5 M, 1.43 mL) was added drop wise. After completed addition, the solution was allowed to warm up to

room temperature and was stirred for 12 h at room temperature. The volume of the solution was then reduced under reduced pressure and stored at $-28\text{ }^{\circ}\text{C}$, yielding colorless crystals (0.24 g, 0.64 mmol, 30%).

$^1\text{H-NMR}$ (300 MHz, Tol-d_8): δ (ppm) 7.57 (s, 1 H, N-H), 5.77 (d, $J = 1.6\text{ Hz}$, 2 H, pyrrole C-H), 3.46 (s, 4 H, linker CH_2), 2.92 (s_{br}, 4 H, N- CH_2 (pyrrolidine)), 2.36 (s_{br}, 4 H, N- CH_2 (pyrrolidine)), 1.31 (s_{br}, 4 H, N- $\text{CH}_2\text{-CH}_2$ (pyrrolidine)), 1.06 (s_{br}, 4 H, N- $\text{CH}_2\text{-CH}_2$ (pyrrolidine)), -0.53 (s, 18 H, AlMe_3).

$^{13}\text{C-NMR}$ (75 MHz, Tol-d_8): δ (ppm) 132.6 (2 C, pyrrole N-C), 112.7 (2 C, pyrrole C-H), 53.02 (4 C, N- CH_2 (pyrrolidine)), 52.15 (2 C, linker CH_2), 24.21 (4 C, N- $\text{CH}_2\text{-CH}_2$ (pyrrolidine)), -8.46 (6 C, CH_3).

Elemental Analysis Anal. Calcd for $\text{C}_{20}\text{H}_{41}\text{Al}_2\text{N}_3$: C, 63.63; H, 10.95; N, 11.13. Found: C, 63.39; H, 10.70; N, 11.34.

4.2.11 Indium-dibromo-{2,5-bis((pyrrolidino)methyl)-pyrrolide} (12)

Lithium[2,5-bis((pyrrolidino)methyl)pyrrolide] (**8**) (0.50 g, 2.08 mmol) was dissolved in toluene and indiumtribromide (0.46 g, 2.08 mmol) was added. The resulting mixture was stirred for 24 h at room temperature and was then filtered through Celite. The residue was washed with cooled toluene (2 x 5 mL) and the volume of the combined filtrates was reduced under reduced pressure to approximately 10 mL. Cooling of this solution to $-28\text{ }^{\circ}\text{C}$ yielded an unidentifiable brownish precipitate. From this precipitate tiny crystals suitable for single crystal X-ray diffractions experiments could be isolated.

4.2.12 Silicon-dichloro-hydrido-{2,5-bis((pyrrolidino)methyl)-pyrrolide} (13)

Lithium[2,5-bis((pyrrolidino)methyl)pyrrolide] (0.50 g, 2.08 mmol) was dissolved in toluene (25 mL) and cooled to $0\text{ }^{\circ}\text{C}$. Subsequently, trichlorosilane (0.21 mL 2.08 mmol) was slowly added to the stirred solution. The resulting mixture was stirred for 24 h at

room temperature and was then filtered through Celite. The residue was washed with cooled toluene (2 x 5 mL) and the volume of the combined filtrates was reduced under reduced pressure to approximately 10 mL. Cooling of this solution to $-40\text{ }^{\circ}\text{C}$ yielded colorless crystals of **13** (0.26 g, 0.78 mmol, 38%). In another approach similar in the synthetic procedure, the solvent was removed completely and the yellowish and highly viscous oil was stored at room temperature for two days, yielding crystalline solid of compound **13a** (0.34 g, 1.02 mmol, 49%).

$^1\text{H-NMR}$ (300 MHz, Tol- d_8): δ (ppm) 6.01 (s, 2 H, pyrrole C-H), 3.54 (s, 4 H, linker CH_2), 2.50 (s_{br} , 8 H, N- CH_2 (pyrrolidine)), 1.42 (s_{br} , 8 H, N- $\text{CH}_2\text{-CH}_2$ (pyrrolidine)), 0.19 (s, 1 H, Si-H).

$^{13}\text{C-NMR}$ (75 MHz, Tol- d_8): δ (ppm) 137.1 (2 C, pyrrole N-C), 108.6 (2 C, pyrrole C-H), 54.57 (2 C, linker CH_2), 54.26 (4 C, N- CH_2 (pyrrolidine)), 23.52 (4 C, N- $\text{CH}_2\text{-CH}_2$ (pyrrolidine)).

$^{29}\text{Si-NMR}$ (59 MHz, Tol- d_8): δ (ppm) -90.3 (s)

MS (EI, 70 eV): m/z (%) 331.1 (14), 261.1 (36), 260.1 (47), 191.0 (98), 163.2 (100), 84.1 (65), 70.1 (39).

Elemental Analysis Anal. Calcd for $\text{C}_{14}\text{H}_{23}\text{Cl}_2\text{N}_3\text{Si}$: C, 50.60; H, 6.98; N, 12.64. Found: C, 47.78; H, 6.20; N, 12.19.

4.2.13 Germanium-chloro-{2,5-bis((pyrrolidino)methyl)-pyrrolide} (**15**)

$[\text{LiN}(\text{SiMe}_3)_2] \cdot \text{Et}_2\text{O}$ (1.00 g, 4.14 mmol) was added to a mixture of $\text{GeCl}_2 \cdot \text{dioxane}$ (0.96 g, 4.14 mmol) in toluene (20 mL). The resulting solution was cooled to $0\text{ }^{\circ}\text{C}$. 2,5-Bis{((pyrrolidino)methyl)-pyrrole} (0.97 g, 4.14 mmol) was added and the solution was stirred for 15 h at room temperature. Filtration of the suspension and reducing the volume of the resulting filtrate yielded crystals of **15** (1.10 g, 3.23 mmol, 78%), suitable for single crystal X-ray diffraction experiments after storage of the solution at $-28\text{ }^{\circ}\text{C}$ for some days.

$^1\text{H-NMR}$ (500 MHz, Tol- d_8): δ (ppm) 6.09 (s, 2 H, pyrrole CH), 3.67 (d, 2 H, linker CH_2), 3.37 (d, 2 H, linker CH_2), 2.77 (s_{br} , 4 H, N- CH_2

	(pyrrolidine)), 2.44 (s _{br} , 4 H, N-CH ₂ (pyrrolidine)), 1.57 (m, 8 H, N-CH ₂ -CH ₂ (pyrrolidine)).
¹³ C-NMR (126 MHz, Tol-d ₈):	δ (ppm) 132.8 (2 C, pyrrole N-C), 104.5 (2 C, pyrrole CH), 54.67 (2 C, linker CH ₂), 54.54 (4 C, N-CH ₂ (pyrrolidine)), 23.77 (4 C, N-CH ₂ -CH ₂ (pyrrolidine)).
MS (EI, 70 eV):	m/z (%) 341 (16), 339 (12), 337 (7), 271 (58), 161 (100), 93 (34), 84 (23).
Elemental Analysis	Anal. Calcd for C ₁₄ H ₂₂ ClGeN ₃ : C, 49.39; H, 6.51; N, 12.34. Found: C, 49.03; H, 6.67; N, 12.14.

4.2.14 Germanium-chloro-{2,5-bis((dimethylamino)methyl)-pyrrolide} (16)

[LiN(SiMe₃)₂] · Et₂O (1.00 g, 4.14 mmol) was added to a mixture of GeCl₂ · dioxane (0.96 g, 4.14 mmol) in toluene (20 mL). The resulting solution was cooled to 0 °C. 2,5-Bis{(dimethylamino)methyl}-pyrrole (0.75 g, 4.14 mmol) was added and the solution was stirred for 15 h at room temperature. Filtration of the suspension and reducing the volume of the resulting filtrate yielded crystals of **15** (1.00 g, 3.46 mmol, 84%), suitable for single crystal X-ray diffraction experiments after storage of the solution at -28 °C for some days.

¹ H-NMR (300 MHz, Tol-d ₈):	δ (ppm) 6.05 (s, 2 H, pyrrole CH), 3.42 (d, 2 H, linker CH ₂), 3.08 (d, 2 H, linker CH ₂), 2.07 (s, 12 H, Me).
¹³ C-NMR (75 MHz, Tol-d ₈):	δ (ppm) 132.4 (2 C, pyrrole N-C), 105.3 (2 C, pyrrole CH), 57.43 (2 C, linker CH ₂), 44.98 (4 C, Me).
MS (EI, 70 eV):	m/z (%) 291 (18), 289 (39), 287 (28), 285 (18), 245 (95), 135 (100).
Elemental Analysis	Anal. Calcd for C ₁₀ H ₁₈ ClGeN ₃ : C, 41.65; H, 6.29; N, 14.57. Found: C, 40.69; H, 6.10; N, 13.82.

4.2.15 Germanium-chloro-[2,5-bis(dimethylamino)methyl]pyrrolidido]-thione (17)

Germanium-chloro-{2,5-bis((dimethylamino)methyl)-pyrrolide} (**16**) (0.20 g, 0.69 mmol) was dissolved in toluene (20 mL). Elemental sulfur (22 mg, 0.69 mmol) was added and the resulting suspension was stirred for 18 h at room temperature. Filtration through Celite afforded a colorless solution. The volume of the filtrate was reduced to approximately 10 mL. After storage of the resulting solution for three days at -28°C , a colorless crystalline solid was obtained after filtration (0.21 g, 0.65 mmol, 94%).

$^1\text{H-NMR}$ (300 MHz, Tol- d_8): δ (ppm) 5.93 (s, 2 H, pyrrole C-H), 3.18 (d, 2 H, linker CH_2), 3.05 (d, 2 H, linker CH_2), 2.18 (s, 9 H, NMe_2).

$^{13}\text{C-NMR}$ (75 MHz, Tol- d_8): δ (ppm) 129.31 (2 C, pyrrole N-C), 106.21 (2 C, pyrrole C-H), 56.46 (2 C, linker CH_2), 45.86 (4 C, NMe_2).

Elemental Analysis Anal. Calcd for $\text{C}_{10}\text{H}_{18}\text{ClGeN}_3\text{S}$: C, 37.48; H, 5.66; N, 13.11; S, 10.01. Found: C, 40.88; H, 6.05; N, 11.28; S, 9.78.

4.2.16 Tin-chloro-{2,5-bis((pyrrolidino)methyl)-pyrrolide} (18)

$[\text{LiN}(\text{SiMe}_3)_2] \cdot \text{Et}_2\text{O}$ (1.00 g, 4.14 mmol) was added to a mixture of SnCl_2 (0.79 g, 4.14 mmol) in toluene (20 mL). The resulting solution was cooled to 0°C . 2,5-Bis{(pyrrolidino)methyl}-pyrrole (0.97 g, 4.14 mmol) was added and the solution was stirred for 15 h at room temperature. Filtration of the suspension and reducing the volume of the resulting filtrate yielded crystals of **18** (1.11 g, 2.86 mmol, 69%), suitable for single crystal X-ray diffraction experiments after storage of the solution at -28°C for some days.

$^1\text{H-NMR}$ (500 MHz, Tol- d_8): δ (ppm) 6.13 (s, 2 H, pyrrole CH), 3.65 (d, 2 H, linker CH_2), 3.39 (d, 2 H, linker CH_2), 2.34 (s_{vbr} , 8 H, N-CH_2 (pyrrolidine)), 1.48 (s_{br} , 8 H, $\text{N-CH}_2\text{-CH}_2$ (pyrrolidine)).

^{13}C -NMR (126 MHz, Tol- d_8): δ (ppm) 133.5 (2 C, pyrrole N-C), 104.8 (2 C, pyrrole CH), 55.40 (2 C, linker CH_2), 54.47 (4 C, N- CH_2 (pyrrolidine)), 23.69 (4 C, N- $\text{CH}_2\text{-CH}_2$ (pyrrolidine)).

^{119}Sn -NMR (187 MHz, Tol- d_8): δ (ppm) -217.1 (s)

MS (EI, 70 eV): m/z (%) 389 (7), 387 (19), 385 (14), 317 (60), 161 (100), 93 (15), 84 (18).

Elemental Analysis Anal. Calcd for $\text{C}_{14}\text{H}_{23}\text{ClN}_3\text{Sn}$: C, 43.50; H, 5.74; N, 10.87. Found: C, 43.21; H, 5.62; N, 10.87.

4.2.17 Lead-chloro-{2,5-bis((pyrrolidino)methyl)-pyrrolide} (**21**)

$[\text{LiN}(\text{SiMe}_3)_2] \cdot \text{Et}_2\text{O}$ (1.00 g, 4.14 mmol) was added to a mixture of PbCl_2 (1.15 g, 4.14 mmol) in toluene (20 mL). The resulting solution was cooled to 0 °C. 2,5-Bis{[(pyrrolidino)methyl]-pyrrole} (0.97 g, 4.14 mmol) was added and the solution was stirred for 15 h at room temperature. Filtration of the suspension and reducing the volume of the resulting filtrate yielded crystals of **21** (1.06 g, 2.24 mmol, 54%), suitable for single crystal X-ray diffraction experiments after storage of the solution at -28 °C for some days.

^1H -NMR (300 MHz, Tol- d_8): δ (ppm) 6.27 (m, 2 H, pyrrole CH), 3.70 (s_{br} , 4 H, linker CH_2), 2.55 (s_{vbr} , 8 H, N- CH_2 (pyrrolidine)), 1.51 (s_{br} , 8 H, N- $\text{CH}_2\text{-CH}_2$ (pyrrolidine)).

^{13}C -NMR (126 MHz, Tol- d_8): δ (ppm) 138.3 (2 C, pyrrole N-C), 105.7 (2 C, pyrrole CH), 56.61 (2 C, linker CH_2), 54.32 (4 C, N- CH_2 (pyrrolidine)), 23.75 (4 C, N- $\text{CH}_2\text{-CH}_2$ (pyrrolidine)).

^{207}Pb -NMR (63 MHz, Tol- d_8): δ (ppm) 1524 (m).

MS (EI, 70 eV): m/z (%) 475 (16), 474 (7), 473 (7), 405 (44), 161 (100), 93 (23), 84 (19).

Elemental Analysis Anal. Calcd for $\text{C}_{14}\text{H}_{23}\text{ClN}_3\text{Pb}$: C, 35.40; H, 4.67; N, 8.85. Found: C, 35.31; H, 4.38; N, 9.15.

4.2.18 Antimony-dichloro-{2,5-bis((pyrrolidino)methyl)-pyrrolide} (22)

Lithium[2,5-bis((pyrrolidino)methyl)pyrrolide] (0.50 g, 2.08 mmol) was dissolved in toluene (25 mL) and subsequently, antimonytrichloride (0.47 g 2.08 mmol) was slowly added to the stirred solution. The resulting mixture was stirred for 24 h at room temperature and was then filtered through Celite. The residue was washed with cooled toluene (2 x 5 mL) and the volume of the combined filtrates was reduced under reduced pressure to approximately 10 mL. Storage of this solution at -28°C yielded colorless crystals of **22** (0.22 g, 0.52 mmol, 25%) after three days.

$^1\text{H-NMR}$ (300 MHz, Tol-d_8): δ (ppm) 6.06 (s, 2 H, pyrrole C-H), 3.78 (s_{vbr} , 4 H, N-CH₂ (pyrrolidine)), 3.76 (s, 4 H, linker CH₂), 2.29 (s_{vbr} , 4 H, N-CH₂ (pyrrolidine)), 1.66 (s_{br} , 4 H, N-CH₂-CH₂ (pyrrolidine)), 1.31 (s_{br} , 4 H, N-CH₂-CH₂ (pyrrolidine)).

$^{13}\text{C-NMR}$ (75 MHz, Tol-d_8): δ (ppm) 131.48 (2 C, pyrrole N-C), 106.32 (2 C, pyrrole C-H), 55.71 (4 C, N-CH₂ (pyrrolidine)), 54.84 (2 C, linker CH₂), 23.02 (4 C, N-CH₂-CH₂ (pyrrolidine)).

MS (EI, 70 eV): m/z (%) 425 (1), 389 (35), 387 (30), 355 (5), 319 (4), 250 (7).

Elemental Analysis Anal. Calcd for $\text{C}_{14}\text{H}_{22}\text{Cl}_2\text{N}_3\text{Sb}$: C, 39.56; H, 5.22; N, 9.89. Found: C, 39.25; H, 4.98; N, 10.13.

4.2.19 Nickel-chloro-{2,5-bis((tertbutyl-thiolato)methyl)pyrrolide} (23)

$[\text{LiN}(\text{SiMe}_3)_2] \cdot \text{Et}_2\text{O}$ (0.50 g, 2.07 mmol) was added to a mixture of $\text{NiCl}_2 \cdot \text{dimethoxyethane}$ (0.45 g, 2.07 mmol) in toluene (20 mL). Then 2,5-bis((tertbutyl-thiolato)methyl)-pyrrole (0.56 g, 2.07 mmol) was added and the solution was stirred for 15 h at room temperature. Filtration of the suspension and reducing the volume of the resulting filtrate yielded purple crystals of **23** (0.61 g, 1.78 mmol, 86%), suitable for single crystal X-ray diffraction experiments after storage of the solution at -28°C for one day.

^1H -NMR (300 MHz, Tol- d_8):	δ (ppm) 5.90 (s, 2 H, pyrrole C-H), 3.52 (s, 2 H, linker CH_2), 3.12 (s, 2 H, linker CH_2), 1.38 (s, 9 H, ^tbu), 1.16 (s, ^tbu).
^{13}C -NMR (75 MHz, Tol- d_8):	δ (ppm) 137.4 (2 C, pyrrole N-C), 105.4 (2 C, pyrrole C-H), 51.47 (2 C, C- CH_3), 34.22 (2 C, linker CH_2), 30.07 (6 C, CH_3).
MS (EI, 70 eV):	m/z (%) 363 (20), 307 (10), 215 (15), 181 (27).

4.2.20 Palladium-dimethylamino-chloro-{2,5-bis((dimethylamino)methyl)-pyrrolide} (**26**)

$[\text{LiN}(\text{SiMe}_3)_2] \cdot \text{Et}_2\text{O}$ (0.50 g, 2.07 mmol) was added to a mixture of PdCl_2 (0.37 g, 2.07 mmol) in toluene (20 mL). Then 2,5-bis((dimethylamino)methyl)-pyrrole (0.38 g, 2.07 mmol) was added and the solution was stirred for 15 h at room temperature. Filtration of the suspension and reducing the volume of the resulting filtrate yielded yellowish crystals of **26** (0.36 g, 0.97 mmol, 47%), suitable for single crystal X-ray diffraction experiments after storage of the solution at -28°C for five days.

^1H -NMR (300 MHz, Tol- d_8):	δ (ppm) 8.25 (s, 1 H, HNMe_2), 6.18 (d, 1 H, pyrrole C-H), 6.11 (d, 1 H, pyrrole C-H), 3.14 (s, 4 H, linker CH_2), 2.35 (s, 3 H, HNMe_2), 2.33 (s, 3 H, HNMe_2), 2.19 (s, 6 H, linker- NMe_2), 1.81 (s, 6 H, linker- NMe_2).
^{13}C -NMR (75 MHz, Tol- d_8):	δ (ppm) 129.20 (2 C, pyrrole N-C), 110.34 (1 C, pyrrole C-H), 102.87 (1 C, pyrrole C-H), 66.81 (1 C, linker CH_2), 58.87 (1 C, linker CH_2), 50.87 (2 C, HNMe_2), 43.63 (2 C, linker- NMe_2), 42.42 (2 C, linker- NMe_2).
MS (EI, 70 eV):	m/z (%) 368 (5), 366 (5), 365 (3), 323 (26), 285 (5), 241 (38), 136 (100).
Elemental Analysis	Anal. Calcd for $\text{C}_{12}\text{H}_{25}\text{ClN}_4\text{Pd}$: C, 39.25; H, 6.86; N, 15.26. Found: C, 39.97; H, 6.38; N, 15.63.

5 Crystallographic section

5.1 General

Single crystals were selected from a *Schlenk* flask under argon atmosphere and covered with perfluorated polyether oil on a microscope slide, which was cooled with an inert gas flow (nitrogen, +25 °C – –100 °C) using the X-TEMP2 device.¹⁴² An appropriate crystal was selected using a microscope equipped with polarization filter, mounted on the tip of a MiTeGen®MicroMount or glass fiber, fixed to a goniometer head and shock cooled by the crystal cooling device.

The data collections were carried out on Bruker APEX2 Ultra or Quazar diffractometers equipped with Bruker TXS Mo, Incoatec I μ S Mo or Incoatec I μ S Ag sources.¹⁴³ The dataset recorded with Cu- $K\alpha$ wavelength was collected on a Bruker SMART6000 diffractometer. The data collection strategy was calculated with the APEX plugin COSMO¹⁴⁴ or entered by hand.

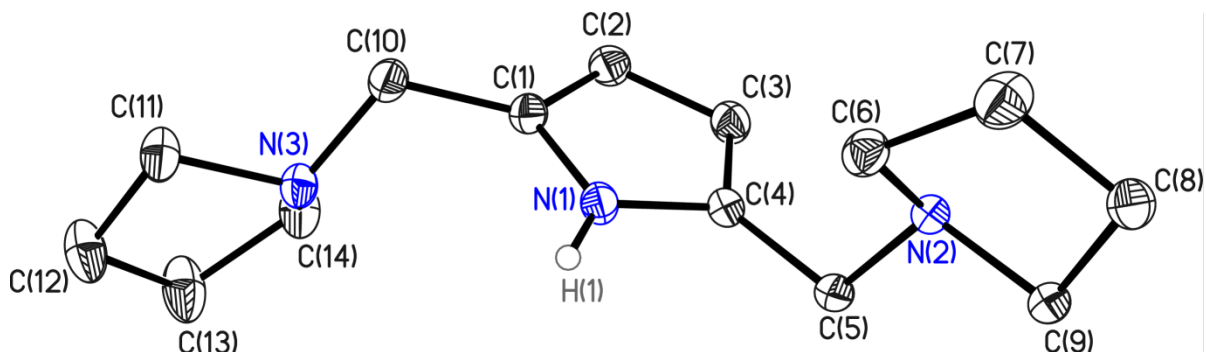
The unit cell was indexed with the tools in the Bruker APEX2 software suite.¹⁴⁵ The intensities on the raw frames were integrated with SAINT 7.68a.¹⁴⁶ The orientation matrix was refined in several integration runs and the maximum resolution was adjusted so that only useable data with a maximum R_{int} of 0.20 were integrated.

The software SADABS 2012/1¹⁴⁷ was used for absorption correction and scaling. TWINABS¹⁴⁸ was used in the cases of non-merohedral twins. XPREP¹⁴⁹ was used for the examination of data statistics and preliminary space group determination. The program SHELXS¹⁵⁰ was used to create a structure solution which was refined using SHELXL-2012¹⁵¹ within the SHELXLE-GUI.¹⁵²

All non-hydrogen-atoms were refined with anisotropic displacement parameters. The C-bound hydrogen atoms were refined isotropically on calculated positions using a riding model with their U_{iso} values constrained equal to 1.5 times the U_{eq} of their pivot atoms for terminal sp³ carbon atoms and 1.2 times for all other carbon atoms. The N-bonded hydrogen atoms were refined freely from the residual density map and constrained to 1.5 U_{eq} of their pivot nitrogen atom. Disordered moieties were refined using bond lengths restraints and isotropic displacement parameter restraints.²⁶

5.2 Determined Structures

5.2.1 2,5-Bis((pyrrolidine)methyl)pyrrole (2)

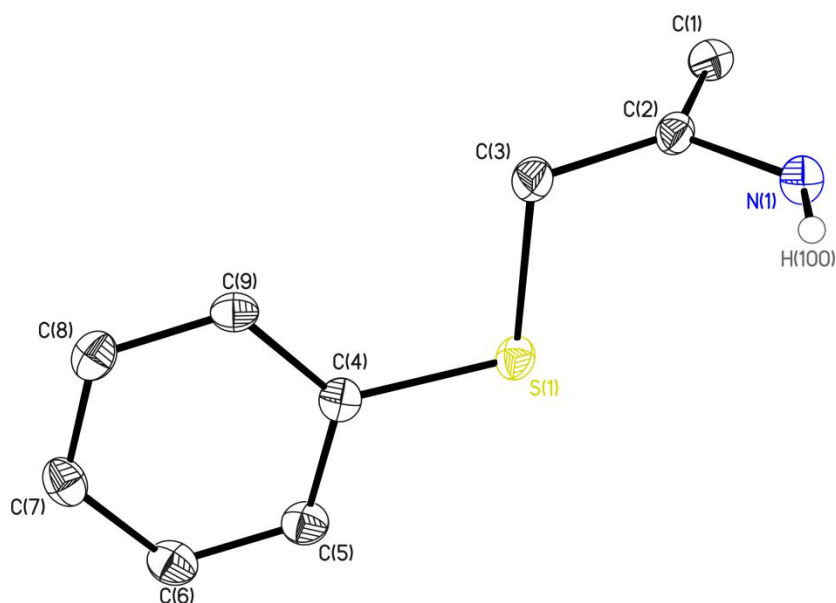


Asymmetric unit of compound **2**. Thermal ellipsoids are depicted at the 50% probability level, hydrogen atoms besides H1 are omitted for clarity.

CCDC no.	928751	<i>Z</i>	8
Empirical formula	C ₁₄ H ₂₃ N ₃	Absorption coefficient	0.070 mm ⁻¹
Formula weight	233.35	<i>F</i> (000)	1024
Temperature	100(2) K	Crystal size	0.2 x 0.1 x 0.1 mm ³
Wavelength	0.71073 Å	Theta range for data collection	2.256 to 30.028°
Crystal system	Orthorhombic	Reflections collected	61880
Space group	<i>Pbca</i>	Independent reflections	3914 [<i>R</i> (int) = 0.0481]
Unit cell dimensions		Completeness to theta = 25.242°	99.4 %
	<i>a</i> = 8.903(2) Å	Data / restraints / parameters	3914 / 3 / 158
	<i>b</i> = 16.681(3) Å	Goodness-of-fit on <i>F</i> ²	1.102
	<i>c</i> = 18.058(3) Å	<i>R</i> 1 [<i>I</i> > 2σ(<i>I</i>)]	0.0426
	α = 90°	w <i>R</i> 2 (all data)	0.1283
	β = 90°	Extinction coefficient	-
	γ = 90°	Largest diff. peak and hole	0.380 and -0.205 e.Å ⁻³
Volume	2681.8(9) Å ³	Absolute structure parameter	-

Selected bond lengths [pm] and angles [°] of (2)

N(1)-C(4)	137.38(13)	N(1)-C(1)-C(10)	122.17(10)
N(1)-C(1)	137.59(13)	C(2)-C(1)-C(10)	130.43(10)
N(1)-H(1)	85.2(17)	C(1)-C(2)-C(3)	107.85(9)
C(1)-C(2)	137.69(15)	C(9)-N(2)-C(5)	112.14(8)
C(1)-C(10)	149.00(15)	C(9)-N(2)-C(6)	103.14(8)
C(2)-C(3)	141.98(15)	C(5)-N(2)-C(6)	113.89(8)
N(2)-C(9)	146.69(13)	C(10)-N(3)-C(14)	113.85(9)
N(2)-C(5)	146.84(13)	C(10)-N(3)-C(11)	111.99(9)
N(2)-C(6)	147.18(13)	C(14)-N(3)-C(11)	104.29(8)
N(3)-C(10)	145.84(14)	C(4)-C(3)-C(2)	107.22(10)
N(3)-C(14)	145.97(14)	N(1)-C(4)-C(3)	107.89(9)
N(3)-C(11)	146.34(14)	N(1)-C(4)-C(5)	121.41(9)
C(3)-C(4)	137.46(15)	C(3)-C(4)-C(5)	130.56(10)
C(4)-C(5)	149.27(14)	N(2)-C(6)-C(7)	103.08(9)
C(6)-C(7)	153.31(16)	N(2)-C(5)-C(4)	111.99(8)
C(9)-C(8)	153.27(14)	N(2)-C(9)-C(8)	103.02(8)
C(8)-C(7)	154.22(16)	C(9)-C(8)-C(7)	104.07(9)
C(11)-C(12)	152.64(16)	C(6)-C(7)-C(8)	104.62(9)
C(12)-C(13)	154.18(18)	N(3)-C(10)-C(1)	113.93(9)
C(13)-C(14)	152.72(17)	N(3)-C(11)-C(12)	104.57(9)
		C(11)-C(12)-C(13)	104.55(10)
C(4)-N(1)-C(1)	109.73(9)	C(14)-C(13)-C(12)	104.41(10)
C(4)-N(1)-H(1)	123.9(11)	N(3)-C(14)-C(13)	103.54(9)
C(1)-N(1)-H(1)	126.0(11)		
N(1)-C(1)-C(2)	107.31(9)		

5.2.2 2,5-bis((thiophenolato)methyl)pyrrole (**6**)

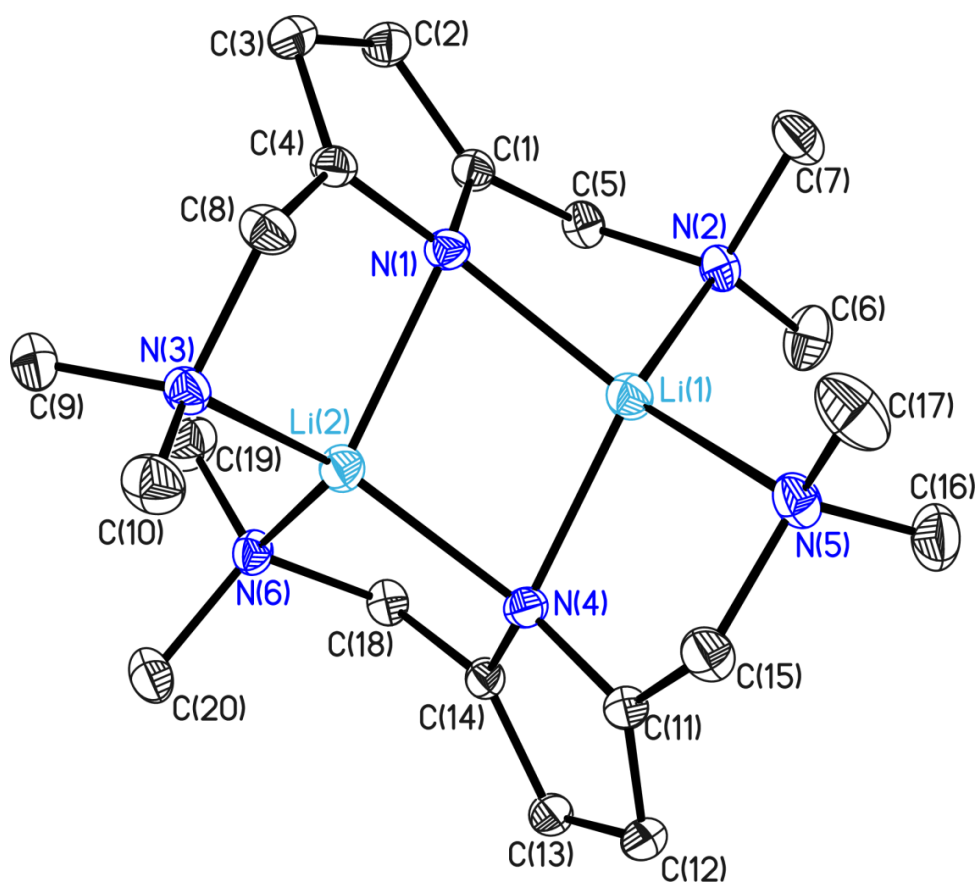
Asymmetric unit of compound **6**, containing a half molecule. Thermal ellipsoids are depicted at the 50% probability level, hydrogen atoms besides H100 are omitted for clarity.

CCDC no.	-	Z	4
Empirical formula	C18 H17 N S2	Absorption coefficient	0.332 mm ⁻¹
Formula weight	311.44	F(000)	656
Temperature	100(2) K	Crystal size	0.15 x 0.1 x 0.1 mm ³
Wavelength	0.71073 Å	Theta range for data collection	1.248 to 25.337°
Crystal system	Orthorhombic	Reflections collected	7618
Space group	<i>Pnma</i>	Independent reflections	1447 [<i>R</i> (int) = 0.0641]
Unit cell dimensions		Completeness to theta = 25.242°	99.7 %
	<i>a</i> = 6.532(2) Å	Data / restraints / parameters	1447 / 0 / 100
	<i>b</i> = 32.631(3) Å	Goodness-of-fit on <i>F</i> ²	1.038
	<i>c</i> = 7.345(2) Å	<i>R</i> 1 [<i>I</i> > 2σ(<i>I</i>)]	0.0378
	α = 90°	w <i>R</i> 2 (all data)	0.0882
	β = 90°	Extinction coefficient	-
	γ = 90°	Largest diff. peak and hole	0.320 and -0.241 e.Å ⁻³
Volume	1566.3(7) Å ³	Absolute structure parameter	-

Selected bond lengths [pm] and angles [°] of (6)

S(1)-C(4)	176.9(2)	C(4)-S(1)-C(3)	104.54(10)
S(1)-C(3)	182.6(2)	C(2)A-N(1)-C(2)	109.6(3)
N(1)-C(2)A	137.8(3)	C(2)-C(1)-C(1)A	107.91(13)
N(1)-C(2)	137.8(3)	C(1)-C(2)-N(1)	107.3(2)
C(1)-C(2)	137.3(3)	C(1)-C(2)-C(3)	130.6(2)
C(1)-C(1)A	140.9(4)	N(1)-C(2)-C(3)	121.9(2)
C(2)-C(3)	148.7(3)	C(5)-C(4)-C(9)	119.3(2)
C(4)-C(5)	139.6(3)	C(5)-C(4)-S(1)	115.65(17)
C(4)-C(9)	139.7(3)	C(9)-C(4)-S(1)	124.97(17)
C(5)-C(6)	138.0(3)	C(2)-C(3)-S(1)	107.41(15)
C(9)-C(8)	138.6(3)	C(6)-C(5)-C(4)	120.6(2)
C(8)-C(7)	138.4(3)	C(8)-C(9)-C(4)	119.4(2)
C(7)-C(6)	139.0(3)	C(7)-C(8)-C(9)	121.1(2)
		C(8)-C(7)-C(6)	119.5(2)
		C(5)-C(6)-C(7)	120.0(2)

5.2.3 Lithium-2,5-bis(dimethylamino)methyl pyrrolide (7)



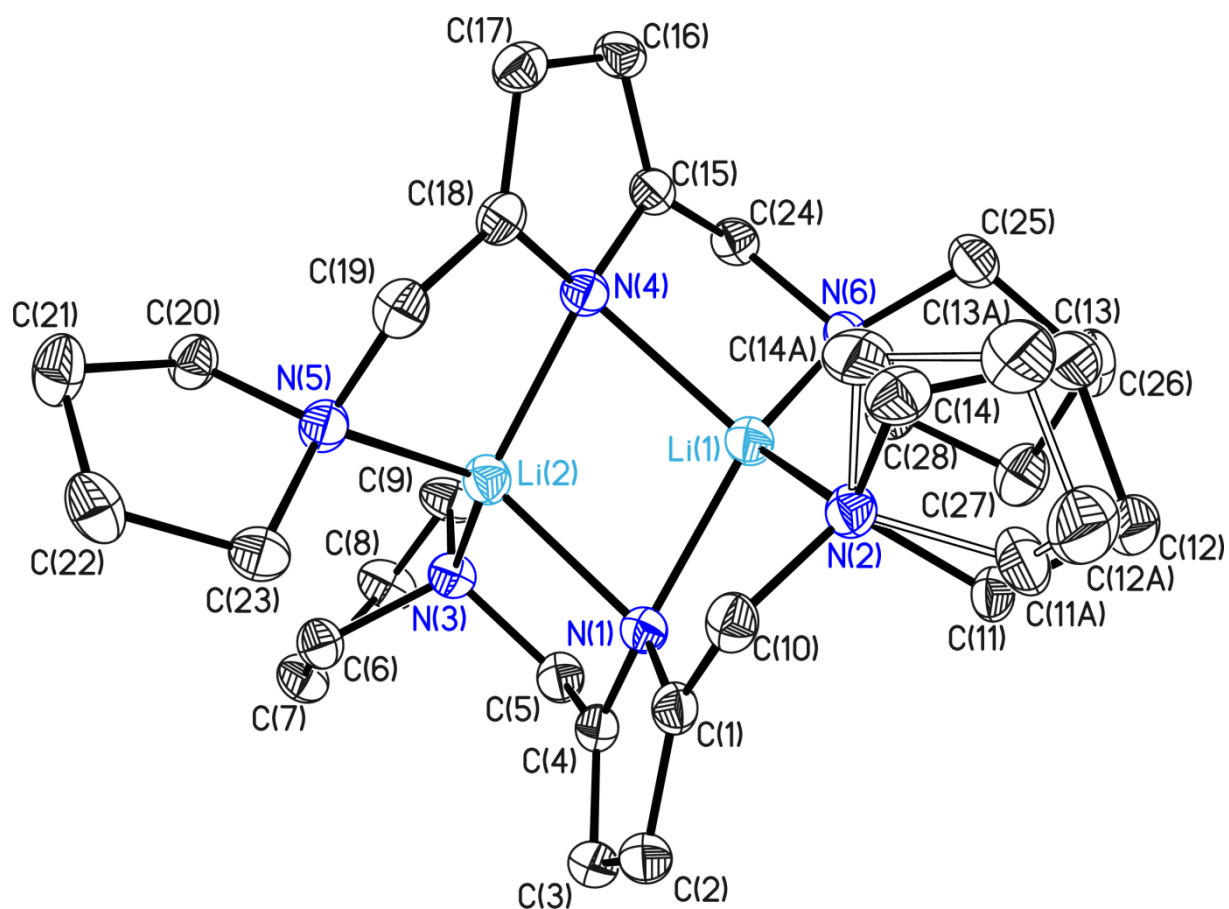
Asymmetric unit of compound 7. Thermal ellipsoids are depicted at the 50% probability level, hydrogen atoms are omitted for clarity.

CCDC no.	-	Z	4
Empirical formula	C ₂₀ H ₃₆ Li ₂ N ₆	Absorption coefficient	0.065 mm ⁻¹
Formula weight	374.43	F(000)	816
Temperature	100(2) K	Crystal size	0.1 x 0.1 x 0.1 mm ³
Wavelength	0.71073 Å	Theta range for data collection	1.596 to 53.895°
Crystal system	Monoclinic	Reflections collected	417443
Space group	<i>P</i> 2 ₁ / <i>c</i>	Independent reflections	28447 [<i>R</i> (int) = 0.0529]
Unit cell dimensions		Completeness to theta = 25.242°	100.0 %
	<i>a</i> = 12.793(3) Å	Data / restraints / parameters	28447 / 0 / 261
	<i>b</i> = 9.709(2) Å	Goodness-of-fit on <i>F</i> ²	1.091
	<i>c</i> = 18.672(3) Å	<i>R</i> 1 [<i>I</i> > 2σ(<i>I</i>)]	0.0386
	α = 90°	w <i>R</i> 2 (all data)	0.1338
	β = 94.31(3)°	Extinction coefficient	-
	γ = 90°	Largest diff. peak and hole	0.582 and -0.212 e.Å ⁻³
Volume	2312.6(8) Å ³	Absolute structure parameter	-

Selected bond lengths [pm] and angles [°] of (7)

N(1)-C(4)	137.44(4)	N(1)-C(1)-C(2)	111.15(3)
N(1)-C(1)	137.51(4)	N(1)-C(1)-C(5)	118.93(2)
N(1)-Li(1)	204.47(8)	C(2)-C(1)-C(5)	129.88(3)
N(1)-Li(2)	212.05(10)	N(1)-C(1)-Li(1)	45.89(2)
C(1)-C(2)	138.75(5)	C(2)-C(1)-Li(1)	153.34(3)
C(1)-C(5)	149.54(5)	C(5)-C(1)-Li(1)	74.21(2)
C(1)-Li(1)	274.75(9)	N(1)-Li(1)-N(4)	102.66(3)
Li(1)-N(4)	207.09(10)	N(1)-Li(1)-N(2)	87.14(3)
Li(1)-N(2)	211.46(8)	N(4)-Li(1)-N(2)	127.88(4)
Li(1)-N(5)	213.06(9)	N(1)-Li(1)-N(5)	139.54(4)
Li(1)-C(11)	271.08(10)	N(4)-Li(1)-N(5)	88.58(3)
Li(1)-C(5)	274.76(9)	N(2)-Li(1)-N(5)	116.38(4)
Li(1)-C(15)	278.99(9)	N(1)-Li(1)-C(11)	127.53(3)
N(2)-C(6)	146.26(5)	N(4)-Li(1)-C(11)	29.724(18)
N(2)-C(7)	146.39(6)	N(2)-Li(1)-C(11)	133.68(4)
N(2)-C(5)	148.06(5)	N(5)-Li(1)-C(11)	59.29(2)
C(2)-C(3)	142.22(5)	N(1)-Li(1)-C(1)	28.875(13)
Li(2)-N(4)	203.56(8)	N(4)-Li(1)-C(1)	114.24(3)
Li(2)-N(6)	210.31(9)	N(2)-Li(1)-C(1)	58.81(2)
Li(2)-N(3)	211.47(8)	N(5)-Li(1)-C(1)	154.70(4)
Li(2)-C(4)	264.14(9)	C(11)-Li(1)-C(1)	143.94(3)
Li(2)-C(14)	269.76(9)	N(1)-Li(1)-C(5)	60.03(2)
Li(2)-C(18)	274.06(8)	N(4)-Li(1)-C(5)	113.32(4)
Li(2)-C(8)	275.41(8)	N(2)-Li(1)-C(5)	32.240(15)
N(3)-C(10)	146.61(5)	N(5)-Li(1)-C(5)	148.52(3)
N(3)-C(9)	147.13(5)	C(11)-Li(1)-C(5)	136.69(3)
N(3)-C(8)	148.15(6)	C(1)-Li(1)-C(5)	31.583(14)
C(3)-C(4)	138.83(5)	N(1)-Li(1)-C(15)	130.87(3)
N(5)-C(17)	146.31(6)	N(4)-Li(1)-C(15)	58.41(3)
N(5)-C(16)	146.54(6)	N(2)-Li(1)-C(15)	141.44(3)
N(5)-C(15)	148.56(6)	N(5)-Li(1)-C(15)	31.690(19)
N(4)-C(11)	137.36(4)	C(11)-Li(1)-C(15)	31.457(15)
N(4)-C(14)	137.57(4)	C(1)-Li(1)-C(15)	159.64(3)
C(4)-C(8)	149.25(5)	C(5)-Li(1)-C(15)	165.79(3)
N(6)-C(19)	146.40(5)	C(6)-N(2)-C(7)	109.88(3)
N(6)-C(20)	146.71(6)	C(6)-N(2)-C(5)	109.95(3)
N(6)-C(18)	148.44(5)	C(7)-N(2)-C(5)	109.85(3)
C(11)-C(12)	138.72(5)	C(6)-N(2)-Li(1)	119.74(3)
C(11)-C(15)	149.30(6)	C(7)-N(2)-Li(1)	108.54(4)
C(12)-C(13)	142.39(6)	C(5)-N(2)-Li(1)	98.13(3)
C(13)-C(14)	138.62(4)	C(1)-C(2)-C(3)	106.00(3)
C(14)-C(18)	149.49(5)	N(4)-Li(2)-N(6)	89.80(3)
		N(4)-Li(2)-N(3)	137.14(4)
C(4)-N(1)-C(1)	105.65(2)	N(6)-Li(2)-N(3)	120.34(3)
C(4)-N(1)-Li(1)	145.11(3)	N(4)-Li(2)-N(1)	101.25(3)
C(1)-N(1)-Li(1)	105.23(3)	N(6)-Li(2)-N(1)	118.48(4)
C(4)-N(1)-Li(2)	95.82(2)	N(3)-Li(2)-N(1)	90.62(3)
C(1)-N(1)-Li(2)	129.53(3)	N(4)-Li(2)-C(4)	129.02(3)
Li(1)-N(1)-Li(2)	76.49(3)	N(6)-Li(2)-C(4)	123.45(4)

N(3)-Li(2)-C(4)	60.96(2)	C(11)-N(4)-Li(1)	101.90(3)
N(1)-Li(2)-C(4)	31.174(16)	C(14)-N(4)-Li(1)	131.83(3)
N(4)-Li(2)-C(14)	29.821(15)	Li(2)-N(4)-Li(1)	77.81(3)
N(6)-Li(2)-C(14)	59.99(2)	N(1)-C(4)-C(3)	111.04(3)
N(3)-Li(2)-C(14)	151.64(4)	N(1)-C(4)-C(8)	118.42(3)
N(1)-Li(2)-C(14)	114.64(3)	C(3)-C(4)-C(8)	130.52(3)
C(4)-Li(2)-C(14)	145.70(3)	N(1)-C(4)-Li(2)	53.00(2)
N(4)-Li(2)-C(18)	60.07(2)	C(3)-C(4)-Li(2)	136.47(3)
N(6)-Li(2)-C(18)	32.424(14)	C(8)-C(4)-Li(2)	78.15(3)
N(3)-Li(2)-C(18)	151.94(3)	C(19)-N(6)-C(20)	109.86(3)
N(1)-Li(2)-C(18)	108.88(3)	C(19)-N(6)-C(18)	110.21(3)
C(4)-Li(2)-C(18)	131.64(3)	C(20)-N(6)-C(18)	109.63(3)
C(14)-Li(2)-C(18)	31.898(14)	C(19)-N(6)-Li(2)	113.90(4)
N(4)-Li(2)-C(8)	131.79(3)	C(20)-N(6)-Li(2)	114.49(3)
N(6)-Li(2)-C(8)	138.34(3)	C(18)-N(6)-Li(2)	98.14(2)
N(3)-Li(2)-C(8)	32.150(17)	N(3)-C(8)-C(4)	111.26(3)
N(1)-Li(2)-C(8)	59.02(2)	N(3)-C(8)-Li(2)	49.43(2)
C(4)-Li(2)-C(8)	32.030(13)	C(4)-C(8)-Li(2)	69.82(3)
C(14)-Li(2)-C(8)	161.60(3)	N(4)-C(11)-C(12)	111.09(3)
C(18)-Li(2)-C(8)	162.30(3)	N(4)-C(11)-C(15)	117.65(3)
C(10)-N(3)-C(9)	109.56(3)	C(12)-C(11)-C(15)	131.15(3)
C(10)-N(3)-C(8)	109.71(3)	N(4)-C(11)-Li(1)	48.38(2)
C(9)-N(3)-C(8)	109.35(3)	C(12)-C(11)-Li(1)	140.58(3)
C(10)-N(3)-Li(2)	123.83(3)	C(15)-C(11)-Li(1)	77.19(3)
C(9)-N(3)-Li(2)	104.99(3)	C(11)-C(12)-C(13)	105.98(3)
C(8)-N(3)-Li(2)	98.42(3)	C(14)-C(13)-C(12)	106.20(3)
C(4)-C(3)-C(2)	106.14(3)	N(4)-C(14)-C(13)	110.94(3)
C(17)-N(5)-C(16)	109.71(4)	N(4)-C(14)-C(18)	118.47(3)
C(17)-N(5)-C(15)	110.63(3)	C(13)-C(14)-C(18)	130.59(3)
C(16)-N(5)-C(15)	109.87(3)	N(4)-C(14)-Li(2)	47.38(2)
C(17)-N(5)-Li(1)	119.65(4)	C(13)-C(14)-Li(2)	148.16(3)
C(16)-N(5)-Li(1)	106.94(3)	C(18)-C(14)-Li(2)	75.63(2)
C(15)-N(5)-Li(1)	99.42(3)	N(5)-C(15)-C(11)	110.48(3)
N(2)-C(5)-C(1)	110.82(3)	N(5)-C(15)-Li(1)	48.89(2)
N(2)-C(5)-Li(1)	49.63(2)	C(11)-C(15)-Li(1)	71.35(3)
C(1)-C(5)-Li(1)	74.20(2)	N(6)-C(18)-C(14)	110.95(2)
C(11)-N(4)-C(14)	105.79(3)	N(6)-C(18)-Li(2)	49.43(2)
C(11)-N(4)-Li(2)	140.39(3)	C(14)-C(18)-Li(2)	72.47(3)
C(14)-N(4)-Li(2)	102.80(3)		

5.2.4 Lithium[2,5-Bis((pyrrolidine)methyl)pyrrolide] (**8**)

Asymmetric unit of compound **8**. Thermal ellipsoids are depicted at the 50% probability level, hydrogen atoms are omitted for clarity. **8** contains a disorder caused by a flipping of the envelope conformation of the pyrrolidine moiety containing N2 (site occupation factor: 0.89)

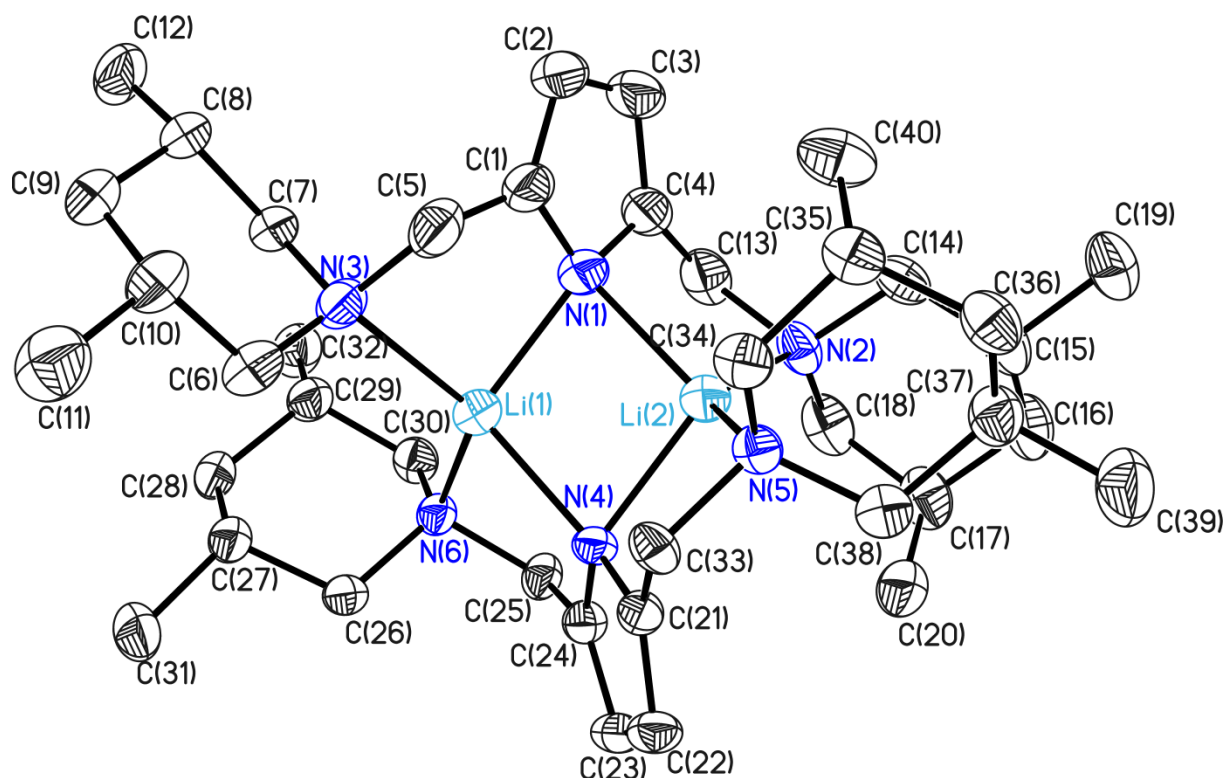
CCDC no.	-	Z	4
Empirical formula	C ₂₈ H ₄₄ Li ₂ N ₆	Absorption coefficient	0.070 mm ⁻¹
Formula weight	478.57	F(000)	1040
Temperature	100(2) K	Crystal size	0.2 x 0.15 x 0.15 mm ³
Wavelength	0.71073 Å	Theta range for data collection	1.60 to 27.13°.
Crystal system	Monoclinic	Reflections collected	59475
Space group	<i>P</i> 2 ₁ / <i>n</i>	Independent reflections	5982 [<i>R</i> (int) = 0.0323]
Unit cell dimensions		Completeness to theta = 25.242°	99.8 %
	<i>a</i> = 9.746(2) Å	Data / restraints / parameters	5982 / 78 / 353
	<i>b</i> = 25.413(3) Å	Goodness-of-fit on <i>F</i> ²	1.046
	<i>c</i> = 11.319(2) Å	<i>R</i> 1 [<i>I</i> > 2σ(<i>I</i>)]	0.0444
	α = 90°	w <i>R</i> 2 (all data)	0.1260
	β = 105.55(2)°	Extinction coefficient	-
	γ = 90°	Largest diff. peak and hole	0.317 and -0.269 e.Å ⁻³
Volume	2700.8(8) Å ³	Absolute structure parameter	-

Selected bond lengths [pm] and angles [°] of (8)

N(1)-C(4)	137.35(17)	C(25)-C(26)	153.9(2)
N(1)-C(1)	137.44(17)	C(26)-C(27)	153.7(2)
N(1)-Li(1)	201.9(2)	C(27)-C(28)	152.2(2)
N(1)-Li(2)	208.3(3)	C(12)-C(13)	152.4(2)
Li(1)-N(4)	207.2(3)	C(13)-C(14)	152.2(3)
Li(1)-N(2)	213.4(3)	C(12A)-C(13A)	157(2)
Li(1)-N(6)	216.8(3)	C(13A)-C(14A)	149.2(10)
Li(1)-C(15)	267.2(3)		
Li(1)-C(1)	275.0(3)	C(4)-N(1)-C(1)	105.33(11)
C(1)-C(2)	138.04(19)	C(4)-N(1)-Li(1)	143.03(12)
C(1)-C(10)	149.7(2)	C(1)-N(1)-Li(1)	106.77(11)
N(2)-C(10)	147.88(17)	C(4)-N(1)-Li(2)	97.32(10)
N(2)-C(14)	148.7(2)	C(1)-N(1)-Li(2)	128.71(11)
N(2)-C(11)	149.19(17)	Li(1)-N(1)-Li(2)	76.32(10)
N(2)-C(14A)	154.5(19)	N(1)-Li(1)-N(4)	102.89(11)
C(2)-C(3)	141.1(2)	N(1)-Li(1)-N(2)	87.21(10)
Li(2)-N(4)	201.3(3)	N(4)-Li(1)-N(2)	121.48(12)
Li(2)-N(5)	206.6(3)	N(1)-Li(1)-N(6)	129.28(12)
Li(2)-N(3)	207.9(3)	N(4)-Li(1)-N(6)	89.09(9)
Li(2)-C(4)	263.7(3)	N(2)-Li(1)-N(6)	127.74(12)
Li(2)-C(18)	272.5(3)	N(1)-Li(1)-C(15)	127.71(11)
Li(2)-C(19)	277.6(3)	N(4)-Li(1)-C(15)	30.43(5)
Li(2)-C(5)	277.8(3)	N(2)-Li(1)-C(15)	130.37(11)
N(3)-C(9)	147.99(17)	N(6)-Li(1)-C(15)	60.29(7)
N(3)-C(6)	148.42(17)	N(1)-Li(1)-C(1)	28.58(5)
N(3)-C(5)	149.25(18)	N(4)-Li(1)-C(1)	114.42(10)
C(3)-C(4)	138.2(2)	N(2)-Li(1)-C(1)	58.70(7)
C(4)-C(5)	149.4(2)	N(6)-Li(1)-C(1)	148.24(11)
N(4)-C(18)	137.03(17)	C(15)-Li(1)-C(1)	144.73(10)
N(4)-C(15)	137.31(17)	N(1)-C(1)-C(2)	111.20(12)
N(5)-C(23)	147.78(17)	N(1)-C(1)-C(10)	118.24(12)
N(5)-C(20)	147.96(17)	C(2)-C(1)-C(10)	130.54(13)
N(5)-C(19)	150.06(18)	N(1)-C(1)-Li(1)	44.64(8)
C(6)-C(7)	153.92(19)	C(2)-C(1)-Li(1)	151.36(12)
N(6)-C(28)	147.14(18)	C(10)-C(1)-Li(1)	75.89(9)
N(6)-C(25)	148.04(17)	C(10)-N(2)-C(14)	111.85(12)
N(6)-C(24)	148.10(17)	C(10)-N(2)-C(11)	110.46(11)
C(7)-C(8)	153.6(2)	C(14)-N(2)-C(11)	105.43(12)
C(9)-C(8)	153.57(19)	C(10)-N(2)-C(14A)	112.8(8)
C(11)-C(12)	150.6(2)	C(14)-N(2)-C(14A)	21.9(7)
C(11)-C(12A)	155.9(9)	C(11)-N(2)-C(14A)	122.2(6)
C(15)-C(16)	138.16(19)	C(10)-N(2)-Li(1)	99.67(10)
C(15)-C(24)	149.62(19)	C(14)-N(2)-Li(1)	121.15(13)
C(16)-C(17)	142.2(2)	C(11)-N(2)-Li(1)	108.11(10)
C(17)-C(18)	138.37(19)	C(14A)-N(2)-Li(1)	100.4(8)
C(18)-C(19)	150.29(19)	C(1)-C(2)-C(3)	106.10(12)
C(20)-C(21)	153.75(19)	N(4)-Li(2)-N(5)	89.05(10)
C(21)-C(22)	152.8(2)	N(4)-Li(2)-N(3)	130.92(13)
C(22)-C(23)	153.0(2)	N(5)-Li(2)-N(3)	124.51(12)

N(4)-Li(2)-N(1)	102.70(11)	C(20)-N(5)-C(19)	109.84(11)
N(5)-Li(2)-N(1)	120.33(12)	C(23)-N(5)-Li(2)	115.21(11)
N(3)-Li(2)-N(1)	90.32(10)	C(20)-N(5)-Li(2)	115.36(11)
N(4)-Li(2)-C(4)	129.34(11)	C(19)-N(5)-Li(2)	101.00(10)
N(5)-Li(2)-C(4)	126.51(11)	N(3)-C(6)-C(7)	106.17(11)
N(3)-Li(2)-C(4)	61.25(7)	C(28)-N(6)-C(25)	103.40(11)
N(1)-Li(2)-C(4)	31.11(5)	C(28)-N(6)-C(24)	112.49(11)
N(4)-Li(2)-C(18)	28.96(5)	C(25)-N(6)-C(24)	112.35(10)
N(5)-Li(2)-C(18)	60.09(7)	C(28)-N(6)-Li(1)	120.85(11)
N(3)-Li(2)-C(18)	147.28(11)	C(25)-N(6)-Li(1)	109.28(10)
N(1)-Li(2)-C(18)	115.90(10)	C(24)-N(6)-Li(1)	98.74(10)
C(4)-Li(2)-C(18)	147.00(10)	C(8)-C(7)-C(6)	104.70(11)
N(4)-Li(2)-C(19)	59.44(7)	N(3)-C(9)-C(8)	106.67(11)
N(5)-Li(2)-C(19)	32.05(6)	C(7)-C(8)-C(9)	104.24(11)
N(3)-Li(2)-C(19)	153.91(11)	N(2)-C(10)-C(1)	111.06(11)
N(1)-Li(2)-C(19)	111.80(10)	N(2)-C(11)-C(12)	108.17(13)
C(4)-Li(2)-C(19)	135.67(10)	N(2)-C(11)-C(12A)	89.4(8)
C(18)-Li(2)-C(19)	31.70(5)	C(12)-C(11)-C(12A)	26.1(8)
N(4)-Li(2)-C(5)	129.21(11)	N(4)-C(15)-C(16)	110.94(12)
N(5)-Li(2)-C(5)	141.73(11)	N(4)-C(15)-C(24)	117.25(11)
N(3)-Li(2)-C(5)	31.85(5)	C(16)-C(15)-C(24)	131.74(12)
N(1)-Li(2)-C(5)	58.68(7)	N(4)-C(15)-Li(1)	49.86(8)
C(4)-Li(2)-C(5)	31.89(5)	C(16)-C(15)-Li(1)	139.61(11)
C(18)-Li(2)-C(5)	158.16(10)	C(24)-C(15)-Li(1)	79.10(9)
C(19)-Li(2)-C(5)	166.76(10)	C(15)-C(16)-C(17)	105.99(12)
C(9)-N(3)-C(6)	102.02(10)	C(18)-C(17)-C(16)	106.30(12)
C(9)-N(3)-C(5)	112.01(11)	N(4)-C(18)-C(17)	110.73(12)
C(6)-N(3)-C(5)	109.35(10)	N(4)-C(18)-C(19)	118.09(11)
C(9)-N(3)-Li(2)	121.45(11)	C(17)-C(18)-C(19)	131.17(13)
C(6)-N(3)-Li(2)	111.10(10)	N(4)-C(18)-Li(2)	45.35(8)
C(5)-N(3)-Li(2)	100.83(10)	C(17)-C(18)-Li(2)	148.36(11)
C(4)-C(3)-C(2)	106.42(12)	C(19)-C(18)-Li(2)	76.03(9)
N(1)-C(4)-C(3)	110.94(12)	N(5)-C(19)-C(18)	110.35(11)
N(1)-C(4)-C(5)	117.93(12)	N(5)-C(19)-Li(2)	46.94(8)
C(3)-C(4)-C(5)	131.13(13)	C(18)-C(19)-Li(2)	72.28(9)
N(1)-C(4)-Li(2)	51.58(8)	N(5)-C(20)-C(21)	106.13(11)
C(3)-C(4)-Li(2)	135.99(11)	C(22)-C(21)-C(20)	104.62(12)
C(5)-C(4)-Li(2)	79.25(9)	C(21)-C(22)-C(23)	104.89(12)
C(18)-N(4)-C(15)	106.03(11)	N(5)-C(23)-C(22)	107.70(12)
C(18)-N(4)-Li(2)	105.69(11)	N(6)-C(24)-C(15)	112.07(11)
C(15)-N(4)-Li(2)	139.54(11)	N(6)-C(25)-C(26)	105.06(12)
C(18)-N(4)-Li(1)	131.78(11)	C(27)-C(26)-C(25)	105.17(12)
C(15)-N(4)-Li(1)	99.71(10)	C(28)-C(27)-C(26)	102.79(12)
Li(2)-N(4)-Li(1)	76.67(10)	N(6)-C(28)-C(27)	102.98(11)
N(3)-C(5)-C(4)	110.25(11)	C(11)-C(12)-C(13)	102.92(14)
N(3)-C(5)-Li(2)	47.32(7)	N(2)-C(14)-C(13)	104.60(14)
C(4)-C(5)-Li(2)	68.85(9)	C(11)-C(12A)-C(13A)	111.7(11)
C(23)-N(5)-C(20)	102.95(11)	C(14A)-C(13A)-C(12A)	105.5(13)
C(23)-N(5)-C(19)	112.77(11)	C(13A)-C(14A)-N(2)	98.1(12)

5.2.5 Lithium-[2,5-bis((3,5-dimethylpiperidino)methyl)pyrrolide] (9)



Asymmetric unit of compound **9**. Thermal ellipsoids are depicted at the 50% probability level, hydrogen atoms are omitted for clarity. The whole molecule is disordered (site occupation factor: 0.83) due to a flipping of the chair conformation of the six-membered rings involving N5 and N2. This disorder is not shown for clarity.

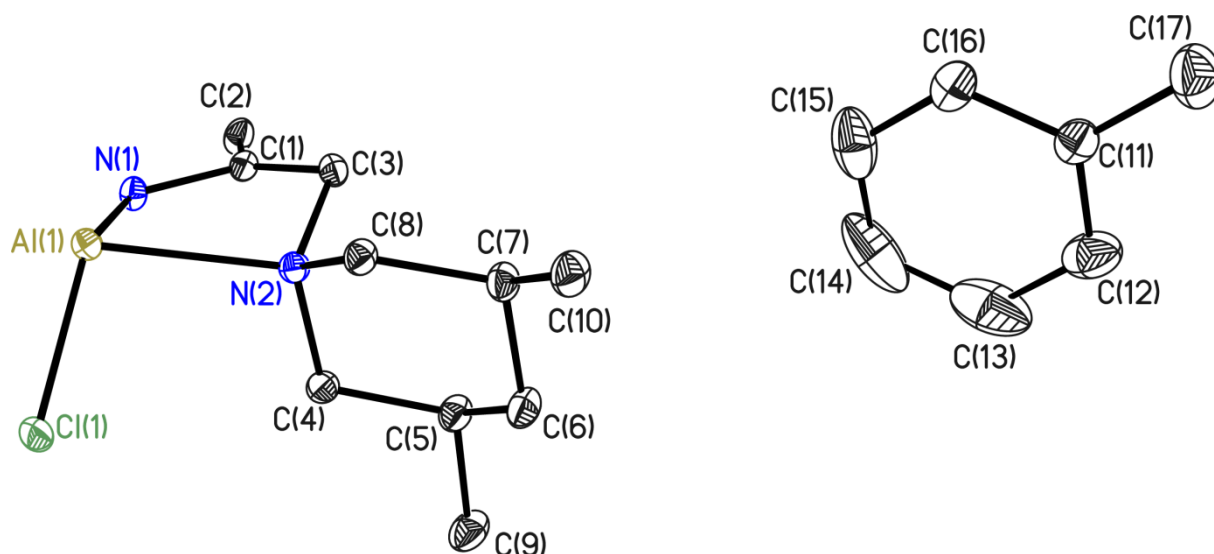
CCDC no.	-	Z	4
Empirical formula	C ₄₀ H ₆₈ Li ₂ N ₆	Absorption coefficient	0.062 mm ⁻¹
Formula weight	646.88	F(000)	1424
Temperature	105(2) K	Crystal size	0.2 x 0.2 x 0.2 mm ³
Wavelength	0.71073 Å	Theta range for data collection	1.337 to 26.416°
Crystal system	Monoclinic	Reflections collected	56034
Space group	<i>P</i> 2 ₁ / <i>c</i>	Independent reflections	8229 [<i>R</i> (int) = 0.0376]
Unit cell dimensions		Completeness to theta = 25.242°	99.9 %
	<i>a</i> = 13.864(3) Å	Data / restraints / parameters	8229 / 1151 / 851
	<i>b</i> = 30.460(3) Å	Goodness-of-fit on <i>F</i> ²	1.060
	<i>c</i> = 9.851(2) Å	<i>R</i> 1 [<i>I</i> > 2σ(<i>I</i>)]	0.0455
	α = 90°	w <i>R</i> 2 (all data)	0.1186
	β = 105.18(2)°	Extinction coefficient	-
	γ = 90°	Largest diff. peak and hole	0.260 and -0.202 e.Å ⁻³
Volume	4014.9(13) Å ³	Absolute structure parameter	-

Selected bond lengths [pm] and angles [°] of (9)

Li(2)-N(1)	203.9(5)	C(32)-C(29)	152.3(3)
Li(2)-N(4)	207.8(5)	C(27)-C(28)	152.5(3)
Li(2)-N(2)	230.6(5)	C(28)-C(29)	153.1(3)
Li(2)-N(5)	236.8(5)	C(34)-C(35)	152.8(3)
N(1)-C(1)	137.2(3)	C(35)-C(36)	152.3(4)
N(1)-C(4)	137.8(3)	C(35)-C(40)	152.4(3)
N(1)-Li(1)	201.3(8)	C(36)-C(37)	152.8(4)
N(2)-C(14)	147.8(4)	C(37)-C(39)	152.5(4)
N(2)-C(18)	147.8(3)	C(37)-C(38)	152.7(3)
N(2)-C(13)	148.9(4)		
N(3)-C(7)	147.4(2)	N(1)-Li(2)-N(4)	98.75(18)
N(3)-C(6)	147.6(3)	N(1)-Li(2)-N(2)	89.57(16)
N(3)-C(5)	149.9(3)	N(4)-Li(2)-N(2)	118.87(18)
N(3)-Li(1)	226.5(7)	N(1)-Li(2)-N(5)	119.44(19)
C(1)-C(2)	138.6(4)	N(4)-Li(2)-N(5)	88.85(17)
C(1)-C(5)	147.9(4)	N(2)-Li(2)-N(5)	137.35(17)
C(2)-C(3)	140.0(4)	N(1)-Li(2)-C(4)	31.06(10)
C(3)-C(4)	137.4(4)	N(4)-Li(2)-C(4)	119.92(18)
C(4)-C(13)	148.2(4)	N(2)-Li(2)-C(4)	60.03(13)
C(6)-C(10)	153.0(3)	N(5)-Li(2)-C(4)	135.27(17)
C(7)-C(8)	153.0(2)	N(1)-Li(2)-C(21)	120.9(2)
C(8)-C(12)	152.3(3)	N(4)-Li(2)-C(21)	30.98(14)
C(8)-C(9)	152.6(3)	N(2)-Li(2)-C(21)	133.1(2)
C(9)-C(10)	152.5(3)	N(5)-Li(2)-C(21)	59.80(15)
C(10)-C(11)	152.9(4)	C(4)-Li(2)-C(21)	148.7(2)
C(14)-C(15)	146.8(9)	C(1)-N(1)-C(4)	105.7(2)
C(15)-C(16)	152.8(4)	C(1)-N(1)-Li(1)	106.9(3)
C(15)-C(19)	153.5(4)	C(4)-N(1)-Li(1)	136.1(4)
C(16)-C(17)	153.5(3)	C(1)-N(1)-Li(2)	129.6(3)
C(17)-C(18)	151.6(4)	C(4)-N(1)-Li(2)	99.2(2)
C(17)-C(20)	153.1(3)	Li(1)-N(1)-Li(2)	81.79(18)
Li(1)-N(4)	206.8(6)	C(14)-N(2)-C(18)	105.9(3)
Li(1)-N(6)	220.7(9)	C(14)-N(2)-C(13)	111.1(3)
N(4)-C(21)	137.7(3)	C(18)-N(2)-C(13)	109.3(3)
N(4)-C(24)	137.7(3)	C(14)-N(2)-Li(2)	111.5(3)
N(5)-C(38)	146.7(4)	C(18)-N(2)-Li(2)	125.4(3)
N(5)-C(34)	148.7(3)	C(13)-N(2)-Li(2)	92.8(2)
N(5)-C(33)	149.3(3)	C(7)-N(3)-C(6)	109.19(14)
N(6)-C(26)	147.4(2)	C(7)-N(3)-C(5)	110.78(16)
N(6)-C(30)	147.7(2)	C(6)-N(3)-C(5)	112.40(17)
N(6)-C(25)	148.3(2)	C(7)-N(3)-Li(1)	110.84(14)
C(30)-C(29)	152.2(3)	C(6)-N(3)-Li(1)	118.48(19)
C(31)-C(27)	153.7(4)	C(5)-N(3)-Li(1)	94.4(2)
C(21)-C(22)	138.0(4)	N(1)-C(1)-C(2)	110.2(3)
C(21)-C(33)	150.1(4)	N(1)-C(1)-C(5)	118.2(2)
C(22)-C(23)	141.3(4)	C(2)-C(1)-C(5)	131.3(2)
C(23)-C(24)	137.2(3)	N(1)-C(1)-Li(1)	44.53(17)
C(24)-C(25)	150.0(3)	C(2)-C(1)-Li(1)	144.7(3)
C(26)-C(27)	151.8(3)	C(5)-C(1)-Li(1)	76.96(15)

C(1)-C(2)-C(3)	106.7(2)	Li(1)-N(4)-Li(2)	79.5(2)
C(4)-C(3)-C(2)	106.7(3)	C(38)-N(5)-C(34)	108.1(3)
C(3)-C(4)-N(1)	110.7(3)	C(38)-N(5)-C(33)	109.9(4)
C(3)-C(4)-C(13)	131.5(3)	C(34)-N(5)-C(33)	108.1(3)
N(1)-C(4)-C(13)	117.7(3)	C(38)-N(5)-Li(2)	111.9(3)
C(3)-C(4)-Li(2)	137.6(3)	C(34)-N(5)-Li(2)	125.5(3)
N(1)-C(4)-Li(2)	49.78(19)	C(33)-N(5)-Li(2)	91.5(3)
C(13)-C(4)-Li(2)	80.6(2)	C(26)-N(6)-C(30)	109.06(14)
C(1)-C(5)-N(3)	110.40(19)	C(26)-N(6)-C(25)	108.33(17)
N(3)-C(6)-C(10)	115.53(15)	C(30)-N(6)-C(25)	109.22(16)
N(3)-C(7)-C(8)	114.88(15)	C(26)-N(6)-Li(1)	110.31(15)
C(12)-C(8)-C(9)	111.32(17)	C(30)-N(6)-Li(1)	120.77(17)
C(12)-C(8)-C(7)	110.07(18)	C(25)-N(6)-Li(1)	98.17(17)
C(9)-C(8)-C(7)	109.87(15)	N(6)-C(30)-C(29)	112.49(15)
C(10)-C(9)-C(8)	113.55(18)	N(4)-C(21)-C(22)	110.5(3)
C(9)-C(10)-C(11)	111.3(3)	N(4)-C(21)-C(33)	117.0(4)
C(9)-C(10)-C(6)	109.29(18)	C(22)-C(21)-C(33)	132.2(4)
C(11)-C(10)-C(6)	110.6(3)	N(4)-C(21)-Li(2)	51.0(3)
C(4)-C(13)-N(2)	113.8(3)	C(22)-C(21)-Li(2)	137.9(5)
C(15)-C(14)-N(2)	115.6(3)	C(33)-C(21)-Li(2)	81.0(3)
C(14)-C(15)-C(16)	107.8(4)	C(21)-C(22)-C(23)	106.4(3)
C(14)-C(15)-C(19)	113.6(4)	C(24)-C(23)-C(22)	106.6(3)
C(16)-C(15)-C(19)	113.3(3)	C(23)-C(24)-N(4)	110.7(3)
C(15)-C(16)-C(17)	110.5(3)	C(23)-C(24)-C(25)	131.2(3)
C(18)-C(17)-C(20)	112.0(2)	N(4)-C(24)-C(25)	118.1(3)
C(18)-C(17)-C(16)	109.5(3)	C(23)-C(24)-Li(1)	148.0(3)
C(20)-C(17)-C(16)	112.5(3)	N(4)-C(24)-Li(1)	45.4(2)
N(2)-C(18)-C(17)	113.4(3)	C(25)-C(24)-Li(1)	76.02(19)
N(1)-Li(1)-N(4)	99.9(2)	N(6)-C(25)-C(24)	111.6(2)
N(1)-Li(1)-N(6)	130.3(2)	N(6)-C(26)-C(27)	112.78(15)
N(4)-Li(1)-N(6)	86.1(3)	C(26)-C(27)-C(28)	110.41(16)
N(1)-Li(1)-N(3)	85.9(4)	C(26)-C(27)-C(31)	109.0(3)
N(4)-Li(1)-N(3)	132.4(2)	C(28)-C(27)-C(31)	111.8(3)
N(6)-Li(1)-N(3)	125.33(19)	C(27)-C(28)-C(29)	111.84(19)
N(1)-Li(1)-C(1)	28.55(16)	C(30)-C(29)-C(32)	110.83(17)
N(4)-Li(1)-C(1)	116.3(3)	C(30)-C(29)-C(28)	109.79(16)
N(6)-Li(1)-C(1)	147.22(18)	C(32)-C(29)-C(28)	111.6(2)
N(3)-Li(1)-C(1)	57.4(2)	N(5)-C(33)-C(21)	114.1(5)
N(1)-Li(1)-C(24)	116.2(2)	N(5)-C(34)-C(35)	113.4(3)
N(4)-Li(1)-C(24)	28.31(15)	C(36)-C(35)-C(40)	113.5(3)
N(6)-Li(1)-C(24)	57.8(2)	C(36)-C(35)-C(34)	110.1(3)
N(3)-Li(1)-C(24)	148.6(2)	C(40)-C(35)-C(34)	112.2(3)
C(1)-Li(1)-C(24)	140.3(2)	C(35)-C(36)-C(37)	110.3(3)
C(21)-N(4)-C(24)	105.7(2)	C(39)-C(37)-C(38)	110.1(3)
C(21)-N(4)-Li(1)	140.1(4)	C(39)-C(37)-C(36)	112.8(3)
C(24)-N(4)-Li(1)	106.3(3)	C(38)-C(37)-C(36)	109.0(3)
C(21)-N(4)-Li(2)	98.0(4)	N(5)-C(38)-C(37)	113.2(3)
C(24)-N(4)-Li(2)	129.0(4)		

5.2.6 Aluminium-dichloro-{2,5-bis((3,5-dimethylpiperidino)methyl)-pyrrolide} (10)



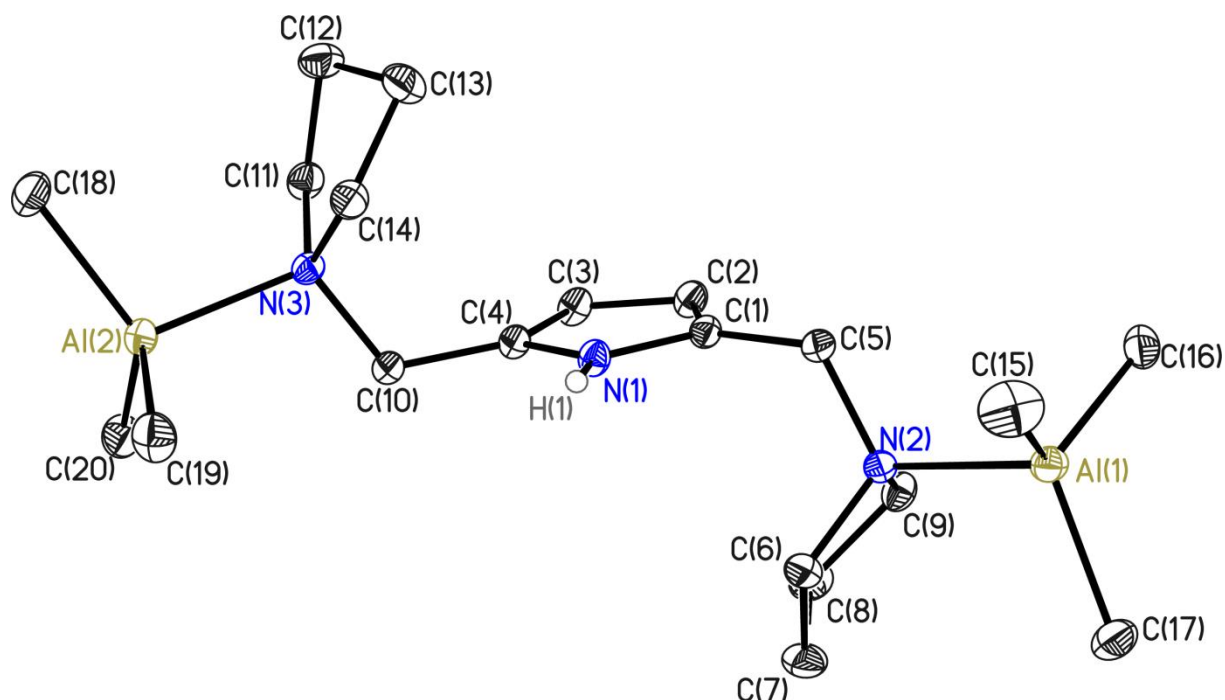
Asymmetric unit of compound **10**. Thermal ellipsoids are depicted at the 50% propability level, hydrogen atoms are omitted for clarity. Half a molecule of **10** is contained in the asymmetric unit, together with a non-disordered toluene solvent molecule.

CCDC no.	-	Z	4
Empirical formula	C ₃₄ H ₅₀ Al Cl ₂ N ₃	Absorption coefficient	0.136 mm ⁻¹
Formula weight	598.65	F(000)	1288
Temperature	100(2) K	Crystal size	0.13 x 0.12 x 0.1 mm ³
Wavelength	0.56086 Å	Theta range for data collection	1.146 to 26.416°
Crystal system	Monoclinic	Reflections collected	28217
Space group	C ₂ /c	Independent reflections	3948 [R(int) = 0.0363]
Unit cell dimensions		Completeness to theta = 25.242°	100.0 %
	a = 13.574(3) Å	Data / restraints / parameters	3948 / 0 / 187
	b = 8.631(2) Å	Goodness-of-fit on F ²	1.091
	c = 28.142(3) Å	R1 [I > 2sigma(I)]	0.0371
	α = 90°	wR2 (all data)	0.0845
	β = 94.60(2)°	Extinction coefficient	-
	γ = 90°	Largest diff. peak and hole	0.347 and -0.296 e.Å ⁻³
Volume	3286.4(11) Å ³	Absolute structure parameter	-

Selected bond lengths [pm] and angles [°] of (10)

Cl(1)-Al(1)	214.30(5)	N(1)-Al(1)-Cl(1)A	123.871(18)
C(1)-N(1)	136.37(15)	Cl(1)-Al(1)-Cl(1)A	112.26(3)
C(1)-C(2)	137.82(18)	N(1)-Al(1)-N(2)A	77.63(3)
C(1)-C(3)	150.00(17)	Cl(1)-Al(1)-N(2)A	95.90(3)
N(1)-C(1)A	136.37(15)	Cl(1)A-Al(1)-N(2)A	97.81(3)
N(1)-Al(1)	181.72(16)	N(1)-Al(1)-N(2)	77.63(3)
Al(1)-Cl(1)A	214.31(5)	Cl(1)-Al(1)-N(2)	97.81(3)
Al(1)-N(2)A	225.21(11)	Cl(1)A-Al(1)-N(2)	95.90(3)
Al(1)-N(2)	225.22(11)	N(2)A-Al(1)-N(2)	155.26(6)
N(2)-C(8)	149.25(16)	C(8)-N(2)-C(4)	108.79(9)
N(2)-C(4)	150.17(15)	C(8)-N(2)-C(3)	111.01(10)
N(2)-C(3)	151.02(16)	C(4)-N(2)-C(3)	109.72(10)
C(2)-C(2)A	143.8(3)	C(8)-N(2)-Al(1)	115.27(8)
C(4)-C(5)	153.00(17)	C(4)-N(2)-Al(1)	108.67(7)
C(7)-C(10)	152.71(18)	C(3)-N(2)-Al(1)	103.21(7)
C(7)-C(6)	152.96(18)	C(1)-C(2)-C(2)A	106.61(7)
C(7)-C(8)	153.15(17)	C(1)-C(3)-N(2)	107.15(10)
C(6)-C(5)	152.57(18)	N(2)-C(4)-C(5)	114.65(10)
C(5)-C(9)	152.81(18)	C(10)-C(7)-C(6)	111.47(11)
C(11)-C(12)	138.3(2)	C(10)-C(7)-C(8)	109.45(11)
C(11)-C(16)	138.9(2)	C(6)-C(7)-C(8)	109.95(10)
C(11)-C(17)	150.6(2)	C(5)-C(6)-C(7)	111.45(11)
C(12)-C(13)	138.5(3)	C(6)-C(5)-C(9)	112.23(11)
C(13)-C(14)	138.5(4)	C(6)-C(5)-C(4)	109.64(11)
C(14)-C(15)	138.3(3)	C(9)-C(5)-C(4)	109.69(11)
C(15)-C(16)	137.7(2)	N(2)-C(8)-C(7)	114.74(10)
		C(12)-C(11)-C(16)	118.71(15)
N(1)-C(1)-C(2)	108.67(11)	C(12)-C(11)-C(17)	120.33(15)
N(1)-C(1)-C(3)	112.26(11)	C(16)-C(11)-C(17)	120.96(14)
C(2)-C(1)-C(3)	138.90(12)	C(11)-C(12)-C(13)	120.20(18)
C(1)A-N(1)-C(1)	109.44(15)	C(14)-C(13)-C(12)	120.36(18)
C(1)A-N(1)-Al(1)	125.28(7)	C(15)-C(14)-C(13)	119.87(17)
C(1)-N(1)-Al(1)	125.28(7)	C(16)-C(15)-C(14)	119.35(18)
N(1)-Al(1)-Cl(1)	123.872(18)	C(15)-C(16)-C(11)	121.51(16)

5.2.7 2,5-bis((pyrrolidino)methyl)-1H-pyrrole · 2 trimethylaluminium (11)



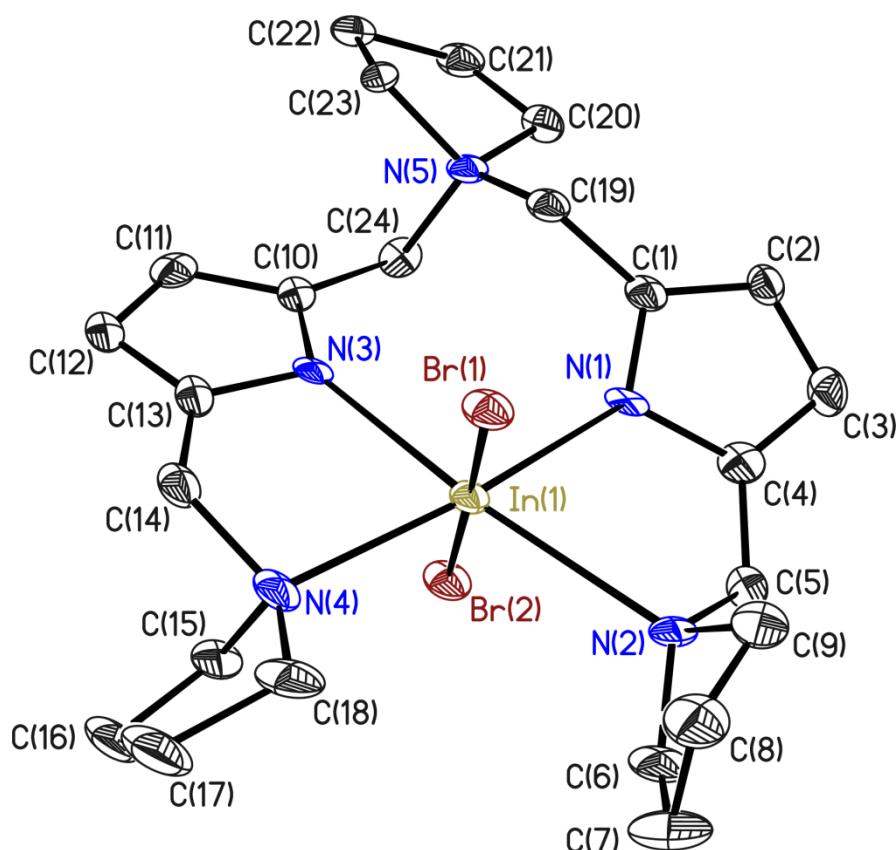
Asymmetric unit of compound **11**. Thermal ellipsoids are depicted at the 50% propability level, hydrogen atoms besides H1 are omitted for clarity.

CCDC no.	-	Z	4
Empirical formula	C ₂₀ H ₄₁ Al ₂ N ₃	Absorption coefficient	0.131 mm ⁻¹
Formula weight	377.52	F(000)	832
Temperature	100(2) K	Crystal size	0.2 x 0.15 x 0.15 mm ³
Wavelength	0.71073 Å	Theta range for data collection	1.767 to 40.361°
Crystal system	Monoclinic	Reflections collected	113567
Space group	<i>P</i> 2 ₁ / <i>c</i>	Independent reflections	14792 [<i>R</i> (int) = 0.0251]
Unit cell dimensions		Completeness to theta = 25.242°	100.0 %
	<i>a</i> = 11.571(2) Å	Data / restraints / parameters	14792 / 0 / 236
	<i>b</i> = 13.830(3) Å	Goodness-of-fit on <i>F</i> ²	1.043
	<i>c</i> = 14.767(3) Å	<i>R</i> 1 [<i>I</i> > 2σ(<i>I</i>)]	0.0307
	α = 90°	w <i>R</i> 2 (all data)	0.0983
	β = 95.15(2)°	Extinction coefficient	-
	γ = 90°	Largest diff. peak and hole	0.613 and -0.253 e.Å ⁻³
Volume	2353.6(7) Å ³	Absolute structure parameter	-

Selected bond lengths [pm] and angles [°] of (11)

Al(1)-C(15)	197.59(7)	C(2)-C(1)-C(5)	130.45(4)
Al(1)-C(16)	198.59(6)	C(4)-N(1)-C(1)	110.45(4)
Al(1)-C(17)	198.68(7)	C(20)-Al(2)-C(18)	116.74(3)
Al(1)-N(2)	204.48(4)	C(20)-Al(2)-C(19)	111.98(3)
C(1)-N(1)	137.61(6)	C(18)-Al(2)-C(19)	114.13(3)
C(1)-C(2)	138.01(6)	C(20)-Al(2)-N(3)	104.59(2)
C(1)-C(5)	149.38(6)	C(18)-Al(2)-N(3)	104.66(2)
N(1)-C(4)	137.31(6)	C(19)-Al(2)-N(3)	102.90(2)
Al(2)-C(20)	197.52(6)	C(1)-C(2)-C(3)	107.59(4)
Al(2)-C(18)	198.38(7)	C(10)-N(3)-C(14)	112.45(3)
Al(2)-C(19)	199.04(6)	C(10)-N(3)-C(11)	110.81(4)
Al(2)-N(3)	203.76(5)	C(14)-N(3)-C(11)	105.94(4)
C(2)-C(3)	142.04(6)	C(10)-N(3)-Al(2)	107.65(3)
N(3)-C(10)	150.57(6)	C(14)-N(3)-Al(2)	108.97(3)
N(3)-C(14)	151.23(6)	C(11)-N(3)-Al(2)	111.04(3)
N(3)-C(11)	151.23(6)	N(1)-C(4)-C(3)	107.09(4)
C(4)-C(3)	138.13(7)	N(1)-C(4)-C(10)	121.51(4)
C(4)-C(10)	149.29(6)	C(3)-C(4)-C(10)	131.35(4)
C(5)-N(2)	151.05(6)	C(1)-C(5)-N(2)	116.19(3)
C(6)-N(2)	151.08(6)	N(2)-C(6)-C(7)	105.95(4)
C(6)-C(7)	152.08(8)	C(6)-C(7)-C(8)	102.51(4)
C(7)-C(8)	152.65(9)	C(9)-C(8)-C(7)	101.47(4)
C(8)-C(9)	152.05(7)	N(2)-C(9)-C(8)	105.88(4)
C(9)-N(2)	151.11(6)	C(4)-C(10)-N(3)	117.08(4)
C(11)-C(12)	152.09(8)	N(3)-C(11)-C(12)	105.86(4)
C(12)-C(13)	152.45(9)	C(11)-C(12)-C(13)	102.72(4)
C(13)-C(14)	151.76(8)	C(14)-C(13)-C(12)	101.63(4)
		N(3)-C(14)-C(13)	105.85(4)
C(15)-Al(1)-C(16)	116.27(3)	C(4)-C(3)-C(2)	107.73(4)
C(15)-Al(1)-C(17)	112.52(3)	C(5)-N(2)-C(6)	111.73(3)
C(16)-Al(1)-C(17)	113.82(3)	C(5)-N(2)-C(9)	111.34(3)
C(15)-Al(1)-N(2)	103.69(3)	C(6)-N(2)-C(9)	105.91(4)
C(16)-Al(1)-N(2)	103.30(2)	C(5)-N(2)-Al(1)	108.48(2)
C(17)-Al(1)-N(2)	105.59(2)	C(6)-N(2)-Al(1)	109.15(3)
N(1)-C(1)-C(2)	107.14(4)	C(9)-N(2)-Al(1)	110.21(3)
N(1)-C(1)-C(5)	122.37(4)		

5.2.8 Indium-dibromo-{2,5-bis((pyrrolidino)methyl)-pyrrolide} (12)



Asymmetric unit of compound **12**. Thermal ellipsoids are depicted at the 50% propability level, hydrogen atoms are omitted for clarity.

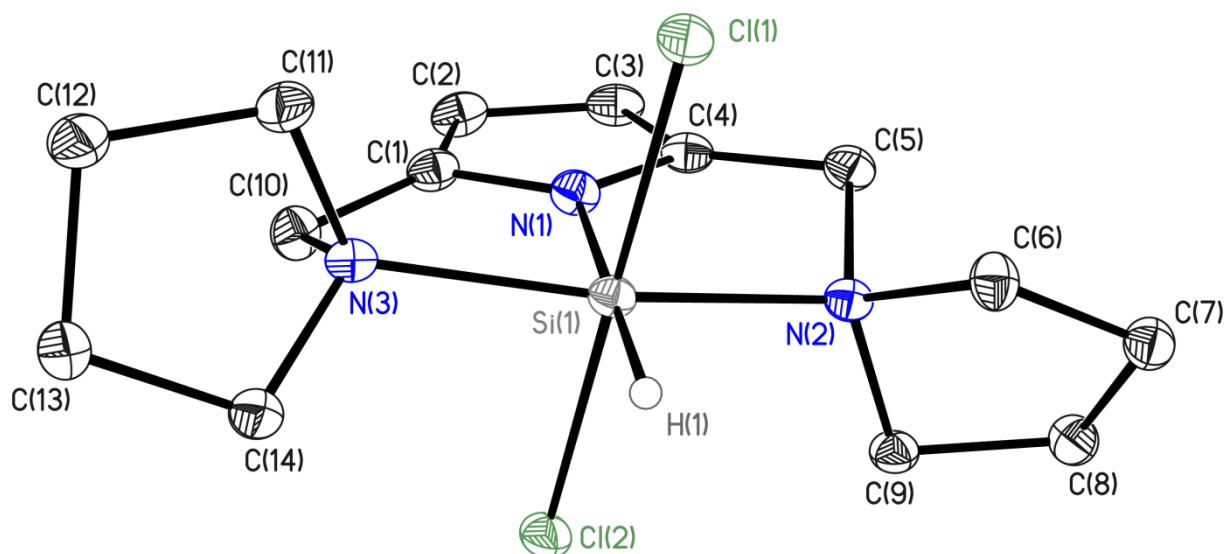
CCDC no.	-	Z	4
Empirical formula	C ₂₄ H ₃₆ Br ₂ In N ₅	Absorption coefficient	4.135 mm ⁻¹
Formula weight	669.22	F(000)	1336
Temperature	106(2) K	Crystal size	0.04 x 0.02 x 0.02 mm ³
Wavelength	0.71073 Å	Theta range for data collection	1.511 to 23.253°
Crystal system	Monoclinic	Reflections collected	14823
Space group	<i>P</i> 2 ₁ / <i>c</i>	Independent reflections	3375 [<i>R</i> (int) = 0.0251]
Unit cell dimensions		Completeness to theta = 25.242°	74.2 %
	<i>a</i> = 13.687(3) Å	Data / restraints / parameters	3375 / 0 / 289
	<i>b</i> = 11.538(2) Å	Goodness-of-fit on <i>F</i> ²	0.999
	<i>c</i> = 16.193(3) Å	<i>R</i> 1 [<i>I</i> > 2σ(<i>I</i>)]	0.0350
	α = 90°	w <i>R</i> 2 (all data)	0.0800
	β = 100.11(3)°	Extinction coefficient	-
	γ = 90°	Largest diff. peak and hole	0.546 and -0.498 e.Å ⁻³
Volume	2517.5(9) Å ³	Absolute structure parameter	-

Selected bond lengths [pm] and angles [°] of (12)

N(1)-C(1)	127.2(8)	N(1)-In(1)-N(2)	74.0(2)
N(1)-C(4)	139.1(9)	N(4)-In(1)-N(2)	109.5(2)
N(1)-In(1)	209.4(5)	N(3)-In(1)-N(2)	172.35(17)
In(1)-N(4)	234.3(5)	Br(2)-In(1)-N(2)	100.69(11)
In(1)-N(3)	239.1(6)	N(1)-In(1)-Br(1)	96.03(14)
In(1)-Br(2)	259.07(10)	N(4)-In(1)-Br(1)	80.92(14)
In(1)-N(2)	262.5(6)	N(3)-In(1)-Br(1)	104.78(12)
In(1)-Br(1)	264.32(10)	Br(2)-In(1)-Br(1)	176.91(3)
C(1)-C(2)	138.0(8)	N(2)-In(1)-Br(1)	79.05(11)
C(1)-C(19)	142.9(9)	N(1)-C(1)-C(2)	109.1(6)
N(2)-C(6)	135.2(8)	N(1)-C(1)-C(19)	117.7(5)
N(2)-C(5)	155.0(8)	C(2)-C(1)-C(19)	133.0(6)
N(2)-C(9)	162.8(9)	C(6)-N(2)-C(5)	116.8(5)
C(2)-C(3)	136.4(10)	C(6)-N(2)-C(9)	89.1(6)
N(3)-C(13)	135.5(7)	C(5)-N(2)-C(9)	114.9(5)
N(3)-C(10)	156.8(10)	C(6)-N(2)-In(1)	118.3(5)
C(3)-C(4)	133.2(8)	C(5)-N(2)-In(1)	92.9(4)
N(4)-C(15)	140.0(8)	C(9)-N(2)-In(1)	127.3(3)
N(4)-C(14)	146.6(9)	C(3)-C(2)-C(1)	110.2(6)
N(4)-C(18)	169.3(10)	C(13)-N(3)-C(10)	104.1(5)
C(4)-C(5)	138.1(10)	C(13)-N(3)-In(1)	112.8(5)
N(5)-C(24)	138.3(7)	C(10)-N(3)-In(1)	141.0(4)
N(5)-C(23)	143.2(8)	C(4)-C(3)-C(2)	102.3(6)
N(5)-C(20)	156.3(8)	C(15)-N(4)-C(14)	92.0(5)
N(5)-C(19)	178.8(9)	C(15)-N(4)-C(18)	113.7(5)
C(6)-C(7)	172.7(11)	C(14)-N(4)-C(18)	117.8(5)
C(7)-C(8)	131.0(9)	C(15)-N(4)-In(1)	112.4(4)
C(9)-C(8)	158.4(10)	C(14)-N(4)-In(1)	105.5(4)
C(10)-C(11)	147.0(10)	C(18)-N(4)-In(1)	113.5(4)
C(10)-C(24)	149.4(8)	C(3)-C(4)-C(5)	130.0(7)
C(11)-C(12)	146.4(10)	C(3)-C(4)-N(1)	112.7(6)
C(12)-C(13)	159.9(11)	C(5)-C(4)-N(1)	117.2(5)
C(13)-C(14)	164.9(11)	C(4)-C(5)-N(2)	117.1(5)
C(15)-C(16)	158.3(9)	C(24)-N(5)-C(23)	99.0(5)
C(16)-C(17)	169.7(12)	C(24)-N(5)-C(20)	105.8(5)
C(17)-C(18)	145.4(9)	C(23)-N(5)-C(20)	99.8(5)
C(20)-C(21)	171.9(11)	C(24)-N(5)-C(19)	115.8(5)
C(21)-C(22)	151.2(8)	C(23)-N(5)-C(19)	118.2(5)
C(22)-C(23)	178.0(10)	C(20)-N(5)-C(19)	115.8(5)
		N(2)-C(6)-C(7)	115.6(5)
C(1)-N(1)-C(4)	105.7(5)	C(8)-C(7)-C(6)	106.3(7)
C(1)-N(1)-In(1)	134.6(5)	C(8)-C(9)-N(2)	113.1(5)
C(4)-N(1)-In(1)	119.6(4)	C(7)-C(8)-C(9)	97.3(6)
N(1)-In(1)-N(4)	174.64(17)	C(11)-C(10)-C(24)	124.2(7)
N(1)-In(1)-N(3)	98.9(2)	C(11)-C(10)-N(3)	115.6(5)
N(4)-In(1)-N(3)	77.8(2)	C(24)-C(10)-N(3)	120.2(6)
N(1)-In(1)-Br(2)	86.83(14)	C(12)-C(11)-C(10)	100.0(7)
N(4)-In(1)-Br(2)	96.32(13)	C(11)-C(12)-C(13)	111.6(6)
N(3)-In(1)-Br(2)	75.86(11)	N(3)-C(13)-C(12)	108.6(6)

N(3)-C(13)-C(14)	114.5(6)	C(1)-C(19)-N(5)	120.6(5)
C(12)-C(13)-C(14)	136.9(5)	N(5)-C(20)-C(21)	111.0(5)
N(4)-C(14)-C(13)	115.8(5)	C(22)-C(21)-C(20)	102.2(5)
N(4)-C(15)-C(16)	97.4(6)	C(21)-C(22)-C(23)	103.5(6)
C(15)-C(16)-C(17)	111.2(5)	N(5)-C(23)-C(22)	110.4(5)
C(18)-C(17)-C(16)	102.8(6)	N(5)-C(24)-C(10)	113.5(5)
C(17)-C(18)-N(4)	101.5(6)		

5.2.9 Silicon-dichloro-hydrido-{2,5-bis((pyrrolidino)methyl)-pyrrolide} (13)



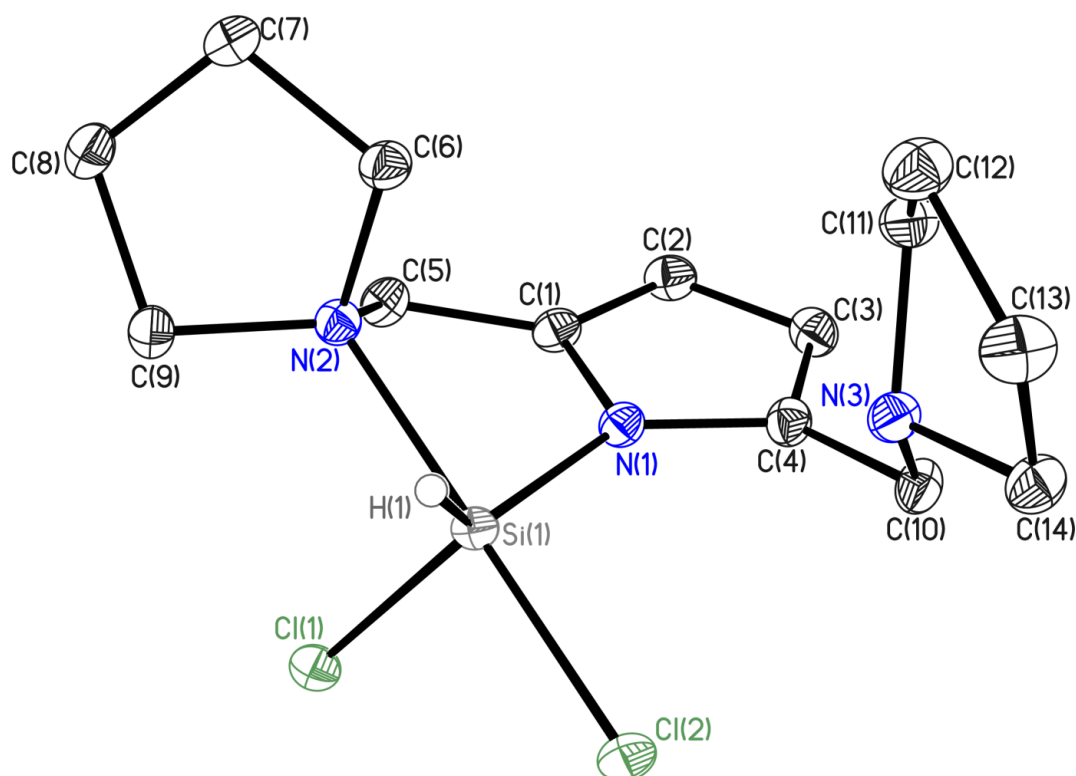
Asymmetric unit of compound **13**. Thermal ellipsoids are depicted at the 50% probability level, hydrogen atoms besides H1 are omitted for clarity.

CCDC no.	-	Z	4
Empirical formula	C ₁₄ H ₂₃ Cl ₂ N ₃ Si	Absorption coefficient	0.510 mm ⁻¹
Formula weight	332.34	F(000)	704
Temperature	106(2) K	Crystal size	0.2 x 0.2 x 0.1 mm ³
Wavelength	0.71073 Å	Theta range for data collection	2.16 to 30.08°
Crystal system	Monoclinic	Reflections collected	31662
Space group	<i>P</i> 2 ₁ / <i>c</i>	Independent reflections	4379 [<i>R</i> (int) = 0.0306]
Unit cell dimensions		Completeness to theta = 25.242°	100.0 %
	<i>a</i> = 8.029(2) Å	Data / restraints / parameters	4379 / 0 / 184
	<i>b</i> = 15.775(3) Å	Goodness-of-fit on <i>F</i> ²	1.098
	<i>c</i> = 12.026(3) Å	<i>R</i> 1 [<i>I</i> > 2σ(<i>I</i>)]	0.0376
	α = 90°	w <i>R</i> 2 (all data)	0.1076
	β = 101.75(2)°	Extinction coefficient	-
	γ = 90°	Largest diff. peak and hole	1.137 and -0.335 e.Å ⁻³
Volume	1491.3(6) Å ³	Absolute structure parameter	-

Selected bond lengths [pm] and angles [°] of (13)

Cl(1)-Si(1)	228.42(7)	N(2)-Si(1)-H(1)	97.1(9)
Si(1)-N(1)	174.72(14)	N(3)-Si(1)-H(1)	98.3(9)
Si(1)-N(2)	206.88(14)	Cl(1)-Si(1)-H(1)	89.8(9)
Si(1)-N(3)	207.23(14)	Cl(2)-Si(1)-H(1)	88.3(9)
Si(1)-Cl(2)	229.47(7)	C(1)-N(1)-C(4)	111.31(13)
Si(1)-H(1)	139(2)	C(1)-N(1)-Si(1)	124.34(11)
N(1)-C(1)	135.21(19)	C(4)-N(1)-Si(1)	123.71(11)
N(1)-C(4)	135.67(19)	N(1)-C(1)-C(2)	107.66(14)
C(1)-C(2)	138.2(2)	N(1)-C(1)-C(10)	112.30(13)
C(1)-C(10)	149.9(2)	C(2)-C(1)-C(10)	139.58(15)
N(2)-C(6)	150.57(19)	C(6)-N(2)-C(9)	101.25(11)
N(2)-C(9)	150.99(19)	C(6)-N(2)-C(5)	111.46(12)
N(2)-C(5)	152.38(19)	C(9)-N(2)-C(5)	108.05(11)
C(2)-C(3)	143.5(3)	C(6)-N(2)-Si(1)	113.08(9)
N(3)-C(14)	150.07(19)	C(9)-N(2)-Si(1)	116.23(9)
N(3)-C(11)	151.36(19)	C(5)-N(2)-Si(1)	106.73(9)
N(3)-C(10)	152.21(19)	C(1)-C(2)-C(3)	106.65(13)
C(3)-C(4)	138.1(2)	C(14)-N(3)-C(11)	101.29(11)
C(4)-C(5)	149.9(2)	C(14)-N(3)-C(10)	111.14(12)
C(6)-C(7)	153.2(2)	C(11)-N(3)-C(10)	108.66(11)
C(8)-C(9)	153.0(2)	C(14)-N(3)-Si(1)	112.32(9)
C(8)-C(7)	154.2(2)	C(11)-N(3)-Si(1)	116.40(10)
C(11)-C(12)	154.1(2)	C(10)-N(3)-Si(1)	106.99(9)
C(12)-C(13)	154.2(2)	C(4)-C(3)-C(2)	107.08(13)
C(13)-C(14)	152.9(2)	N(1)-C(4)-C(3)	107.29(14)
		N(1)-C(4)-C(5)	111.91(13)
N(1)-Si(1)-N(2)	82.66(6)	C(3)-C(4)-C(5)	140.64(14)
N(1)-Si(1)-N(3)	81.97(6)	C(4)-C(5)-N(2)	106.57(12)
N(2)-Si(1)-N(3)	164.61(5)	N(2)-C(6)-C(7)	106.83(12)
N(1)-Si(1)-Cl(1)	91.27(4)	C(9)-C(8)-C(7)	104.33(12)
N(2)-Si(1)-Cl(1)	87.53(4)	C(6)-C(7)-C(8)	105.20(13)
N(3)-Si(1)-Cl(1)	93.55(4)	N(2)-C(9)-C(8)	105.28(12)
N(1)-Si(1)-Cl(2)	90.58(4)	C(1)-C(10)-N(3)	107.70(12)
N(2)-Si(1)-Cl(2)	93.06(4)	N(3)-C(11)-C(12)	105.61(12)
N(3)-Si(1)-Cl(2)	86.36(4)	C(11)-C(12)-C(13)	103.95(13)
Cl(1)-Si(1)-Cl(2)	178.11(2)	C(14)-C(13)-C(12)	105.57(13)
N(1)-Si(1)-H(1)	178.9(9)	N(3)-C(14)-C(13)	107.20(12)

5.2.10 Silicon-dicloro-hydrido2,5-bis(pyrrolidino)methylpyrrolide (13a)



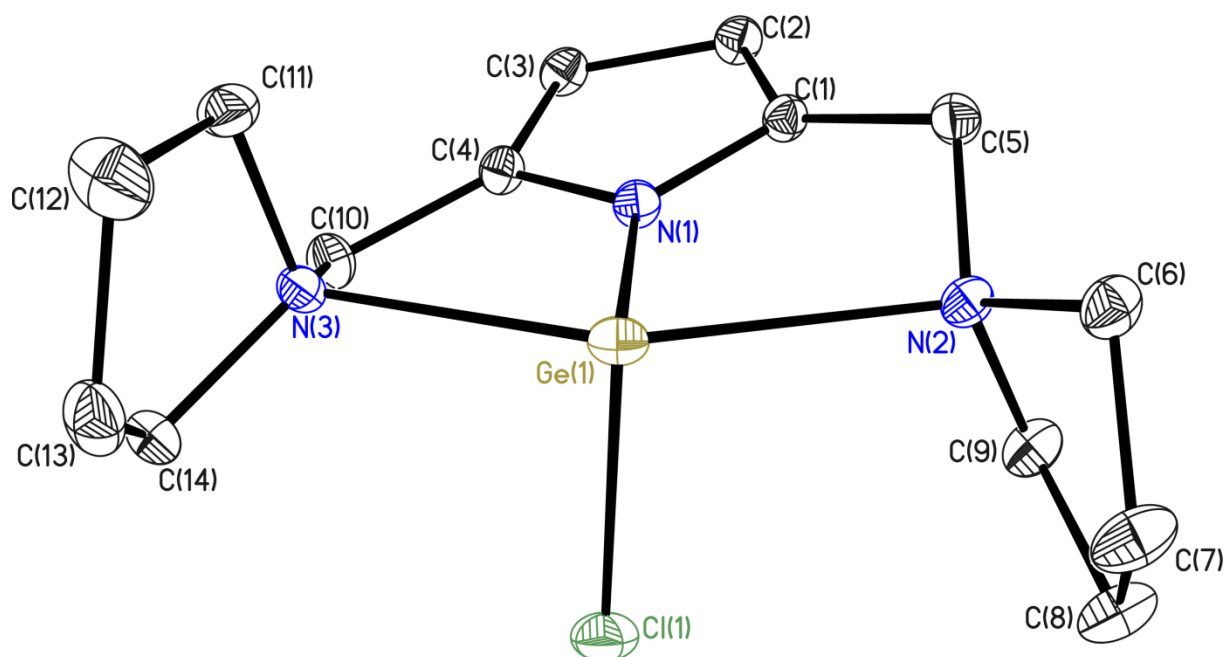
Asymmetric unit of compound **13a**. Thermal ellipsoids are depicted at the 50% propability level, hydrogen atoms besides H1 are omitted for clarity. The silicon bonded substituents are disordered due to a mixture of tetrachlorosilane, trichlorosilane and dichlorosilane in the commercially available trichlorosilane (site occupation factors: 0.01, 0.88, 0.11).

CCDC no.	-	Z	4
Empirical formula	C14 H23.1 Cl1.9 N3 Si	Absorption coefficient	0.461 mm ⁻¹
Formula weight	329.00	F(000)	698
Temperature	100(2) K	Crystal size	0.13 x 0.12 x 0.09 mm ³
Wavelength	0.71073 Å	Theta range for data collection	2.323 to 34.661°
Crystal system	Monoclinic	Reflections collected	43019
Space group	<i>P</i> 2 ₁ / <i>n</i>	Independent reflections	6762 [<i>R</i> (int) = 0.0271]
Unit cell dimensions		Completeness to theta = 25.242°	99.9 %
	<i>a</i> = 9.000(2) Å	Data / restraints / parameters	6762 / 210 / 211
	<i>b</i> = 10.087(2) Å	Goodness-of-fit on <i>F</i> ²	1.074
	<i>c</i> = 17.928(3) Å	<i>R</i> 1 [<i>I</i> > 2σ(<i>I</i>)]	0.0279
	α = 90°	w <i>R</i> 2 (all data)	0.0793
	β = 102.07(2)°	Extinction coefficient	-
	γ = 90°	Largest diff. peak and hole	0.587 and -0.235 e.Å ⁻³
Volume	1591.6(2) Å ³	Absolute structure parameter	-

Selected bond lengths [pm] and angles [°] of (13a)

Si(1)-N(1)	177.24(7)	N(2)-Si(1)-Cl(1)	178.97(2)
Si(1)-N(2)	204.47(7)	Cl(3)-Si(1)-Cl(1)	91.3(7)
Si(1)-Cl(3)	208.5(16)	Cl(2A)-Si(1)-Cl(1)	95.9(16)
Si(1)-Cl(2A)	209.2(18)	Cl(2)-Si(1)-Cl(1)	91.694(19)
Si(1)-Cl(2)	210.35(4)	C(4)-N(1)-C(1)	107.05(6)
Si(1)-Cl(1)	217.64(3)	C(4)-N(1)-Si(1)	137.26(5)
N(1)-C(4)	139.56(10)	C(1)-N(1)-Si(1)	115.62(5)
N(1)-C(1)	139.79(10)	C(2)-C(1)-N(1)	109.77(7)
C(1)-C(2)	136.79(11)	C(2)-C(1)-C(5)	134.92(7)
C(1)-C(5)	149.22(11)	N(1)-C(1)-C(5)	115.01(6)
N(2)-C(9)	149.54(10)	C(9)-N(2)-C(5)	112.56(6)
N(2)-C(5)	149.62(10)	C(9)-N(2)-C(6)	102.94(6)
N(2)-C(6)	150.51(10)	C(5)-N(2)-C(6)	110.28(6)
C(2)-C(3)	142.65(12)	C(9)-N(2)-Si(1)	116.33(5)
N(3)-C(10)	145.90(10)	C(5)-N(2)-Si(1)	104.34(5)
N(3)-C(14)	146.17(10)	C(6)-N(2)-Si(1)	110.49(5)
N(3)-C(11)	146.32(10)	C(1)-C(2)-C(3)	106.33(7)
C(3)-C(4)	137.10(11)	C(10)-N(3)-C(14)	112.62(6)
C(4)-C(10)	149.30(11)	C(10)-N(3)-C(11)	114.13(6)
C(6)-C(7)	153.79(12)	C(14)-N(3)-C(11)	103.95(6)
C(8)-C(9)	152.50(12)	C(4)-C(3)-C(2)	108.50(7)
C(8)-C(7)	153.96(13)	C(3)-C(4)-N(1)	108.32(7)
C(11)-C(12)	153.17(12)	C(3)-C(4)-C(10)	127.20(7)
C(12)-C(13)	154.47(13)	N(1)-C(4)-C(10)	123.32(7)
C(13)-C(14)	153.49(12)	C(1)-C(5)-N(2)	103.48(6)
		N(2)-C(6)-C(7)	106.57(6)
N(1)-Si(1)-N(2)	81.62(3)	C(9)-C(8)-C(7)	104.24(7)
N(1)-Si(1)-Cl(3)	116.5(8)	C(6)-C(7)-C(8)	105.47(7)
N(2)-Si(1)-Cl(3)	87.7(7)	N(2)-C(9)-C(8)	105.09(6)
N(1)-Si(1)-Cl(2A)	104.8(15)	N(3)-C(10)-C(4)	110.10(6)
N(2)-Si(1)-Cl(2A)	84.7(16)	N(3)-C(11)-C(12)	102.93(6)
Cl(3)-Si(1)-Cl(2A)	136.3(18)	C(11)-C(12)-C(13)	104.05(7)
N(1)-Si(1)-Cl(2)	112.64(3)	C(14)-C(13)-C(12)	104.53(7)
N(2)-Si(1)-Cl(2)	88.80(3)	N(3)-C(14)-C(13)	103.75(7)
N(1)-Si(1)-Cl(1)	99.02(2)		

5.2.11 Germanium-chloro-{2,5-bis((pyrrolidino)methyl)-pyrrolide} (15)



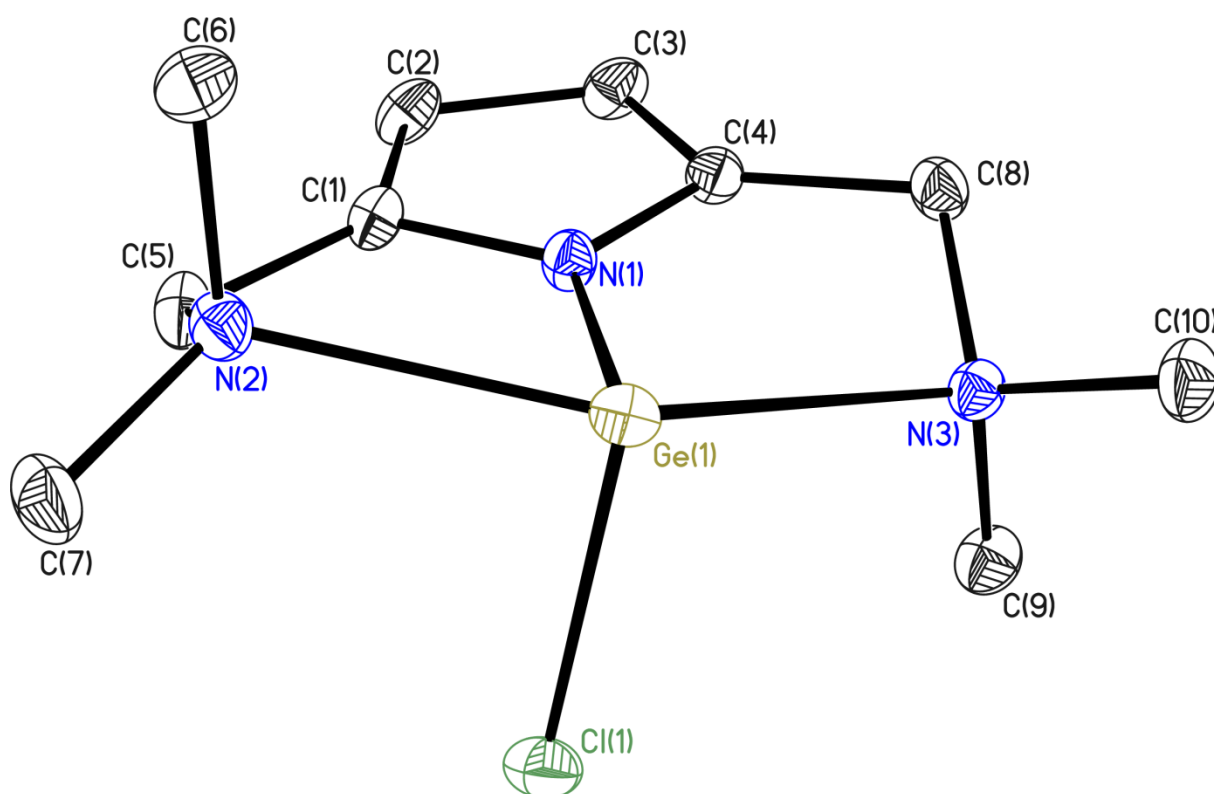
Asymmetric unit of compound **15**. Thermal ellipsoids are depicted at the 50% probability level, hydrogen atoms are omitted for clarity. **15** crystallizes as a racemic twin in the tetragonal space group $I\bar{4}$.

CCDC no.	928750	Z	8
Empirical formula	C ₁₄ H ₂₂ Cl Ge N ₃	Absorption coefficient	2.182 mm ⁻¹
Formula weight	340.38	F(000)	1408
Temperature	105(2) K	Crystal size	0.12 x 0.12 x 0.08 mm ³
Wavelength	0.71073 Å	Theta range for data collection	1.321 to 40.278°
Crystal system	Tetragonal	Reflections collected	61670
Space group	$I\bar{4}$	Independent reflections	9581 [$R(\text{int}) = 0.0374$]
Unit cell dimensions		Completeness to theta = 25.242°	99.9 %
	$a = 21.087(4)$ Å	Data / restraints / parameters	9581 / 0 / 173
	$b = 21.087(4)$ Å	Goodness-of-fit on F^2	1.043
	$c = 6.392(3)$ Å	$R1$ [$I > 2\sigma(I)$]	0.0176
	$\alpha = 90^\circ$	w $R2$ (all data)	0.0422
	$\beta = 90^\circ$	Extinction coefficient	-
	$\gamma = 90^\circ$	Largest diff. peak and hole	0.340 and -0.196 e.Å ⁻³
Volume	3039.7(18) Å ³	Absolute structure parameter	-

Selected bond lengths [pm] and angles [°] of (15)

Ge(1)-N(1)	190.95(9)	C(1)-N(1)-Ge(1)	125.09(6)
Ge(1)-Cl(1)	230.69(5)	N(1)-C(1)-C(2)	108.81(8)
Ge(1)-N(3)	238.01(10)	N(1)-C(1)-C(5)	115.73(8)
Ge(1)-N(2)	249.78(9)	C(2)-C(1)-C(5)	135.07(9)
N(1)-C(4)	137.07(12)	C(6)-N(2)-C(5)	113.65(8)
N(1)-C(1)	137.12(12)	C(6)-N(2)-C(9)	104.82(8)
C(1)-C(2)	137.74(13)	C(5)-N(2)-C(9)	112.58(8)
C(1)-C(5)	149.19(14)	C(6)-N(2)-Ge(1)	110.98(6)
N(2)-C(6)	147.56(14)	C(5)-N(2)-Ge(1)	100.50(5)
N(2)-C(5)	147.62(12)	C(9)-N(2)-Ge(1)	114.63(6)
N(2)-C(9)	148.07(13)	C(1)-C(2)-C(3)	106.97(8)
C(2)-C(3)	143.48(14)	C(4)-C(3)-C(2)	106.46(8)
C(3)-C(4)	137.91(13)	C(14)-N(3)-C(10)	113.04(9)
N(3)-C(14)	147.57(12)	C(14)-N(3)-C(11)	104.53(8)
N(3)-C(10)	147.60(14)	C(10)-N(3)-C(11)	113.12(8)
N(3)-C(11)	148.44(13)	C(14)-N(3)-Ge(1)	116.27(6)
C(4)-C(10)	149.48(13)	C(10)-N(3)-Ge(1)	106.41(6)
C(6)-C(7)	152.37(16)	C(11)-N(3)-Ge(1)	103.22(7)
C(7)-C(8)	153.87(17)	N(1)-C(4)-C(3)	109.08(8)
C(9)-C(8)	153.44(14)	N(1)-C(4)-C(10)	114.94(8)
C(11)-C(12)	153.20(16)	C(3)-C(4)-C(10)	135.85(8)
C(12)-C(13)	153.90(18)	N(2)-C(5)-C(1)	108.33(7)
C(13)-C(14)	152.41(17)	N(2)-C(6)-C(7)	102.37(8)
		C(6)-C(7)-C(8)	103.91(9)
N(1)-Ge(1)-Cl(1)	98.49(3)	N(2)-C(9)-C(8)	105.25(8)
N(1)-Ge(1)-N(3)	74.44(3)	C(9)-C(8)-C(7)	105.05(9)
Cl(1)-Ge(1)-N(3)	88.85(3)	N(3)-C(10)-C(4)	107.73(8)
N(1)-Ge(1)-N(2)	73.22(3)	N(3)-C(11)-C(12)	105.23(9)
Cl(1)-Ge(1)-N(2)	93.73(2)	C(11)-C(12)-C(13)	105.41(9)
N(3)-Ge(1)-N(2)	147.59(3)	C(14)-C(13)-C(12)	103.87(9)
C(4)-N(1)-C(1)	108.67(7)	N(3)-C(14)-C(13)	103.07(9)
C(4)-N(1)-Ge(1)	125.88(6)		

5.2.12 Germanium-chloro-{2,5-bis((dimethylamino)methyl)-pyrrolide} (16)



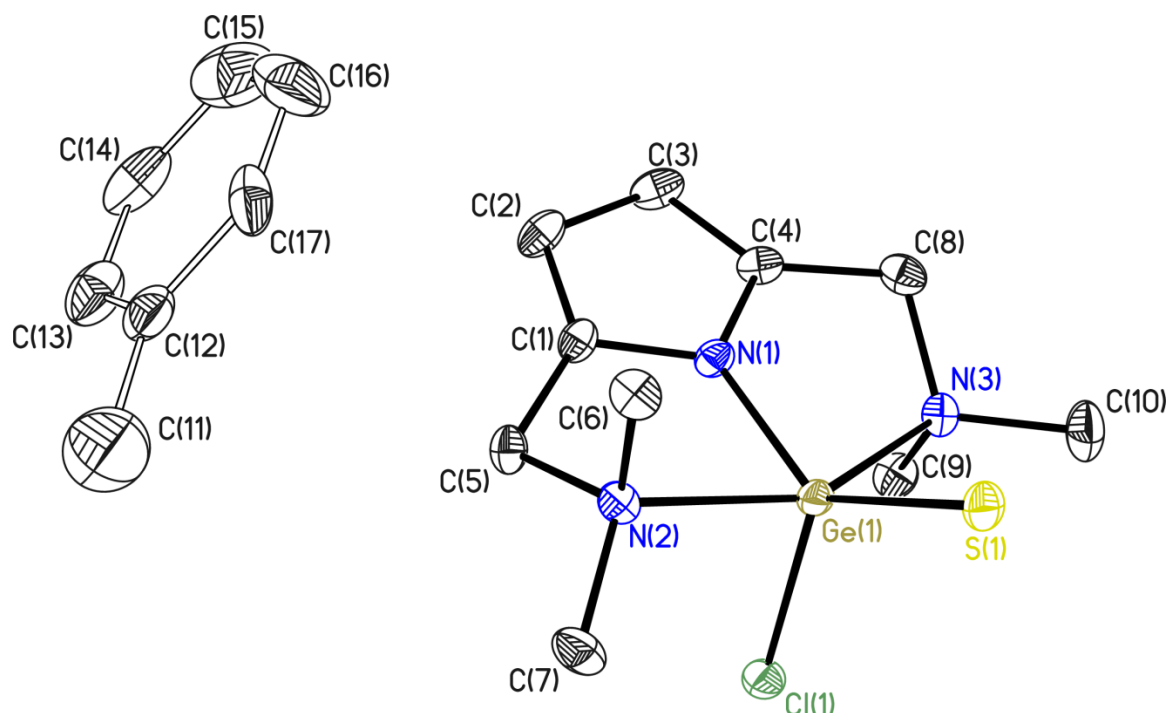
Asymmetric unit of compound **16**. Thermal ellipsoids are depicted at the 50% probability level, hydrogen atoms are omitted for clarity.

CCDC no.	-	Z	4
Empirical formula	C ₁₀ H ₁₈ Cl Ge N ₃	Absorption coefficient	2.573 mm ⁻¹
Formula weight	288.31	F(000)	592
Temperature	100(2) K	Crystal size	0.15 x 0.12 x 0.1 mm ³
Wavelength	0.71073 Å	Theta range for data collection	1.374 to 36.311°
Crystal system	Monoclinic	Reflections collected	38876
Space group	<i>P</i> 2 ₁ / <i>c</i>	Independent reflections	6128 [<i>R</i> (int) = 0.0298]
Unit cell dimensions		Completeness to theta = 25.242°	100.0 %
	<i>a</i> = 15.246(3) Å	Data / restraints / parameters	6128 / 0 / 140
	<i>b</i> = 6.024(2) Å	Goodness-of-fit on <i>F</i> ²	1.040
	<i>c</i> = 14.348(3) Å	<i>R</i> 1 [<i>I</i> > 2σ(<i>I</i>)]	0.0199
	α = 90°	w <i>R</i> 2 (all data)	0.0527
	β = 103.52(3)°	Extinction coefficient	-
	γ = 90°	Largest diff. peak and hole	0.550 and -0.269 e.Å ⁻³
Volume	1281.2(6) Å ³	Absolute structure parameter	-

Selected bond lengths [pm] and angles [°] of (16)

Ge(1)-N(1)	191.56(8)	N(1)-C(1)-C(5)	115.01(7)
Ge(1)-Cl(1)	231.14(5)	C(2)-C(1)-C(5)	136.17(8)
Ge(1)-N(2)	236.24(9)	C(7)-N(2)-C(6)	110.01(7)
Ge(1)-N(3)	250.22(11)	C(7)-N(2)-C(5)	110.41(7)
C(1)-N(1)	137.32(11)	C(6)-N(2)-C(5)	110.45(7)
C(1)-C(2)	137.97(13)	C(7)-N(2)-Ge(1)	116.39(6)
C(1)-C(5)	149.10(13)	C(6)-N(2)-Ge(1)	103.81(6)
N(2)-C(7)	147.30(12)	C(5)-N(2)-Ge(1)	105.50(5)
N(2)-C(6)	147.41(11)	C(1)-C(2)-C(3)	106.76(8)
N(2)-C(5)	148.59(12)	C(9)-N(3)-C(10)	110.37(7)
C(2)-C(3)	143.22(14)	C(9)-N(3)-C(8)	109.94(7)
N(3)-C(9)	147.00(11)	C(10)-N(3)-C(8)	111.03(7)
N(3)-C(10)	147.10(12)	C(9)-N(3)-Ge(1)	113.21(6)
N(3)-C(8)	148.20(12)	C(10)-N(3)-Ge(1)	110.25(5)
C(4)-N(1)	137.10(11)	C(8)-N(3)-Ge(1)	101.78(5)
C(4)-C(3)	137.86(12)	N(1)-C(4)-C(3)	108.83(7)
C(4)-C(8)	149.64(12)	N(1)-C(4)-C(8)	115.61(7)
		C(3)-C(4)-C(8)	135.32(8)
N(1)-Ge(1)-Cl(1)	97.52(3)	N(2)-C(5)-C(1)	107.80(7)
N(1)-Ge(1)-N(2)	74.94(3)	N(3)-C(8)-C(4)	108.51(7)
Cl(1)-Ge(1)-N(2)	89.99(3)	C(4)-C(3)-C(2)	106.88(8)
N(1)-Ge(1)-N(3)	72.81(3)	C(4)-N(1)-C(1)	108.74(7)
Cl(1)-Ge(1)-N(3)	93.81(2)	C(4)-N(1)-Ge(1)	126.29(6)
N(2)-Ge(1)-N(3)	147.74(3)	C(1)-N(1)-Ge(1)	124.79(6)
N(1)-C(1)-C(2)	108.79(8)		

5.2.13 Germanium-chloro-[2,5-bis(dimethylamino)methyl]pyrrolidido]-thione (17)

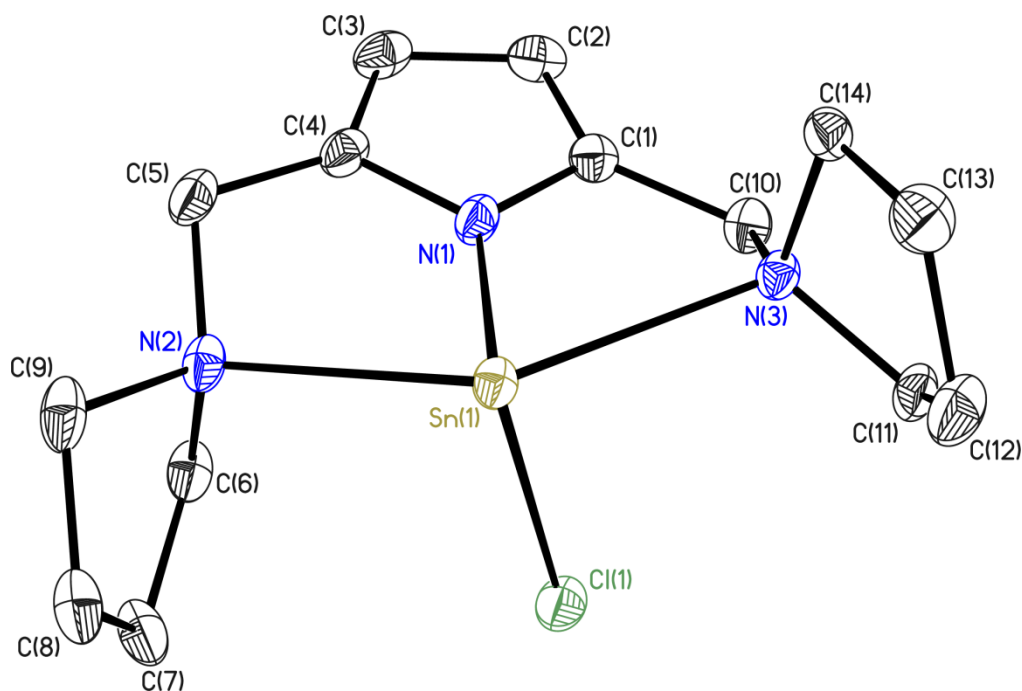


Asymmetric unit of compound **17**. Thermal ellipsoids are depicted at the 50% probability level, hydrogen atoms are omitted for clarity. The site occupation factor of the toluene molecule in the asymmetric unit is 0.5. This explains the empirical formula given in the table. Instead it should be written C₁₀ H₁₈ Cl Ge N₃ S, 0.5 (C₇ H₈).

CCDC no.	-	Z	4
Empirical formula	C _{13.5} H ₂₂ Cl Ge N ₃ S	Absorption coefficient	1.117 mm ⁻¹
Formula weight	366.44	F(000)	756
Temperature	100(2) K	Crystal size	0.1 x 0.08 x 0.08 mm ³
Wavelength	0.56086 Å	Theta range for data collection	1.690 to 24.745°
Crystal system	Monoclinic	Reflections collected	33310
Space group	P2 ₁ /c	Independent reflections	5749 [R(int) = 0.0496]
Unit cell dimensions		Completeness to theta = 25.242°	99.9 %
	a = 8.460(2) Å	Data / restraints / parameters	5749 / 81 / 212
	b = 17.142(3) Å	Goodness-of-fit on F ²	1.019
	c = 11.487(3) Å	R1 [I > 2sigma(I)]	0.0254
	α = 90°	wR2 (all data)	0.0569
	β = 95.92(2)°	Extinction coefficient	-
	γ = 90°	Largest diff. peak and hole	0.418 and -0.496 e.Å ⁻³
Volume	1657.0(7) Å ³	Absolute structure parameter	-

Selected bond lengths [pm] and angles [°] of (17)

Ge(1)-N(1)	185.03(11)	N(2)-Ge(1)-N(3)	151.71(4)
Ge(1)-S(1)	208.07(6)	C(1)-N(1)-C(4)	110.14(11)
Ge(1)-Cl(1)	217.12(5)	C(1)-N(1)-Ge(1)	122.43(9)
Ge(1)-N(2)	219.48(12)	C(4)-N(1)-Ge(1)	127.43(9)
Ge(1)-N(3)	243.21(13)	C(7)-N(2)-C(6)	109.22(11)
N(1)-C(1)	137.12(17)	C(7)-N(2)-C(5)	110.93(10)
N(1)-C(4)	137.24(17)	C(6)-N(2)-C(5)	109.23(11)
N(2)-C(7)	148.38(17)	C(7)-N(2)-Ge(1)	114.34(9)
N(2)-C(6)	148.50(18)	C(6)-N(2)-Ge(1)	106.91(8)
N(2)-C(5)	150.13(17)	C(5)-N(2)-Ge(1)	106.02(8)
N(3)-C(10)	147.44(18)	C(10)-N(3)-C(9)	109.03(12)
N(3)-C(9)	147.96(19)	C(10)-N(3)-C(8)	111.16(12)
N(3)-C(8)	149.04(19)	C(9)-N(3)-C(8)	108.99(11)
C(1)-C(2)	137.68(19)	C(10)-N(3)-Ge(1)	113.25(9)
C(1)-C(5)	149.54(19)	C(9)-N(3)-Ge(1)	112.14(8)
C(2)-C(3)	143.2(2)	C(8)-N(3)-Ge(1)	102.08(8)
C(3)-C(4)	137.39(19)	N(1)-C(1)-C(2)	107.65(12)
C(4)-C(8)	149.8(2)	N(1)-C(1)-C(5)	114.05(11)
C(11)-C(12)	145.1(13)	C(2)-C(1)-C(5)	138.16(12)
C(12)-C(13)	138.0(9)	C(1)-C(2)-C(3)	107.19(12)
C(12)-C(17)	140.1(9)	C(4)-C(3)-C(2)	107.39(12)
C(13)-C(14)	138.5(9)	N(1)-C(4)-C(3)	107.63(12)
C(14)-C(15)	141.4(10)	N(1)-C(4)-C(8)	113.96(11)
C(15)-C(16)	137.6(10)	C(3)-C(4)-C(8)	138.36(13)
C(16)-C(17)	137.1(9)	C(1)-C(5)-N(2)	105.92(10)
		N(3)-C(8)-C(4)	107.06(11)
N(1)-Ge(1)-S(1)	133.53(4)	C(13)-C(12)-C(17)	118.1(6)
N(1)-Ge(1)-Cl(1)	107.12(4)	C(13)-C(12)-C(11)	122.5(7)
S(1)-Ge(1)-Cl(1)	119.055(15)	C(17)-C(12)-C(11)	119.4(6)
N(1)-Ge(1)-N(2)	78.30(5)	C(12)-C(13)-C(14)	122.4(8)
S(1)-Ge(1)-N(2)	102.28(4)	C(13)-C(14)-C(15)	119.2(7)
Cl(1)-Ge(1)-N(2)	94.00(3)	C(16)-C(15)-C(14)	117.6(9)
N(1)-Ge(1)-N(3)	73.56(5)	C(17)-C(16)-C(15)	123.2(7)
S(1)-Ge(1)-N(3)	99.09(3)	C(16)-C(17)-C(12)	119.5(7)
Cl(1)-Ge(1)-N(3)	91.60(3)		

5.2.14 Tin-chloro-{2,5-bis((pyrrolidino)methyl)-pyrrolide} (**18**)

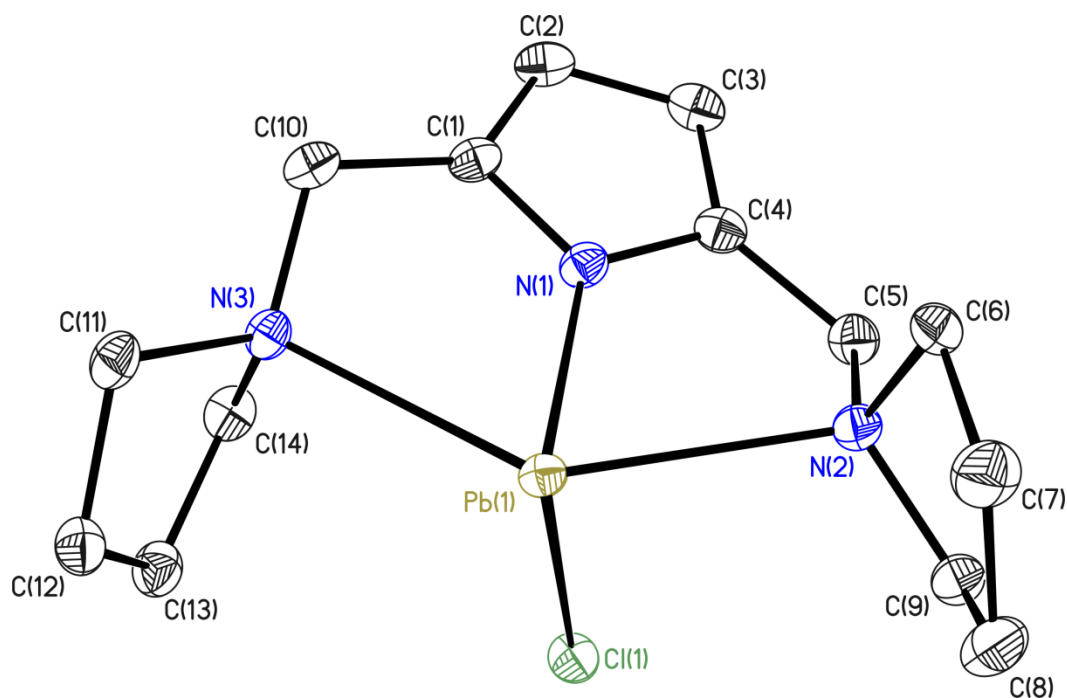
Asymmetric unit of compound **18**. Thermal ellipsoids are depicted at the 50% propability level, hydrogen atoms are omitted for clarity.

CCDC no.	928753	<i>Z</i>	4
Empirical formula	C ₁₄ H ₂₂ Cl N ₃ Sn	Absorption coefficient	0.957 mm ⁻¹
Formula weight	386.48	<i>F</i> (000)	776
Temperature	100(2) K	Crystal size	0.2 x 0.1 x 0.1 mm ³
Wavelength	0.56086 Å	Theta range for data collection	1.398 to 26.464°
Crystal system	Monoclinic	Reflections collected	47581
Space group	<i>P</i> 2 ₁ / <i>c</i>	Independent reflections	6540 [<i>R</i> (int) = 0.0352]
Unit cell dimensions		Completeness to theta = 25.242°	100.0 %
	<i>a</i> = 11.645(2) Å	Data / restraints / parameters	6540 / 0 / 172
	<i>b</i> = 14.595(3) Å	Goodness-of-fit on <i>F</i> ²	1.053
	<i>c</i> = 9.281(2) Å	<i>R</i> 1 [<i>I</i> > 2σ(<i>I</i>)]	0.0226
	α = 90°	w <i>R</i> 2 (all data)	0.0549
	β = 99.28(2)°	Extinction coefficient	-
	γ = 90°	Largest diff. peak and hole	1.969 and -0.381 e.Å ⁻³
Volume	1556.7(5) Å ³	Absolute structure parameter	-

Selected bond lengths [pm] and angles [°] of (18)

Sn(1)-N(1)	211.83(12)	C(1)-N(1)-Sn(1)	126.64(9)
Sn(1)-Cl(1)	245.87(5)	C(4)-N(1)-Sn(1)	124.40(10)
Sn(1)-N(2)	257.68(12)	N(1)-C(1)-C(2)	109.39(13)
Sn(1)-N(3)	258.56(12)	N(1)-C(1)-C(10)	115.95(12)
N(1)-C(1)	137.16(19)	C(2)-C(1)-C(10)	134.43(14)
N(1)-C(4)	137.43(17)	C(5)-N(2)-C(9)	112.74(11)
C(1)-C(2)	137.8(2)	C(5)-N(2)-C(6)	112.63(11)
C(1)-C(10)	150.0(2)	C(9)-N(2)-C(6)	103.47(11)
N(2)-C(5)	147.8(2)	C(5)-N(2)-Sn(1)	103.69(8)
N(2)-C(9)	147.91(18)	C(9)-N(2)-Sn(1)	112.89(8)
N(2)-C(6)	148.81(17)	C(6)-N(2)-Sn(1)	111.73(8)
C(2)-C(3)	143.0(2)	C(1)-C(2)-C(3)	106.44(13)
C(3)-C(4)	138.1(2)	C(4)-C(3)-C(2)	107.12(12)
N(3)-C(11)	147.79(17)	C(11)-N(3)-C(10)	113.55(11)
N(3)-C(10)	147.87(18)	C(11)-N(3)-C(14)	103.97(10)
N(3)-C(14)	148.13(17)	C(10)-N(3)-C(14)	113.27(11)
C(4)-C(5)	150.0(2)	C(11)-N(3)-Sn(1)	114.27(8)
C(11)-C(12)	152.0(2)	C(10)-N(3)-Sn(1)	106.84(8)
C(12)-C(13)	154.3(2)	C(14)-N(3)-Sn(1)	104.73(8)
C(13)-C(14)	153.8(2)	N(1)-C(4)-C(3)	108.70(13)
C(8)-C(9)	152.0(2)	N(1)-C(4)-C(5)	116.18(13)
C(8)-C(7)	154.0(2)	C(3)-C(4)-C(5)	134.95(13)
C(7)-C(6)	154.0(2)	N(2)-C(5)-C(4)	109.51(11)
		N(3)-C(10)-C(1)	109.21(11)
N(1)-Sn(1)-Cl(1)	95.01(4)	N(3)-C(11)-C(12)	102.52(11)
N(1)-Sn(1)-N(2)	69.22(4)	C(11)-C(12)-C(13)	104.00(12)
Cl(1)-Sn(1)-N(2)	93.97(3)	C(14)-C(13)-C(12)	105.11(12)
N(1)-Sn(1)-N(3)	69.50(4)	N(3)-C(14)-C(13)	104.26(11)
Cl(1)-Sn(1)-N(3)	84.65(3)	C(9)-C(8)-C(7)	104.18(13)
N(2)-Sn(1)-N(3)	138.39(4)	C(8)-C(7)-C(6)	105.02(12)
C(1)-N(1)-C(4)	108.35(12)	N(2)-C(6)-C(7)	104.45(12)
		N(2)-C(9)-C(8)	102.92(11)

5.2.15 Lead-chloro-{2,5-bis((pyrrolidino)methyl)-pyrrolide} (21)



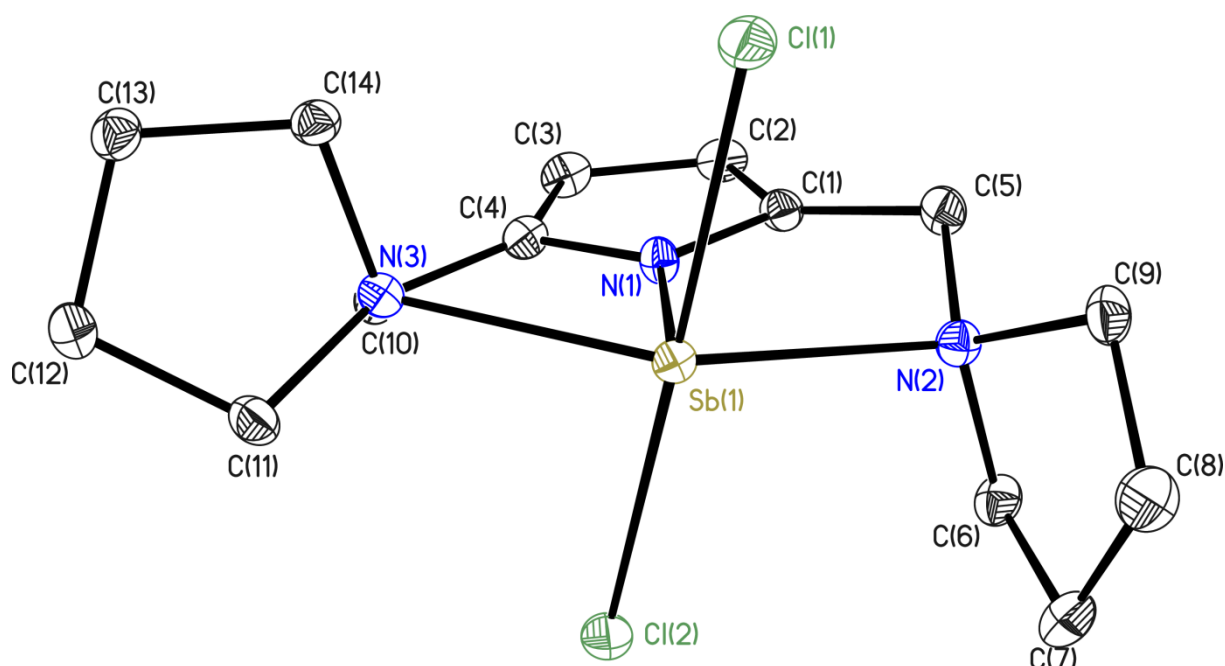
Asymmetric unit of compound **21**. Thermal ellipsoids are depicted at the 50% probability level, hydrogen atoms are omitted for clarity.

CCDC no.	928752	Z	4
Empirical formula	C ₁₄ H ₂₂ Cl N ₃ Pb	Absorption coefficient	10.889 mm ⁻¹
Formula weight	474.98	F(000)	904
Temperature	100(2) K	Crystal size	0.10 x 0.05 x 0.05 mm ³
Wavelength	0.71073 Å	Theta range for data collection	2.032 to 27.875°
Crystal system	Monoclinic	Reflections collected	30844
Space group	<i>P</i> 2 ₁ / <i>c</i>	Independent reflections	3750 [<i>R</i> (int) = 0.0264]
Unit cell dimensions		Completeness to theta = 25.242°	100.0 %
	<i>a</i> = 10.050(2) Å	Data / restraints / parameters	3750 / 0 / 172
	<i>b</i> = 14.313(3) Å	Goodness-of-fit on <i>F</i> ²	1.068
	<i>c</i> = 10.965(2) Å	<i>R</i> 1 [<i>I</i> > 2σ(<i>I</i>)]	0.0136
	α = 90°	w <i>R</i> 2 (all data)	0.0326
	β = 94.38(2)°	Extinction coefficient	-
	γ = 90°	Largest diff. peak and hole	0.808 and -0.392 e.Å ⁻³
Volume	1572.7(5) Å ³	Absolute structure parameter	-

Selected bond lengths [pm] and angles [°] of (21)

Pb(1)-N(1)	220.00(18)	C(1)-N(1)-Pb(1)	125.85(14)
Pb(1)-N(2)	261.62(18)	C(9)-N(2)-C(5)	112.55(17)
Pb(1)-N(3)	268.05(19)	C(9)-N(2)-C(6)	104.47(17)
Pb(1)-Cl(1)	275.58(7)	C(5)-N(2)-C(6)	113.75(17)
N(1)-C(4)	136.7(3)	C(9)-N(2)-Pb(1)	114.34(13)
N(1)-C(1)	136.8(3)	C(5)-N(2)-Pb(1)	107.24(13)
N(2)-C(9)	147.6(3)	C(6)-N(2)-Pb(1)	104.35(12)
N(2)-C(5)	148.1(3)	C(14)-N(3)-C(10)	113.09(17)
N(2)-C(6)	148.6(3)	C(14)-N(3)-C(11)	103.14(17)
N(3)-C(14)	147.1(3)	C(10)-N(3)-C(11)	114.35(17)
N(3)-C(10)	147.7(3)	C(14)-N(3)-Pb(1)	109.56(13)
N(3)-C(11)	148.0(3)	C(10)-N(3)-Pb(1)	104.78(13)
C(1)-C(2)	138.2(3)	C(11)-N(3)-Pb(1)	112.05(13)
C(1)-C(10)	149.6(3)	N(1)-C(1)-C(2)	108.6(2)
C(2)-C(3)	142.0(3)	N(1)-C(1)-C(10)	117.18(18)
C(3)-C(4)	138.1(3)	C(2)-C(1)-C(10)	133.9(2)
C(4)-C(5)	149.5(3)	C(1)-C(2)-C(3)	107.0(2)
C(6)-C(7)	153.3(3)	C(4)-C(3)-C(2)	106.9(2)
C(7)-C(8)	153.9(3)	N(1)-C(4)-C(3)	108.7(2)
C(8)-C(9)	152.4(3)	N(1)-C(4)-C(5)	117.57(19)
C(11)-C(12)	152.8(3)	C(3)-C(4)-C(5)	133.4(2)
C(12)-C(13)	155.7(3)	N(2)-C(5)-C(4)	110.55(17)
C(13)-C(14)	152.7(3)	N(2)-C(6)-C(7)	103.64(17)
		C(6)-C(7)-C(8)	105.41(19)
N(1)-Pb(1)-N(2)	68.64(6)	C(9)-C(8)-C(7)	105.03(19)
N(1)-Pb(1)-N(3)	67.46(6)	N(2)-C(9)-C(8)	103.98(18)
N(2)-Pb(1)-N(3)	136.05(6)	N(3)-C(10)-C(1)	109.72(18)
N(1)-Pb(1)-Cl(1)	90.02(5)	N(3)-C(11)-C(12)	102.51(17)
N(2)-Pb(1)-Cl(1)	82.30(4)	C(11)-C(12)-C(13)	104.52(18)
N(3)-Pb(1)-Cl(1)	95.72(4)	C(14)-C(13)-C(12)	104.05(18)
C(4)-N(1)-C(1)	108.85(18)	N(3)-C(14)-C(13)	103.82(17)
C(4)-N(1)-Pb(1)	125.29(14)		

5.2.16 Antimony-dichloro-{2,5-bis((pyrrolidino)methyl)-pyrrolide} (22)



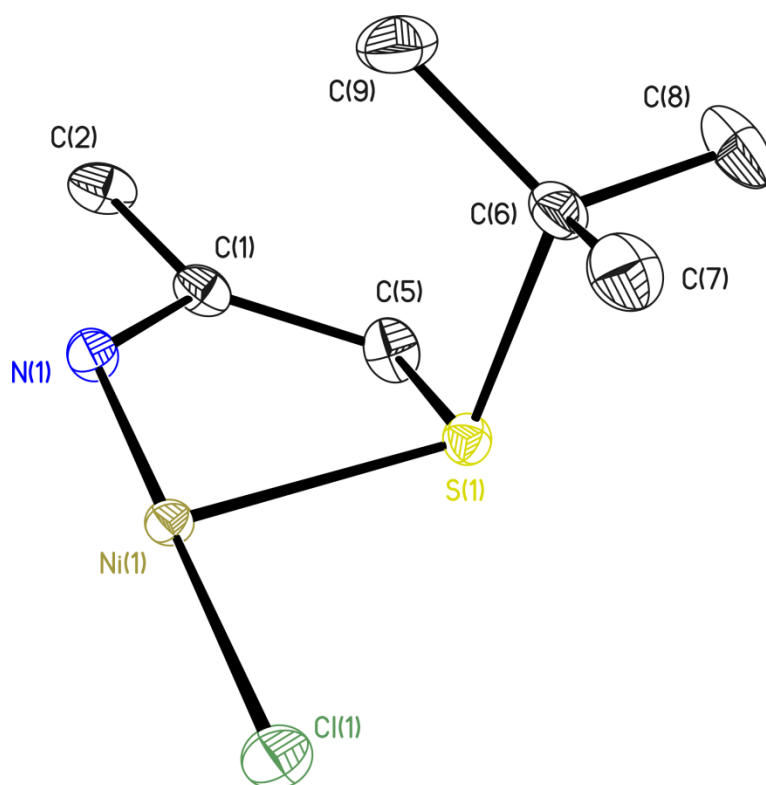
Asymmetric unit of compound **22**. Thermal ellipsoids are depicted at the 50% probability level, hydrogen atoms are omitted for clarity.

CCDC no.	-	Z	4
Empirical formula	C14 H22 Cl2 N3 Sb	Absorption coefficient	1.097 mm ⁻¹
Formula weight	422.99	F(000)	848
Temperature	100(2) K	Crystal size	0.12 x 0.08 x 0.08 mm ³
Wavelength	0.56086 Å	Theta range for data collection	1.527 to 23.648°
Crystal system	Monoclinic	Reflections collected	26921
Space group	<i>P</i> 2 ₁ / <i>n</i>	Independent reflections	4823 [<i>R</i> (int) = 0.0408]
Unit cell dimensions		Completeness to theta = 25.242°	99.9 %
	<i>a</i> = 8.453(2) Å	Data / restraints / parameters	4823 / 0 / 181
	<i>b</i> = 21.043(3) Å	Goodness-of-fit on <i>F</i> ²	1.049
	<i>c</i> = 8.901(2) Å	<i>R</i> 1 [<i>I</i> > 2σ(<i>I</i>)]	0.0266
	α = 90°	w <i>R</i> 2 (all data)	0.0540
	β = 92.95(2)°	Extinction coefficient	-
	γ = 90°	Largest diff. peak and hole	1.038 and -0.738 e.Å ⁻³
Volume	1581.2(6) Å ³	Absolute structure parameter	-

Selected bond lengths [pm] and angles [°] of (22)

Sb(1)-N(1)	202.87(17)	Cl(1)-Sb(1)-Cl(2)	173.997(19)
Sb(1)-N(3)	240.19(18)	C(4)-N(1)-C(1)	109.54(17)
Sb(1)-N(2)	247.39(18)	C(4)-N(1)-Sb(1)	124.86(14)
Sb(1)-Cl(1)	258.05(7)	C(1)-N(1)-Sb(1)	125.59(14)
Sb(1)-Cl(2)	259.35(7)	C(5)-N(2)-C(9)	111.68(17)
N(1)-C(4)	136.6(3)	C(5)-N(2)-C(6)	112.66(17)
N(1)-C(1)	137.0(3)	C(9)-N(2)-C(6)	103.47(16)
N(2)-C(5)	148.5(3)	C(5)-N(2)-Sb(1)	106.17(12)
N(2)-C(9)	148.6(3)	C(9)-N(2)-Sb(1)	112.40(13)
N(2)-C(6)	149.0(3)	C(6)-N(2)-Sb(1)	110.60(13)
N(3)-C(11)	149.2(3)	C(11)-N(3)-C(14)	102.54(16)
N(3)-C(14)	149.6(3)	C(11)-N(3)-C(10)	112.21(17)
N(3)-C(10)	150.2(3)	C(14)-N(3)-C(10)	109.72(16)
C(1)-C(2)	137.2(3)	C(11)-N(3)-Sb(1)	111.17(12)
C(1)-C(5)	148.8(3)	C(14)-N(3)-Sb(1)	114.39(13)
C(2)-C(3)	142.5(3)	C(10)-N(3)-Sb(1)	106.91(12)
C(3)-C(4)	137.5(3)	N(1)-C(1)-C(2)	108.03(19)
C(4)-C(10)	148.9(3)	N(1)-C(1)-C(5)	116.01(18)
C(6)-C(7)	152.7(3)	C(2)-C(1)-C(5)	135.6(2)
C(7)-C(8)	154.4(3)	C(1)-C(2)-C(3)	107.27(19)
C(8)-C(9)	151.5(3)	C(4)-C(3)-C(2)	106.99(19)
C(11)-C(12)	153.3(3)	N(1)-C(4)-C(3)	108.16(19)
C(12)-C(13)	154.4(3)	N(1)-C(4)-C(10)	115.31(18)
C(13)-C(14)	152.8(3)	C(3)-C(4)-C(10)	136.3(2)
		N(2)-C(5)-C(1)	109.24(17)
N(1)-Sb(1)-N(3)	72.73(7)	N(2)-C(6)-C(7)	103.57(17)
N(1)-Sb(1)-N(2)	71.89(7)	C(6)-C(7)-C(8)	105.10(18)
N(3)-Sb(1)-N(2)	144.59(6)	C(9)-C(8)-C(7)	105.12(18)
N(1)-Sb(1)-Cl(1)	87.64(6)	N(2)-C(9)-C(8)	104.30(18)
N(3)-Sb(1)-Cl(1)	93.49(5)	C(4)-C(10)-N(3)	108.31(17)
N(2)-Sb(1)-Cl(1)	83.73(5)	N(3)-C(11)-C(12)	105.89(17)
N(1)-Sb(1)-Cl(2)	86.35(6)	C(11)-C(12)-C(13)	104.84(17)
N(3)-Sb(1)-Cl(2)	84.83(5)	C(14)-C(13)-C(12)	104.83(17)
N(2)-Sb(1)-Cl(2)	94.29(5)	N(3)-C(14)-C(13)	104.76(17)

5.2.17 Nickel-chloro-{2,5-bis((tertbutyl-thiolato)methyl)pyrrolide} (23)



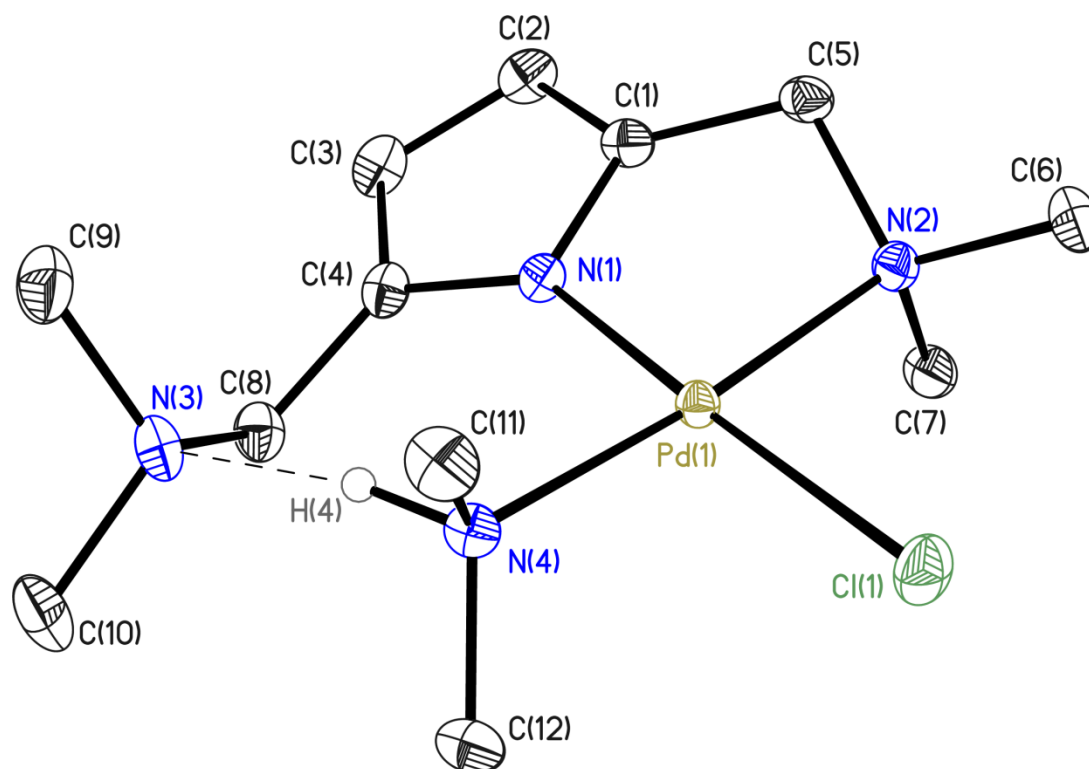
Asymmetric unit of compound **23**, containing a half molecule. Thermal ellipsoids are depicted at the 50% propability level, hydrogen atoms are omitted for clarity. The data for **23** was collected with support of M. Granitzka.

CCDC no.	-	Z	4
Empirical formula	C14 H24 Cl N Ni S2	Absorption coefficient	0.812 mm ⁻¹
Formula weight	364.62	F(000)	768
Temperature	100(2) K	Crystal size	0.1 x 0.1 x 0.1 mm ³
Wavelength	0.56086 Å	Theta range for data collection	3.121 to 25.548°
Crystal system	Orthorhombic	Reflections collected	35723
Space group	<i>Pbca</i>	Independent reflections	3174 [<i>R</i> (int) = 0.0521]
Unit cell dimensions		Completeness to theta = 25.242°	99.5 %
	<i>a</i> = 9.431(2) Å	Data / restraints / parameters	3174 / 84 / 91
	<i>b</i> = 14.118(3) Å	Goodness-of-fit on <i>F</i> ²	1.026
	<i>c</i> = 12.527(3) Å	<i>R</i> 1 [<i>I</i> > 2σ(<i>I</i>)]	0.0239
	α = 90°	w <i>R</i> 2 (all data)	0.0593
	β = 90°	Extinction coefficient	-
	γ = 90°	Largest diff. peak and hole	0.504 and -0.642 e.Å ⁻³
Volume	1667.9(6) Å ³	Absolute structure parameter	-

Selected bond lengths [pm] and angles [°] of (23)

Ni(1)-N(1)	182.20(13)	Cl(1)-Ni(1)-S(1)A	94.812(9)
Ni(1)-Cl(1)	218.33(6)	S(1)-Ni(1)-S(1)A	170.375(17)
Ni(1)-S(1)	222.14(5)	C(5)-S(1)-C(6)	103.62(6)
Ni(1)-S(1)A	222.15(5)	C(5)-S(1)-Ni(1)	98.74(4)
S(1)-C(5)	183.09(12)	C(6)-S(1)-Ni(1)	107.44(4)
S(1)-C(6)	186.85(12)	C(1)A-N(1)-C(1)	108.62(13)
N(1)-C(1)A	136.88(13)	C(1)A-N(1)-Ni(1)	125.69(7)
N(1)-C(1)	136.88(13)	C(1)-N(1)-Ni(1)	125.69(7)
C(6)-C(9)	152.49(18)	C(9)-C(6)-C(7)	110.43(10)
C(6)-C(7)	152.85(17)	C(9)-C(6)-C(8)	111.38(11)
C(6)-C(8)	152.95(18)	C(7)-C(6)-C(8)	110.52(11)
C(2)-C(1)	138.23(16)	C(9)-C(6)-S(1)	112.23(8)
C(2)-C(2)A	142.4(3)	C(7)-C(6)-S(1)	105.28(8)
C(1)-C(5)	149.01(17)	C(8)-C(6)-S(1)	106.79(8)
		C(1)-C(2)-C(2)A	106.80(7)
N(1)-Ni(1)-Cl(1)	180.0	N(1)-C(1)-C(2)	108.89(11)
N(1)-Ni(1)-S(1)	85.188(9)	N(1)-C(1)-C(5)	115.91(10)
Cl(1)-Ni(1)-S(1)	94.812(9)	C(2)-C(1)-C(5)	135.20(11)
N(1)-Ni(1)-S(1)A	85.188(9)	C(1)-C(5)-S(1)	108.33(8)

5.2.18 Palladium-dimethylamino-chloro-{2,5-bis((dimethylamino)methyl)-pyrrolide} (26)



Asymmetric unit of compound **26**. Thermal ellipsoids are depicted at the 50% propability level, hydrogen atoms besides H4 are omitted for clarity.

CCDC no.	-	Z	4
Empirical formula	C ₁₂ H ₂₅ Cl N ₄ Pd	Absorption coefficient	0.705 mm ⁻¹
Formula weight	367.21	F(000)	752
Temperature	100(2) K	Crystal size	0.12 x 0.1 x 0.08 mm ³
Wavelength	0.56086 Å	Theta range for data collection	1.392 to 23.625°
Crystal system	Monoclinic	Reflections collected	48620
Space group	<i>P</i> 2 ₁ / <i>c</i>	Independent reflections	4823 [<i>R</i> (int) = 0.0437]
Unit cell dimensions		Completeness to theta = 25.242°	99.9 %
	<i>a</i> = 11.622(3) Å	Data / restraints / parameters	4823 / 0 / 169
	<i>b</i> = 10.422(2) Å	Goodness-of-fit on <i>F</i> ²	1.011
	<i>c</i> = 13.166(3) Å	<i>R</i> 1 [<i>I</i> > 2σ(<i>I</i>)]	0.0216
	α = 90°	w <i>R</i> 2 (all data)	0.0479
	β = 96.56(3)°	Extinction coefficient	-
	γ = 90°	Largest diff. peak and hole	0.580 and -0.510 e.Å ⁻³
Volume	1584.3(6) Å ³	Absolute structure parameter	-

Selected bond lengths [pm] and angles [°] of (26)

Pd(1)-N(1)	202.84(13)	C(1)-N(1)-C(4)	107.02(13)
Pd(1)-N(4)	204.66(13)	C(1)-N(1)-Pd(1)	111.82(10)
Pd(1)-N(2)	209.35(13)	C(4)-N(1)-Pd(1)	141.13(11)
Pd(1)-Cl(1)	233.36(6)	C(2)-C(1)-N(1)	110.19(14)
N(1)-C(1)	138.26(19)	C(2)-C(1)-C(5)	132.80(14)
N(1)-C(4)	138.60(19)	N(1)-C(1)-C(5)	116.98(13)
C(1)-C(2)	138.2(2)	C(6)-N(2)-C(7)	109.02(12)
C(1)-C(5)	148.7(2)	C(6)-N(2)-C(5)	108.65(12)
N(2)-C(6)	148.5(2)	C(7)-N(2)-C(5)	110.10(12)
N(2)-C(7)	148.9(2)	C(6)-N(2)-Pd(1)	116.08(10)
N(2)-C(5)	150.63(19)	C(7)-N(2)-Pd(1)	108.47(9)
C(2)-C(3)	141.5(2)	C(5)-N(2)-Pd(1)	104.38(9)
C(3)-C(4)	139.0(2)	C(1)-C(2)-C(3)	106.29(14)
N(3)-C(9)	146.6(2)	C(4)-C(3)-C(2)	107.73(14)
N(3)-C(10)	147.2(2)	C(9)-N(3)-C(10)	110.47(14)
N(3)-C(8)	148.1(2)	C(9)-N(3)-C(8)	111.87(13)
C(4)-C(8)	149.3(2)	C(10)-N(3)-C(8)	109.96(13)
N(4)-C(11)	148.31(19)	N(1)-C(4)-C(3)	108.75(14)
N(4)-C(12)	148.70(19)	N(1)-C(4)-C(8)	124.83(14)
		C(3)-C(4)-C(8)	126.05(15)
N(1)-Pd(1)-N(4)	94.70(5)	C(11)-N(4)-C(12)	110.70(12)
N(1)-Pd(1)-N(2)	81.62(5)	C(11)-N(4)-Pd(1)	111.90(10)
N(4)-Pd(1)-N(2)	175.11(5)	C(12)-N(4)-Pd(1)	114.80(10)
N(1)-Pd(1)-Cl(1)	175.25(4)	C(1)-C(5)-N(2)	108.46(12)
N(4)-Pd(1)-Cl(1)	89.57(4)	N(3)-C(8)-C(4)	114.89(13)
N(2)-Pd(1)-Cl(1)	94.23(4)		

6 Conclusion and outlook

Within this thesis two new ligand species namely the {*NNN*}-pyrrole based pincer ligand with increased steric demand and the {*SNS*}-pyrrole based pincer ligand could be prepared and were proven to be highly suitable for the coordination of a variety of metal species.

These complexes with metal ions as small as germanium(IV) (39 pm) and big as lead(II) comprising an ion radius of 119 pm, convey the coordination flexibility of this type of ligand. Consequently, the distance of both side arm nitrogen donor atoms varies between 440.0 pm for aluminium(III) (**10**) and 491.2 pm for lead(II) (**21**) (Figure 65). The ligand flexibility is further mirrored by the variable coordination mode which can be tridentate or bidentate in the presence of another *Lewis*-acidic molecule as shown in the palladium compound (**26**).

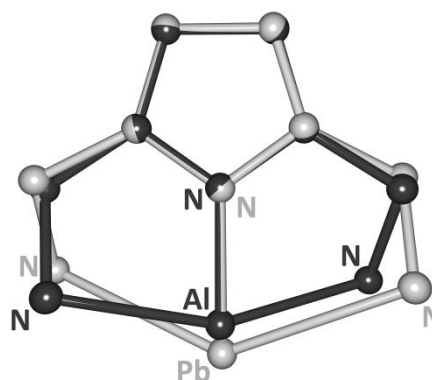


Figure 65. Superposition plot of compounds **10** (dark gray) and **21** (light gray).

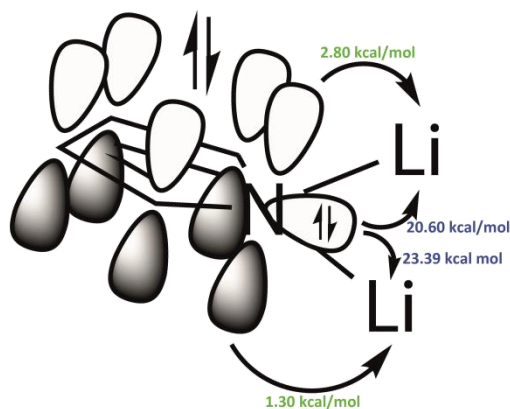


Figure 66. Pyrrole→lithium interaction in compound **7**. Energy values depicted in the figure belong to σ - and π - interaction energies of N1 in compound **7**.

An example for this coordination diversity is the dimeric lithium pyrrolide species (**7-9**). The pyrrole nitrogen atom coordinates to both lithium ions in the μ_2 -bridging mode. This could be expected for sp^3 -hybridized nitrogen atoms¹⁵³ as they comprise a tetrahedral geometry, however, this coordination mode was not explained for aromatic nitrogen atoms showing a similar tetrahedral motif.⁹² High resolution X-ray diffraction data for compound **7** together with an extensive computational

study confirmed the assumption of a lithium- π interaction in dimeric structures of aromatic lithium amides (Figure 66).

Apart from the prove of ligand flexibility, it could be shown that the alkyl chains bonded to the side arm donor functionalities are stereochemically active. Even the slight

increase in steric bulk from dimethylamino- to pyrrolidino-groups drastically affects the reactivity of N_{Pyrrole} bonded atoms. In compound **11** the bulkier pyrrolidine groups, with respect to dimethylamine, prevent the pyrrole N–H from being deprotonated by the rather basic trimethylaluminium compound. Replacing the pyrrolidine groups by dimethylamine moieties leads to a quantitative deprotonation of the pyrrole heterocycle. Both products could be confirmed by crystallization. The N -metallated species symbolizes the thermodynamic product and the N -protonated compound, forming a C–H \cdots N interaction between pyrrole and a trimethylaluminium molecule represents the kinetic product.

This reactivity can be transferred to the $\{NNN\}\text{GeCl}$ species (**15**). Reacting **15** with methyllithium exclusively yielded the $[\{NNN\}\text{Li}]_2$ lithium pyrrolide species (**8**) (Figure 67). By increasing the size of the lithiumorganic compound from methyllithium to TMS-methyllithium which is similar in size to trimethylaluminium it should be possible to synthesize the desired $\{NNN\}\text{Ge-alkyl}$ species.

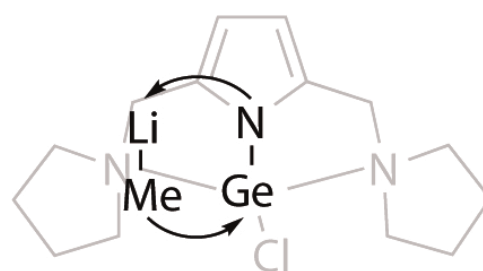


Figure 67. Intermediate species in the reaction of **15** with MeLi, explaining the formation of compound **8**.

Further investigation of the tetrele complexes afforded an absolutely unknown phenomenon in metal organic chemistry. The silicon compound $\{NNN\}\text{HSiCl}_2$ crystallizes in two different connectivity modes. Depending on the crystallization conditions, the ligand can coordinate as a tridentate ligand yielding an octahedral environment at the silicon atom or the ligand can act as a bidentate species with a trigonal bipyramidal surrounding at the silicon atom. This observation of thermodynamic vs. kinetic crystallization product was confirmed by a computational investigation showing a difference in energy of only 7.8 kJ/mol for both isomers.

Descending group 14 the interaction of the heavier elements with the pyrrole π -system was focused on. By analyzing the C–C bond lengths of the pyrrole heterocycle in combination with a computational investigation and a NMR-spectroscopic study on the heavy group 14 pincer complexes a decreasing interaction of the pyrrole π -system with the tetrele element going from germanium to lead was noticed. It could be clearly pointed out that within the heavy tetrele elements, tin is much more similar to

germanium than it is to lead. Lead does not show a significant interaction with the π -system. Evaluation of the data yielded a similar metal- π interaction for lead than for lithium in **7** and **8**.

Unexpectedly, none of the prepared group 14 compounds contained a metal \rightarrow ligand π -back donation. To visualize the consequences of a π -back donation on the pyrrole π -system a transition metal complex with nickel(II) was prepared. The molecular orbitals computed for this compound do not comprise an overlap between the unoccupied pyrrole π -orbital and a d-orbital of the nickel(II) ion. Related compounds^{3c,139e} hint to the fact that the empty pyrrole π -orbital is too high in energy which could be an explanation for the lacking π -back donation in the tetrele complexes as well.

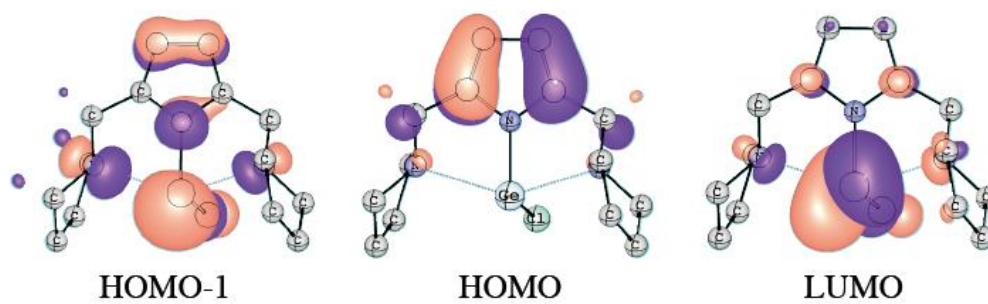


Figure 68. Molecular orbitals of $\{NNN\}GeCl$ (**15**). HOMO-1 clearly shows the metal centered lone pair, whereas the empty pyrrole π -orbital shows only small orbital coefficients in the LUMO. It seems to be higher in energy, indicating an even larger gap between the metal centered lone pair and the empty pyrrole π -orbital.

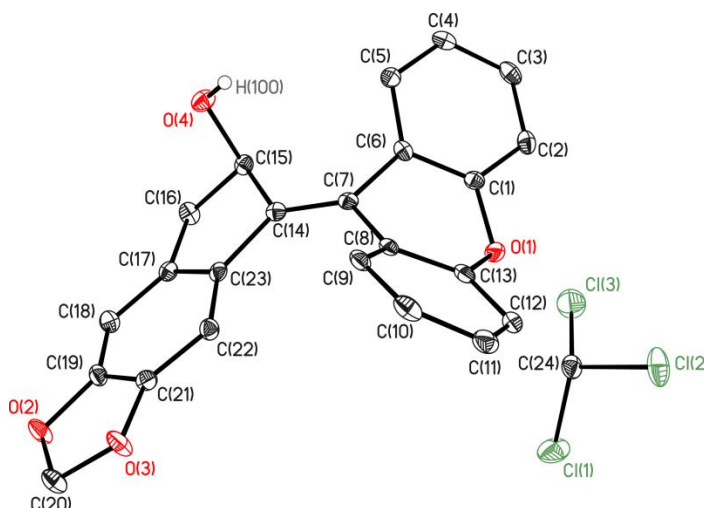
A way to tune the orbital energies is to replace the remaining metal bonded substituent. It was shown, that replacement of chlorine by methyl elevates the HOMO and thus narrows the HOMO-LUMO gap by approximately 1 eV. Another approach can be the substitution of the side arms as the compounds with pyridyl side arms^{3c} clearly show. By enlarging the pyrrole π -system they contain a LUMO with equal contributions of the pyrrole π -system and a metal centered d-orbital (Figure 68). By varying the metal bonded substituent it should be possible to obtain pyrrole based pincer ligands containing a rather small HOMO-LUMO gap, which makes π -back donation likely. Those species will contain new properties with a quasi-open-shell orbital configuration and a stronger metal ligand bond. This stronger ligand metal bond should make new reactions feasible, like the reduction of a metal species, yielding germanium in the oxidation state +1, which was not possible with compound **15**. These yet unknown properties will open a new field of chemistry in the area of pyrrole based pincer ligands. With the properties of the Frustrated Lewis Pairs⁵⁷ combined at a single atom, similar to the metalylenes but

rather convenient to synthesize, they comprise high potential in molecule/bond activation.

7 Crystal structure determination in collaborations

7.1 Structures determined for Dr. Tim Hungerland (Prof. Dr. Dr. h. c. L. F. Tietze)

7.1.1 CM_THD391

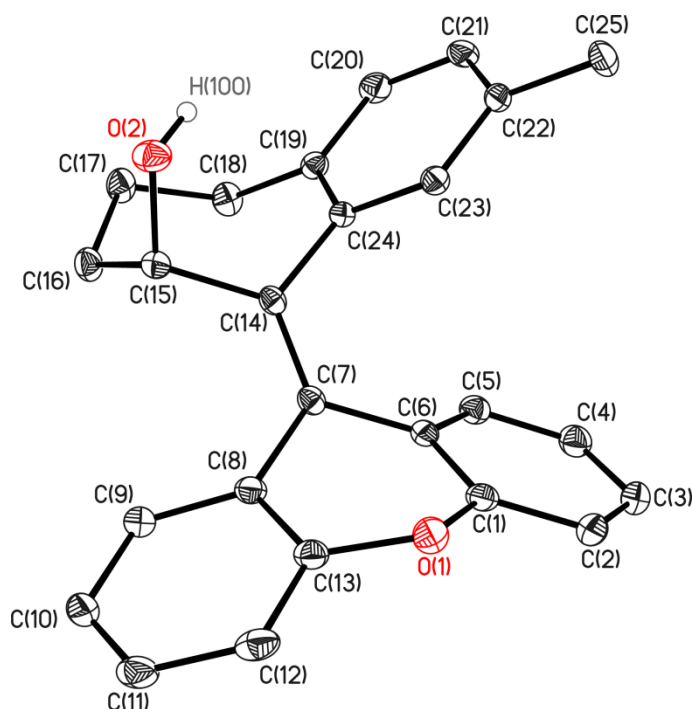


Asymmetric unit of CM_THD391. Hydrogen atoms besides H100 have been omitted. H100 has been freely refined and the thermal ellipsoid was modeled isotropic.

The structure has been published in *"Palladium-catalyzed domino carbopalladation/C-H activation for the synthesis of tetrasubstituted alkenes bearing five- and seven-membered rings."* L. F. Tietze, T. Hungerland, C. Depken, C. Maass, D. Stalke, *Synlett*, **2012**, 23, 2516.

CCDC no.	881349	Z	2
Empirical formula	C ₂₄ H ₁₇ Cl ₃ O ₄	Absorption coefficient	0.250 mm ⁻¹
Formula weight	475.73	F(000)	488
Temperature	100(2) K	Crystal size	0.2 x 0.1 x 0.05 mm ³
Wavelength	0.56086 Å	Theta range for data collection	1.19 to 21.38°
Crystal system	Triclinic	Reflections collected	19632
Space group	<i>P</i> $\bar{1}$	Independent reflections	4721 [<i>R</i> (int) = 0.0459]
Unit cell dimensions		Completeness to theta = 25.242°	99.9 %
	<i>a</i> = 8.061(2) Å	Data / restraints / parameters	4721 / 0 / 284
	<i>b</i> = 9.785(2) Å	Goodness-of-fit on <i>F</i> ²	1.021
	<i>c</i> = 13.815(3) Å	<i>R</i> 1 [<i>I</i> > 2σ(<i>I</i>)]	0.0362
	α = 93.21(2)°	w <i>R</i> 2 (all data)	0.0838
	β = 100.01(3)°	Extinction coefficient	-
	γ = 105.82(3)°	Largest diff. peak and hole	0.405 and -0.284 e.Å ⁻³
Volume	1026.3(4) Å ³	Absolute structure parameter	-

7.1.2 CM_THD398

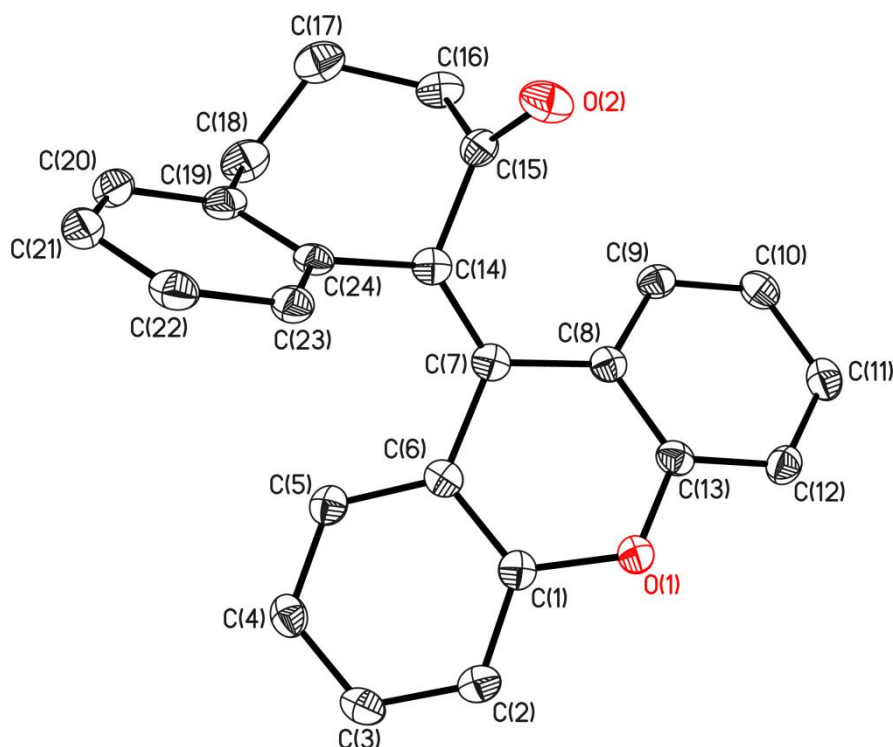


Asymmetric unit of CM_THD398. Hydrogen atoms besides H100 have been omitted. H100 has been freely refined and the thermal ellipsoid was modeled isotropic.

The structure has been published in “*Palladium-catalyzed domino carbopalladation/C-H activation for the synthesis of tetrasubstituted alkenes bearing five- and seven-membered rings.*” L. F. Tietze, T. Hungerland, C. Depken, C. Maass, D. Stalke, *Synlett*, **2012**, 23, 2516.

CCDC no.	881350	Z	8
Empirical formula	C ₂₅ H ₂₂ O ₂	Absorption coefficient	0.051 mm ⁻¹
Formula weight	354.43	F(000)	1504
Temperature	100(2) K	Crystal size	0.2 x 0.2 x 0.1 mm ³
Wavelength	0.56086 Å	Theta range for data collection	0.95 to 21.97°.
Crystal system	Monoclinic	Reflections collected	38666
Space group	C2/c	Independent reflections	4721 [R(int) = 0.0459]
Unit cell dimensions		Completeness to theta = 25.242°	99.9 %
	a = 34.504(3) Å	Data / restraints / parameters	4721 / 0 / 284
	b = 6.390(2) Å	Goodness-of-fit on F ²	1.021
	c = 17.026(2) Å	R1 [I > 2sigma(I)]	0.0362
	α = 90°	wR2 (all data)	0.0838
	β = 101.39(2)°	Extinction coefficient	-
	γ = 90°	Largest diff. peak and hole	0.405 and -0.284 e.Å ⁻³
Volume	3680.0(13) Å ³	Absolute structure parameter	-

7.1.3 CM_THDDWV7NK

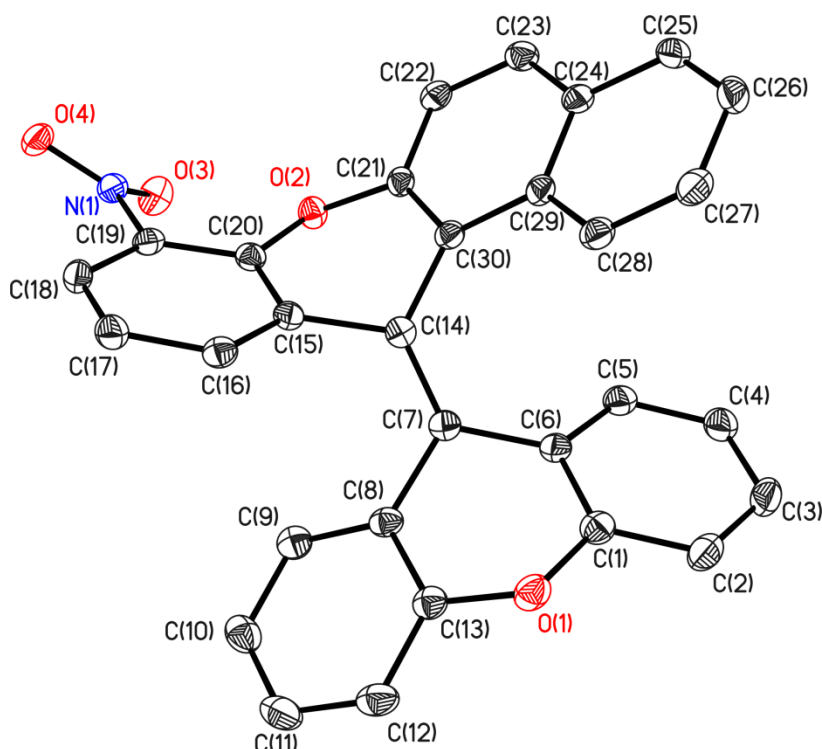


Asymmetric unit of CM_THDDWV7NK. Hydrogen atoms have been omitted. The crystal was non-merohedrally twinned. The structure was refined against HKLF5 data, including both domains, with a batch scale factor of 0.51.

The structure has been published in "Palladium-catalyzed domino carbopalladation/C-H activation for the synthesis of tetrasubstituted alkenes bearing five- and seven-membered rings." L. F. Tietze, T. Hungerland, C. Depken, C. Maass, D. Stalke, *Synlett*, **2012**, 23, 2516.

CCDC no.	881351	Z	4
Empirical formula	C ₂₄ H ₁₈ O ₂	Absorption coefficient	0.083 mm ⁻¹
Formula weight	338.38	F(000)	712
Temperature	100(2) K	Crystal size	0.2 x 0.04 x 0.04 mm ³
Wavelength	0.71073 Å	Theta range for data collection	2.23 to 23.26°
Crystal system	Monoclinic	Reflections collected	13216
Space group	<i>P</i> 2 ₁ / <i>n</i>	Independent reflections	4429 [<i>R</i> (int) = -]
Unit cell dimensions		Completeness to theta = 25.242°	99.0 %
	<i>a</i> = 9.392(2) Å	Data / restraints / parameters	4429 / 0 / 235
	<i>b</i> = 16.481(3) Å	Goodness-of-fit on <i>F</i> ²	1.102
	<i>c</i> = 11.341(2) Å	<i>R</i> 1 [<i>I</i> > 2σ(<i>I</i>)]	0.0403
	α = 90°	w <i>R</i> 2 (all data)	0.1045
	β = 105.26(2)°	Extinction coefficient	-
	γ = 90°	Largest diff. peak and hole	0.312 and -0.206 e.Å ⁻³
Volume	1693.6(6) Å ³	Absolute structure parameter	-

7.1.4 CM_THD533B

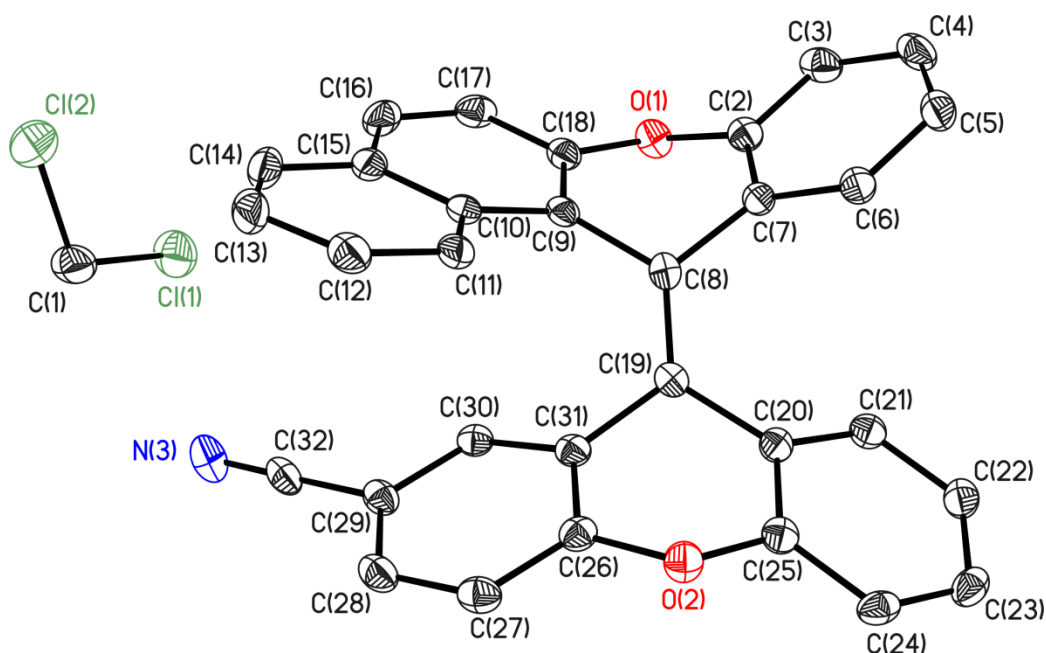


Asymmetric unit of CM_THD533B. Hydrogen atoms have been omitted.

The structure has been published in “Efficient Synthesis of Helical Tetrasubstituted Alkenes as Potential Molecular Switches: A Two-Component Palladium-Catalyzed Triple Domino Process.” L. F. Tietze, T. Hungerland, C. Eichhorst, A. Duefert, C. Maass, D. Stalke, *Angew. Chem. Int. Ed.* **2013**, 52, 3668.

CCDC no.	911711	Z	4
Empirical formula	C ₃₀ H ₁₇ N O ₄	Absorption coefficient	0.094 mm ⁻¹
Formula weight	455.45	F(000)	944
Temperature	100(2) K	Crystal size	0.12 x 0.1 x 0.1 mm ³
Wavelength	0.71073 Å	Theta range for data collection	1.904 to 27.487°
Crystal system	Monoclinic	Reflections collected	48344
Space group	<i>P</i> 2 ₁ / <i>c</i>	Independent reflections	4944 [<i>R</i> (int) = 0.0495]
Unit cell dimensions		Completeness to theta = 25.242°	99.9 %
	<i>a</i> = 9.454(2) Å	Data / restraints / parameters	4944 / 306 / 316
	<i>b</i> = 21.390(3) Å	Goodness-of-fit on <i>F</i> ²	1.056
	<i>c</i> = 10.709(2) Å	<i>R</i> 1 [<i>I</i> > 2σ(<i>I</i>)]	0.0434
	α = 90°	w <i>R</i> 2 (all data)	0.1125
	β = 94.75(2)°	Extinction coefficient	-
	γ = 90°	Largest diff. peak and hole	0.282 and -0.334 e.Å ⁻³
Volume	2158.1(7) Å ³	Absolute structure parameter	-

7.1.5 CM_THD563



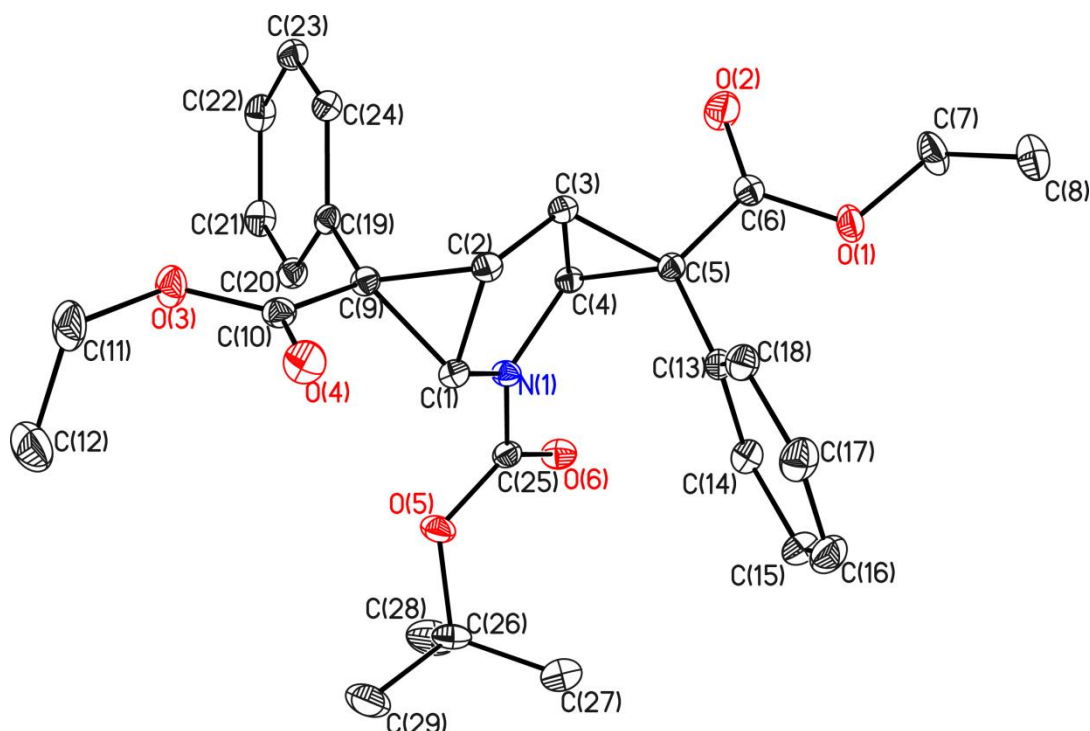
Asymmetric unit of CM_THD563. Hydrogen atoms have been omitted. The dichloromethane molecule is not disordered, however, the position is not fully occupied with a site occupation factor of 0.92.

The structure has been published in “*Efficient Synthesis of Helical Tetrasubstituted Alkenes as Potential Molecular Switches: A Two-Component Palladium-Catalyzed Triple Domino Process.*” L. F. Tietze, T. Hungerland, C. Eichhorst, A. Duefert, C. Maass, D. Stalke, *Angew. Chem. Int. Ed.* **2013**, 52, 3668.

CCDC no.	911712	Z	4
Empirical formula	C _{31.92} H ₁₉ Cl _{1.84} N O ₂	Absorption coefficient	0.283 mm ⁻¹
Formula weight	513.81	F(000)	1059
Temperature	100(2) K	Crystal size	0.1 x 0.1 x 0.05 mm ³
Wavelength	0.71073 Å	Theta range for data collection	1.638 to 25.411°
Crystal system	Monoclinic	Reflections collected	38816
Space group	<i>P</i> 2 ₁ / <i>n</i>	Independent reflections	4450 [<i>R</i> (int) = 0.0665]
Unit cell dimensions		Completeness to theta = 25.242°	99.9 %
	<i>a</i> = 13.301(3) Å	Data / restraints / parameters	4450 / 0 / 334
	<i>b</i> = 8.518(2) Å	Goodness-of-fit on <i>F</i> ²	1.013
	<i>c</i> = 21.991(3) Å	<i>R</i> 1 [<i>I</i> > 2σ(<i>I</i>)]	0.0406
	α = 90°	w <i>R</i> 2 (all data)	0.0979
	β = 103.64(2)°	Extinction coefficient	-
	γ = 90°	Largest diff. peak and hole	0.281 and -0.246 e.Å ⁻³
Volume	2421.3(9) Å ³	Absolute structure parameter	-

7.2 Structures determined for Dr. Tobias Schneider (Prof. Dr. D. B. Werz)

7.2.1 CM_ST413b

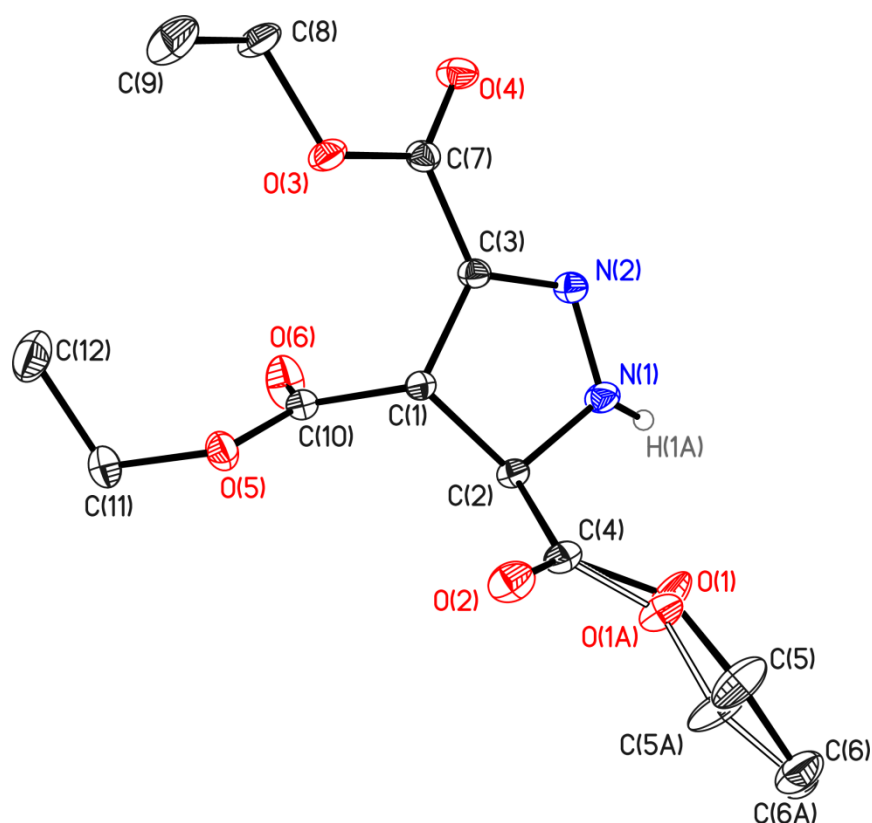


Asymmetric unit of CM_ST413b. Hydrogen atoms have been omitted.

The structure has been published in "Rearrangements of Furan-, Thiophene- and *N*-Boc-Pyrrole-Derived Donor-Acceptor Cyclopropanes: Scope and Limitations" J. Kaschel, T. F. Schneider, P. Schirmer, C. Maass, D. Stalke, D. B. Werz, *Eur. J. Org. Chem.* **2013**, 21, 4539.

CCDC no.	925485	<i>Z</i>	2
Empirical formula	C ₂₉ H ₃₃ N O ₆	Absorption coefficient	0.055 mm ⁻¹
Formula weight	491.56	<i>F</i> (000)	524
Temperature	100(2) K	Crystal size	0.2 x 0.15 x 0.15 mm ³
Wavelength	0.56086 Å	Theta range for data collection	1.201 to 23.269°
Crystal system	Triclinic	Reflections collected	35353
Space group	<i>P</i> $\bar{1}$	Independent reflections	7554 [<i>R</i> (int) = 0.0357]
Unit cell dimensions		Completeness to theta = 25.242°	100.0 %
	<i>a</i> = 9.071(2) Å	Data / restraints / parameters	7554 / 0 / 330
	<i>b</i> = 10.908(2) Å	Goodness-of-fit on <i>F</i> ²	1.029
	<i>c</i> = 14.325(3) Å	<i>R</i> 1 [<i>I</i> > 2σ(<i>I</i>)]	0.0409
	α = 69.14(2)°	w <i>R</i> 2 (all data)	0.1107
	β = 87.03(3)°	Extinction coefficient	-
	γ = 77.38(3)°	Largest diff. peak and hole	0.382 and -0.233 e.Å ⁻³
Volume	1292.0(5) Å ³	Absolute structure parameter	-

7.2.2 CM_ST440d

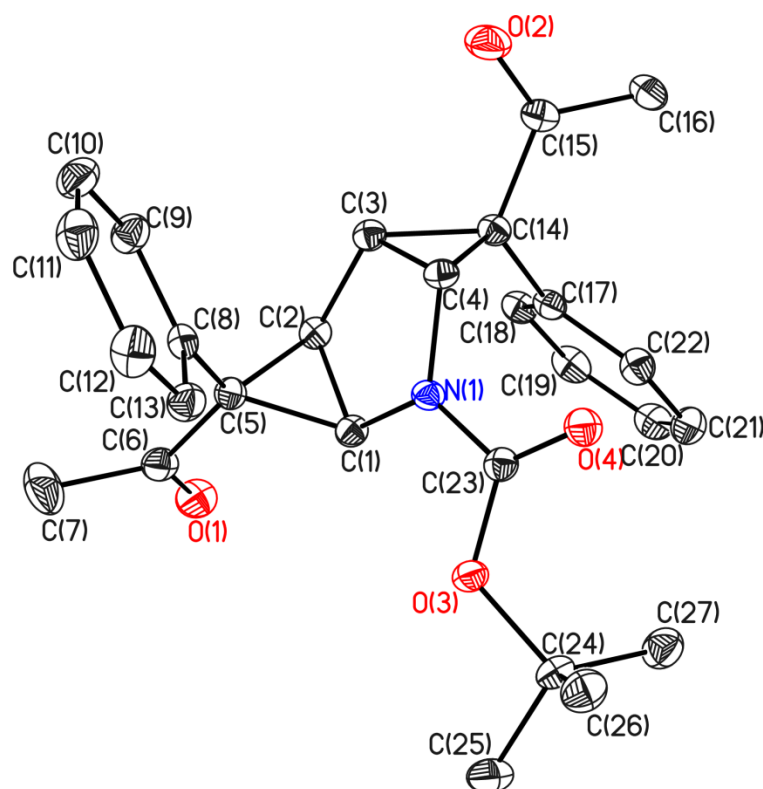


Asymmetric unit of CM_ST440d. Hydrogen atoms, besides H1A, have been omitted. H1A was freely refined with an isotropic thermal displacement parameter. The molecule fragment bonded to C2 shows a disorder with a site occupation factor of 0.62.

CM_ST440d has not been published, however, it is deposited at the CSD with the number 949463.

CCDC no.	949463	Z	4
Empirical formula	C12 H18 N2 O6	Absorption coefficient	0.110 mm ⁻¹
Formula weight	286.28	F(000)	608
Temperature	100(2) K	Crystal size	0.2 x 0.1 x 0.1 mm ³
Wavelength	0.71073 Å	Theta range for data collection	2.308 to 30.531°
Crystal system	Orthorhombic	Reflections collected	21067
Space group	<i>P</i> 2 ₁ 2 ₁ 2 ₁	Independent reflections	4242 [<i>R</i> (int) = 0.0612]
Unit cell dimensions		Completeness to theta = 25.242°	99.6 %
	<i>a</i> = 7.844(2) Å	Data / restraints / parameters	4242 / 94 / 217
	<i>b</i> = 10.274(3) Å	Goodness-of-fit on <i>F</i> ²	1.056
	<i>c</i> = 17.229(3) Å	<i>R</i> 1 [<i>I</i> > 2σ(<i>I</i>)]	0.0361
	α = 90°	w <i>R</i> 2 (all data)	0.0971
	β = 90°	Extinction coefficient	-
	γ = 90°	Largest diff. peak and hole	0.382 and -0.218 e.Å ⁻³
Volume	1388.5(6) Å ³	Absolute structure parameter	-

7.2.3 CM_ST4202b

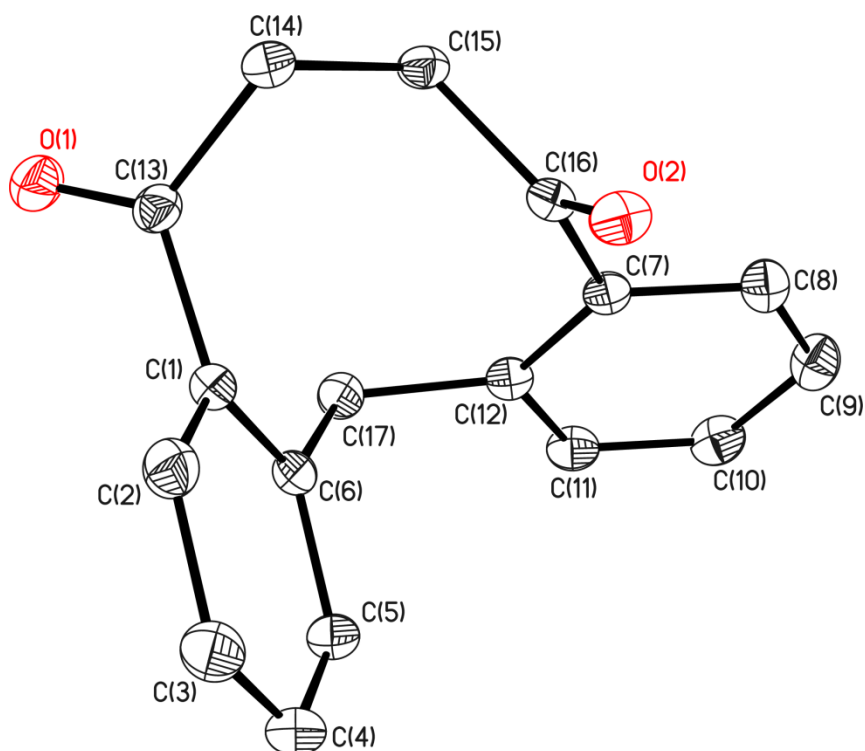


Asymmetric unit of CM_ST4202b. Hydrogen atoms have been omitted.

The structure has been published in "Rearrangements of Furan-, Thiophene- and *N*-Boc-Pyrrole-Derived Donor-Acceptor Cyclopropanes: Scope and Limitations" J. Kaschel, T. F. Schneider, P. Schirmer, C. Maass, D. Stalke, D. B. Werz, *Eur. J. Org. Chem.* **2013**, 21, 4539.

CCDC no.	925486	Z	2
Empirical formula	C ₂₇ H ₂₉ N O ₄	Absorption coefficient	0.080 mm ⁻¹
Formula weight	431.51	F(000)	460
Temperature	101(2) K	Crystal size	0.15 x 0.1 x 0.1 mm ³
Wavelength	0.71073 Å	Theta range for data collection	1.393 to 28.312°
Crystal system	Triclinic	Reflections collected	27001
Space group	<i>P</i> $\bar{1}$	Independent reflections	5926 [<i>R</i> (int) = 0.0345]
Unit cell dimensions		Completeness to theta = 25.242°	99.8 %
	<i>a</i> = 8.994(2) Å	Data / restraints / parameters	5926 / 0 / 294
	<i>b</i> = 9.359(2) Å	Goodness-of-fit on <i>F</i> ²	1.031
	<i>c</i> = 14.816(3) Å	<i>R</i> 1 [<i>I</i> > 2σ(<i>I</i>)]	0.0392
	α = 80.65(3)°	w <i>R</i> 2 (all data)	0.1023
	β = 86.50(3)°	Extinction coefficient	-
	γ = 76.62(2)°	Largest diff. peak and hole	0.338 and -0.241 e.Å ⁻³
Volume	1196.8(5) Å ³	Absolute structure parameter	-

7.2.4 CM_B3Al55



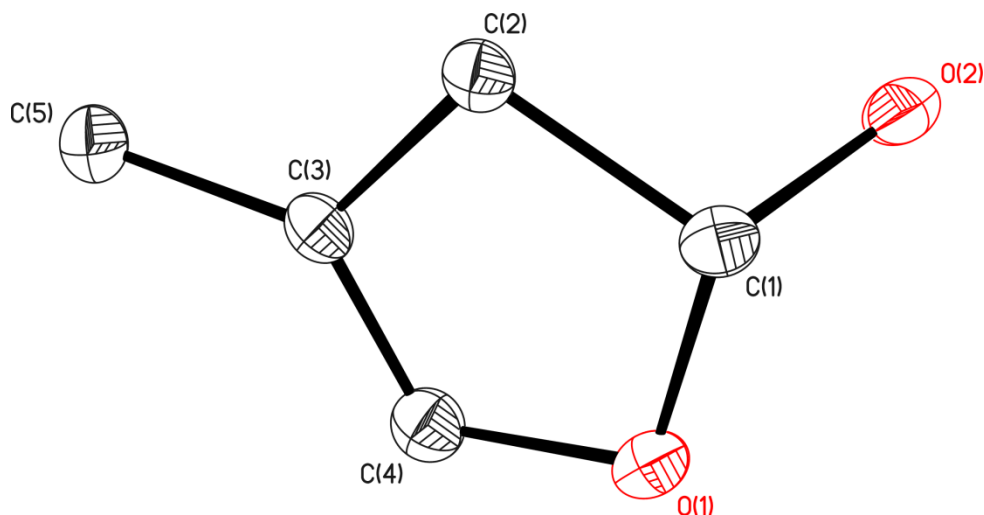
Asymmetric unit of CM_B3Al55. Hydrogen atoms have been omitted.

CM_B3Al55 has not been published, however, it is deposited at the CSD with the CCDC-number 949461.

CCDC no.	949461	Z	4
Empirical formula	C17 H14 O2	Absorption coefficient	0.085 mm ⁻¹
Formula weight	250.28	F(000)	528
Temperature	100(2) K	Crystal size	0.2x 0.2x 0.1 mm ³
Wavelength	0.71073 Å	Theta range for data collection	1.871 to 30.032°
Crystal system	Monoclinic	Reflections collected	38795
Space group	<i>P</i> 2 ₁ / <i>c</i>	Independent reflections	3702 [<i>R</i> (int) = 0.0275]
Unit cell dimensions		Completeness to theta = 25.242°	99.5 %
	<i>a</i> = 11.209(3) Å	Data / restraints / parameters	3702 / 0 / 172
	<i>b</i> = 15.124(4) Å	Goodness-of-fit on <i>F</i> ²	1.047
	<i>c</i> = 7.728(3) Å	<i>R</i> 1 [<i>I</i> > 2σ(<i>I</i>)]	0.0404
	α = 90°	w <i>R</i> 2 (all data)	0.1136
	β = 103.83(3)°	Extinction coefficient	-
	γ = 90°	Largest diff. peak and hole	0.402 and -0.208 e.Å ⁻³
Volume	1272.1(7) Å ³	Absolute structure parameter	-

7.3 Structures determined for Dr. Johannes Kaschel (Prof. Dr. D. B. Werz)

7.3.1 CM_JKF73



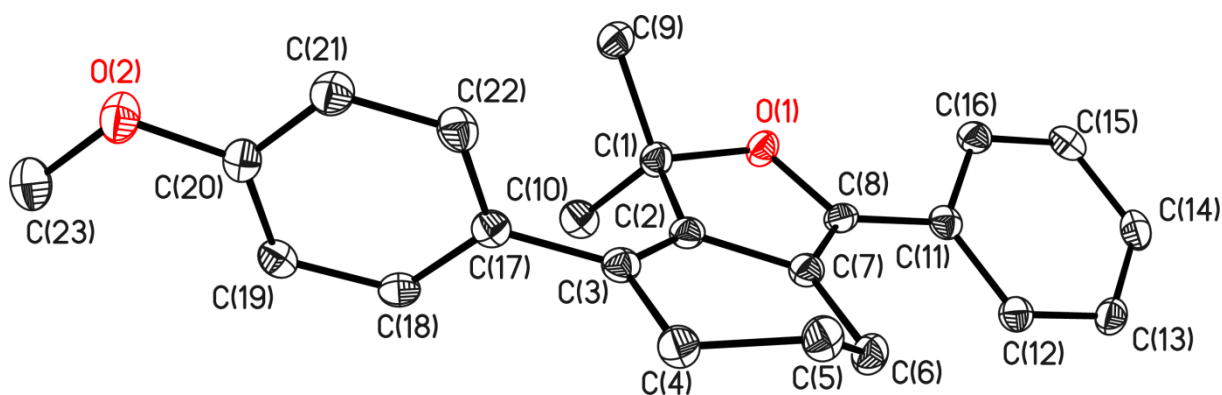
Asymmetric unit of CM_JKF73. Hydrogen atoms have been omitted.

The structure has been published in “Rearrangements of Furan-, Thiophene- and *N*-Boc-Pyrrole-Derived Donor-Acceptor Cyclopropanes: Scope and Limitations” J. Kaschel, T. F. Schneider, P. Schirmer, C. Maass, D. Stalke, D. B. Werz, *Eur. J. Org. Chem.* **2013**, 21, 4539.

CCDC no.	925484	Z	8
Empirical formula	C ₁₀ H ₁₂ O ₂	Absorption coefficient	0.062 mm ⁻¹
Formula weight	180.20	F(000)	768
Temperature	100(2) K	Crystal size	0.2 x 0.1 x 0.04 mm ³
Wavelength	0.56086 Å	Theta range for data collection	2.615 to 20.493°
Crystal system	Orthorhombic	Reflections collected	4978
Space group	<i>Fdd2</i>	Independent reflections	897 [<i>R</i> (int) = 0.0325]
Unit cell dimensions		Completeness to theta = 25.242°	99.8 %
	<i>a</i> = 10.495(2) Å	Data / restraints / parameters	897 / 3 / 65
	<i>b</i> = 24.590(3) Å	Goodness-of-fit on <i>F</i> ²	1.059
	<i>c</i> = 6.828(2) Å	<i>R</i> 1 [<i>I</i> > 2σ(<i>I</i>)]	0.0316
	α = 90°	w <i>R</i> 2 (all data)	0.0799
	β = 90°	Extinction coefficient	-
	γ = 90°	Largest diff. peak and hole	0.156 and -0.143 e.Å ⁻³
Volume	1762.1(7) Å ³	Absolute structure parameter	-

7.4 Structures determined for Matrin Pawliczek (Prof. Dr. D. B. Werz)

7.4.1 CM_PM411



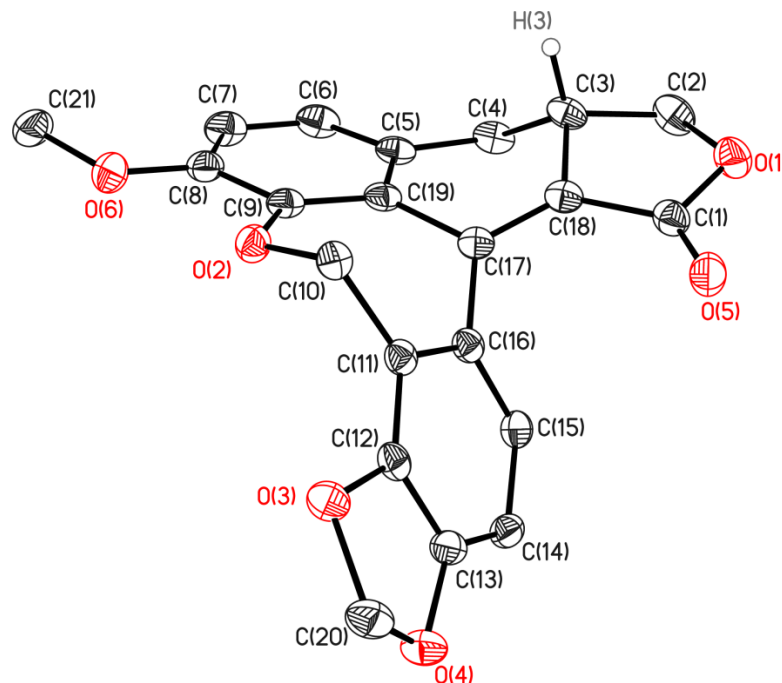
Asymmetric unit of CM_PM411. Hydrogen atoms are omitted for clarity.

CM_PM411 is part of the manuscript "Pd-Catalyzed Domino Reaction of Propargylic Diynols to Dienol Ethers: A Formal anti-Carbopalladation Process." M. Pawliczek, C. Maass, D. Stalke, D. B. Werz, submitted.

CCDC no.	941402	Z	8
Empirical formula	C ₂₃ H ₂₄ O ₂	Absorption coefficient	0.079 mm ⁻¹
Formula weight	332.42	F(000)	1424
Temperature	100(2) K	Crystal size	0.15 x 0.15 x 0.05 mm ³
Wavelength	0.71073 Å	Theta range for data collection	1.857 to 25.678°
Crystal system	Monoclinic	Reflections collected	26410
Space group	C2/c	Independent reflections	3315 [R(int) = 0.0283]
Unit cell dimensions		Completeness to theta = 25.242°	99.8 %
	a = 9.888(2) Å	Data / restraints / parameters	3315 / 0 / 230
	b = 16.130(3) Å	Goodness-of-fit on F ²	1.074
	c = 21.940(3) Å	R1 [I > 2sigma(I)]	0.0358
	α = 90°	wR2 (all data)	0.0905
	β = 91.46(2)°	Extinction coefficient	-
	γ = 90°	Largest diff. peak and hole	0.273 and -0.180 e.Å ⁻³
Volume	3498.2(11) Å ³	Absolute structure parameter	-

7.5 Structures determined for Svenia C. Düfert (Prof. Dr. Dr. h. c. L. F. Tietze)

7.5.1 CM_JCLINOXEPIN



Asymmetric unit of of CM_JCLINOXEPIN, showing the crystal structure of (-)-S-Linoxepin. Hydrogen atoms, besides H3, have been omitted. The absolute structure was determined using Cu-K α radiation (Flack x parameter: -0.05(8))¹⁵⁴.

The structure has been published in “Total Synthesis of Linoxepin through a Palladium-Catalyzed Domino Reaction” L. F. Tietze, S.-C. Duefert, J. Clerc, M. Bischoff, C. Maass, D. Stalke, *Angew. Chem. Int. Ed.* **2013**, 52, 3191.

CCDC no.	913693	Z	2
Empirical formula	C ₂₁ H ₁₆ O ₆	Absorption coefficient	0.914 mm ⁻¹
Formula weight	364.34	F(000)	380
Temperature	100(2) K	Crystal size	0.12 x 0.08 x 0.03 mm ³
Wavelength	1.54178 Å	Theta range for data collection	4.118 to 68.547°
Crystal system	Monoclinic	Reflections collected	8931
Space group	P2 ₁	Independent reflections	2186 [R(int) = 0.0290]
Unit cell dimensions		Completeness to theta = 25.242°	99.3 %
	a = 4.845(2) Å	Data / restraints / parameters	2186 / 1 / 245
	b = 15.655(3) Å	Goodness-of-fit on F ²	1.060
	c = 10.918(3) Å	R1 [I > 2sigma(I)]	0.0265
	α = 90°	wR2 (all data)	0.0683
	β = 100.47(3)°	Extinction coefficient	-
	γ = 90°	Largest diff. peak and hole	0.134 and -0.214 e.Å ⁻³
Volume	814.3(4) Å ³	Absolute structure parameter	-0.05(8)

8 References

- 1 G. van Koten, J. T. B. H. Jastrzebski, J. G. Noltes, A. L. Spek, J. C. Schoone, *J. Organomet. Chem.* **1978**, *148*, 233.
- 2 C. J. Moulton, B. L. Shaw, *J. Chem. Soc. Dalton Trans.* **1976**, 1020.
- 3 (a) C. Mazet, L. H. Gade, *Chem. Eur. J.* **2003**, *9*, 1759; (b) S. Kumar, G. Mani, S. Mondal, P.-K. Chata-taraj, *Inorg. Chem.* **2012**, *51*, 12527; (c) G. H. Immler, Z. Lu, K. A. Kistler, P. J. Carroll, B. B. Wayland, M. J. Zdilla, *Inorg. Chem.* **2012**, *51*, 10122; (d) N. Grüger, H. Wadepohl, L. H. Gade, *Dalton Trans.* **2012**, *41*, 14028; (e) M. C. Denney, V. Pons, T. J. Hebden, D. M. Heinekey, K. I. Goldberg, *J. Am. Chem. Soc.* **2006**, *128*, 12048; (f) A. S. Goldman, A. H. Roy, Z. Huang, R. Ahuja, W. Schinski, M. Brookhart, *Science*, **2006**, *312*, 257; (g) J. Zhao, A. S. Goldman, J. F. Hartwig, *Science*, **2005**, *307*, 1080; (h) S. W. Kohl, L. Weiner, L. Swartsburd, L. Kostanikowski, L. J. W. Shimon, Y. Ben-David, M. A. Iron, D. Milstein, *Science*, **2009**, *324*, 74; (i) F. E. Hahn, M. C. Jahnke, V. Gomez-Benitez, D. Morales-Morales, T. Pape, *Organometallics*, **2005**, *24*, 6458; (j) E. Khaskin, M. A. Iron, L. J. W. Shimon, J. Zhang, D. Milstein, *J. Am. Chem. Soc.* **2010**, *132*, 8542; (k) E. Balaraman, C. Gunanathan, J. Zhang, L. J. W. Shimon, D. Milstein, *Nat. Chem.* **2011**, *3*, 609; (l) R. Tian, Y. Ng, R. Ganguly, F. Mathey, *Organometallics*, **2012**, *31*, 2486; (m) A. Friedrich, M. Drees, M. Käss, E. Herdtweck, S. Schneider, *Inorg. Chem.* **2010**, *49*, 5482; (n) B. Askevold, J. T. Nieto, S. Tussupbayev, M. Diefenbach, E. Herdtweck, M. C. Holthausen, S. Schneider, *Nature Chem.* **2011**, *3*, 532; (o) B. Askevold, H. W. Roesky, S. Schneider, *ChemCatChem*, **2012**, *4*, 307; (p) M. G. Scheibel, B. Askevold, F. W. Heinemann, E. J. Reijerse, B. de Bruin, S. Schneider, *Nature Chem.* **2012**, *4*, 552; (q) S. Y. de Boer, Y. Gloaguen, J. N. H. Reek, M. Lutz, J. I. van der Vlugt, *Dalton Trans.* **2012**, *41*, 11276; (r) M. W. Löble, M. Casimiro, D. T. Thielemann, P. Ona-Burgos, I. Fernandez, P. W. Roesky, F. Breher, *Chem. Eur. J.* **2012**, *18*, 5325.
- 4 (a) S. Khan, R. Michel, J. M. Dieterich, R. A. Mata, H. W. Roesky, J.-P. Demers, A. Lange, D. Stalke, *J. Am. Chem. Soc.* **2011**, *133*, 17889; (b) J. Jentner, M. T. Gamer, P. W. Roesky, *Organometallics*, **2010**, *29*, 4410; (c) J. Jenter, P. W. Roesky, *New. J. Chem.* **2010**, *34*, 1541; (d) S. Khan, P. P. Samuel, R. Michel, J. M. Dieterich, R. A. Mata, J.-P. Demers, A. Lange, H. W. Roesky, D. Stalke, *Chem. Commun.* **2012**, *48*, 4890; (e) L. Mahalakshmi, D. Stalke „The R_2M^+ Group 13 Organometallic Fragment Chelated by P-centered Ligands“ in *Structure and Bonding - Group 13 Chemistry I*, Springer Verlag Heidelberg, **2002**, *103*, 85; (f) T. Kottke, D. Stalke, *Chem. Ber./Recl.* **1997**, *130*, 1365; (g) F. Baier, Z. Fei, H. Gornitzka, A. Murso, S. Neufeld, M. Pfeiffer, I. Rüdenauer, A. Steiner, T. Stey, D. Stalke, *J. Organomet. Chem.* **2002**, *661*, 111.
- 5 R. G. Pearson, J. Songstad, *J. Am. Chem. Soc.* **1967**, *89*, 1827.
- 6 S. K. Russell, C. Milsmann, E. Lobkovsky, T. Weyhermuller, P. J. Chirik, *Inorg. Chem.* **2011**, *50*, 3159.
- 7 A. P. Singh, H. W. Roesky, E. Carl, D. Stalke, J.-P. Demers, A. Lange, *J. Am. Chem. Soc.* **2012**, *134*, 4998.
- 8 S. Katagiri, R. Sakamoto, H. Maeda, Y. Nishimori, T. Kurita, H. Nishihara, *Chem. Eur. J.* **1996**, *19*, 5088.
- 9 C. Mazet, L. H. Gade, *Chem. Eur. J.* **2002**, *8*, 4308.
- 10 M. Contel, D. Nobel, A. L. Spek, G. van Koten, *Organometallics*, **2000**, *19*, 3288.

-
- 11 J. L. Lien, Y. C. Chang, N. T. Chuang, A. Datta, S. J. Chen, C. H. Hu, W. Y. Huang, C. H. Lin, J. H. Huang, *Inorg. Chem.* **2010**, *49*, 136.
- 12 H. C. L. Abbenhuis, N. Feiken, D. M. Grove, J. T. B. H. Jastrzebski, H. Kooijman, P. van der Sluis, W. J. J. Smeets, A. L. Spek, G. van koten, *J. Am. Chem. Soc.* **1992**, *114*, 9773.
- 13 W. J. J. Smeets, A. L. Spek, A. J. M. Duisenberg, J. A. M. van Beek, G. van Koten, *Acta Crystallographica Section C: Crystal Structure Communications*, **1987**, *C43*, 463.
- 14 H. C. L. Sbbenhuis, N. Feiken, H. F. Haarman, D. M. Grove, E. Horn, H. Kooijman, A. L. Spek, G. van Koten, *Angew. Chem. Int. Ed.* **1991**, *30*, 996.
- 15 J.-P. Sutter, S. L. James, P. Steenwinkel, T. Karlen, D. M. Grove, N. Veldman, W. J. J. Smeets, A. L. Spek, G. van Koten, *Organometallics*, **1996**, *15*, 941.
- 16 A. D. Ryabov, *Chem. Rev.* **1990**, *90*, 403.
- 17 J. A. M. van Beek, G. van Koten, M. J. Ramp, N. C. Coenjaarts, D. M. Grove, K. Goubnitz, M. C. Zoutberg, C. H. Stam, W. J. J. Smeets, A. L. Spek, *Inorg. Chem.* **1991**, *30*, 3059.
- 18 F. F. Runge, *Pogg. Ann.* **1834**, *31*, 65.
- 19 H. J. Anderson, *J. Chem. Edu.* **1995**, *72*, 10, 875.
- 20 a) M. J. Cook, A. R. Katritzky, P. Linda, *Adv. Heterocycl. Chem.* **1974**, *17*, 257; b) R. A. Hosmane, J. F. Liebman, *Tetrahedron Lett.* **1991**, *32*, 3949; c) V. G. S. Box, *Heterocycles*, **1991**, *32*, 2023; d) A. R. Katritzky, M. Karelson, N. Malhotra, *Heterocycles*, **1991**, *32*, 127; e) B. Y. Simkin, V. I. Minkin, M. N. Glukhovtsev, *Adv. Heterocycl. Chem.* **1993**, *56*, 303.
- 21 T. Eicher, S. Hauptmann, *The Chemistry of Heteroycles*, Wiley-VCH, Weinheim, **2003**.
- 22 C. Elschenbroich, *Organometallchemie*, 5th ed, Teubner, Wiesbaden, **2005**.
- 23 J. Hey, D. M. Andrada, R. Michel, R. A. Mata, D. Stalke, *Angew. Chem. Int. Ed.* **2013**, DOI: 10.1002/anie.201304498.
- 24 J. A. Joule, K. Mills, *Heterocyclic Chemistry*, 4th ed, Blackwell Science, Malden, **2004**.
- 25 a) E. Hückel, *Z. Phys.* **1931**, *70*, 204; b) E. Hückel, *Z. Phys.* **1932**, *72*, 310; c) E. Hückel, *Z. Phys.* **1932**, *76*, 628; d) E. Hückel, *Grundzüge der Theorie ungesättigter und aromatischer Verbindungen*, Verlag Chemie, Berlin, **1938**.
- 26 P. Müller, R. Herbst-Irmer, A. L. Spek, T. R. Schneider, M. R. Sawaya in *Crystal Structure Refinement - A Crystallographer's Guide to SHELXL*, 8th ed, Oxford University Press, Oxford, **2006**.
- 27 D. R. Lide, *Handbook of Chemistry and Physics*, 87th ed, CRC Press, Boca Raton, **2006**.
- 28 F. G. Bordwell, G. E. Drucker, H. E. Fried, *J. Org. Chem.* **1981**, *46*, 632.

-
- 29 A. A. Frost, B. Musulin, *J. Chem. Phys.* **1953**, *21*, 572.
- 30 a) J. Goubeau, *Angew. Chem.* **1957**, *69*, 77; b) P. Jutzi, *Angew. Chem. Int. Ed.* **1975**, *14*, 232; c) L. E. Guselnikov, N. S. Nametkin, *Chem. Rev.* **1979**, *79*, 529; d) M. C. Kuchta, G. Parkin, *Coord. Chem. Rev.* **1998**, *176*, 323.
- 31 a) P. J. Davidson, D. H. Harris, M. F. Lappert, *J. Chem. Soc., Dalton Trans.* **1976**, 2268; b) D. E. Goldberg, P. B. Hitchcock, M. F. Lappert, K. M. Thomas, T. Fjelberg, A. Haaland, B. E. R. Schilling, *J. Chem. Soc., Dalton Trans.* **1986**, 2387.
- 32 A. F. Wells, *Structural Inorganic Chemistry*, 5th ed, Clarendon Press, Oxford, **1984**.
- 33 M. F. Lappert, *Adv. Chem. Ser.* **1976**, *214*, 1343.
- 34 M. Stürmann, W. Saak, M. Weidenbruch, K. W. Klinkhammer, *Eur. J. Inorg. Chem.* **1999**, 579.
- 35 M. Driess, H. Grützmacher, *Angew. Chem.* **1996**, *108*, 900.
- 36 P. P. Power, *Nature*, **2010**, *463*, 171.
- 37 a) R. West, M. J. Fink, J. Michl, *Science*, **1981**, *214*, 1343; b) M. J. Fink, M. J. Michalczyk, K. J. Haller, R. West, J. Michl, *J. Chem. Soc., Chem. Commun.* **1983**, 1010.
- 38 P. B. Hitchcock, M. F. Lappert, S. J. Miles, A. J. Thorne, *J. Chem. Soc., Chem. Commun.* **1984**, 480.
- 39 a) M. Stürmann, M. Weidenbruch, K. W. Klinkhammer, F. Lissner, H. Marsmann, *Organometallics*, **1998**, *17*, 4425; b) M. Weidenbruch, *Eur. J. Inorg. Chem.* **1999**, 373.
- 40 a) R. F. W. Bader, *Can. J. Chem.* **1962**, *40*, 1164; b) R. G. Pearson, *J. Am. Chem. Soc.* **1969**, *91*, 4947; c) R. S. Grev, *Adv. Organomet. Chem.* **1991**, *33*, 125.
- 41 P. P. Power, *Chem. Commun.* **2003**, 2091.
- 42 a) W. Kutzelnigg, *Angew. Chem. Int. Ed.* **1984**, *23*, 272; b) K. P. Huber, G. Herzberg, *Molecular Spectra and Molecular Structures IV. Constants of Diatomic Molecules*. Van Nostrand, New York, **1979**.
- 43 H. Watanabe, K. Takeuchi, N. Fukawa, M. Kato, M. Goto, Y. Nagai, *Chem. Lett.* **1987**, 1341.
- 44 M. Kaupp, B. Metz, H. Stoll, *Angew. Chem. Int. Ed.* **2000**, *39*, 4607.
- 45 P. P. Power, *J. Chem. Soc., Dalton Trans.* **1998**, 2939.
- 46 L. Pu, B. Twamley, P. P. Power, *J. Am. Chem. Soc.* **2000**, *122*, 3524.
- 47 A. D. Phillips, R. J. Wright, M. M. Olmstead, P. P. Power, *J. Am. Chem. Soc.* **2002**, *124*, 5930.
- 48 M. Stender, A. D. Phillips, R. J. Wright, P. P. Power, *Angew. Chem. Int. Ed.* **2002**, *41*, 1785.
- 49 A. Sekiguchi, R. Kingo, M. A. Ichinohe, *Science*, **2004**, *305*, 1755.

-
- 50 a) G. J. Kubas, *Metal Dihydrogen and σ -Bonded Complexes: Structure, Theory and Reactivity*, Kluwer Academic/Plenum Publishers, London, **2001**; b) D. M. Heinekey, W. J. Oldman Jr. *Chem. Rev.* **1993**, 93, 913; c) P. G. Jessop, R. H. Morris, *Coord. Chem. Rev.* **1992**, 121, 155.
- 51 G. H. Spikes, J. C. Fettingner, P. P. Power, *J. Am. Chem. Soc.* **2005**, 127, 12232.
- 52 H.-J. Himmel, H. Schnöckel, *Chem. Eur. J.* **2002**, 8, 2397.
- 53 Z. D. Brown, P. P. Power, *Inorg. Chem.* **2013**, 52, 6248.
- 54 T. L. Allen, W. H. Fink, P. P. Power, *J. Chem. Soc., Dalton Trans.* **2000**, 407.
- 55 C. Cui, M. M. Olmstead, J. C. Fettingner, G. H. Spikes, P. P. Power, *J. Am. Chem. Soc.* **2005**, 127, 17530.
- 56 G. D. Frey, V. Lavallo, D. Donnadiou, W. W. Schoeller, G. Bertrand, *Science*, **2007**, 316, 439.
- 57 a) G. C. Welch, R. R. San Juan, J. D. Masuda, D. W. Stephan, *Science*, **2006**, 314, 1124; b) G. C. Welch, D. W. Stephan, *J. Am. Chem. Soc.* **2007**, 129, 1880; c) D. W. Stephan, *Chem. Commun.* **2010**, 46, 8526.
- 58 Z. D. Brown, P. Vasko, J. C. Fettingner, H. M. Tuononen, P. P. Power, *J. Am. Chem. Soc.* **2012**, 134, 4045.
- 59 Z. D. Brown, P. Vasko, J. D. Erickson, H. M. Tuononen, P. P. Power, *J. Am. Chem. Soc.* **2013**, 135, 6257.
- 60 J. Escudie, H. Ranaivonjatovo, *Organometallics*, **2007**, 26, 1542.
- 61 K. Klinkhammer, *Polyhedron*, **2002**, 21, 587.
- 62 H. Grützmacher, S. Freitag, R. Herbst-Irmer, G. M. Sheldrick, *Angew. Chem. Int. Ed.* **1992**, 31, 437.
- 63 X. Wang, Z. Zhu, Y. Peng, H. Lei, J. C. Fettingner, P. P. Power, *J. Am. Chem. Soc.* **2009**, 131, 6912.
- 64 Y. Peng, J. D. Guo, B. D. Ellis, Z. Zhu, J. C. Fettingner, S. Nagase, P. P. Power, *J. Am. Chem. Soc.* **2009**, 131, 16272.
- 65 Z. D. Brown, J.-D. Guo, S. Nagase, P. P. Power, *Organometallics*, **2012**, 31, 3768.
- 66 C. Maaß, *Pinzetten-Liganden in der Koordination von Hauptgruppenmetallen*, Diplomarbeit, Göttingen, **2010**.
- 67 a) H. W. Gschwend, H. R. Rodriguez, *Organic Reactions*, 26th ed, John Wiley, New York, **1979**; b) J. M. Mallan, R. L. Bebb, *Chem. Rev.* **1969**, 69, 693.
- 68 a) V. Snieckus, *Chem. Rev.* **1990**, 90, 879; b) H. Gilman, R. L. Bebb, *J. Am. Chem. Soc.* **1939**, 61, 109; c) G. Wittig, G. Fuhrmann, *Chem. Ber.* **1940**, 73, 1197

-
- 69 D. J. Nielsen, K. J. Cavell, M. S. Viciu, S. P. Nolan, B. W. Skelton, A. H. White, *J. Organomet. Chem.* **2005**, 690, 6133.
- 70 D. E. B. H. M. Gilow, *J. Org. Chem.* **1981**, 46, 2221.
- 71 V. A. Knizhnikov, N. E. Borisova, N. Y. Yurashevich, L. A. Popova, A. Y. Chernyadev, Z. P. Zubreichuk, M. D. Reshetova, *Russ. J. Org. Chem.* **2007**, 43, 855.
- 72 a) N. Meyer, J. Jentner, P. W. Roesky, G. Eickerling, W. Scherer, *Chem. Commun.* **2009**, 4693; b) N. Meyer, M. Kuzdrowska, P. W. Roesky, *Eur. J. Inorg. Chem.* **2008**, 1475.
- 73 a) C. Mannich, W. Krösche, *Archiv der Pharmazie*, **1912**, 250, 647; b) S. Hauptmann, *Organische Chemie*, 3rd ed, Wiley-VCH, Weinheim, **1991**.
- 74 I. T. Kim, R. L. Elsenbaumer, *Tetrahedron Letters*, **1998**, 39, 1087.
- 75 P.-C. Kuo, J.-C. Chang, W.-Y. Lee, H. M. Lee, J.-H. Huang, *J. Organomet. Chem.* **2005**, 690, 4168.
- 76 J.-H. Huang, H.-J. Chen, J.-C. Chang, C.-C. Zhou, G.-H. Lee, S.-M. Peng, *Organometallics*, **2001**, 20, 2647.
- 77 a) J.-W. Hsu, Y.-C. Lin, C.-S. Hsiao, A. Datta, C.-H. Lin, J.-H. Huang, J.-C. Tsai, W.-C. Hsu, *Dalton Trans.* **2012**, 41, 7700; b) J.-C. Chang, Y.-C. Chen, A. Datta, C.-H. Lin, C.-S. Hsiao, J.-H. Huang, *J. Organomet. Chem.* **2011**, 696, 3673; c) W.-Y. Lee, C.-C. Hsieh, J.-W. Hsu, A. Datta, Y.-C. Lin, J.-H. Huang, T.-Y. Lee, *J. Organomet. Chem.* **2001**, 696, 3816; d) S. Banerjee, Y. Shi, C. Cao, A. L. Odom, *J. Organomet. Chem.* **2005**, 690, 5066; e) Y. Li, S. Banerjee, A. L. Odom, *Organometallics*, **2005**, 24, 3272; f) P.-C. Kuo, J.-H. Huang, C.-H. Hung, G.-H. Lee, S.-M. Peng, *Eur. J. Inorg. Chem.* **2003**, 1440; g) A. Xia, M. J. Heeg, C. H. Winter, *Organometallics*, **2002**, 21, 4718; h) W.-Y. Huang, S.-J. Chuang, N.-T. Chunag, C.-S. Hsiao, A. Datta, S.-J. Chen, C.-H. Hu, J.-H. Huang, T.-Y. Lee, C.-H. Lin, *Dalton Trans.* **2011**, 40, 7423; i) J.-H. Huang, H.-J. Chen, C.-C. Hsieh, G.-H. Lee, S.-M. Peng, *Inorg. Chim. Acta*, **2001**, 321, 142; j) J.-C. Chang, C.-H. Hung, J.-H. Huang, *Organometallics*, **2001**, 20, 4445; k) I.-C. Chen, S.-M. Ho, Y.-C. Chen, C.-Y. Lin, C.-H. Hu, C.-Y. Tu, A. Datta, J.-H. Huang, C.-H. Lin, *Dalton Trans.* **2009**, 8631.
- 78 Compound **2** published in the CSD by Y.-X. Li. CCDC-no. 768580.
- 79 R. Brückner, *Reaktionsmechanismen*, 3rd ed, Elsevier, Heidelberg, **2004**.
- 80 M. A. Spackman, D. Jayatilaka, *CrystEngComm*, **2009**, 11, 19.
- 81 J. J. McKinnon, D. Jayatilaka, M. A. Spackman, *Chem. Commun.* **2007**, 3814.
- 82 a) J. J. McKinnon, M. A. Spackman, A. S. Mitchell, *Acta Cryst. B*, **2004**, 60, 627; b) F. L. Hirshfeld, *Theor. Chim. Acta*, **1977**, 44, 129.
- 83 U. Baisch, S. Pagano, M. Zeuner, N. Barros, L. Maron, W. Schnick, *Chem. Eur. J.* **2006**, 12, 4785.
- 84 N. Mohan, K. P. Vijayalakshmi, N. Koga, C. H. Suresh, *J. Comput. Chem.* **2010**, 31, 2874.
- 85 S. Tsuzuki, K. Honda, T. Uchimaru, M. Mikami and A. Fujii, *J. Phys. Chem. A*, **2006**, 110, 10163.

-
- 86 S. Tsuzuki, A. Fujii, *Phys. Chem. Chem. Phys.* **2008**, *10*, 2584.
- 87 A. Szabo, N. S. Ostlund, *Modern Quantum Chemistry: Introduction to Advanced Electronic Structure Theory*, 1st ed, Dover Publications, New York, **1996**.
- 88 C. C. J. Roothaan, *Reviews of Modern Physics*, **1951**, *23*, 69.
- 89 J. E. Lennard-Jones, *Trans. Faraday Soc.* **1929**, *25*, 668.
- 90 P. Hohenberg, W. Kohn, *Phys. Rev.* **1964**, *136*, B864.
- 91 (a) A. D. Becke, *J. Chem. Phys.* **1993**, *98*, 5648; (b) C. Lee, W. Yang, R. G. Parr, *Phys. Rev. B*, **1988**, *37*, 785; (c) P. J. Stephens, F. J. Devlin, C. F. Chabalowski, M. J. Frisch, *J. Phys. Chem.* **1994**, *98*, 11623; (d) A. D. Becke, *Phys. Rev. A*, **1988**, *38*, 3098.
- 92 R. von Bülow, H. Gornitzka, T. Kottke, D. Stalke, *Chem. Comm.* **1996**, 1639.
- 93 F. Neese, *Wiley Interdisciplinary Reviews: Computational Molecular Science* **2012**, *2*, 73.
- 94 F. Weigend, R. Ahlrichs, *Phys. Chem. Chem. Phys.* **2005**, *7*, 3297.
- 95 H.-J. Werner, P. J. Knowles, G. Knizia, F. R. Manby, M. Schütz, P. Celani, T. Korona, R. Lindh, A. Mitrushenkov, G. Rauhut, K. R. Shamasundar, T. B. Adler, R. D. Amos, A. Bernhardsson, A. Berning, D. L. Cooper, M. J. O. Deegan, A. J. Dobbyn, F. Eckert, E. Goll, C. Hampel, A. Hesselmann, G. Hetzer, T. Hrenar, G. Jansen, C. Köppl, Y. Liu, A. W. Lloyd, R. A. Mata, A. J. May, S. J. McNicholas, W. Meyer, M. E. Mura, A. Nicklass, D. P. O'Neill, P. Palmieri, D. Peng, K. Pflüger, R. Pitzer, M. Reiher, T. Shiozaki, H. Stoll, A. J. Stone, R. Tarroni, T. Thorsteinsson, M. Wang, <http://www.molpro.net>, **2012**.
- 96 (a) Kaupp, M.; Metz, B.; Stoll, H. *Angew. Chem. Int. Ed.* **2000**, *39*, 4607; (b) Kaupp, M.; Metz, B.; Stoll, H. *Angew. Chem.* **2000**, *112*, 4780.
- 97 a) T. H. Dunning, Jr. *J. Chem. Phys.* **1989**, *90*, 1007; b) D. E. Woon, T. H. Dunning, Jr. *J. Chem. Phys.* **1993**, *98*, 1358.
- 98 D. E. Woon, T. H. Dunning Jr, *The Journal of Chemical Physics* **1995**, *103*, 4572.
- 99 a) A. E. Reed, F. Weinhold, *J. Chem. Phys.* **1983**, *78*, 4066; b) A. E. Reed, F. Weinhold, *J. Chem. Phys.* **1985**, *83*, 1736; c) A. E. Reed, L. A. Curtiss, F. Weinhold, *Chem. Rev.* **1988**, *88*, 899; d) A. E. Reed, R. B. Weinstock, F. Weinhold, *J. Chem. Phys.* **1985**, *83*, 735.
- 100 M. J. Frisch, G. W. Trucks, H. B. Schlegel, G. E. Scuseria, M. A. Robb, J. R. Cheeseman, G. Scalmani, V. Barone, B. Mennucci, G. A. Petersson, H. Nakatsuji, M. Caricato, X. Li, H. P. Hratchian, A. F. Izmaylov, J. Bloino, G. Zheng, J. L. Sonnenberg, M. Hada, M. Ehara, K. Toyota, R. Fukuda, J. Hasegawa, M. Ishida, T. Nakajima, Y. Honda, O. Kitao, H. Nakai, T. Vreven, J. A. J. Montgomery, J. E. Peralta, F. Ogliaro, M. Bearpark, J. J. Heyd, E. Brothers, K. N. Kudin, V. N. Staroverov, T. Keith, R. Kobayashi, J. Normand, K. Raghavachari, A. Rendell, J. C. Burant, S. S. Iyengar, J. Tomasi, M. Cossi, N. Rega, J. M. Millam, M. Klene, J. E. Knox, J. B. Cross, V. Bakken, C. Adamo, J. Jaramillo, R. Gomperts, R. E. Stratmann, O. Yazyev, A. J. Austin, R. Cammi, C. Pomelli, J. W. Ochterski, R. L. Martin, K. Morokuma,

- V. G. Zakrzewski, G. A. Voth, P. Salvador, J. J. Dannenberg, S. Dapprich, A. D. Daniels, O. Farkas, J. B. Foresman, J. V. Ortiz, J. Cioslowski, D. J. Fox, Gaussian 09, Revision A.02, **2010**, Gaussian.
- 101 J. C. Ma, D. A. Dougherty, *Chem. Rev.* **1997**, 97, 1303.
- 102 a) R. A. Kumpf, D. A. Dougherty, *Science*, **1993**, 261, 1708; b) J. W. Caldwell, P. A. Kollman, *J. Am. Chem. Soc.* **1995**, 338, 303.
- 103 K. Yuan, Y. Liu, L. Lü, Y. Zhu, J. Zhang, J. Zhang, *Chin. J. Chem.* **2009**, 27, 697.
- 104 a) A. D. Shannon, *Acta Crystallogr.* **1976**, A32, 751; b) Y. Q. Jia, *Solid State Chem.* **1991**, 95, 184.
- 105 D. Jayatilaka, D. J. Grimwood, *Computational Science – ICCS*, **2003**, 4, 142.
- 106 S. Tsuzuki, *Annu. Rep. Prog. Chem., Sect. C: Phys. Chem.* **2012**, 108, 69.
- 107 M. Nishio, *CrystEngComm*, **2004**, 6, 27, 130.
- 108 a) J. J. Byers, W. T. Pennington, G. H. Robinson, *Acta Crystallogr., Sect. C: Cryst. Struct. Commun.* **1992**, 48, 2023; b) T. Gelbrich, J. Sieler, U. Dumichen, *Z. Kristallogr.* **2000**, 215, 127.
- 109 F. G. Bordwell, *Acc. Chem. Res.* **1988**, 21, 456.
- 110 M. J. Bruce, *Angew. Chem. Int. Ed.* **1977**, 16, 73.
- 111 B.-K. Kim, S.-B. Choi, S. D. Kloos, P. Boudjouk, *Inorg. Chem.* **2000**, 39, 728.
- 112 P. Boudjouk, S. D. Kloos, B.-K. Kim, M. Page, D. Thweatt, *J. Chem. Soc., Dalton Trans.* **1998**, 877.
- 113 J. Li, A. Stasch, C. Schenk, C. Jones, *Dalton Trans.* **2011**, 40, 11448.
- 114 a) W. J. Hehre, R. Ditchfield, J. A. Pople, *J. Chem. Phys.* **1972**, 56, 2257; b) M. M. Francl, W. J. Pietro, W. J. Hehre, J. S. Binkley, M. S. Gordon, D. J. DeFrees, J. A. Pople, *J. Chem. Phys.* **1982**, 77, 3654.
- 115 a) I. I. Chernyaev, *Ann. Inst. Platine*, **1926**, 4, 243; b) K. M. Anderson, A. G. Orpen, *Chem. Commun.* **2001**, 2682.
- 116 (a) S. Grimme, *J. Comput. Chem.* **2006**, 27, 1787; (b) T. Schwabe, S. Grimme, *Acc. Chem. Res.* **2008**, 41, 569; (c) S. Grimme, J. Antony, S. Ehrlich, H. Krieg, *J. Chem. Phys.* **2010**, 132, 154104.
- 117 K. Eichkorn, F. Weigend, O. Treutler, R. Ahlrichs, *Theor. Chem. Acc.* **1997**, 97, 119.
- 118 (a) C. Møller and M. S. Plesset, *Phys. Rev.* **1934**, 46, 618; (b) M. Head-Gordon, J. A. Pople, M. J. Frisch, *Chem. Phys. Lett.* **1988**, 153, 503; (c) S. Saebø, J. Almlöf, *Chem. Phys. Lett.* **1989**, 154, 83; (d) M. J. Frisch, M. Head-Gordon, J. A. Pople, *Chem. Phys. Lett.* **1990**, 166, 275; (e) M. J. Frisch, M. Head-Gordon, J. A. Pople, *Chem. Phys. Lett.* **1990**, 166, 281; (f) M. Head-Gordon, T. Head-Gordon, *Chem. Phys. Lett.* **1994**, 220, 122.
- 119 C. Maaß, D. M. Andrada, R. A. Mata, R. Herbst-Irmer, D. Stalke, *Inorg. Chem.* **2013**, 52, 9539.

- 120 a) P. v. R. Schleyer, C. Maerker, A. Dransfeld, H. Jiao, N. J. R. Van Eikema Hommes, *J. Am. Chem. Soc.* **1996**, *118*, 6317-6318; b) Z. Chen, C. S. Wannere, C. Corminboeuf, R. Puchta, P. v. R. Schleyer, *Chem. Rev.* **2005**, *105*, 3842-3888; c) H. Fallah-Bagher-Shaidei, C. S. Wannere, C. Corminboeuf, R. Puchta, P. v. R. Schleyer, *Org. Lett.* **2006**, *8*, 863-866.
- 121 M. J. Frisch, J. A. Pople, J. S. Binkley, *J. Chem. Phys.*, **1984**, *80*, 3265.
- 122 a) H. Günther *NMR Spectroscopy: Basic Principles, Concepts, and Applications in Chemistry*, 2nd ed, Wiley, Chichester, **1995**; b) N. H. Matrin, D. Brown, *Int. J. Mol. Sci.* **2000**, *1*, 84; c) C. S. Wannere, P. v. R. Schleyer, *Org. Lett.* **2003**, *5*, 605; d) S. Pelloni, A. Ligabue, P. Lazzeretti, *Org. Lett.* **2004**, *6*, 4451; e) R. Soriano Jartin, A. Ligabue, A. Soncini, P. Lazzeretti, *J. Phys. Chem. A*, **2002**, *106*, 11806; f) U. Fleischer, W. Kutzelnigg, P. Lazzeretti, V. Mühlkamp, *J. Am. Chem. Soc.* **1994**, *116*, 5298.
- 123 a) T. M. Krygowski, K. Ejsmont, B. T. Stepien, M. K. Cryanski, J. Poater, M. Sola, *J. Org. Chem.* **2004**, *69*, 6634; b) T. M. Krygowski, B. T. Stepien, M. K. Cryanski, K. Ejsmont, *J. Phys. Org. Chem.* **2005**, *18*, 886.
- 124 B.T. Psciuk, R. L. Lord, C. H. Winter, H. B. Schlegel, *J. Chem. Theory Comput.* **2012**, *8*, 4950.
- 125 (a) C. Jones, S. J. Bonyhady, N. Holzmann, G. Frenking, A. Stasch, *Inorg. Chem.* **2011**, *50*, 12315; (b) D. Matioszek, N. Kafir, N. Saffon, A. Castel, *Organometallics*, **2010**, *29*, 3039; (c) T. Chlupaty, Z. Padelkova, A. Lycka, J. Bruns, A. Ruzicka, *Dalton Trans.* **2012**, *41*, 5010; (d) I. L. Fedushkin, N. M. Khvoinova, *Inorg. Chem.* **2004**, *43*, 7807; (e) W.-P. Leung, C.-W. So, Y.-S. Wu, H.-W. Li, T. C. W. Mak, *Eur. J. Inorg. Chem.* **2005**, 513; (f) H. Arai, F. Nakadate, K. Mochida, T. Kawashima, *Organometallics*, **2011**, *30*, 4471; (g) A. Chrostowska, V. Lemierre, T. Pigot, G. Pfister-Guillouzo, I. Saur, K. Miqueu, G. Rima, J. Barrau, *Main Group Met. Chem.* **2002**, *25*, 469; (h) I. L. Fedushkin, M. Hummert, H. Schumann, *Eur. J. Inorg. Chem.* **2006**, 3266; (i) C. Jones, R. P. Rose, A. Stasch, *Dalton Trans.* **2008**, 2871; (j) W. Wang, S. Inoue, S. Yao, M. Driess, *Organometallics*, **2011**, *30*, 6490; (k) N. D. Reddy, A. Jana, H. W. Roesky, P. P. Samuel, C. Schulzke, *Dalton Trans.* **2010**, *39*, 234; (l) W. D. Woodul, A. F. Richards, A. Stasch, M. Driess, C. Jones, *Organometallics*, **2010**, *29*, 3655; (m) S. P. Sarish, S. S. Sen, H. W. Roesky, I. Objartel, D. Stalke, *Chem. Commun.* **2011**, *47*, 7206; (n) R. K. Siwatch, S. Kundu, D. Kumar, S. Nagendran, *Organometallics*, **2011**, *30*, 1998; (o) A. E. Ayers, T. M. Klapotke, H. V. R. Dias, *Inorg. Chem.* **2001**, *40*, 1000; (p) K. V. Vasudevan, J. Vargas-Baca, A. H. Cowley, *Angew. Chem. Int. Ed.* **2009**, *48*, 8369; (q) S. P. Green, C. Jones, P. C. Junk, K.-A. Lippert, A. Stasch, *Chem. Commun.* **2006**, 3978; (r) H. V. Dias, Z. Wang, *J. Am. Chem. Soc.* **1997**, *119*, 4650; (s) A. C. Filippou, P. Portius, G. Kociok-Kohn, *Chem. Commun.* **1998**, 2327; (t) S. Nagendran, S. S. Sen, H. W. Roesky, D. Koley, H. Grubmüller, A. Pal R. Herbst-Irmer, *Organometallics*, **2008**, *27*, 5459; (u) A. E. Ayers, H. V. R. Dias, *Inorg. Chem.* **2002**, *41*, 3259; (v) A. F. Gushwa, A. F. Richards, *J. Chem. Cryst.* **2006**, *36*, 851; (w) Y. Ding, H. W. Roesky, M. Noltemeyer, H.-G. Schmidt, P. P. Power, *Organometallics*, **2001**, *20*, 1190; (x) Z. Yang, X. Ma, H. W. Roesky, Y. Yang, H. Zhu, J. Magull, A. Ringe, *Z. Anorg. Allg. Chem.* **2008**, *634*, 1490.
- 126 a) L. W. Pineda, V. Jancik, H. W. Roesky, R. Herbst-Irmer, *Angew. Chem. Int. Ed.* **2004**, *43*, 5534; b) I. Saur, G. Rima, H. Gornitzka, K. Miqueu, J. Barrau, *Organometallics*, **2003**, *22*, 1106; c) M. Veith, S. Becker, V. Huch, *Angew. Chem. Int. Ed.* **1989**, *28*, 1237; d) A. Jana, D. Ghoshal, H. W. Roesky, I. Objartel, G. Schwab, D. Stalke, *J. Am. Chem. Soc.* **2009**, *131*, 1288.
- 127 Y. Ding, H. Hao, H. W. Roesky, M. Noltemeyer, H.-G. Schmidt, *Organometallics*, **2001**, *20*, 4806.
- 128 A. Jana, D. Ghoshal, H. W. Roesky, I. Objartel, G. Schwab, D. Stalke, *J. Am. Chem. Soc.* **2009**, *131*, 1288.

- 129 A. Jana, H. W. Roesky, C. Schulzke, *Dalton Trans.* **2010**, 39, 132.
- 130 Y. Ding, Q. Ma, H. W. Roesky, R. Herbst-Irmer, I. Usón, M. Noltemeyer, H.-G. Schmidt, *Organometallics*, **2002**, 21, 5216.
- 131 I. Saur, K. Miqueu, G. Rima, J. Barrau, V. Lemierre, A. Chrostowska, J.-M. Sotiropoulos, G. Pfister-Guillouzo, *Organometallics*, **2003**, 22, 3143.
- 132 (a) A. H. Cowley, R. L. Geerts, C. M. Nurm, C. J. Carrano, *J. Organomet. Chem.* **1988**, 341, C27; (b) D. J. Doyle, P. B. Hitchcock, M. F. Lappert, G. Li, *J. Organomet. Chem.* **2009**, 694, 2611; (c) S. S. Sen, M. P. Kritzer-Kosch, S. Nagendran, H. W. Roesky, T. Beck, A. Pal, R. Herbst-Irmer, *Eur. J. Inorg. Chem.* **2010**, 5304; (d) L. Ferro, P. B. Hitchcock, M. P. Coles, H. Cox, J. R. Futton, *Inorg. Chem.* **2011**, 50, 1879; (e) D. L. Reger, S. J. Knox, M. F. Huff, A. L. Rheingold, B. J. Haggerty, *Inorg. Chem.* **1991**, 30, 1754; (f) P. B. Hitchcock, J. Hu, M. F. Lappert, J. R. Severn, *Dalton Trans.* **2004**, 4193; (g) A. Akkari, J. J. Byrne, I. Saur, G. Rima, H. Gornitzka, J. Barrau, *J. Organomet. Chem.* **2001**, 622, 190; (h) M. Bryn, M. D. Francis, G. Jin, C. Jones, D. P. Mills, A. Stasch, *Organometallics*, **2006**, 25, 4799; (i) J. Kobayasi, T. Kushida, T. Kawashima, *J. Am. Chem. Soc.* **2009**, 131, 10836; (j) H. V. R. Dias, W. Jin, *J. Am. Chem. Soc.* **1996**, 118, 9123; (k) J. T. B. H. Jastrzebski, P. A. van der Schaaf, J. Boersma, G. van Koten, M. C. Zoutberg, D. Heijdenrijk, *Organometallics*, **1989**, 8, 1373; (l) N. Nimitsiriwat, V. C. Gibson, E. L. Marshall, A. J. P. With, S. H. Dale, N. R. J. Elsegood, *Dalton Trans.* **2007**, 4464.
- 133 Y. Zhao, D. G. Truhlar, *Theor. Chem. Acc.* **2008**, 120, 215.
- 134 K. Jurkschat, K. Peveling, M. Schürmann, *Eur. J. Inorg. Chem.* **2003**, 3563.
- 135 R. W. Chorley, P. B. Hitchcock, M. F. Lappert, W.-P. Leung, P. P. Power, M. M. Olmstead, *Inorg. Chim. Acta*, **1992**, 198, 203.
- 136 T. Fjeldberg, H. Hope, M. F. Lappert, P. P. Power, A. J. Thorne, *Chem. Commun.* **1983**, 639.
- 137 M. Chen, J. R. Fulton, P. B. Hitchcock, N. C. Johnstone, M. F. Lappert, A. V. Protchenko, *Dalton Trans.* **2007**, 2770.
- 138 a) J. Vrana, R. Jambor, A. Ruzicka, J. Holecek, L. Dostal, *Collect. Czech. Chem. Commun.* **2010**, 75, 1041; b) B. Lyhs, S. Schulz, U. Westphal, D. Blaser, R. Boese, M. Bolte, *Eur. J. Inorg. Chem.* **2009**, 2247; c) S. P. Green, C. Jones, G. Jin, A. Stasch, *Inorg. Chem.* **2007**, 46, 8; d) P. B. Hitchcock, M. F. Lappert, G. Li, M. P. Coles, *Dalton Trans.* **2009**, 7820; e) L. A. Lesikar, A. F. Richards, *J. Organomet. Chem.* **2006**, 691, 4250.
- 139 a) T. D. Manuel, J.-U. Rohde, *J. Am. Chem. Soc.* **2009**, 131, 15582; b) S. Yuan, S. Bai, H. Tomg, D. Liu, W.-H. Sun, *Inorg. Chim. Acta*, **2011**, 370, 215; c) J.-C. Wasilke, G. Wu, X. Bu, G. Kehr, G. Erker, *Organometallics*, **2005**, 24, 4289; d) P. L. Holland, T. R. Cundari, L. L. Perez, N. A. Eckert, R. J. Lachicotte, *J. Am. Chem. Soc.* **2002**, 124, 14416; e) K. Okamoto, T. Kanbara, T. Yamamoto, *Chem. Lett.* **2006**, 35, 558.
- 140 J. C. Jeffrey, T. B. Rauchfuss, *Inorg. Chem.* **1979**, 18, 2658.
- 141 a) W. Schlenk, A. Thal, *Ber. Dtsch. Chem. Ges.* **1913**, 46, 2840; b) W. Schlenk, J. Holtz, *Ber. Dtsch. Chem. Ges.* **1917**, 50, 262; c) W. Schlenk, *Die Methoden der Organischen Chemie*, G. Thieme, Leipzig, **1924**; d) T. T. Tidwell, *Angew. Chem. Int. Ed.* **2001**, 40, 331.

-
- 142 (a) T. Kottke, D. Stalke, *J. Appl. Crystallogr.* **1993**, 26, 615; (b) T. Kottke, R. J. Lagow, D. Stalke, *J. Appl. Crystallogr.* **1996**, 29, 465; (c) D. Stalke, *Chem. Soc. Rev.* **1998**, 27, 171.
- 143 T. Schulz, K. Meindl, D. Leusser, D. Stern, J. Graf, C. Michaelson, M. Ruf, G. M. Sheldrick, D. Stalke, *J. Appl. Crystallogr.* **2009**, 42, 885.
- 144 COSMO, Madison (WI), Bruker-AXS, **2011**.
- 145 Bruker APEX v2012.10-0, Madison, WI, USA, **2012**.
- 146 SAINT, v7.68A, Bruker-AXS, Madison (WI), **2009**.
- 147 G. M. Sheldrick, SADABS-2012/1, Madison, WI, USA, **2012**.
- 148 G. M. Sheldrick, TWINABS-2012/1, Göttingen, **2012**.
- 149 G. M. Sheldrick, XPREP 2013/1, Madison, WI, USA, **2013**.
- 150 G. M. Sheldrick, *Acta Crystallogr., Sect. A.* **1990**, 46, 467.
- 151 G. M. Sheldrick, *Acta Crystallogr. Sect. A*, **2008**, 64, 112.
- 152 C. B. Huebschle, G. M. Sheldrick, B. Dittrich, *J. Appl. Cryst.* **2011**, 44, 1281.
- 153 D. Mootz, A. Zinnius, B. Bottcher, *Angew. Chem.* **1969**, 81, 398.
- 154 (a) H. Flack, *Acta Crystallogr.* **1983**, A39, 876; (b) H. Flack, G. Bernardinelli, *J. Appl. Cryst.* **2000**, 33, 1143; (c) S. Parsons H. Flack, *Acta Cryst.* **2004**, A60, 61.